

# Phase Behaviour of Alternative Solvents

Marijana Blešić



Dissertation presented to obtain the Ph.D. degree  
in Chemistry (Physical Chemistry) at the Instituto de Tecnologia  
Química e Biológica da Universidade Nova de Lisboa

Oeiras, December 2008.

## **CONTENTS:**

|                                                                 |           |
|-----------------------------------------------------------------|-----------|
| <b>Acknowledgements</b>                                         | <b>I</b>  |
| <b>Summary</b>                                                  | <b>II</b> |
| <b>General Introduction</b>                                     | <b>1</b>  |
| <b>Solvent Properties</b>                                       | <b>1</b>  |
| <b>Alternative Solvent Strategy</b>                             | <b>2</b>  |
| <b>Multiphasic Solvent System</b>                               | <b>3</b>  |
| <b>Fluorinated Solvents</b>                                     | <b>4</b>  |
| <b>Water</b>                                                    | <b>5</b>  |
| <b>Ionic Liquids</b>                                            | <b>6</b>  |
| Structure of Ionic Liquids                                      | <b>8</b>  |
| Physicochemical Properties of Ionic Liquids                     | <b>8</b>  |
| <b>References</b>                                               | <b>11</b> |
| <br>                                                            |           |
| <b>Chapter 1</b>                                                | <b>14</b> |
| <b>How Hydrophilic Ionic Liquids Behave in Aqueous Solution</b> | <b>16</b> |
| <b>Abstract</b>                                                 | <b>16</b> |
| <b>Introduction</b>                                             | <b>16</b> |
| <b>Experimental</b>                                             | <b>18</b> |
| <b>Results and Discussion</b>                                   | <b>19</b> |
| <b>Conclusion</b>                                               | <b>23</b> |
| <b>References</b>                                               | <b>23</b> |
| <br>                                                            |           |
| <b>Chapter 2</b>                                                | <b>26</b> |

|                                                                                                                                                                                 |           |
|---------------------------------------------------------------------------------------------------------------------------------------------------------------------------------|-----------|
| <b>On the Self-Aggregation and Fluorescence Quenching Aptitude of Surfactant Ionic Liquids</b>                                                                                  | <b>28</b> |
| Abstract                                                                                                                                                                        | 28        |
| Introduction                                                                                                                                                                    | 28        |
| Experimental                                                                                                                                                                    | 28        |
| Results and Discussion                                                                                                                                                          | 29        |
| Conclusion                                                                                                                                                                      | 32        |
| References                                                                                                                                                                      | 32        |
| <br>                                                                                                                                                                            |           |
| <b>Chapter 3</b>                                                                                                                                                                | <b>34</b> |
| <b>1-Alkyl-3-Methylimidazolium Alkylsulfonate Ionic Liquids: Synthesis and Physicochemical Properties</b>                                                                       | <b>36</b> |
| Introduction                                                                                                                                                                    | 36        |
| Experimental                                                                                                                                                                    | 38        |
| Results and Discussion                                                                                                                                                          | 41        |
| Conclusion                                                                                                                                                                      | 53        |
| References                                                                                                                                                                      | 54        |
| <br>                                                                                                                                                                            |           |
| <b>Chapter 4</b>                                                                                                                                                                | <b>56</b> |
| <b>Anion and Cation Effects on the Self-Aggregation of 1-Alkyl-3-Methylimidazolium Alkylsulfonate, <math>[C_nH_{2n+1}mim][C_mH_{2m+1}SO_3]</math>, Ionic Liquid Surfactants</b> | <b>58</b> |
| Abstract                                                                                                                                                                        | 58        |
| Introduction                                                                                                                                                                    | 59        |
| Experimental                                                                                                                                                                    | 61        |
| Results and Discussion                                                                                                                                                          | 64        |

|                                                                                                                                                |            |
|------------------------------------------------------------------------------------------------------------------------------------------------|------------|
| <b>Conclusion</b>                                                                                                                              | <b>72</b>  |
| <b>References</b>                                                                                                                              | <b>73</b>  |
| <br>                                                                                                                                           |            |
| <b>Chapter 5</b>                                                                                                                               | <b>76</b>  |
| <b>Phase Equilibria in Ionic Liquid Plus Aromatic<br/>Compound Binary Systems</b>                                                              | <b>78</b>  |
| <b>Abstract</b>                                                                                                                                | <b>78</b>  |
| <b>Introduction</b>                                                                                                                            | <b>78</b>  |
| <b>Experimental</b>                                                                                                                            | <b>80</b>  |
| <b>Results and Discussion</b>                                                                                                                  | <b>81</b>  |
| <b>Conclusion</b>                                                                                                                              | <b>85</b>  |
| <b>References</b>                                                                                                                              | <b>86</b>  |
| <br>                                                                                                                                           |            |
| <b>Chapter 6</b>                                                                                                                               | <b>88</b>  |
| <b>Solubility of Fluorinated Compounds in a Range of<br/>Ionic Liquids: Cloud-Point Temperature Dependence on<br/>Composition and Pressure</b> | <b>90</b>  |
| <b>Abstract</b>                                                                                                                                | <b>90</b>  |
| <b>Introduction</b>                                                                                                                            | <b>90</b>  |
| <b>Experimental</b>                                                                                                                            | <b>91</b>  |
| <b>Results and Discussion</b>                                                                                                                  | <b>94</b>  |
| <b>Conclusion</b>                                                                                                                              | <b>100</b> |
| <b>References</b>                                                                                                                              | <b>100</b> |

|                                                                                                                  |            |
|------------------------------------------------------------------------------------------------------------------|------------|
| <b>Chapter 7</b>                                                                                                 | <b>101</b> |
| <b>7.1 Liquid-Liquid Equilibrium of (Perfluoralkane + Alkane)<br/>    Binary Mixures</b>                         | <b>103</b> |
| Abstract                                                                                                         | 103        |
| Introduction                                                                                                     | 103        |
| Experimental                                                                                                     | 105        |
| Modelling                                                                                                        | 106        |
| Results and Discussion                                                                                           | 108        |
| Conclusion                                                                                                       | 110        |
| References                                                                                                       | 111        |
| <b>7.2 Liquid-Liquid Equilibrium of (1H,1H,7H-Perfluorheptan-1-ol<br/>    + Perfluoroalkane) Binary Mixtures</b> | <b>113</b> |
| Abstract                                                                                                         | 113        |
| Introduction                                                                                                     | 113        |
| Experimental                                                                                                     | 114        |
| Modelling                                                                                                        | 115        |
| Results and Discussion                                                                                           | 115        |
| Conclusion                                                                                                       | 119        |
| References                                                                                                       | 120        |
| <b>General Discussion</b>                                                                                        | <b>121</b> |
| <b>Appendix 1</b>                                                                                                | <b>125</b> |
| <b>Appendix 2</b>                                                                                                | <b>132</b> |
| <b>Appendix 3</b>                                                                                                | <b>139</b> |

## Acknowledgements

Marijana Blesic is grateful to:

- Supervisors Prof. Luís Paulo S. Nieto M. Rebelo and Prof. António Manuel Gonçalves Lopes;
- Prof. Kenneth Richard Seddon, Dr. Vesna Najdanovic-Visak, Dr. Joanna Lachwa, Dr. Zoran Visak, Prof. José N. Canongia Lopes, Malgorzata Swadzba-Kwasny, Dr. John Holbrey, Dr. Margarida F. Costa Gomes, Dr. Nimal Gunaratne, Dr. Natalia V. Plechkova, Prof. Agilio A. H. Padua, Prof. Eurico Melo, Dr. Zeljko Petrovski, Dr. Jose´ M.S.S. Esperança, and other collaborators;
- Instituto de Tecnologia Química e Biológica da Universidade Nova de Lisboa, The QUILL Centre, The Queen’s University of Belfast, and Laboratoire de Thermodynamique et Interactions Moléculaires, Université Blaise Pascal, Clermont-Ferrand;
- The Fundação para a Ciência e Tecnologia for the PhD grant and Marie Curie Fellowships for Early Stage Research Training.

## Summary

This Thesis is mainly focused on phase behaviour in macro and nano domains and thermodynamic properties of mixtures containing ionic liquids and water, fluorinated or organic solvents. A broad list of commercially available ionic liquids or specific and functionalised, synthesised and characterised by the author of the Thesis is included in this study. The used ionic liquids contained the following cations: 1-alkyl-3-methylimidazolium  $[C_n\text{mim}]^+$ , 1-alkyl-3-methylpyridinium  $[C_n\text{mpyr}]^+$ , 1-alkyl-1-methylpyrrolidinium  $[C_n\text{mpyrr}]^+$ , 1-alkyl-1-methylpiperidinium  $[C_n\text{mpip}]^+$ , and tetraalkylphosphonium  $[C_xC_yC_zC_w\text{P}]^+$  and some of the anions: chloride  $\text{Cl}^-$ ,  $\text{Br}^-$ , hexafluorophosphate  $[\text{PF}_6]^-$ , bis{(trifluoromethyl)sulfonyl}amide  $[\text{NTf}_2]^-$ , alkylsulfonate  $[C_m\text{SO}_3]^-$ , trifluoromethanesulfonate  $[\text{OTf}]^-$ , dicyanamide  $[\text{dca}]^-$  and acetate  $[\text{Ac}]^-$ .

In the first Chapter we studied aqueous solutions of ionic liquids of the 1-alkyl-3-methylimidazolium chloride family,  $[C_n\text{mim}]\text{Cl}$ , with  $n$  ranging from 8 to 14. Evidence for self-aggregation of  $[C_n\text{mim}]^+$  cations into micellar aggregates has been found.

In the Chapter 2 we investigated both the influence of the alkyl side chain length and the type of ring in the cation (head) on the surface activity of 1-alkyl-3-methylpyridinium ionic liquids. It was observed that these ionic liquids could be used as quenchers for some fluorescence probes. As a consequence, a simple and convenient method to search for early evidence of aggregate formation was established.

A comprehensive study on the synthesis and characterisation, including melting point, decomposition temperature, density and viscosity as a function of temperature, of a range of 1-alkyl-3-methylimidazolium alkylsulfonates  $[C_n\text{mim}][C_m\text{SO}_3]$  is given in Chapter 3.

We have also investigated thermotropic and lyotropic properties for the same family of the ionic liquids  $[C_n\text{mim}][C_m\text{SO}_3]$  with greater amphiphilic character in either or both the cation and anion. In Chapter 4 we reported on the surfactant properties of this family and demonstrated how new materials having exceptional performance characteristics can be developed by applying an ionic liquid design strategy.

In Chapter 5 the solid - liquid and liquid-liquid phase diagrams of mixtures of several ionic liquids with benzene, or totally or partially fluorinated benzene were presented. Systems with congruent melting temperature or simple eutectic point but with different crystalline phases were obtained. It was found that the behaviour is controlled by temperature of annealing during crystallization and by solvent selection.

The potential of fluorinated solvents for biphasic catalysis is recognized, yet not well explored. In Chapters 6 and 7 we investigated the mutual solubility of several mixtures of alternative solvents: commonly used ionic liquids (imidazolium, pyridinium, phosphonium and ammonium ionic liquids) plus partially fluorinated alcohols, or fluorinated alkanes plus alkanes or fluorinated alcohols.

# GENERAL INTRODUCTION

“Τα υγρά μικτά μάλιστα των σωμάτων”, Aristotle (384-322 B.C.)

Solvents are used in many different aspects of chemistry: in synthesis, extraction, purification, dilution, separation, cleaning and many others. Most chemical reactions take place in solution where the reactants are molecularly dispersed in a solvent. In a chemical process the solvent is usually added to the reactant to facilitate reaction and later removed by distillation, since they are mainly highly volatile. Unfortunately, the high volatility of organic solvents (desirable from processing point of view) linked with their loss by leak and spillage became one of the main environmental issues today because many traditional organic solvents have detrimental effect on human health and on the environment. The use of large quantities of volatile organic solvents as liquid media for chemical reactions and extractions, with worldwide cost estimated at € 6,000,000,000 per year is a major concern for today's chemical processing industry.<sup>1</sup> It is the reason why many approaches have been made in order to minimize the use of traditional organic solvents by replacing them with alternative solvents which include water, fluorinated solvents, ionic liquids and supercritical fluids. Toxic and carcinogenic solvents (CCl<sub>4</sub>, benzene), ozone depleters (chlorofluorocarbons, bromofluorocarbons), chlorinated solvents, and aromatic hydrocarbons (xylene, mesitylene) were partially already removed from use.<sup>2</sup> Oxygenated solvents are more acceptable because they undergo degradation in the environment more quickly than hydrocarbon and halogenated solvents. In this Thesis the main accent will be put on the application of ionic liquids as solvents.

## Solvent properties

From the macroscopic point of view, a solvent is a continuum characterized by its boiling point, vapour pressure, density, index of refraction, relative permittivity, thermal conductivity, surface tension, etc. From the microscopic point of view, a solvent is a discontinuum which consists of individual, mutually interacting solvent molecules, characterized by molecular properties such as dipole moment, electronic polarizability, hydrogen-bond donor (HBD) and hydrogenbond acceptor (HBA) capability, electron-pair donor (EPD) and electron-pair acceptor (EPA) capability, etc.



On dissolution of solutes, solvents break the crystal lattice of solid reactants, they dissolve liquid or gaseous reactants, and they have a significant influence on the reaction rate and equilibrium.<sup>3</sup>

The solvent effects originate from the non-specific intermolecular interactions (ion-dipole, dipole-dipole, dipole-induced dipole, instantaneous dipole-induced dipole forces) and specific interactions (HBD-HBA, EPD-EPA, and solvophobic interactions) between solute and solvent.<sup>3</sup> These interactions will also be reflected in solvent polarity. The quantitative determination of solvent polarity is difficult, since pure electrostatic approach, based on the dipolar moment or relative permittivity, can not correlate complex solvent effects. Solvent polarity can be measured by means of the solvent-sensitive processes which reflect all possible solute/solvent interactions, for example, the UV/Vis absorption of solvatochromic dyes.<sup>3, 4</sup>

Density and boiling temperature are as well important properties of solvent. Usually, a high difference in densities between phases in a process is required for an efficient phase separation. Boiling temperatures are determined by the strength of dispersive forces, permanent dipole moment, H-bonding and electrostatic interactions.

The selection of an appropriate solvent or solvent mixture is fundamental for not only chemical but also for physical processes such as recrystallization, extraction processes, chromatographic separations, and phase transfer catalytic reactions.

## **Alternative solvent strategy**

Although a huge variety of available solvents are able to meet the requirements in respect to the suitable liquid temperature range for certain reaction, the effect of solvent on the reaction rate and equilibrium, solvent volatility and cost, problems related to solvent losses in the reaction, separation or purification steps, their recovery and reuse still remain. Therefore, the development of solvent-free processes as well as the application of environmentally benign solvents, such as water and perfluorinated solvents (as used in biphasic systems), supercritical fluids and ambient temperature ionic liquids, has become a major issue. Water and CO<sub>2</sub> are non-toxic solvents present in the environment in a huge amount, and generally they do not require recovery. CO<sub>2</sub> is a gas at ambient conditions and is easily removed from a process without energy-consuming distillation. Perfluorinated solvents can be used in biphasic systems because of their low polarity. Reactants and catalyst are usually captured in fluorophilic phase with

fluorinated ligands, while products remain in higher polarity non-fluorous phase and they can be removed from reaction mixture by simply phase-separation. There are also many examples of similar use of ionic liquids in biphasic systems. Water is the most desirable solvent and can be used in the best case as a single solvent in a chemical reaction or in combination with other organic or fluorous solvents and ionic liquids.

## **Multiphasic solvent systems**

The main goals of multiphasic systems are to enable catalysts recovery, efficient product separation and to reduce the use of traditional solvents by their replacement by alternative ones.

Depending on the number of phases in a multiphase system this can be termed as biphasic or triphasic which are the most common. However, the number of phases can be even higher.

The phases present in a multiphasic system must be very different in their nature, so that they are mutually immiscible. Usually, two phases, one with the catalyst and the other with the substrate, are mixed to form an emulsion in order to allow a good contact between the starting materials and the catalyst. When the reaction is finished, two phases separate, leaving the catalyst in one phase, and product in the other. However, usually some degree of mutual phase contamination is present.

In some cases systems consisting of two immiscible phases at room temperature can form a single homogenous phase just by the temperature increase, thus maximising the contact area catalyst-substrate. The phase separation of product and catalyst can be achieved by cooling.<sup>5</sup>

There are also some ideal cases of biphasic processes when the product of the reaction is not soluble with the solvent which contains starting material and catalyst.<sup>6</sup> Combination of different types and number of solvents can result in multiphase systems (Figure 1.). Some possible solvent combinations were investigated by the author of this thesis.

Some of the most important advantages of biphasic process are: (i) the use of traditional solvents is reduced; (ii) enables reuse of catalyst; and (iii) avoids expensive distillation of product required for homogeneous catalysed reaction, since the product extraction can be done by separation.

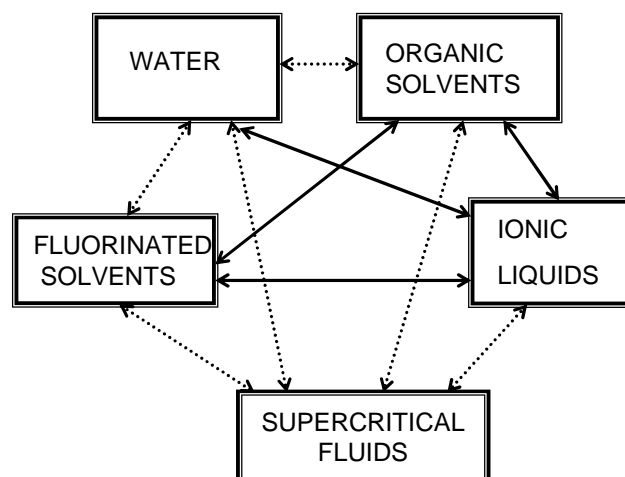


**Figure 1.** Possible solvent combinations which result in biphasic system formation. Solid arrows connect the systems investigated in this Thesis.

The key disadvantage of multiphase methods is the fact that solvents are almost always partially miscible which results in loss of catalyst as well as in product contamination. Catalysts are expensive and often toxic. Hence, efforts must be done to modify the catalyst usually by different types of ligands which will make the catalyst strongly immobilised in one phase and immiscible in the other product phase

## Fluorinated solvents

The most used fluorinated solvents are n-perfluorooctane, n-perfluorohexane, perfluorodecalin, perfluoromethyl cyclohexane, perfluorotributyl amine, etc.

Usually they are synthesised by electrochemical substitution.

Their most important properties are: (i) high density (1.7-1.9 g cm<sup>3</sup>); (ii) very low polarity and consequently low solubility in polar solvents like water, alcohols, and ketones; (iii) they are not hydrogen-bond donors (HBD) and they are very bad hydrogen bond acceptors (HBA) It means that only very weak van der Waals forces are present between their molecules. Thus, they are relatively volatile; (iv) chemically inert (this characteristic together with high oxygen solubility in fluorinated solvents make them good candidates for blood substitution); (v) non-flammable, and presenting low toxicity.

Contrary to halofluorocarbons, perfluorinated compounds are not ozone depleters, but degradation of perfluorinated compounds caused by their high chemical stability is very difficult and slow. The other disadvantage of perfluorinated compounds is their high cost. Therefore, the application is still limited to the production of only very expensive chemicals or processes where the recovery of the catalyst is crucial.

Perfluorinated compounds have low miscibility with hydrocarbons<sup>7</sup> and many organic solvents because of their very low polarity. This property plays the main role in biphasic catalysed reactions<sup>8</sup> and liquid-liquid extractions. In some cases, by a careful selection of the organic and the fluorinated solvents it is possible to have a system of two compounds immiscible at room temperature, but completely miscible at higher temperature.<sup>5,7</sup> In such case reactions can be carried out in the homogenous phase.

For biphasic catalysed reactions it is essential to modify the catalyst making it strongly immobilised in the fluorinated phase. This is done by attaching a fluorinated group (usually a perfluoroalkyl chain) which gives sufficient solubility in the fluorinated solvent. It is also necessary to include an organic group between the fluorinated domain and the active centre in order to prevent drawing electrons by fluorine atoms.<sup>9</sup> Such structure prevents product contamination and enables efficient catalyst recycling. With a good selection of the modified catalyst and both a fluorinated and an organic solvent the product of reaction can be obtained by simple phase separation.

Although fluorinated technology has started to develop in 1990s, it has been already shown that numerous chemical reactions can be performed in fluorinated solvents. To mention only a few: polymerisation,<sup>10</sup> hydroformylation,<sup>5, 11</sup> hydrogenation,<sup>12</sup> oxidation,<sup>13</sup> hydroboration,<sup>14</sup> and Heck reaction<sup>15</sup>.

## Water

Most technological and biological processes occur in aqueous media. Water is in many ways an excellent and unique solvent. Thanks to its high polarity water is able to dissolve many ionic compounds and compounds with covalent bond. In the liquid phase water shows diverse structures. It contains regions with regular arrangements (with holes or vacancies), chains, regions with random structures, and single unbound molecules. The ability of water molecules to form two H-bonds as a donor, and two as an acceptor is reflected in its high melting and boiling temperature, and high surface tension and viscosity.

The high value of the Gordon parameter, which is a measure of the solvent cohesive energy (defined as  $(\gamma / V_m^{1/3})$  where  $\gamma$  is the surface tension, and  $V_m$  is molar volume), makes water the best medium for aggregation of amphiphilic molecules. Aggregation of hydrocarbon molecules is consequence of the hydrophobic effect.

Namely, there is an interaction between water dipoles and induced dipoles present in hydrocarbon molecules which overcomes a weak van der Waals interaction between the hydrocarbon molecules. In order to minimise disruption of H-bonds water itself forms an arranged cage-like structure around the hydrocarbon chains and this leads to a decrease of entropy. In order to reduce the number of water molecules with restricted motion and unfavourable water re-structuring, hydrocarbon molecules in aqueous solution spontaneously aggregate and a phase separation occurs. Amphiphilic molecules present a similar behaviour. This explains the decrease of surface tension of aqueous solution and micelle formation upon adding amphiphilic compounds. Hydrocarbon chains of the amphiphilic molecules are not soluble in water and it causes their concentration at the air-water interface, with the hydrocarbon chains oriented towards the vapour phase. Since the surface tension of water is higher than that of hydrocarbons, adding more amphiphilic molecules results in a surface tension decrease. The surface tension decreases up to a certain concentration known as a critical micelle concentration and above this concentration the surface tension changes only slightly. What actually happens, is a compromise between the extremes of a complete phase separation and molecular disperse solution.<sup>16</sup> As a result the amphiphilic molecules create a nano-phase in which the hydrocarbon chains sequester themselves inside the aggregate and polar head groups orient themselves toward the aqueous phase.<sup>16</sup>

Thanks to its high polarity and density, and ability to form a H-bond network, water can be used for biphasic catalysis in which the catalyst is immobilised in the aqueous phase.<sup>6</sup> Water is immiscible with fluorinated compounds, hydrocarbons, many ionic liquids, many organic solvents and supercritical CO<sub>2</sub>.

Besides plenty of desirable characteristics water has some disadvantages which constrain its application: (i) high heat capacity and enthalpy of vaporization, and hence distillation requires a lot of energy; (ii) low miscibility with many organic compounds; (iii) many catalysts can be deactivated by reaction with water; and (iv) it is expensive and inefficient to purify water after contamination.

## **Ionic liquids**

The term 'ionic liquid' refers to the liquid state of matter exhibited by salts in an ambient temperature regime. Ionic liquids are typically organic salts, of which examples containing 1,3-dialkylimidazolium cations have probably been the most extensively

studied.<sup>17-19</sup> The cations are usually bulky and with low symmetry which prevents the charges to come together, thus reducing the melting points. Charge delocalisation over many atoms also helps in weakening the attraction between ions lowering the melting point. The first report on an ionic liquid (ethylammonium nitrate) was published in 1914.<sup>20</sup> An amazing increase in ionic liquids research started in the 1990s when it was found that many combinations of the anions and cations could form air- and water-stable ionic liquids. Since then their potential application in synthesis, catalysis, biocatalysis, separation technology, electrochemistry, analytical chemistry, and nanotechnology have been investigated. For a long time ionic liquids have been advertised as promising replacements for conventional organic solvents since they are generally nonvolatile, nonflammable, and recyclable. More recently, research activity has shown that the application of the ionic liquids goes far beyond solvents replacement. It is reported that they can be used as surfactants, additives, stabilizers, lubricants, working fluids or as protective layers.

Some of beneficial properties of ionic liquids are: (i) good solvent ability for a wide range of organic and inorganic compounds; (ii) they can as well be designed to be immiscible with water and a number of organic solvents, thus providing alternative for aqueous and non-aqueous biphasic systems; (iii) low vapour pressure; (iv) the combination of ionic liquids and supercritical carbon dioxide gives gas-liquid equilibrium where in the most cases carbon dioxide can be dissolved readily in an ionic liquids, but no ionic liquid dissolves in the carbon dioxide. This offers an excellent opportunity for extraction of organic compounds; (v) their properties such as melting points, viscosity, density, hydrophobicity etc., can be designed by careful selection of their ions' nature and structures.

Many physicochemical properties of ionic liquids have been determined and can be found in data basis, such as "IL Thermo" given by the U.S. National Institute of Standards and Technology (<http://ilthermo.boulder.nist.gov/ILThermo/>). On the other hand, there is a huge number of potential anion and cation combinations, that it is crucial to understand their structure at a molecular level in order to predict their behaviour and make a good selection of anion-cation pair for a desired application. Of course, this is an extremely difficult task due to the complexity and interplay of different molecular interactions.

## *The Structure of Ionic Liquids*

The most common cations are the 1-alkyl-3-methylimidazolium, pyridinium, pyrrolidinium, tetraalkylammonium and tetraalkylphosphonium.

Among the anions, in the past a lot of work has been performed on  $[\text{BF}_4]^-$  and  $[\text{PF}_6]^-$  but since it was found that in the presence of water they hydrolyse forming HF, they are not recommended for use anymore. Commonly in use are the halides (which are unfortunately very hygroscopic), the bis(trifluoromethanesulfonyl)amide  $[\text{NTf}_2]^-$ , the trifluoromethane-sulfonate  $[\text{OTf}]^-$ , alkylsulfates, alkanesulfonates and the tosylate.

Some authors consider that between the imidazolium cations and anions a three-dimensional hydrogen bond network is formed. This is still a controversial issue based on different criteria used for characterizing hydrogen bonds.

By small angle x-ray scattering it was found that longer chain ( $C_n \geq 12$ ) imidazolium salts form liquid-crystalline phases.<sup>21-24</sup> Comprehensive simulation studies have confirmed segregation and the existence of hydrophilic domains formed by the head groups of the cations and anions and nonpolar domains formed by alkyl chains.<sup>25, 26</sup> Such segregation was found even for short chain ionic liquids  $C_n \geq 4$ .<sup>27, 28</sup> The inhomogeneity on a mesoscopic scale should be taken into account when the processes of solvation, gas solubility and diffusion are considered.

## *Physicochemical Properties of ionic Liquids*

The determination of the melting temperature of ionic liquids is difficult and influenced by their complex structure and high viscosity. Some problems in the thermal determination are supercooling and pronounced metastability (Chapter 3), glass formation, polymorphism (Chapter 6), and dependence of reproducibility on experimental factors like cooling / heating rates. An increase in size and anisotropy of the ions generally lowers the melting temperatures. For some homologous imidazolium salts with  $[\text{BF}_4]^-$  or  $[\text{PF}_6]^-$  anions it was reported that cations with short alkyl chain ( $C_n \leq 3$ ) form crystalline phases with relatively high melting points. Ionic liquids with intermediate lengths ( $4 \leq C_n \leq 12$ ) exhibit a broad liquid range and form glasses on cooling due to a reduction of the lattice energy owing to disruption of packing efficiencies. For the longer alkyl chains imidazolium salts ( $C_n \geq 12$ ) higher melting points and liquid crystalline behaviour have been observed.<sup>23, 24</sup> However, in the Chapter 3 of this Thesis

it is shown, that there are some exceptions to this general rule, like for example the 1-alkyl-3-methylimidazolium alkylsulfonate ionic liquids.

Ionic liquids have negligible vapour pressure, a fact that offers opportunity for an alternative, environmentally “greener” solvent strategy. Although ionic liquids have high boiling points, it was shown that they can be distilled using high vacuum and high temperature around 400-500K.<sup>29-31</sup> Extrapolation of the vapour pressure curves to the atmospheric pressure gives hypothetical boiling temperatures in the range 800- 1200 K. Of course many ionic liquids have decomposition temperatures at a much lower temperature range of 500-600K as determined by thermogravimetric analysis. Actually, in real conditions the decomposition of many ionic liquids starts at a much lower temperature during longer exposure. On the other hand, analysis of the vapour-pressure curve is important because it provides us with the enthalpy of vaporisation. The enthalpy of vaporisation is an important parameter in thermodynamic modelling of equations of state, but as well it gives information on molecular interactions in the liquid phase, since there is a correlation between the molar energy of vaporisation and cohesive energy density. For this purposes as well direct calorimetric measurements of enthalpies of vaporization have been performed for a series of commonly used 1-alkyl-3-methylimidazolium bis(trifluoromethyl sulfonyl)-imides, [C<sub>n</sub>mim][NTf<sub>2</sub>].<sup>30</sup>

Viscosity is one of the most important characteristics of solvents for their industrial application and, unfortunately, a disadvantage of ionic liquids whenever used in the pure form. Ionic liquids have viscosities from 10 to 1000 times higher than classical organic solvents. Because of their high viscosity many chemical reactions and diffusion controlled processes are significantly slower in ionic liquids than in organic solvents. As well, the high viscosity has a negative impact on processes of mixing, transport and handling. Contrary to simple liquids where the temperature dependence of the viscosity in a logarithmic scale versus the inverse of temperature gives a straight line (Arrhenius plot), in the case of ionic liquids a deviation from linearity is observed (Chapter 3), a behaviour which classifies ionic liquid into group of “glass formers”.<sup>32</sup> The viscosity of 1-alkyl-3methyl imidazolium ionic liquids increases with the length of the alkyl chain, because of the increased van der Waals interaction (Chapter 3). It seems as well that symmetry and bulkiness of anion have a key influence on the viscosity.

Ionic liquids are also of a great interest for electrochemical purposes because they have a high electrical conductivity up to 10<sup>-2</sup> S cm<sup>-1</sup> and wide electrochemical windows that can reach values of more than 6 volts. They allow deposition of elements



and compounds, especially less-noble nanocrystalline materials that otherwise cannot be electrodeposited from aqueous or organic solutions.<sup>33</sup>

Polarity is the most important solvent characteristic and reflects a complex interplay of molecular interactions. The polarity of an ionic liquid determines its solubility with other organic solvents, but it also has an influence on chemical reactions in solution. There are many methods for polarity determination which are based on different criteria, and hence there are several polarity scales. Polarity can be expressed by relative dielectric permittivity, UV/VIS and fluorescence spectra of solvatochromic dyes, IR and Raman spectra of dissolved molecules, liquid-liquid distribution coefficients, solvent effect on chemical reaction, to mention only some of them. Based on dielectric constant measurements imidazolium ionic liquids can be classified as moderately polar solvents. However, anions with high dipole moments like alkylsulfates have significantly higher dielectric constants.<sup>34, 35</sup> The most important solvatochromic method for polarity determination is based on the shift of the low frequency band in the Vis absorption spectrum of Reichardt's zwitter-ionic dye betaine-30. This shift defines a normalized polarity parameter  $E_T^N$ . According to parameter  $E_T^N$  the polarity of imidazolium based ionic liquids is higher than that expressed by relative dielectric permittivity and is similar to polarity of methanol, acetonitrile or DMSO.<sup>36, 37</sup>

There are numerous reports on the miscibility of ionic liquids in water and organic solvents. Generally, for the partially miscible systems, it was found that water or organic solvents can be dissolved in an ionic liquids, but ionic liquids can not be dissolved in molecular solvents.<sup>38</sup> Imidazolium ionic liquids with common anions ( $[NTf_2]^-$ ,  $Cl^-$ ,  $[BF_4]^-$ ,  $[OTf_2]^-$ ) are immiscible with non polar hydrocarbons, and partially miscible with alcohols and benzene.<sup>39-41</sup> Hydrophobic ionic liquids with  $[NTf_2]^-$  or  $[PF_6]^-$  anions are also water immiscible. 1-alkyl-3-methylimidazolium and 1-alkyl-3-methylpyrdinium salts with the  $[Cl]^-$  anion are water miscible even for cations with long hydrocarbon chains ( $C_n \geq 12$ ).<sup>42, 43</sup> Significantly different phase behaviour in respect to the solubility in water, short or long chains alcohols and alkanes was found for phosphonium based ILs.<sup>44</sup>

## References:

1. K. R. Seddon, *Journal of Chemical Technology and Biotechnology*, 1997, **68**, 351-356.
2. P. J. D. Dave J. Adams, Steward J. Tavener, *Chemistry in Alternative Media*, John Wiley & Sons Ltd, Chichester, 2004.
3. C. Reichardt, *Org. Process Res. Dev.*, 2007, **11**, 105-113.
4. C. Reichardt, *Chem. Rev.*, 1994, **94**, 2319-2358.
5. I. T. Horvath and J. Rabai, *Science*, 1994, **266**, 72-75.
6. B. Cornils, W. A. Herrmann and R. W. Eckl, *J. Mol. Catal. A-Chem.*, 1997, **116**, 27-33.
7. M. J. P. de Melo, A. M. A. Dias, M. Blesic, L. P. N. Rebelo, L. F. Vega, J. A. P. Coutinho and I. M. Marrucho, *Fluid Phase Equilibria*, 2006, **242**, 210-219.
8. C. M. Haar, J. Huang, S. P. Nolan and J. L. Petersen, *Organometallics*, 1998, **17**, 5018-5024.
9. Adams D.J., Dyson P.J. and Tavener S.J., John Wiley & Sons Ltd, Chichester, 2004.
10. D. M. Haddleton, S. G. Jackson and S. A. F. Bon, *Journal of the American Chemical Society*, 2000, **122**, 1542-1543.
11. D. F. Foster, D. Gudmunsen, D. J. Adams, A. M. Stuart, E. G. Hope, D. J. Cole-Hamilton, G. P. Schwarz and P. Pogorzelec, *Tetrahedron*, 2002, **58**, 3901-3910.
12. D. Rutherford, J. J. J. Juliette, C. Rocaboy, I. T. Horvath and J. A. Gladysz, *Catalysis Today*, 1998, **42**, 381-388.
13. B. Betzemeier, M. Cavazzini, S. Quici and P. Knochel, *Tetrahedron Letters*, 2000, **41**, 4343-4346.
14. J. J. J. Juliette, D. Rutherford, I. T. Horvath and J. A. Gladysz, *Journal of the American Chemical Society*, 1999, **121**, 2696-2704.
15. M. Moreno-Manas, R. Pleixats and S. Villarroya, *Organometallics*, 2001, **20**, 4524-4528.
16. D. F. W. Evans, H. , *The Colloidal Domain: Where Physics, Chemistry, Biology and Technology Meet*, VCH, New York.
17. W. T. Wasserscheid P., ed., *Ionic Liquids in Synthesis*, Wiley VCH, Weinheim, , 2007.

18. C. P. Fredlake, J. M. Crosthwaite, D. G. Hert, S. Aki and J. F. Brennecke, *Journal of Chemical and Engineering Data*, 2004, **49**, 954-964.
19. J. G. Huddleston, A. E. Visser, W. M. Reichert, H. D. Willauer, G. A. Broker and R. D. Rogers, *Green Chemistry*, 2001, **3**, 156-164.
20. P. Walden, *Bull. Acad. Imp. Sci.*, 1914., **8**, 405
21. A. E. Bradley, C. Hardacre, J. D. Holbrey, S. Johnston, S. E. J. McMath and M. Nieuwenhuyzen, *Chemistry of Materials*, 2002, **14**, 629-635.
22. A. Downard, M. J. Earle, C. Hardacre, S. E. J. McMath, M. Nieuwenhuyzen and S. J. Teat, *Chemistry of Materials*, 2004, **16**, 43-48.
23. C. M. Gordon, J. D. Holbrey, A. R. Kennedy and K. R. Seddon, *Journal of Materials Chemistry*, 1998, **8**, 2627-2636.
24. J. D. Holbrey and K. R. Seddon, *Journal of the Chemical Society-Dalton Transactions*, 1999, 2133-2139.
25. J. N. C. Lopes, M. F. C. Gomes and A. A. H. Padua, *Journal of Physical Chemistry B*, 2006, **110**, 16816-16818.
26. A. A. H. Padua, M. F. Gomes and J. Lopes, *Accounts of Chemical Research*, 2007, **40**, 1087-1096.
27. S. Dorbritz, W. Ruth and U. Kragl, *Advanced Synthesis & Catalysis*, 2005, **347**, 1273-1279.
28. J. Sung, Y. Jeon, D. Kim, T. Iwahashi, T. Iimori, K. Seki and Y. Ouchi, *Chemical Physics Letters*, 2005, **406**, 495-500.
29. M. J. Earle, J. Esperanca, M. A. Gilea, J. N. C. Lopes, L. P. N. Rebelo, J. W. Magee, K. R. Seddon and J. A. Widegren, *Nature*, 2006, **439**, 831-834.
30. L. Santos, J. N. C. Lopes, J. A. P. Coutinho, J. Esperanca, L. R. Gomes, I. M. Marrucho and L. P. N. Rebelo, *Journal of the American Chemical Society*, 2007, **129**, 284-285.
31. D. H. Zaitsau, G. J. Kabo, A. A. Strechan, Y. U. Paulechka, A. Tschersich, S. P. Verevkin and A. Heintz, *Journal of Physical Chemistry A*, 2006, **110**, 7303-7306.
32. K. R. Seddon, A. Stark and M. J. Torres, *Clean Solvents*, 2002, **819**, 34-49.
33. F. Endres and S. Z. El Abedin, *Physical Chemistry Chemical Physics*, 2006, **8**, 2101-2116.
34. C. Wakai, A. Oleinikova, M. Ott and H. Weingartner, *Journal of Physical Chemistry B*, 2005, **109**, 17028-17030.

35. H. Weingartner, *Zeitschrift Fur Physikalische Chemie-International Journal of Research in Physical Chemistry & Chemical Physics*, 2006, **220**, 1395-1405.
36. M. Caricato, B. Mennucci and J. Tomasi, *Molecular Physics*, 2006, **104**, 875-887.
37. C. Reichardt, *Green Chemistry*, 2005, **7**, 339-351.
38. L. P. N. Rebelo, V. Najdanovic-Visak, R. G. de Azevedo, J. M. Esperanca, M. N. da Ponte, H. J. Guedes, Z. P. Visak, H. C. de Sousa, J. Szydowski and J. N. C. Lopes, *Abstracts of Papers of the American Chemical Society*, 2003, **226**, U616-U616.
39. J. M. Crosthwaite, S. Aki, E. J. Maginn and J. F. Brennecke, *Journal of Physical Chemistry B*, 2004, **108**, 5113-5119.
40. J. M. Crosthwaite, S. Aki, E. J. Maginn and J. F. Brennecke, *Fluid Phase Equilibria*, 2005, **228**, 303-309.
41. J. Lachwa, J. Szydowski, A. Makowska, K. R. Seddon, J. Esperanca, H. J. R. Guedes and L. P. N. Rebelo, *Green Chemistry*, 2006, **8**, 262-267.
42. M. Blesic, A. Lopes, E. Melo, Z. Petrovski, N. V. Plechkova, J. N. C. Lopes, K. R. Seddon and L. P. N. Rebelo, *Journal of Physical Chemistry B*, 2008, **112**, 8645-8650.
43. M. Blesic, M. H. Marques, N. V. Plechkova, K. R. Seddon, L. P. N. Rebelo and A. Lopes, *Green Chemistry*, 2007, **9**, 481-490.
44. M. Blesic, J. N. C. Lopes, M. F. Costa Gomes and L. P. N. Rebelo, *Manuscript in preparation*, 2008.

# **CHAPTER 1.**

## **HOW HYDROPHILIC IONIC LIQUIDS BEHAVE IN AQUEOUS SOLUTIONS**

*The results presented in this Chapter were published as a full article:*

Blesic M., Marques M.H., Plechkova N.V., Seddon, K.R., Rebelo L.P.N., Lopes, A., "Self-aggregation of ionic liquids: micelle formation in aqueous solution", *Green Chemistry*, 2007, **9**, 481.

*and as a Chapter in a Book:*

Blesic M., Plechkova N.V., Gunaratne N., Lopes A., Seddon K.R., Rebelo L.P.N., "How hydrophilic ionic liquids behave in aqueous solutions", *In Ionic Liquids: Never the Twain*; Gaune-Escard, M., Seddon, K. R., Eds.; Wiley: Hoboken, NJ, 2008.

**Note:** The author of this Thesis has obtained all experimental results presented in this Chapter. All ionic liquid used in this work were synthesised and characterised at QUILL, Belfast.

# How Hydrophilic Ionic Liquids Behave in Aqueous Solutions

Marijana Blesic,<sup>a, b</sup> Natalia V. Plechkova,<sup>b</sup> Nimal Gunaratne,<sup>b</sup> Kenneth R. Seddon,<sup>a, b</sup> António Lopes,<sup>a</sup> and Luís Paulo N. Rebelo<sup>a</sup>

<sup>a</sup>*Instituto de Tecnologia Química e Biológica, ITQB 2, Universidade Nova de Lisboa, Apartado 127, 2780-901 Oeiras, Portugal*

<sup>b</sup>*The QUILL Centre, The Queen's University of Belfast, Stranmillis Road, Belfast BT9 5AG, United Kingdom*

*Keywords:* ionic liquids; interfacial tension (IFT); self-aggregation; critical micelle concentration (CMC)

## Abstract

Self-aggregation behaviour of a number of ionic liquids has been investigated using two techniques: interfacial tension, and fluorescence. The list of ionic liquids includes:  $[C_n\text{mim}]\text{Cl}$  (1-alkyl-3-methylimidazolium chlorides) with different linear alkyl chain lengths ( $n = 4\text{--}14$ , only even numbers),  $[C_{10}\text{mim}][\text{PF}_6]$  (1-decyl-3-methylimidazolium hexafluorophosphate), and  $[C_{10}\text{mim}][\text{NTf}_2]$  (1-decyl-3-methylimidazolium bis{(trifluoromethyl)sulfonyl}amide (bistriflamide)). Two factors were varied: the length of alkyl chain on the ring, and the nature of the anion. Only  $[C_n\text{mim}]\text{Cl}$  ionic liquids with  $n$  greater than 8 unambiguously form aggregates in solution. The transitional ionic liquid,  $[C_6\text{mim}]\text{Cl}$  is able to develop a monolayer at the aqueous solution-air interface, but shows no noticeable self-aggregation in the bulk fluid. Ionic liquids based on more hydrophobic and large anions, namely  $[\text{PF}_6]^-$  and  $[\text{NTf}_2]^-$ , do not form micellar aggregates in aqueous solutions. The nature of this self-aggregation is discussed in terms of the electrostatic *vs.* hydrophobic contributions.

## Introduction

The innate amphiphilic nature of some cations, *e.g.*  $[C_n\text{mim}]^+$  suggests the possibility of interfacial and aggregation phenomena in aqueous solutions, and their

ultimate organisation into micelles displaying surfactant behaviour.<sup>1-3</sup> Ionic liquids are very similar in structure to traditional ionic surfactants (most the latter are solid salts). Ionic liquids have low melting points, usually a consequence of the presence of bulky and asymmetric cations, compared to considerably smaller size anions, while ionic surfactants typically have higher melting points – *e.g.*, sodium dodecyl sulphate (SDS), [C<sub>12</sub>H<sub>25</sub>SO<sub>4</sub>]Na, has a melting point close to 200 °C. Longer chain ionic liquids self-assemble to form thermotropic liquid crystalline mesophase ionic liquids,<sup>4-6</sup> and lyotropic mesophases in concentrated aqueous solutions of 1-decyl-3-methylimidazolium bromide.<sup>7</sup>

With the possibility of fine-tuning of the ionic liquids' hydrophobicity by changing the alkyl chain length, the type of the head (cation), and/or the nature and size of the counter-ion (anion), one can affect both the structure and the delicate dynamics of these micellar aggregates. This can lead to the modification of their major characteristics such as the critical micelle concentration, CMC, and the aggregation number (micellar size). It is interesting that even some short chain ionic liquids, for example 1-butyl-3-methylimidazolium tetrafluoroborate [C<sub>4</sub>mim][BF<sub>4</sub>] can form very small aggregates in aqueous solution.<sup>8</sup>

On the other hand, the addition of ionic liquids to aqueous solutions of surfactants affects the CMC of the surfactant and offers the possibility of their usage as co-surfactants.<sup>1, 9, 10</sup>

Furthermore, it was shown that solvophobic interactions are present between ionic liquids and the hydrocarbon portion of the surfactant, thus leading to the formation of surfactant micelles in ionic liquids and enhancing the solvation characteristics of ionic liquids + surfactant system.<sup>11, 12</sup>

However, different previous studies<sup>2, 9</sup> report contradictory conclusions and do not confirm an obvious differentiation between electrostatic and hydrophobic contributions for the self-aggregation of [C<sub>n</sub>mim]Cl family. Fortunately, the formation of aggregates, particularly micelles, can be detected using several instrumental methods: equivalent conductivity, turbidity, surface tension, self-diffusion, magnetic resonance and many others.<sup>13</sup> Hence, it is generally possible to obtain comparative results.

The aim of the current contribution is to offer a more systematic study and establish the role of the alkyl chain length, concentration and the nature of the anion, on the aggregation behaviour of the compounds belonging to the [C<sub>n</sub>mim]X (X= Cl,



[PF<sub>6</sub>]<sup>-</sup> and [NTf<sub>2</sub>]<sup>-</sup>) families in aqueous solutions, as well as to elucidate those hydrophobic and electrostatic contributions for the building up of the micellar aggregates.

## Experimental

### Chemicals

The 1-alkyl-3-methylimidazolium chlorides, [C<sub>*n*</sub>mim]Cl (*n* = 4–14, even numbers), [C<sub>10</sub>mim][PF<sub>6</sub>], and [C<sub>10</sub>mim][NTf<sub>2</sub>], were all synthesised and initially purified at QUILL (The Queen's University Ionic Liquid Laboratories, Belfast) according to recipes found elsewhere.<sup>4, 14, 15</sup>

<sup>1</sup>H and <sup>13</sup>C NMR analyses showed no major impurities in the untreated, original samples, except for the presence of adventitious water (Karl-Fischer analysis). All samples were then further thoroughly degassed and dried to remove any small traces of volatile compounds by applying vacuum (0.1 Pa) at moderate temperatures (60–80 °C) for typically 72 h. Doubly-distilled deionised water was obtained from a Millipore Milli-Q water purification system (Millipore, USA). [C<sub>*n*</sub>mim][X] stock solutions were prepared in a 1.74×10<sup>-6</sup> M pyrene aqueous solution and all work solutions were prepared from the stock solutions diluting with the same pyrene aqueous solution. Pyrene (Fluka, Germany, 99%) was recrystallised from benzene

### Interfacial tension measurements

Interfacial tension (IFT) was measured using a Drop Shape Analysis Tensiometer Kruss DSA1 v 1.80 working in the pendant drop mode at a constant temperature of (23 ± 1) °C. IFT is derived from the fit of the pendant drop profile, and care was taken to ensure that the apparatus was calibrated with several solvents of known IFT in the range of interest. The drops were left to equilibrate close to the rupture point and at least three consistent measurements per solution were recorded.

### Fluorescence spectroscopy

Steady-state fluorescence spectra of the pyrene-containing solutions were recorded with a Cary Varian Eclipse Fluorescence Spectrometer and collected from a 1 cm<sup>2</sup> quartz cuvette at 25 °C. Excitation was set to a wavelength of 337 nm and all emission spectra measured were corrected for emission monochromator response and were background subtracted using appropriate blanks. Intensities of first (I1) and third (I3) vibronic bands in the pyrene emission spectra located at 373 and 384 nm, respectively, were measured and used to determine the ratio I3/I1, a well known “solvent” polarity scale<sup>16</sup>. Band I1 corresponds to a S0 (v = 0) ← S1 (v = 0) transition and band I3 is a S0 (v = 1) ← S1 (v = 0) transition.

## Results and Discussion

As 1-alkyl-3-methylimidazolium chlorides,  $[C_n\text{mim}]\text{Cl}$ , are completely miscible with water at all compositions of interest, the first group of experiments examined the behaviour of the aqueous solution-air interface for this series of compounds ( $n = 4-14$ , even numbers). The results of the IFT for the aqueous solutions as a function of the total concentration of  $[C_n\text{mim}]\text{Cl}$  are presented in Figure 1(a). It is well known that a sharp decrease of the IFT followed by a plateau reveals the aforementioned amphiphilic characteristic of the cation, which is the cause for the possible micelle formation.<sup>17</sup> The break point of each concentration-surface tension curve determines the saturation of the outer monolayer of the surface of the drop, and the consequent onset of aggregation in the bulk, the CMC, when the dissolution permits.

Figure 1(a) clearly shows that the plateau, which indicate micelle formation, are present only in the case of alkyl chains with a hydrocarbon “tail” equal or greater than  $n = 8$ .  $[C_4\text{mim}]\text{Cl}$  does not achieve any plateau, even in the limit of tending to the pure compound (higher concentration point). For pure and highly concentrated solutions of  $[C_6\text{mim}]\text{Cl}$ , it was not possible to determine IFT due to the high viscosity of the solutions. The longer hydrocarbon chain members for the higher concentrations show the lower values of the IFT of the plateau region and higher compactness of surface monolayer. The experimental values for the break points in the IFT measurement are presented in Table 1 (along with other CMC results from different techniques). An interesting comparison with the measured CMC values of  $[C_n\text{mim}]\text{Br}$  family, recently reported by R. Vanyúr et al.<sup>18</sup> is shown in Figure 2. The slightly lower values obtained for  $[C_n\text{mim}]\text{Br}$  are expected since it is well known that the binding of anionic counterions to cationic micelles increases in the order  $\text{F}^- < \text{Cl}^- < \text{Br}^- < \text{I}^-$ .<sup>19</sup> The binding of counterions influences not only the CMC value, but increases the binding of counterions, decreases the head repulsion and enables denser packing of monomers in monolayers. This leads to lower values for the plateau region at concentrations greater than the CMC. In this regard we notice that Bowers et al. reported the surface tension value of  $35\text{mNm}^{-1}$ , in the plateau region for  $[C_8\text{mim}]\text{I}$ , which is much lower than the value achieved for  $[C_8\text{mim}]\text{Cl}$  ( $43\text{mNm}^{-1}$ ).<sup>2</sup>

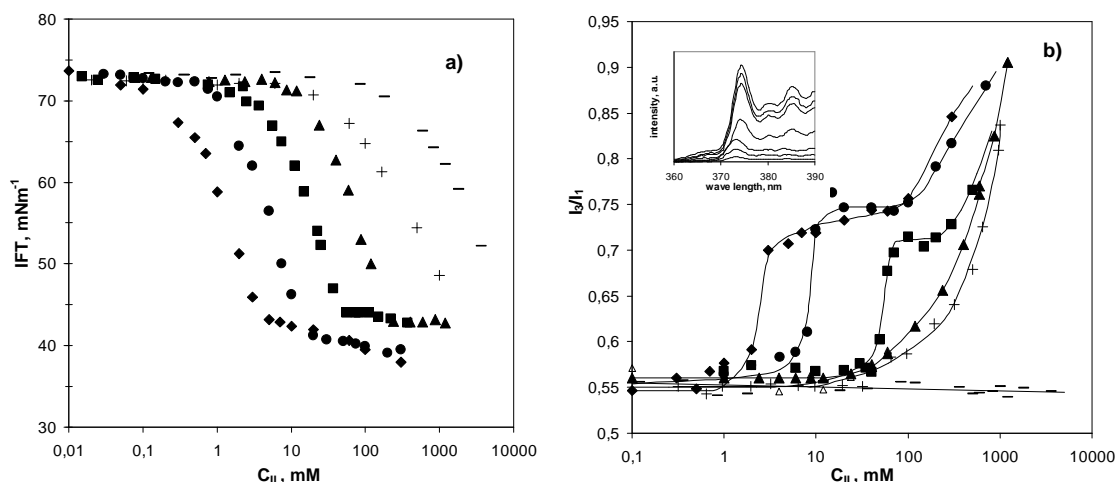


**Figure 1** – Monitoring the self-aggregation of  $[C_n\text{mim}]\text{Cl}$  using different techniques: (a) IFT, (b) Fluorescence for different chain lengths:  $n = (\blacksquare)4, (+) 6, (\blacktriangle)8, (\blacksquare)10, (\bullet)12, (\blacklozenge)14$ .

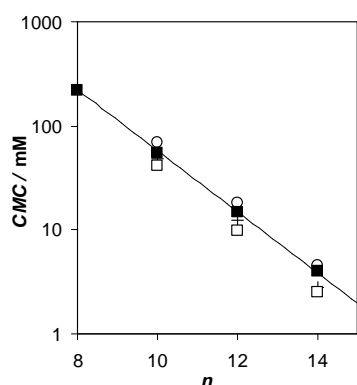


**Figure 2** CMC values for  $[C_n\text{mim}]\text{Cl}$  ( $\blacksquare$ ) as a function of the number of carbon atoms. Data for  $[C_n\text{mim}]\text{Br}$  ( $\square$ ),<sup>18</sup>  $[\text{N}_{111n}]\text{Cl}$  ( $\circ$ ), and  $[\text{H}_3\text{N}_n]\text{Cl}$  ( $+$ ) are included for comparison purposes.<sup>1</sup>

In order to corroborate the results mentioned above fluorescence measurements that involve a pyrene solvatochromic probe were also used. Intensities of first (I<sub>1</sub>) and third (I<sub>3</sub>) vibronic bands in the pyrene emission spectra were measured and used to determine the ratio I<sub>3</sub>/I<sub>1</sub>. The ratio I<sub>3</sub>/I<sub>1</sub> is function of polarity of the pyrene environment and it increases with decreasing solvent polarity (Figure 1b insert). I<sub>3</sub>/I<sub>1</sub> ratio as a function of the total surfactant (in our case the ionic liquid) concentration shows a specific sigmoidal type curve, which increases due to the formation of micelles with a well-defined hydrophobic core into which pyrene

partitions preferentially.<sup>20</sup> Figure 1(b) shows the pyrene response for aqueous  $[C_n\text{mim}]\text{Cl}$  solutions as a function of  $[C_n\text{mim}]\text{Cl}$  concentration. In agreement with the surface tension measurements above, Figure 1(b) provides evidence that in solutions for  $n < 6$  either no hydrophobic environment is formed or the volume of formed aggregates is too small to “protect” pyrene from the polar environment. Although the I3/I1 ratio shows a typical increase indicating the presence of hydrophobic environment for tails equal to or greater than 6 carbons, it is only certain that a plateau is reached for  $n = 10, 12,$  and  $14$ . Consequently, the intersection point between that plateau and the descending part is used for the CMC determination only for these three  $[C_n\text{mim}]^+$  salts. The reason for the absence of a plateau at higher concentrations in the case of  $[C_6\text{mim}]\text{Cl}$  or  $[C_8\text{mim}]\text{Cl}$  may be attributed to the progressive dense packing of the individual cations. This produces a steady increase in the hydrophobicity sensed by pyrene that reflects the continuous increase in the probe response. However, these observations are speculative, as tentative measurements with the light scattering technique did not clarify this point. Small angle neutron scattering, applied for  $[C_8\text{mim}]\text{Cl}$  solution by Bowers *et al.*, did not clarify the size and shape of the micelles as well.<sup>2</sup>

|                               | IFT | Fluor | NMR |
|-------------------------------|-----|-------|-----|
| $[C_8\text{mim}]\text{Cl}$    | 220 | –     | 200 |
| $[C_{10}\text{mim}]\text{Cl}$ | 55  | 45    | 55  |
| $[C_{12}\text{mim}]\text{Cl}$ | 15  | 7     | 13  |
| $[C_{14}\text{mim}]\text{Cl}$ | 4   | 3     | 4   |

**Table 1.** Critical micelle concentration, CMC (mM) of  $[C_n\text{mim}]\text{Cl}$  ( $n = 8-14$ ), measured by Interfacial Tension (IFT), Fluorescence (Fluor), and  $^1\text{H}$  NMR spectroscopy.<sup>1</sup>

The CMC values obtained by the IFT, fluorescence and  $^1\text{H}$  NMR<sup>1</sup> are given in Table 1.

Figure 2 summarises the CMC values obtained with the IFT methodology plotted as a function of the number of carbons for  $[C_n\text{mim}]\text{Cl}$ ,  $n = 8 -14$ . For comparison purposes, data obtained for cationic surfactants of the alkyltrimethylammonium and alkylammonium chloride families,  $[N_{111n}]\text{Cl}$ ,  $[\text{H}_3\text{N}_n]\text{Cl}$ , with similar hydrocarbon chain lengths are depicted.<sup>1</sup> Published data for  $[C_n\text{mim}]\text{Br}$  family measured by conductivity are also included.<sup>18</sup> As one can perceive,

there is a good free energy correlation for all the  $[C_n\text{mim}]\text{Cl}$  family and the results show the same dependence for micellisation as a function of  $n$  as observed for the other two families. It is even possible to notice that the CMC values for  $[C_n\text{mim}]\text{Cl}$  are located between those of  $[\text{H}_3\text{N}_n]\text{Cl}$  and  $[\text{N}_{111n}]\text{Cl}$ . This probably reflects the effect of solute polarity and consequent heads' repulsion. Namely,  $[\text{N}_{111n}]\text{Cl}$  is a very stable ammonium salt and more polar than both  $[C_n\text{mim}]\text{Cl}$  (where the positive charge is delocalised) and  $[\text{H}_3\text{N}_n]\text{Cl}$  (that can even dissociate to some extent).

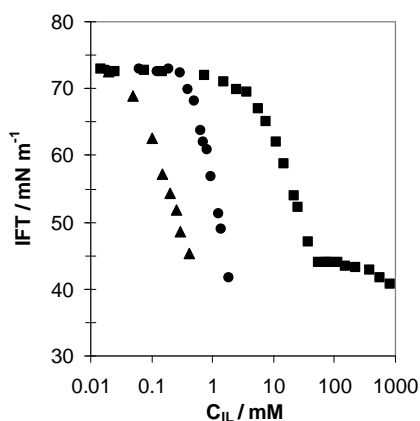


**Figure 3** Counterion effect on  $[\text{C}_{10}\text{mim}]\text{X}$  aggregation from IFT measurements: X = ( $\blacktriangle$ )  $[\text{NTf}_2]^-$ , ( $\bullet$ )  $[\text{PF}_6]^-$ , ( $\blacksquare$ )  $\text{Cl}^-$ .

Figure 3 shows the effect of the anion of the ionic liquid on the surface tension of aqueous solutions of  $[\text{C}_{10}\text{mim}]\text{X}$  (where X is  $\text{Cl}^-$ ,  $[\text{NTf}_2]^-$  or  $[\text{PF}_6]^-$ ). The concentrations of ionic liquid at which the surface tension starts to lower decrease as the hydrophobicity and bulkiness of the anion increase. This is believed to result from decreased electrostatic repulsion between head groups in the monolayer due to both the relatively strong binding of the hydrophobic counterions to the ionic liquids' cations and the hydrophobicity of the anions themselves. Generally this may lead to lower CMC values, thus promoting micelle formation.<sup>19</sup> This statement can be confirmed if we compare our IFT vs. concentration curve for  $[\text{C}_4\text{mim}]\text{Cl}$  and a similar curve for  $[\text{C}_4\text{mim}][\text{BF}_4]$  measured by Bowers *et al.*<sup>2</sup>. The more hydrophobic  $[\text{BF}_4]^-$  anion is more strongly bound to the surface of micelles and consequently is more efficient in decreasing the electrostatic repulsion. As a result,  $[\text{C}_4\text{mim}][\text{BF}_4]$  has the CMC at  $(0.8 \pm 0.1) \text{ mol dm}^{-3}$  concentration while  $[\text{C}_4\text{mim}]\text{Cl}$  does not reach a plateau even at a concentration higher than  $3 \text{ mol dm}^{-3}$ . However, in the cases of the  $[\text{NTf}_2]^-$  and  $[\text{PF}_6]^-$  anions (Figure 3), no micelle formation was detected, as the low solubility

of the corresponding ionic liquids induced phase separation before any bulk aggregation occurred. Probably, a lack of hydration prevents dissolving of these ILs in water and the system separates into two phases

## Conclusions

This contribution suggests general methodologies that can be used to find out whether ionic liquids are capable of forming aggregates in aqueous solutions. More classes of ionic liquids can be checked for their micellar behaviour using the techniques described in this chapter.

Aqueous solutions of ionic liquids of the 1-alkyl-3-methylimidazolium chloride family,  $[C_n\text{mim}]\text{Cl}$ , with  $n$  ranging from 8 to 14, when scrutinised using interfacial tension, fluorescence, and  $^1\text{H}$  NMR techniques,<sup>1</sup> present evidence for the self-aggregation of the  $[C_n\text{mim}]^+$  cations into micellar aggregates.

The exchange of the chloride anion for a more hydrophobic and larger counter ion such as  $[\text{NTf}_2]^-$  or  $[\text{PF}_6]^-$  (besides surface tension diminution) brings the system to a non-micellar state: system separates into two phases.

It seems that aggregation is an inherent characteristic of ionic liquids; they aggregate in neat,<sup>21-23</sup> bulk state, and in aqueous<sup>1-3, 18</sup> and non-aqueous solution. Their ability to act as surfactants (longer alkyl chain) or hydrotropes (shorter alkyl chain) can be combined with other unique highly advantageous characteristic of these materials.

## Acknowledgements

This work was supported by the Fundação para a Ciência e Tecnologia (FCT), Portugal (Projects POCTI/QUI/35413/2000 and POCI/QUI/57716/2004). M. B. thanks FCT for a Ph.D. grant SFRH/BD/13763/2003, and KRS thanks the EPSRC (Portfolio Partnership Scheme, grant no. EP/D029538/1)

## References

1. M. Blesic, M. H. Marques, N. V. Plechkova, K. R. Seddon, L. P. N. Rebelo and A. Lopes, *Green Chemistry*, 2007, **9**, 481-490.

2. J. Bowers, C. P. Butts, P. J. Martin, M. C. Vergara-Gutierrez and R. K. Heenan, *Langmuir*, 2004, **20**, 2191-2198.
3. J. Sirieix-Plenet, L. Gaillon and P. Letellier, *Talanta*, 2004, **63**, 979-986.
4. C. J. Bowlas, D. W. Bruce and K. R. Seddon, *Chemical Communications*, 1996, 1625-1626.
5. A. E. Bradley, C. Hardacre, J. D. Holbrey, S. Johnston, S. E. J. McMath and M. Nieuwenhuyzen, *Chemistry of Materials*, 2002, **14**, 629-635.
6. J. D. Holbrey and K. R. Seddon, *Journal of the Chemical Society-Dalton Transactions*, 1999, 2133-2139.
7. M. A. Firestone, J. A. Dzielawa, P. Zapol, L. A. Curtiss, S. Seifert and M. L. Dietz, *Langmuir*, 2002, **18**, 7258-7260.
8. S. Dorbritz, W. Ruth and U. Kragl, *Advanced Synthesis & Catalysis*, 2005, **347**, 1273-1279.
9. A. Beyaz, W. S. Oh and V. P. Reddy, *Colloids and Surfaces B-Biointerfaces*, 2004, **35**, 119-124.
10. Z. Miskolczy, K. Sebok-Nagy, L. Biczok and S. Gokturk, *Chemical Physics Letters*, 2004, **400**, 296-300.
11. J. L. Anderson, V. Pino, E. C. Hagberg, V. V. Sheares and D. W. Armstrong, *Chemical Communications*, 2003, 2444-2445.
12. K. A. Fletcher and S. Pandey, *Langmuir*, 2004, **20**, 33-36.
13. D. F. W. Evans, H. , *The Colloidal Domain: Where Physics, Chemistry, Biology and Technology Meet*, VCH, New York.
14. P. Bonhote, A. P. Dias, N. Papageorgiou, K. Kalyanasundaram and M. Gratzel, *Inorganic Chemistry*, 1996, **35**, 1168-1178.
15. C. M. Gordon, J. D. Holbrey, A. R. Kennedy and K. R. Seddon, *Journal of Materials Chemistry*, 1998, **8**, 2627-2636.
16. J. Lakowicz, *Principles of Fluorescence Spectroscopy*, Kluwer Academic/Plenum Publishers, New York, 1999.
17. D. F. Evans and H. Wennerstrom, *The Colloidal Domain: Where Physics, Chemistry, Biology and Technology Meet*, VCH, New York, 1994.
18. R. Vanyur, L. Biczok and Z. Miskolczy, *Colloids and Surfaces a-Physicochemical and Engineering Aspects*, 2007, **299**, 256-261.
19. Y. Moroi, *Micelles: Theoretical and Applied Aspects*, Kluwer Academic Plenum Publishers, New York, 1992.

20. R. Zana, *Surfactant Solutions: New Methods of Investigation*, Marcel Dekker, New York, 1986.
21. J. N. C. Lopes, M. F. C. Gomes and A. A. H. Padua, *Journal of Physical Chemistry B*, 2006, **110**, 16816-16818.
22. A. A. H. Padua, M. F. Gomes and J. Lopes, *Accounts of Chemical Research*, 2007, **40**, 1087-1096.
23. L. P. N. Rebelo, J. N. C. Lopes, J. Esperanca, H. Lachwa, V. Najdanovic-Visak and Z. P. Visak, *Accounts of Chemical Research*, 2007, **40**, 1114-1121.



## **CHAPTER 2.**

# **ON THE SELF-AGGREGATION AND FLUORESCENCE QUENCHING APTITUDE OF SURFACTANT IONIC LIQUIDS**

*This Chapter is published as a full article:*

Blesic M., Lopes A., Melo E., Petrovski Z., Plechkova N.V., Canongia Lopes J.N., Seddon K.R., Rebelo L.P.N., “On the Self-Aggregation and Fluorescence Quenching Aptitude of Surfactant Ionic Liquids“, *Journal of Physical Chemistry B*, **2008**, 112, 8645.

**Note:** The synthesis and the characterisation of the ionic liquids used in the study, and the experimental measurements were done by the author of this Thesis.

$^1\text{H}$  and  $^{13}\text{C}$  NMR, the melting and decomposition temperatures of the ionic liquids used in this Chapter and the results of *ab-initio* calculations are given in **Appendix 1**.

# On the Self-Aggregation and Fluorescence Quenching Aptitude of Surfactant Ionic Liquids

Marijana Blesic,<sup>†,‡</sup> António Lopes,<sup>\*,†</sup> Eurico Melo,<sup>†</sup> Zeljko Petrovski,<sup>§</sup> Natalia V. Plechkova,<sup>‡</sup> José N. Canongia Lopes,<sup>†,⊥</sup> Kenneth R. Seddon,<sup>†,‡</sup> and Luís Paulo N. Rebelo<sup>\*,†</sup>

*Instituto de Tecnologia Química e Biológica, ITQB 2, Universidade Nova de Lisboa, Apartado 127, 2780-901 Oeiras, Portugal, The QUILL Centre, The Queen's University of Belfast, Stranmillis Road, Belfast BT9 5AG, U.K., and CQFM, Departamento de Engenharia Química e Biológica and Centro de Química Estrutural, Instituto Superior Técnico, 1049-001 Lisboa, Portugal*

Received: March 12, 2008

The aggregation behavior in aqueous solution of a number of ionic liquids was investigated at ambient conditions by using three techniques: fluorescence, interfacial tension, and <sup>1</sup>H NMR spectroscopy. For the first time, the fluorescence quenching effect has been used for the determination of critical micelle concentrations. This study focuses on the following ionic liquids: [C<sub>n</sub>mpy]Cl (1-alkyl-3-methylpyridinium chlorides) with different linear alkyl chain lengths (*n* = 4, 10, 12, 14, 16, or 18), [C<sub>12</sub>mpip]Br (1-dodecyl-1-methylpiperidinium bromide), [C<sub>12</sub>mpy]Br (1-dodecyl-3-methylpyridinium bromide), and [C<sub>12</sub>mpyr]Br (1-dodecyl-1-methylpyrrolidinium bromide). Both the influence of the alkyl side-chain length and the type of ring in the cation (head) on the CMC were investigated. A comparison of the self-aggregation behavior of ionic liquids based on 1-alkyl-3-methylpyridinium and 1-alkyl-3-methylpyridinium cations is provided. It was observed that 1-alkyl-3-methylpyridinium ionic liquids could be used as quenchers for some fluorescence probes (fluorophores). As a consequence, a simple and convenient method to probe early evidence of aggregate formation was established.

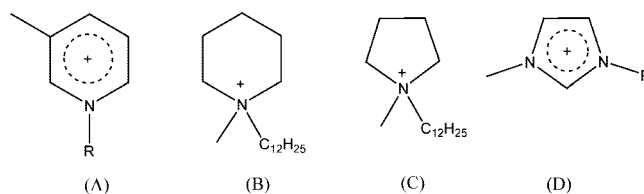
## 1. Introduction

Considering the growing number of reported investigations in which the dual nature of ionic liquids<sup>1</sup> has been studied, it seems that their roles in both surfactant science and its applications are promising. Surveying the recent literature, three possible directions for the development and applications of ionic liquids can be identified:

In the first group of publications, the amphiphilic nature of some cations, for example, [C<sub>n</sub>mim]<sup>+</sup>, leading to aggregation phenomena in aqueous solutions (and in some cases to organization into micelles displaying surfactant behavior) was analyzed.<sup>2–14</sup> With the possibility of the fine-tuning of the ionic liquids' hydrophobicity by changing the alkyl chain length and/or the nature and size of the counterion (anion), one can affect both the structure and the delicate dynamics of these micellar aggregates. Second, impressive solvation abilities toward the dissolution of a series of different common surfactants,<sup>15,16</sup> amphiphilic polymers<sup>17</sup> or ionic liquids<sup>18,19</sup> in neat ionic liquids have been demonstrated. Third, ionic liquids can be added as a cosurfactant or hydrotrope to aqueous solutions of common surfactants, thus affecting the surface activity and the critical micelle concentration (CMC) of these solutions.<sup>3,6</sup>

In our previous work,<sup>3</sup> we reported the role of the alkyl chain length, the concentration, and the nature of the anion on the aggregation behavior of the ionic compounds belonging to the [C<sub>n</sub>mim]X (X = Cl, [PF<sub>6</sub>]<sup>-</sup> or [NTf<sub>2</sub>]<sup>-</sup>) family. In the current contribution, we also examine the influence of different cationic

**SCHEME 1: Cations of Ionic Liquids Discussed: (A) 1-Alkyl-3-methylpyridinium, [C<sub>n</sub>mpy]<sup>+</sup>; (B) 1-Methyl-1-dodecylpiperidinium, [C<sub>12</sub>mpip]<sup>+</sup>; (C) 1-Methyl-1-dodecylpyrrolidinium, [C<sub>12</sub>mpyr]<sup>+</sup>; (D) 1-Alkyl-3-methylimidazolium, [C<sub>n</sub>mim]<sup>+</sup>**



ring types on the aggregation behavior by using aqueous solutions of [C<sub>12</sub>Y]Br (Y = mpyrr, mpy, or mpip).

Recently, a few studies on the fluorescence behavior of imidazolium and pyrrolidinium ionic liquids were published.<sup>20</sup> Here, we show a unique characteristic of some ionic liquids, namely, in the case of the 1-alkyl-3-methylpyridinium family: besides their ability to act as surfactants, they present also a quencher aptitude for the most commonly used fluorescence probes for micellar characterization (fluorophores). Probably, this characteristic has its origin at the pyridinium ring (head), for it is known that other pyridinium-containing cations can also act as quenchers.

## 2. Experimental Section

**Ionic Liquids.** The 1-alkyl-3-methylpyridinium chlorides, [C<sub>n</sub>mpy]Cl (*n* = 4, 10, 12, 14, 16, or 18), 1-dodecyl-1-methylpyrrolidinium bromide, 1-dodecyl-3-methylpyridinium bromide, and 1-dodecyl-1-methylpiperidinium bromide {[C<sub>12</sub>Y]Br; Y = mpyrr, mpy, or mpip; see Scheme 1) were synthesized by the reaction of one mole equivalent of the amine 3-methylpyridine, 1-methylpyrrolidine, or 1-methylpiperidine

\* Corresponding authors. E-mail: luis.rebelo@itqb.unl.pt and alopes@itqb.unl.pt.

<sup>†</sup> Universidade Nova de Lisboa.

<sup>‡</sup> The Queen's University of Belfast.

<sup>§</sup> Departamento de Engenharia Química e Biológica, Instituto Superior Técnico.

<sup>⊥</sup> Centro de Química Estrutural, Instituto Superior Técnico.

with an excess of the appropriate haloalkane (1.3 mol equivalents). This excess also allows for the reactants to be stirred without additional solvent at 70 °C; the progress of reactions was monitored by  $^1\text{H}$  NMR spectroscopy in  $\text{CDCl}_3$ . Upon completion of the reaction, there was no evidence for the presence of unreacted amine. The ionic liquids were purified with ethyl ethanoate. The volume of ethyl ethanoate used for the recrystallization was approximately half that of the halide salt. The ethyl ethanoate was decanted, followed by the addition of fresh ethyl ethanoate, and this step was repeated five times. The remaining ethyl ethanoate was removed in vacuo, and the ionic liquids were dried in vacuo (0.1 Pa) to remove any small traces of volatile compounds at moderate temperatures (60–80 °C) for typically 72 h. The detailed syntheses and spectroscopic (NMR, MS) and thermophysical (DSC, TGA) characterization will be reported elsewhere.<sup>21</sup> All chemicals were purchased from Sigma-Aldrich; the more volatile liquids were purified by distillation under vacuum before use. For the NMR experiments,  $d^1$ -trichloromethane (D+0.03%, Euriso-top) was used:  $^1\text{H}$ - and  $^{13}\text{C}$  NMR analyses showed no major impurities in the ionic liquids as prepared above by using a Bruker Avance spectrometer DPX 300.

**Chemicals for IFT, Fluorescence, and NMR Measurements.** Doubly distilled deionized water was obtained from a Millipore Milli-Q water purification system (Millipore). Both for the interfacial tension (IFT) and fluorescence measurements,  $[\text{C}_n\text{mpy}]\text{Cl}$  stock solutions were prepared in either  $1.74 \times 10^{-6}$  M pyrene or slightly less than saturated anthracene aqueous solution, and all studied solutions were prepared from the stock solutions, diluting with the same pyrene or anthracene aqueous solution. Pyrene (Fluka, Germany, 99%) was recrystallized from benzene. Anthracene (Fluka, Germany, *puriss.*, for scintillation) and ethanenitrile (Merck, Germany, gradient grade) were used without further purification. For the NMR experiments,  $\text{D}_2\text{O}$  (Cambridge Isotope Laboratory, Andover, MA, D, 99.9%) was used.

Details about the experimental techniques and instrumentation for IFT, fluorescence, and  $^1\text{H}$  NMR spectroscopy are found in the Supporting Information.

**Ab Initio Calculations.** The molecular geometry and charge distribution of isolated 1,1-dimethylpyrrolidinium and 1,1-dimethylpiperidinium cations were obtained by quantum chemical (*ab initio*) calculations. These were performed by using the Gaussian 03 program<sup>22</sup> at the HF/6-31G(d) level of theory for geometry optimization and the MP2/cc-pVTZ-f level for single-point energy and electronic density calculations, as is current practice in the development of force-field parameters for ions present in ionic liquids.<sup>23</sup> The point-charge assignment was done by using the CHelpG algorithm.

### 3. Results and Discussion

**Self-Aggregation Assessment by Surface Tension.** The surface tension of aqueous solutions of 1-alkyl-3-methylpyridinium chlorides,  $[\text{C}_n\text{mpy}]\text{Cl}$ , ( $n = 10, 12, 14, 16, \text{ or } 18$ ) was measured, see Figure 1a. The results of the IFT for the aqueous solutions as a function of the total concentration of  $[\text{C}_n\text{mpy}]\text{Cl}$  were used to determine the CMC and to study adsorption parameters: the efficiency of adsorption,  $\text{pC}_{20}$ , (defined as the negative logarithm to the base 10 of the concentration of amphiphilic molecules required to reduce the surface tension of the pure solvent by 20  $\text{mN m}^{-1}$ ), the effectiveness of the surface tension reduction,  $\Pi_{\text{CMC}}$ , (defined as  $\Pi_{\text{CMC}} = \gamma_0 - \gamma_{\text{CMC}}$ , where  $\gamma_0$  is surface tension of the pure solvent (water) and  $\gamma_{\text{CMC}}$  the surface tension of the solution

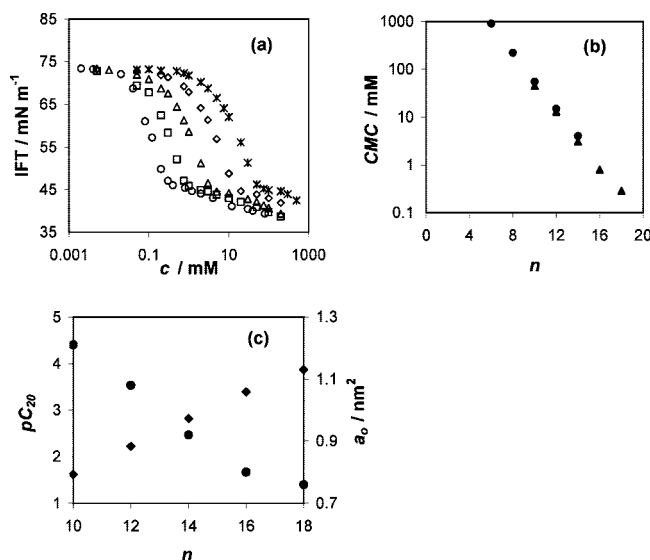


**Figure 1.** (a) Monitoring the self-aggregation of  $[\text{C}_n\text{mpy}]\text{Cl}$  by using IFT for different chain lengths:  $n = (*)$  10, ( $\diamond$ ) 12, ( $\Delta$ ) 14, ( $\circ$ ) 16, ( $\circ$ ) 18. (b) CMC values for  $[\text{C}_n\text{mpy}]\text{Cl}$  ( $\blacktriangle$ ) and  $[\text{C}_n\text{mim}]\text{Cl}$  ( $\bullet$ ) as a function of  $n$ . (c) Efficiency of adsorption  $\text{pC}_{20}$  ( $\blacklozenge$ ) and minimum area per ionic liquid molecule,  $a_0$  ( $\bullet$ ) as a function of  $n$   $[\text{C}_n\text{mpy}]\text{Cl}$ .

**TABLE 1: CMC (in mM) of  $[\text{C}_n\text{mpy}]\text{Cl}$  ( $n = 10\text{--}18$ ),  $[\text{C}_{12}\text{Y}]\text{Br}$ , ( $\text{Y} = \text{mpyrr}$ ,  $\text{mpy}$ ,  $\text{mpip}$ , and  $\text{mim}$ ) Measured by IFT, Fluorescence Quenching of Pyrene, Fluor, and  $^1\text{H}$  NMR Spectroscopy<sup>a</sup>**

| Ionic Liquid                           | IFT                                       | fluor           | $^1\text{H}$ NMR |
|----------------------------------------|-------------------------------------------|-----------------|------------------|
| $[\text{C}_{10}\text{mpy}]\text{Cl}$   | 45                                        | 44 <sup>b</sup> |                  |
| $[\text{C}_{12}\text{mpy}]\text{Cl}$   | 13                                        | 13.5            | 12.5             |
| $[\text{C}_{14}\text{mpy}]\text{Cl}$   | 3.1                                       | 3.1             | 3.2              |
| $[\text{C}_{16}\text{mpy}]\text{Cl}$   | 0.8                                       | 0.77            | 0.9              |
| $[\text{C}_{18}\text{mpy}]\text{Cl}$   | 0.3                                       | 0.23            | 0.25             |
| $[\text{C}_{12}\text{mpy}]\text{Br}$   | 10                                        |                 |                  |
| $[\text{C}_{12}\text{mpip}]\text{Br}$  | 11                                        |                 |                  |
| $[\text{C}_{12}\text{mpyrr}]\text{Br}$ | 1.2                                       |                 |                  |
| $[\text{C}_{12}\text{mim}]\text{Br}$   | 9, 10, 12 <sup>c</sup> , 9.8 <sup>d</sup> |                 |                  |

<sup>a</sup> The experimental errors for all used techniques are  $\leq 5\%$ .

<sup>b</sup> Result obtained by using anthracene as a fluorophore. <sup>c</sup> From ref 9. CMCs obtained by using conductivity, volume, and fluorescence measurements. <sup>d</sup> From ref 7. CMC obtained by using conductivity measurements.

at the CMC), and the minimum area per amphiphilic molecule at the interface,  $a_0$ .<sup>24</sup>

**Micellisation.** If aggregation phenomena occur, then, as the concentration of an ionic liquid increases, the surface tension of the solution initially decreases and then becomes almost constant. The CMC is determined as the intersection of two linearly extrapolated lines. It is obvious that the decrease in the CMC of aqueous solutions of  $[\text{C}_n\text{mpy}]\text{Cl}$  is a consequence of the growth of the alkyl chain. The experimental values for the break points in the IFT measurement are presented in Table 1 (along with other CMC results from different techniques). Figure 1b summarizes the CMC values obtained with the IFT methodology plotted as a function of the number of carbon atoms,  $n$ , in the cationic side chain of  $[\text{C}_n\text{mpy}]\text{Cl}$ ,  $n = 10\text{--}18$ . For comparison purposes, data obtained for the  $[\text{C}_n\text{mim}]\text{Cl}$  family with similar hydrocarbon chain lengths are depicted.<sup>3</sup> The expected slightly higher hydrophobicity of the  $[\text{C}_n\text{mpy}]$  cation in comparison with the  $[\text{C}_n\text{mim}]$  cation is probably the reason for the lower CMC values of the former.

**Adsorption.** The lowering of the surface tension values,  $\gamma$ , is a consequence of the increased concentration of the ionic

**TABLE 2: Efficiency of Adsorption,  $pC_{20}$ , Effectiveness of Surface Tension Reduction,  $\Pi_{CMC}$ , and Minimum Area per Ionic Liquid Molecule at the Interface Air/Liquid,  $a_o$  of  $[C_n\text{mpy}]\text{Cl}$  ( $n = 10-18$ )**

| ionic liquid                  | $pC_{20}$ | $\Pi_{CMC}/\text{mN m}^{-1}$ | $a_o/\text{nm}^2$ |
|-------------------------------|-----------|------------------------------|-------------------|
| $[C_{10}\text{mpy}]\text{Cl}$ | 1.62      | 27.9                         | 1.21              |
| $[C_{12}\text{mpy}]\text{Cl}$ | 2.22      | 27.9                         | 1.08              |
| $[C_{14}\text{mpy}]\text{Cl}$ | 2.82      | 28.0                         | 0.92              |
| $[C_{16}\text{mpy}]\text{Cl}$ | 3.39      | 27.9                         | 0.80              |
| $[C_{18}\text{mpy}]\text{Cl}$ | 3.87      | 27.8                         | 0.76              |

liquid at the air–water surface. Because of the almost invariant condition of the surface for concentrations greater than that of the CMC, the chemical potential of the ionic liquid changes only slightly.<sup>25</sup> Although the adsorption efficiency,  $pC_{20}$ , increases with increasing alkyl chain length (Figure 1c), the effectiveness of the surface tension reduction,  $\Pi_{CMC}$ , varies only slightly. They follow tendencies published for both  $[C_n\text{mim}]\text{Cl}$ <sup>13</sup> and classical cationic surfactants.<sup>24</sup>

From surface tension data, by assuming for these low-concentration regimes a monolayer structure at the surface, we calculated the minimum area per ionic liquid molecule,  $a_o$ , by using the well-known Gibbs equation.<sup>24</sup> Values for  $a_o$ ,  $pC_{20}$ , and  $\Pi_{CMC}$  are listed in Table 2. The dependence of the minimum area per amphiphilic molecule versus the number of carbon atoms in the alkyl chain,  $n$  (up to 16 carbon atoms), for  $[C_n\text{mpy}]\text{Cl}$  is linear and can be described by  $a_o = 1.906 - 0.0695n$  (Figure 1c). A similar dependence for  $[C_n\text{mim}]\text{Cl}$  was recently reported,<sup>13</sup> and the corresponding equation is  $a_o = 1.461 - 0.062n$ . A comparison of the equations for these two families suggests a higher degree of packing of adsorbed  $[C_n\text{mim}]\text{Cl}$  molecules. A slightly lower surface tension in the plateau region reported in our previous paper<sup>3</sup> for  $[C_n\text{mim}]\text{Cl}$  in comparison with  $[C_n\text{mpy}]\text{Cl}$  (Figure 1a) also leads to the same conclusion.

It is well-known that surface tension measurements are a very sensitive test for the presence of impurities, usually being unreacted surface active compounds (long chain chloroalkane in the case of chloride-based ionic liquids that are usually used in excess during the synthesis). The absence of a minimum<sup>24</sup> around the CMC confirms the high purity of the ionic liquids used in this study.

**CMC Determination by Changes in the Fluorescence of Added Probes.** A widely used method for the determination of the aggregation of amphiphilic molecules (surfactants, polymers, and so forth) is the comparison of the intensities of the first, I1, and third, I3, vibronic bands of the pyrene emission spectrum. The ratio I3/I1 is a function of the polarity of the pyrene environment, and it increases with decreasing solvent polarity.<sup>26,27</sup>

Obviously, the method cannot be applied when the fluorescence of pyrene is quenched by the surfactant itself. This is found to be the case for the 1-alkyl-3-methylpyridinium ionic liquids, in analogy with other cases containing the same common pyridinium ring (head).<sup>28</sup> In fact, it was witnessed that the fluorescence of both pyrene and anthracene in water vanished (indistinguishable from the noise level) for all  $[C_n\text{mpy}]\text{Cl}$  ionic liquids used in this study, at concentrations for which aggregation is expected. Therefore, it seems that once in the aggregate, the close contact between the fluorophore probe and the 1-alkyl-3-methylpyridinium group results in an efficient static fluorescence quenching. In order to verify that the 1-alkyl-3-methylpyridinium group is able to quench the fluorescence of these probes, Stern–Volmer quenching constants,  $K_{SV}$ , for the steady-state fluorescence quenching were determined from the

variation of fluorescence intensity in the absence ( $I_0$ ) and presence ( $I$ ) of low concentrations,  $c$ , of 1-alkyl-3-methylpyridinium in ethanenitrile. In order to quantify the quenching effect of the monomer (preventing aggregation), we have chosen the short chain  $[C_4\text{mpy}]\text{Cl}$  homologue to perform the experiments, and (for  $c < 0.6$  mM) a linear Stern–Volmer plot,  $(I_0/I) = 1 + cK_{SV}$ , was obtained (Figure 2a). From the slopes of the Stern–Volmer plots, values of  $K_{SV} = (0.3 \pm 0.04)$  and  $(0.07 \pm 0.005)$   $\text{mM}^{-1}$  for pyrene and anthracene, respectively, were obtained. For the quenching of an excited state, we have  $K_{SV} = k_q\tau_0$ ,<sup>28,29</sup> where  $\tau_0$  is the fluorescence lifetime of the excited state and  $k_q$  is the rate constant for bimolecular quenching. By taking as reasonable approximations the published values of  $\tau_0$  of pyrene and anthracene in polar aerated solvents, respectively 18.9 ns (19.0 ns without  $O_2$ ) and 4.2 ns (5.3 ns without  $O_2$ ),<sup>30</sup> we calculated the values of the bimolecular quenching constant  $k_q(\text{pyrene}) = (1.58 \pm 0.23) \times 10^{10}$   $\text{L mol}^{-1} \text{s}^{-1}$  and  $k_q(\text{anthracene}) = (1.67 \pm 0.12) \times 10^{10}$   $\text{L mol}^{-1} \text{s}^{-1}$ . This demonstrates that within the experimental error, the quenching is diffusion controlled ( $k_{\text{diff}} = 1.9 \times 10^{10}$   $\text{L mol}^{-1} \text{s}^{-1}$ ). The quenching mechanism probably involves electron transfer, but this is out of the scope of the current work.

The fact that the  $[C_n\text{mpy}]\text{Cl}$  family may act as fluorescence quenchers opens the possibility of determining CMCs by detecting the surfactant concentration for which the quenching deviates from the normal Stern–Volmer equation, that is, from a slope comparable to that which occurs in homogeneous media. The onset of micellization, defined as the CMC, can be recognized as a pronounced break-point in the dependence of  $I_0/I$  versus the concentration of  $[C_n\text{mpy}]\text{Cl}$  in aqueous solution. Typical graphs of this type for  $[C_n\text{mpy}]\text{Cl}$  ( $n = 12, 14, 16,$  or  $18$ ) in aqueous solution by using pyrene as a fluorescence probe are shown in Figure 2b. The values of CMCs for all systems are presented in Table 1. In order to apply this new method, it is necessary that the CMC of certain compound–quencher combinations is not greater than the concentration at which complete quenching of fluorescence probes occurs. It means that this method requires an appropriate match between the fluorescence probe and the quencher. One should note here the very good agreement between values determined by using distinct methodologies. Having a good agreement between this new method and two well-established methods for the onset of aggregation, surface tension and  $^1\text{H}$  NMR (see next section), is important. This avoids potentially fallacious interpretations which are a common occurrence when novel methods are used without the proof of concept.

**Self-Aggregation Assessment by  $^1\text{H}$  NMR.**  $^1\text{H}$  NMR resonances for the protons of  $[C_n\text{mpy}]\text{Cl}$  undergo reasonable shifts as a function of the  $[C_n\text{mpy}]\text{Cl}$  concentration, namely, the protons of the ring and the protons of the terminal  $\text{CH}_3$  group. Figure 3 shows the evolution of the chemical shifts ( $\delta$ , ppm) in the  $^1\text{H}$  NMR spectra for the protons of the terminal  $\text{CH}_3$  group as a function of the reciprocal concentration (logarithmic scale) of  $[C_n\text{mpy}]\text{Cl}$ .

Once again, in agreement with the previous methodologies, the chemical shift shows a distinctive decrease for all  $n > 12$ , indicating the change in the environment for these molecules as a function of their concentration, related to the self-aggregation in small micellar-type aggregates.

**Self-Aggregation for Other Types of Cationic Rings—Assessment by Surface Tension and Ab Initio Calculations.** The influence of the type of ring in the cation on the aggregation behavior was also investigated. The underlying influence of this effect is very complex because head groups have opposing



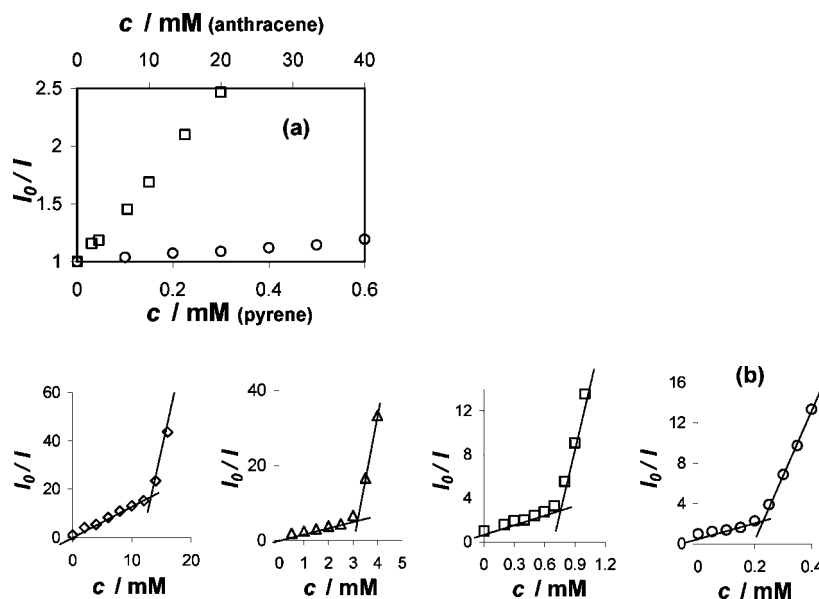


**Figure 2.** (a) Stern–Volmer relation for  $[\text{C}_4\text{mpy}]\text{Cl}$  in ethanenitrile solutions of anthracene ( $\square$ ) and pyrene ( $\circ$ ). (b) Monitoring the self-aggregation of  $[\text{C}_n\text{mpy}]\text{Cl}$  in aqueous solution by using the fluorescence quenching technique for pyrene for different alkyl side-chain lengths of the ionic liquid:  $n = (\diamond)12$ ,  $(\Delta)14$ ,  $(\square)16$ , and  $(\circ)18$ .

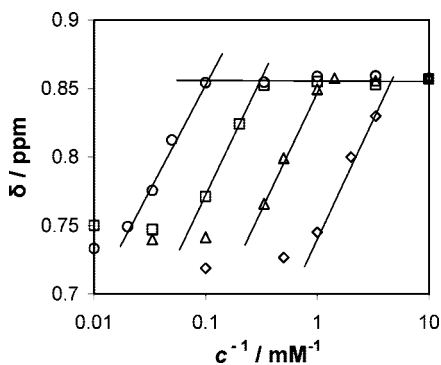


**Figure 3.** Monitoring the self-aggregation of  $[\text{C}_n\text{mpy}]\text{Cl}$  by using  $^1\text{H}$  NMR spectroscopy.  $\delta$  is the observed chemical shift, and  $c$  is the ionic liquid concentration. Results for protons of the terminal  $\text{CH}_3$  group for different chain lengths:  $n = (\diamond)12$ ,  $(\Delta)14$ ,  $(\square)16$ , and  $(\circ)18$ .

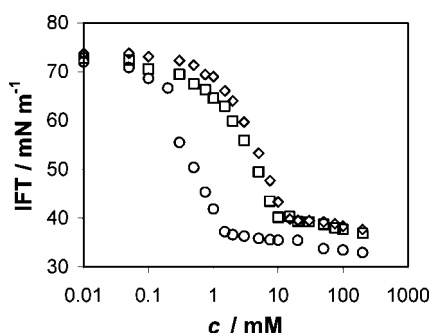


**Figure 4.** - Monitoring the self-aggregation of  $[\text{C}_{12}\text{Y}]\text{Br}$  by using the IFT technique:  $(\diamond)[\text{C}_{12}\text{mpip}]\text{Br}$ ,  $(\square)[\text{C}_{12}\text{mpy}]\text{Br}$ , and  $(\circ)[\text{C}_{12}\text{mpyr}]\text{Br}$ .

tendencies to keep close to minimize hydrocarbon–water contacts and to repel as a result of electrostatic repulsion, hydration, and steric hindrance.<sup>25</sup> Three ionic liquids with the same anion and the same alkyl chain length but with different types of hydrocarbon rings have been analyzed. Figure 4 shows the surface tension curves for  $[\text{C}_{12}\text{Y}]\text{Br}$  ( $\text{Y} = \text{mpyr}$ ,  $\text{mpy}$ , and  $\text{mpip}$ ). Surprisingly, two very similar curves with almost the same CMC values were obtained for  $[\text{C}_{12}\text{mpy}]\text{Br}$  and  $[\text{C}_{12}\text{mpip}]\text{Br}$ . Probably, in the case of  $[\text{C}_{12}\text{mpip}]\text{Br}$ , two effects

compensate each other. On the one hand, the higher hydrophobicity of the  $[\text{C}_{12}\text{mpip}]^+$  cation and stronger bound anion,  $\text{Br}^-$ , in comparison with the  $[\text{C}_{12}\text{mpy}]^+$  cation, where the positive charge is delocalized, would give a lower CMC. On the other hand, because these two molecules have a different geometry and volume, we can expect that the more space-demanding  $[\text{C}_{12}\text{mpip}]^+$  cation (we are comparing boat and/or chair structures of a cyclic six-membered ring with a planar aromatic molecule) has a higher CMC because of steric hindrance. One can also notice that the CMC value for  $[\text{C}_{12}\text{mpy}]\text{Br}$  (10 mM) is lower than that for  $[\text{C}_{12}\text{mpy}]\text{Cl}$  (13 mM). The slightly lower values obtained for  $[\text{C}_n\text{mpy}]\text{Br}$  are expected because it is known that the binding of anionic counterions to cationic micelles increases in the order  $\text{F}^- < \text{Cl}^- < \text{Br}^- < \text{I}^-$ .<sup>31</sup>

It is even more difficult to explain the significantly lower CMC and surface tension in the plateau region of the five-membered heterocyclic ring of  $[\text{C}_{12}\text{mpyr}]\text{Br}$  in comparison with the six-membered heterocyclic ring of  $[\text{C}_{12}\text{mpip}]\text{Br}$ . Without further studies, we are unable to speculate whether this is only the effect of their different volume and geometry and consequent head packing in the micelles or in the monolayers. However, a complementary interpretation can be developed if one compares the geometry and internal charge distribution of the two isolated cations.

The necessary data were calculated *ab initio* (cf. Table S1 of the Supporting Information), and different conclusions can be drawn from. First, the geometry (bond lengths and angles) around the nitrogen atom are very similar in both cases ( $\text{N}-\text{C}(\text{methyl})$  and  $\text{N}-\text{C}(\text{methylene})$  distances of 149 and 151 pm, respectively, and angles close to  $109.5^\circ$ ). This can be seen in Figure 5, where the most stable conformation of each cation is represented. In fact, the chair conformation of the piperidinium cation can be thought as an envelope conformation (like that of the pyrrolidinium cation) with an extra flap. Because that extra flap occupies a position opposite to the nitrogen atom, the influence of the former on the latter is very limited from a geometrical perspective. Also, the charge distribution in the two cations is quite different because of different hyper-conjugation effects on the five- and six-membered rings (cf. Figure 5).

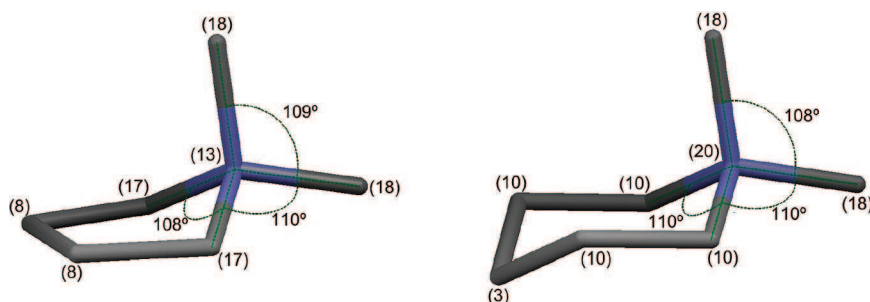


**Figure 5.** Most stable conformers of 1,1-dimethylpyrrolidinium (envelope conformation, left) and 1,1-dimethylpiperidinium (chair conformation, right). When a long alkyl chain is present, it will occupy an equatorial position relative to the pseudo-plane of the ring. The numbers in brackets are the point charges (in % acu) attributed by the model to the nitrogen, methylene, and methyl groups.

Taken together, these conclusions mean that the headgroup of the anion will interact with the two cations at a similar position (the most positive charge is centered around the geometrically similar nitrogen atoms) but with different magnitude. In fact, the larger charge density on the nitrogen of the piperidinium cation will lead to weaker interactions because this atom (surrounded by four carbon atoms) cannot be approached by the anion. On the other hand, the pyrrolidinium cation has greater charge densities in the 2,6-methylene groups (taken as the sum of the charge of the ortho carbon atom plus its two hydrogen atoms) where most of the interactions with the anion will take place. This fact can compensate for the lower charge density of its nitrogen atom and lead to an effectively higher counteranion binding, and consequently, to a lower CMC, as experimentally measured. These observations have to be examined in deeper detail by using other classes of ionic liquids and other methods.

#### 4. Conclusions

We propose a novel methodology that can be used to find out whether ionic liquids are capable of forming aggregates in aqueous solutions. This technique is based on the fluorescence quenching effect that specific ionic liquids provoke in common fluorophores. This procedure was successfully tested against two well-established methodologies. Additional classes of ionic liquids can now be checked for their micellar behavior by using this new technique.

Quenching of fluorescence has found wide utility in biochemical research.<sup>28</sup> The current new result, connected to aggregation phenomena in ionic-liquids-containing systems, may find application in other fields too.

It was found that pyridinium ionic liquids are more biodegradable than imidazolium ionic liquids and biodegradation rates increase with longer alkyl chain length.<sup>32</sup> The ability of pyridinium ionic liquids to act as a quencher for some fluorophores can be used as a very sensitive method for following their degradation rates or generally concentration change. This method can be used in broad concentration range and in the presence of many other species in solution, because quenching requires specific contact pyridinium nucleus–fluorophore.

Besides the length of the alkyl chain and the nature of the anion, both the structure of the headgroup and the point-charge density distribution are parameters which play important roles in the geometry and packing of micelles, in particular by controlling the magnitude of the steric repulsions between the head groups. However, the issue of the influence of the headgroup on the aggregation behavior deserves further investigations.

**Acknowledgment.** This work was supported by the Fundação para a Ciência e Tecnologia (FC&T), Portugal (Projects POCTI/

QUI/35413/2000 and POCTI/QUI/57716/2004). M.B. thanks FC&T for a Ph.D. Grant SFRH/BD/13763/2003) and Marie Curie Fellowships for Early Stage Research Training (EST No505613). K.R.S. thanks the EPSRC (Portfolio Partnership Scheme, Grant no. EP/D029538/1).

**Supporting Information Available:** Experimental methods and detailed ab initio results. This material is available free of charge via the Internet at <http://pubs.acs.org>.

#### References and Notes

- Rebello, L. P. N.; Canongia Lopes, J. N.; Esperança, J. M. S. S.; Guedes, H. J. R.; Łachwa, J.; Najdanovic-Visak, V.; Visak, Z. P. *Acc. Chem. Res.* **2007**, *40*, 1114.
- Bowers, J.; Butts, C. P.; Martin, P. J.; Vergara-Gutierrez, M. C.; Heenan, R. K. *Langmuir* **2004**, *20*, 2191.
- Blesic, M.; Marques, M. H.; Plechkova, N. V.; Seddon, K. R.; Rebello, L. P. N.; Lopes, A. *Green Chem.* **2007**, *9*, 481.
- Blesic, M.; Gunaratne, N.; Lopes, A.; Plechkova, N. V.; Rebello, L. P. N.; Seddon, K. R. In *Ionic Liquids: Never the Twain*; Gaune-Escard, M., Seddon, K. R., Eds.; Wiley: Hoboken, NJ, 2008. In preparation.
- Sirieux-Plénet, J.; Gaillon, L.; Letellier, P. *Talanta* **2004**, *63*, 979.
- Miskolczy, Z.; Sebök-Nagy, K.; Biczók, L.; Göktütük, S. *Chem. Phys. Lett.* **2004**, *400*, 296.
- Vanyúr, R.; Biczók, L.; Miskolczy, Z. *Colloid Surf., A* **2007**, *299*, 25.
- Goodchild, I.; Collier, L.; Millar, S. L.; Prokeš, I.; Lord, J. C. D.; Butts, C. P.; Bowers, J.; Webster, J. R. P.; Heenan, R. K. *J. Colloid Interface Sci.* **2007**, *307*, 455.
- Wang, J.; Wang, H.; Zhang, S.; Zhang, H.; Zhao, Y. *J. Phys. Chem. B* **2007**, *111*, 6181.
- Modarelli, A.; Sifaoui, H.; Mielcarz, M.; Domańska, U.; Rogalski, M. *Colloid Surf., A* **2007**, *302*, 181.
- Dong, B.; Li, N.; Zheng, L.; Yu, L.; Inoue, T. *Langmuir* **2007**, *23*, 4178.
- Singh, T.; Kumar, A. *J. Phys. Chem. B* **2007**, *111*, 7843.
- El Seoud, O. A.; Pires, P. A. R.; Abdel-Moghny, T.; Bastos, E. L. *J. Colloid Interface Sci.* **2007**, *313*, 296.
- (a) Najdanovic-Visak, V.; Canongia Lopes, J. N.; Visak, Z. P.; Trindade, J.; Rebello, L. P. N. *Int. J. Mol. Sci.* **2007**, *8*, 736. (b) Lopes, J. N. C.; Rebello, L. P. N. *Chimica Oggi/Chem. Today* **2007**, *25*, 37.
- Anderson, J. L.; Pino, V.; Hagberg, E. C.; Sheares, V. V.; Armstrong, D. W. *Chem. Comm.* **2003**, *19*, 2444.
- Fletcher, K. A.; Pandey, S. *Langmuir* **2004**, *20*, 33.
- He, Y.; Li, Z.; Simone, P.; Lodge, T. P. *J. Am. Chem. Soc.* **2006**, *128*, 2745.
- Thomaier, S.; Kunz, W. *J. Mol. Liq.* **2007**, *130*, 104.
- Velasco, S. B.; Turmine, M.; Di Caprio, D.; Letellier, P. *Colloid Surf., A* **2006**, *275*, 50.
- (a) Mandal, P. K.; Samanta, A. *J. Phys. Chem. B* **2005**, *109*, 15172. (b) Paul, A.; Mandal, P. K.; Samanta, A. *J. Phys. Chem. B* **2005**, *109*, 9148.
- Blesic, M.; Plechkova, N. V.; Rebello, L. P. N.; Seddon, K. R. *J. Mater. Chem.* To be submitted.
- Frisch, M. J.; Trucks, G. W.; Schlegel, H. B.; Scuseria, G. E.; Robb, M. A.; Cheeseman, J. R.; Montgomery, J. A., Jr.; Vreven, T.; Kudin, K. N.; Burant, J. C.; Millam, J. M.; Iyengar, S. S.; Tomasi, J.; Barone, V.; Mennucci, B.; Cossi, M.; Scalmani, G.; Rega, N.; Petersson, G. A.; Nakatsuji, H.; Hada, M.; Ehara, M.; Toyota, K.; Fukuda, R.; Hasegawa, J.; Ishida, M.; Nakajima, T.; Honda, Y.; Kitao, O.; Nakai, H.; Klene, M.; Li, X.; Knox, J. E.; Hratchian, H. P.; Cross, J. B.; Bakken, V.; Adamo, C.; Jaramillo, J.; Gomperts, R.; Stratmann, R. E.; Yazyev, O.; Austin, A. J.; Cammi, R.; Pomelli, C.; Ochterski, J. W.; Ayala, P. Y.; Morokuma, K.;

Voth, G. A.; Salvador, P.; Dannenberg, J. J.; Zakrzewski, V. G.; Dapprich, S.; Daniels, A. D.; Strain, M. C.; Farkas, O.; Malick, D. K.; Rabuck, A. D.; Raghavachari, K.; Foresman, J. B.; Ortiz, J. V.; Cui, Q.; Baboul, A. G.; Clifford, S.; Cioslowski, J.; Stefanov, B. B.; Liu, G.; Liashenko, A.; Piskorz, P.; Komaromi, I.; Martin, R. L.; Fox, D. J.; Keith, T.; Al-Laham, M. A.; Peng, C. Y.; Nanayakkara, A.; Challacombe, M.; Gill, P. M. W.; Johnson, B.; Chen, W.; Wong, M. W.; Gonzalez, C.; Pople, J. A. *Gaussian 03*, revision B.04; Gaussian, Inc.: Wallingford, CT, 2003.

(23) Canongia Lopes, J. N.; Deschamps, J.; Padua, A. A. H. *J. Phys. Chem. B* **2004**, *108*, 2038.

(24) Rosen, M. J. *Surfactant and Interfacial Phenomena*; Wiley-Interscience, John Wiley & Sons: NJ, 2004.

(25) Evans, D. F.; Wennerstrom, H. *The Colloidal Domain: Where Physics, Chemistry, Biology and Technology Meet*; VCH: New York, 1994.

(26) Zana, R. *Surfactant Solutions: New Methods of Investigation*, Marcel Dekker: New York, 1986.

(27) Aguiar, J.; Carpena, P.; Molina-Bolívar, J. A.; Carnero Ruiz, C. *J. Colloid Interface Sci.* **2003**, *258*, 116.

(28) Lackowicz, J. *Principles of Fluorescence Spectroscopy*; Plenum Press: New York, 1983.

(29) Birks, J. B. *Photophysics of Aromatic Molecules*; Wiley-Interscience: London, 1970.

(30) Murov, S. L.; Carmichael, I.; Hug, G. L. *Handbook of Photochemistry*, 2nd ed.; Marcel Dekker: New York, 1993.

(31) Anacker, E. W.; Ghose, H. M. *J. Am. Chem. Soc.* **1968**, *90*, 3161.

(32) Docherty, K. M.; Dixon, J. K.; Kulpa, C. F., Jr *Biodegradation* **2007**, *18*, 481.

JP802179J



## **CHAPTER 3.**

# **1-ALKYL-3-METHYLIMIDAZOLIUM ALKYLSULFONATE IONIC LIQUIDS: SYNTHESIS AND PHYSICOCHEMICAL PROPERTIES**

*This Chapter will be submitted as a full article:*

Blesic M., Swadzba-Kwasny M., Belhocine T., Gunaratne N., Seddon K.R., Padua A.A.H., Costa Gomes M.F., Lopes J.N.C., Rebelo L.P.N., “1-Alkyl-3-methylimidazolium alkanesulfonate ionic liquids: synthesis and physicochemical properties”.

**Note:** The experimental part - synthesis and characterisation of the ionic liquids used in this study- was done by the author of this Thesis.

$^1\text{H}$  NMR,  $^{13}\text{C}$  NMR and mass spectroscopy results of the ionic liquids are given in **Appendix 2**.

# 1-Alkyl-3-Methylimidazolium Alkanesulfonate Ionic Liquids: Synthesis and Physicochemical Properties

Marijana Blesic,<sup>a, b</sup> Malgorzata Swadzba-Kwasny,<sup>b</sup> Tayeb Belhocine,<sup>b</sup>  
Nimal Gunaratne,<sup>b</sup> Kenneth R. Seddon,<sup>a, b</sup> Agilio A. H. Padua,<sup>c</sup> Margarida F. Costa  
Gomes,<sup>c</sup> José N. Canongia Lopes,<sup>a, d</sup> Luís Paulo N. Rebelo<sup>a</sup>

<sup>a</sup>*Instituto de Tecnologia Química e Biológica, ITQB 2, Universidade Nova de Lisboa, Apartado  
127, 2780-901 Oeiras, Portugal*

<sup>b</sup>*The QUILL Centre, The Queen's University of Belfast, Stranmillis Road, Belfast BT9 5AG, United  
Kingdom*

<sup>c</sup>*Laboratoire de Thermodynamique et Interactions Moléculaires, Université Blaise Pascal, Clermont-  
Ferrand/CNRS, 63177 Aubière, France*

<sup>d</sup>*Centro de Química Estrutural, Instituto Superior Técnico, 1049-001 Lisboa, Portugal*

**Keywords:** ionic liquids; 1-alkyl-3-methylimidazolium; alkanesulfonate; synthesis;  
physicochemical properties.

## Introduction

Ionic liquids are now undisputedly considered as possible alternatives to volatile organic compounds. They can replace more conventional media to perform chemical reactions, to support homogeneous or heterogeneous catalytic processes or to carry out extractions and separations. Moreover, the ionic liquids myriad and its consequent diversity permit us to create tailored liquids whose study contributes to increase fundamental knowledge about their molecular characteristics, and to establish molecular engineering strategies for particular processes.<sup>1</sup>

In this work, a family of ionic liquids based on alkanesulfonate anions,  $[C_kSO_3]^-$ , and 1-alkyl-3-methylimidazolium cations,  $[C_nmim]^+$ , was synthesized for the first time, where the size of the alkyl side chain can simultaneously be varied in the cation or in the anion. This represents a departure from the usual way of conceiving the relation between structure and the properties along a family of ionic liquids. Traditionally, an ionic liquid family is established by using one fixed anion or cation and varying the nature of the counter-ion in a systematic way – for example by increasing the alkyl side-chain length on a homologous series or the degree of substitution. Herein, the family of

ionic liquids was designed by altering the nature of both the cation and the anion in a systematic way – creating a bi-dimensional homologous series of ionic liquids (see Figure 1).

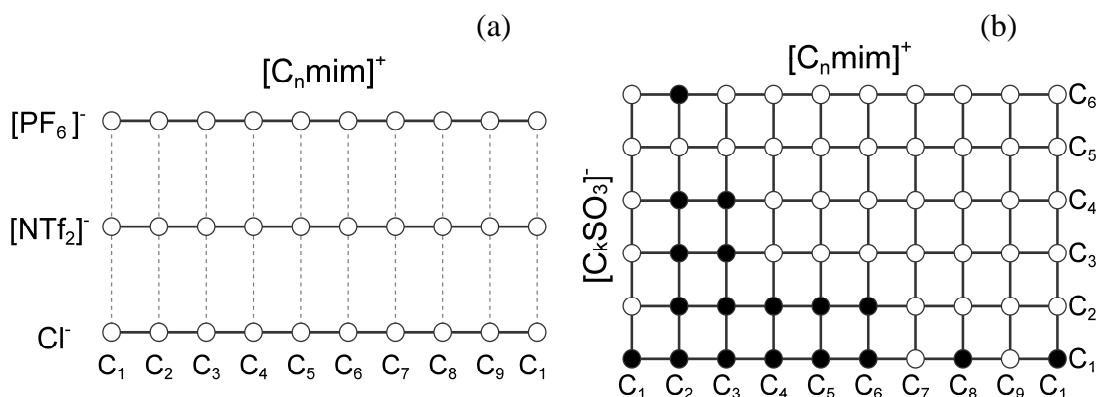


**Figure 1.** Schematic representation showing different families of ionic liquids. In (a) different members of the 1-alkyl-3-methylimidazolium family are shown with different anions, defining traditional homologous series (different rows represented by the solid lines) that can be correlated whenever two ionic liquids have a common cation (dashed lines). In (b) different members of the 1-alkyl-3-methylimidazolium,  $[C_n\text{mim}]^+$ , alkanesulfonate,  $[C_k\text{SO}_3]^-$ , ionic liquid family are shown. This family is characterised by a matrix-like arrangement of its members (solid lines). The filled dots represent ionic liquids actually synthesized and characterized in the present study.

We wish to judge if it could *a priori* be anticipated that the study of the current family yields recognizable patterns as far as the correlation between structure and properties of the different ionic liquids is concerned; and, if so, whether this can be rationalized in a useful way – both from the application and fundamental points of view. For instance, the properties of the 1-alkyl-3-methylimidazolium alkanesulfonate family should follow a trend compatible with the assumption that ionic liquids are nano-structured media<sup>2,3</sup>, a fact now largely supported by different experimental information.<sup>4-8</sup> In other words, the existence of polar and non-polar domains in the ionic liquids, the latter formed by the aggregation of the alkyl chains of both the cation and the anion, should influence the way the properties vary along the family. Another interesting aspect is to check how these alkanesulfonate-based salts differ, in terms of their physicochemical properties, from the related alkanesulfate family. The latter have been suggested as particularly environmentally friendly ionic liquids<sup>9, 10</sup> and, more recently as potential candidates to be used in the construction of a liquid-mirror lunar telescope<sup>11</sup>.

A series of 1-alkyl-3-methylimidazolium alkanesulfonate  $[C_n\text{mim}] [C_k\text{SO}_3]$  ionic liquids were prepared with  $n = 1-6, 8, 10$ , and  $k = 1-4, 6$ . In order to characterize this

family of ionic liquids, their melting point and decomposition temperatures were determined. Their physicochemical properties were also measured – namely, the density and the viscosity as a function of temperature- provided the samples are liquid at about room temperature and large enough quantities are available.

## Experimental

### Materials

The eighteen ionic liquids used in this study were synthesized following the procedure described below. These include  $[C_n\text{mim}][C_1\text{SO}_3]$ ,  $n = 1-6, 8$  or  $10$ ;  $[C_n\text{mim}][C_2\text{SO}_3]$ ,  $n = 2-6$ ;  $[C_n\text{mim}][C_3\text{SO}_3]$ ,  $n = 2$  or  $3$ ;  $[C_n\text{mim}][C_4\text{SO}_3]$ ,  $n = 2$  or  $3$ ; and  $[C_2\text{mim}][C_6\text{SO}_3]$  (see Figure 1).

1-Methylimidazole ( $\geq 99\%$ ), dichloromethane, ethyl ethanoate, ethyl methanesulfonate ( $\geq 98\%$ ), ethanesulfonyl chloride ( $\geq 99\%$ ), 1-propanesulfonyl chloride ( $\geq 98\%$ ), 1-butan-1-ylsulfonyl chloride ( $\geq 98\%$ ), 1-propanol ( $\geq 99.8\%$ ), 1-butanol ( $\geq 99.8\%$ ), 1-hexanol ( $\geq 99.5\%$ ), 1-octanol ( $\geq 99\%$ ), 1-decanol ( $\geq 99\%$ ), sodium hexanesulfonate (98%), and trimethylamine ( $\geq 99\%$ ) were purchased from Aldrich. Methyl methanesulfonate,  $\text{CH}_3\text{SO}_3\text{CH}_3$ , (99%) was purchased from Acros Organics. All purity values listed above are given as a mole fraction.

### General procedure 1

The different ionic liquids were prepared as follows:

a) The desired alkyl-1-ol ( $C_nH_{2n+1}OH$ ;  $n = 2 \dots 10$ ) (1.1 mol eq.) and triethylamine (1.1 mol eq.) dissolved in dichloromethane ( $430 \text{ cm}^3$ ) were placed in a round-bottomed flask and stirred vigorously. The mixture was cooled in an ice-bath, and alkylsulfonyl chloride ( $C_kH_{2k+1}SO_2Cl$ ,  $k = 1-4$ , or  $6$ ) (1 mol eq.) dissolved in dichloromethane ( $100 \text{ cm}^3$ ) was added dropwise to maintain the reaction temperature below  $0^\circ\text{C}$ . The reaction mixture was then stirred for several hours at room temperature (monitored by  $^1\text{H-NMR}$ ). Filtration of triethylammonium chloride and removal of dichloromethane yielded the corresponding alkyl alkanesulfonate esters ( $C_nH_{2n+1}OSO_2C_kH_{2k+1}$ ) which were obtained as colourless liquids after purification by fractional vacuum distillation.

b) The freshly distilled alkyl alkanesulfonate esters ( $C_nH_{2n+1}SO_3C_kH_{2k+1}$ ) (1.1 mol eq.) and 1-methylimidazole (1 mol eq.) were placed in a round-bottomed flask and dissolved in ethyl ethanoate ( $150 \text{ cm}^3$ ). The reaction mixture was stirred under reflux for several hours. Upon completion of the reaction, the crude products (ionic liquid layer) were washed 6 times with ethyl ethanoate and the remaining solvent removed under reduced pressure to yield the corresponding ionic liquids  $[C_nH_{2n+1}\text{mim}][C_kH_{2k+1}\text{SO}_3]$ .

$^1\text{H}$  and  $^{13}\text{C}$  NMR analyses showed no major impurities in the untreated, original samples, except for the presence of residual water (detected independently by Karl-Fischer analysis). All NMR spectra were recorded at room temperature on a Bruker Avance spectrometer DPX 300, using deuteriated chloroform as solvent. They are given together with mass spectroscopy results in Appendix 2. All samples were then further thoroughly degassed and dried to remove any small traces of volatile compounds by applying vacuum (*ca.* 0.1 Pa) at moderate temperatures (60–80 °C) for typically 24 h.

#### Melting point measurements

The melting points of the synthesized ionic liquids were measured by differential scanning calorimetry, using a Modulated DSC 2920 from TA Instruments. Cooling was accomplished by using a refrigerated cooling system capable of controlling the temperature down to 220 K. Dry nitrogen gas, with a flow rate of approximately 20 mL min<sup>-1</sup> was purged through the DSC cell.

Different experimental procedures were followed depending on the ionic liquids. Because some samples could remain liquid well below their melting points as metastable, supercooled melts, the procedure used to measure melting points and/or crystallization temperatures was different from sample to sample. For 1-alkyl-3-methylimidazolium alkanesulfonate that are solid at room temperature a standard heating and cooling ramp of 5 Kmin<sup>-1</sup> was used for determination of their melting points. For those that are liquids or metastable liquids at room temperature much lower cooling and heating rates were used, namely from 0.2 up to 1 Kmin<sup>-1</sup>. Both the onset and the peak melting temperatures were measured and, for each ionic liquid, the enthalpy of fusion was determined by integration of the experimental heat flow curves as functions of temperature.

In some cases ([C<sub>2</sub>mim][C<sub>2</sub>SO<sub>3</sub>], [C<sub>2</sub>mim][C<sub>3</sub>SO<sub>3</sub>], [C<sub>2</sub>mim][C<sub>4</sub>SO<sub>3</sub>], and [C<sub>6</sub>mim][C<sub>1</sub>SO<sub>3</sub>] ionic liquids) it was impossible to detect the phase transitions (crystallisation and melting) using the DSC cell. The melting points of those samples were then determined visually in a glass vial by slow heating (the temperature considered was that of the disappearance of the last crystal). In this case, the uncertainty of the melting point temperatures ( $\pm 3$  K in most cases) is much greater than that of measurements in the DSC cell.

#### Thermogravimetric Analysis

Decomposition temperature measurements were performed in a Thermogravimetric Analyzer, TGA Q50. The temperature calibration of the instrument was carried out by

analyzing high purity magnetic standard for its Curie temperature. The measurements were done in platinum pans with a heating rate of 10 Kmin<sup>-1</sup> in air atmosphere. The onset of weight loss in each thermogram was used to determine the corresponding decomposition temperature.

#### Density Measurements

Density was measured with an Anton Paar vibrating tube densimeter, model DMA 5000, operating at atmospheric pressure and within the temperature range (293 to 333) K. The internal calibration of the instrument was confirmed by measuring the densities of atmospheric air and bi-distilled water, according to the recommendations of the manufacturer. The DMA 5000 cell is embedded in a metallic block, the temperature of which is controlled by several Peltier units. This arrangement allows a temperature stability better than  $\pm 2$  mK. Under these operating conditions, we found that the repeatability of the density measurements was better than 0.05 kgm<sup>-3</sup> and the expanded uncertainty was estimated as ranging from  $\pm 0.3$  kgm<sup>-3</sup> to  $\pm 2$  kgm<sup>-3</sup> for low-viscosity and high-viscosity samples, respectively<sup>12</sup>. All reported density data were corrected for the effect of viscosity on density determinations with a vibrating tube densimeter, according to the empirical equation,  $(\rho - \rho_{\text{raw}}) / \rho_{\text{raw}} = (0.5 - 0.45 (\eta/\text{mPa s})^{0.5})10^{-4}$ , where  $\rho$  and  $\rho_{\text{raw}}$  are the corrected and measured (raw) densities, respectively, and  $\eta$  is the sample viscosity.<sup>12</sup> Herein, the correction can be as high as 1.7 kg m<sup>-3</sup> for samples with viscosities greater than 1700 mPa s.

All ionic liquids used in the density determinations were degassed under vacuum and moderate temperature conditions for periods longer than 24 hours and maintained in sealed vials before being injected in the densimeter using non-lubricated disposable syringes. Nine out of the eighteen synthesized ionic liquids were available in large enough quantities as liquids near room temperature conditions to perform the density measurements. The studied samples were [C<sub>2</sub>mim][C<sub>1</sub>SO<sub>3</sub>], [C<sub>2</sub>mim][C<sub>2</sub>SO<sub>3</sub>], [C<sub>2</sub>mim][C<sub>4</sub>SO<sub>3</sub>], [C<sub>3</sub>mim][C<sub>1</sub>SO<sub>3</sub>], [C<sub>3</sub>mim][C<sub>2</sub>SO<sub>3</sub>], [C<sub>3</sub>mim][C<sub>4</sub>SO<sub>3</sub>], [C<sub>4</sub>mim][C<sub>1</sub>SO<sub>3</sub>], [C<sub>6</sub>mim][C<sub>1</sub>SO<sub>3</sub>], and [C<sub>8</sub>mim][C<sub>1</sub>SO<sub>3</sub>].

#### Viscosity Measurements

The viscosity was determined using a rheometer, Rheometrics Scientific SR200, that allows measurements from (293 to 393) K at atmospheric pressure, and in a wide viscosity range (from 1 to 3000 mPa s) depending on the geometry used. A Couette geometry (concentric cylinders) was chosen for this study. Temperature was maintained constant to within 0.01 K by means of a recirculating bath and was measured with the

same accuracy using a PRT calibrated against a secondary reference temperature standard from Hart Scientific (model 5612, accuracy of  $\pm 0.018^\circ\text{C}$  at  $0^\circ\text{C}$ ). To decrease the water contamination of the sample during the measurements, the rheometer was placed inside a glove-box in an isolating atmosphere of purified and dried air. In order to improve the accuracy of the viscosity measurements, the rheometer was calibrated, as a function of temperature, with high viscosity standard oils N100 from Cannon Instruments Company (280 mPa s at 293 K).

Viscosity measurements were performed in steps of approximately 10 K from 293 K up to 360 K in all the ionic liquid samples in which a sufficient amount (approximately 13 mL) was available. Similar measurements done before in the same equipment<sup>13</sup> permitted a statistical analysis of the results that has indicated a precision in the viscosities of 0.2% and an overall uncertainty lower than 1%. The same precision cannot be claimed in the present measurements. It was observed that the ionic liquid samples were highly hygroscopic and, even when all the appropriate precautions were taken, water uptake by the samples could nevertheless be detected. The effect of this water uptake was evaluated by measuring the viscosity of the ionic liquid samples at regular time intervals. By the analysis of the values obtained, which implied a decrease of the viscosity by less than 10% after 10 hours of viscosity measurements at temperatures from 295 to 360 K, the overall uncertainty of the present measurements can be estimated as being always better than 5%.

Eight out of the eighteen synthesized ionic liquids were available in large enough quantities as liquids near room temperature conditions to perform the viscosity measurements. The studied samples were [C<sub>2</sub>mim][C<sub>1</sub>SO<sub>3</sub>], [C<sub>2</sub>mim][C<sub>2</sub>SO<sub>3</sub>], [C<sub>2</sub>mim][C<sub>4</sub>SO<sub>3</sub>], [C<sub>3</sub>mim][C<sub>1</sub>SO<sub>3</sub>], [C<sub>3</sub>mim][C<sub>2</sub>SO<sub>3</sub>], [C<sub>3</sub>mim][C<sub>4</sub>SO<sub>3</sub>], [C<sub>4</sub>mim][C<sub>2</sub>SO<sub>3</sub>], and [C<sub>10</sub>mim][C<sub>1</sub>SO<sub>3</sub>].

## Results and Discussion

The melting points measured for the ionic liquids studied are reported in Table 1. No clear pattern was found in the variation of the melting point temperatures. The majority of the ionic liquids studied have melting temperatures above ambient, except in the cases of [C<sub>2</sub>mim][C<sub>3</sub>SO<sub>3</sub>], [C<sub>2</sub>mim][C<sub>6</sub>SO<sub>3</sub>] and [C<sub>3</sub>mim][C<sub>2</sub>SO<sub>3</sub>] that have melting points below 20°C. Three other ionic liquids – [C<sub>2</sub>mim][C<sub>1</sub>SO<sub>3</sub>], [C<sub>2</sub>mim][C<sub>2</sub>SO<sub>3</sub>] and [C<sub>3</sub>mim][C<sub>4</sub>SO<sub>3</sub>] – have melting points close to 30°C and all other 1-alkyl-3-



methylimidazolium alkanesulfonate ionic liquids melt at higher temperatures with a maximum of 91 °C for [C<sub>1</sub>mim][C<sub>1</sub>SO<sub>3</sub>].

This somehow irregular behaviour of the melting point temperatures with the structure of the ionic liquid can also be found in other families of ionic liquids where the size of the alkyl chain varies in the anion. It is the case of 1-ethyl-3-methylimidazolium alkanesulfate ionic liquids<sup>10</sup>, [C<sub>2</sub>mim][C<sub>k</sub>SO<sub>4</sub>], where the melting point temperature varies in a non-monotonous way from ≤ - 65 °C for [C<sub>2</sub>mim][C<sub>2</sub>SO<sub>4</sub>]<sup>10</sup>, 23-25 °C for [C<sub>2</sub>mim][C<sub>4</sub>SO<sub>4</sub>], 7 °C for [C<sub>2</sub>mim][C<sub>6</sub>SO<sub>4</sub>], up to 79 °C for [C<sub>2</sub>mim][C<sub>8</sub>SO<sub>4</sub>]<sup>14</sup>. These observations contrast with the regular, and relatively easy to explain, variation of the melting point temperature of 1-alkyl-3-methylimidazolium tetrafluoroborate ionic liquids with the size of the alkyl chain in the cation.<sup>15</sup> A non-monotonous dependence of melting temperature on alkyl side-chain length is expected to be related to different crystal structures adopted by the salts. As such, this property should give more information about the stability of the solid phase than about the structure of the liquid.

The enthalpies of fusion were determined by integration of the experimental curves and are also reported in Table 1. The higher value was found for [C<sub>10</sub>mim][C<sub>1</sub>SO<sub>3</sub>] with approximately 38 kJmol<sup>-1</sup>, the majority of the samples studied having enthalpies of fusion between 14 and 22 kJmol<sup>-1</sup>.

Decomposition temperatures (onset of weight loss in the thermogravimetric run) are reported in Table 2. The ionic liquids studied have shown good thermal stability, with decomposition temperatures ranging from 330 to 380 °C. For comparison, the decomposition temperature of 1-ethyl-3-methylimidazolium ethanesulfate ionic liquids (ECOENG 212) is also given in the table. The significantly lower decomposition temperature of 1-ethyl-3-methylimidazolium ethanesulfate (230 °C) in comparison to 1-ethyl-3-methylimidazolium ethanesulfonate (343 °C) confirms that [C<sub>k</sub>SO<sub>4</sub>]<sup>-</sup> anions are not stable at very high temperature and in the presence of traces of impurities (water, amines) they can undergo hydrolysis. The lack of a bridging oxygen atom between the alkyl and (-SO<sub>3</sub>) moieties makes 1-alkyl-3-methylimidazolium alkanesulfate ionic liquids resistant to hydrolysis at high temperature.

| <b>[C<sub>n</sub>mim]<br/>[C<sub>k</sub>SO<sub>3</sub>]</b> | <b>C<sub>1</sub>SO<sub>3</sub></b>                          |                               | <b>C<sub>2</sub>SO<sub>3</sub></b>                          |                               | <b>C<sub>3</sub>SO<sub>3</sub></b>                          |                               | <b>C<sub>4</sub>SO<sub>3</sub></b>                          |                               | <b>C<sub>6</sub>SO<sub>3</sub></b>                          |                               |
|-------------------------------------------------------------|-------------------------------------------------------------|-------------------------------|-------------------------------------------------------------|-------------------------------|-------------------------------------------------------------|-------------------------------|-------------------------------------------------------------|-------------------------------|-------------------------------------------------------------|-------------------------------|
|                                                             | MP                                                          | $\Delta_{\text{fus}}\text{H}$ | MP                                                          | $\Delta_{\text{fus}}\text{H}$ | MP                                                          | $\Delta_{\text{fus}}\text{H}$ | MP                                                          | $\Delta_{\text{fus}}\text{H}$ | MP                                                          | $\Delta_{\text{fus}}\text{H}$ |
|                                                             | $\frac{t_{\text{onset}}}{t_{\text{peak}}}/^{\circ}\text{C}$ | $\text{kJmol}^{-1}$           | $\frac{t_{\text{onset}}}{t_{\text{peak}}}/^{\circ}\text{C}$ | $\text{kJmol}^{-1}$           | $\frac{t_{\text{onset}}}{t_{\text{peak}}}/^{\circ}\text{C}$ | $\text{kJmol}^{-1}$           | $\frac{t_{\text{onset}}}{t_{\text{peak}}}/^{\circ}\text{C}$ | $\text{kJmol}^{-1}$           | $\frac{t_{\text{onset}}}{t_{\text{peak}}}/^{\circ}\text{C}$ | $\text{kJmol}^{-1}$           |
| <b>C<sub>1</sub>mim</b>                                     | 90.8<br>91.0                                                | 17.5                          |                                                             |                               |                                                             |                               |                                                             |                               |                                                             |                               |
| <b>C<sub>2</sub>mim</b>                                     | 22.5<br>30.6                                                | 16.0                          | 29 <sup>a</sup>                                             |                               | 40 <sup>a</sup>                                             |                               | 4 <sup>a</sup>                                              |                               | 14.1<br>19.1                                                | 12.4                          |
| <b>C<sub>3</sub>mim</b>                                     | 35.2<br>39.8                                                | 15.2                          | 17.1<br>19.0                                                | 14.0                          | 24.6<br>32.0                                                | 11.3                          | 45.1<br>47.2                                                | 20.8                          |                                                             |                               |
| <b>C<sub>4</sub>mim</b>                                     | 67.6<br>73.7                                                | 22.0                          | 53.2<br>57.3                                                | 19.6                          | 47.8<br>53.0                                                | 14.1                          |                                                             |                               |                                                             |                               |
| <b>C<sub>5</sub>mim</b>                                     | 69.9<br>76.7                                                | 21.9                          | 51.2<br>54.4                                                | 16.1                          |                                                             |                               |                                                             |                               |                                                             |                               |
| <b>C<sub>6</sub>mim</b>                                     | 47 <sup>a</sup>                                             |                               | 61.3<br>65.7                                                | 16.9                          |                                                             |                               |                                                             |                               |                                                             |                               |
| <b>C<sub>8</sub>mim</b>                                     | 34.6<br>38.4                                                | 33.9                          |                                                             |                               |                                                             |                               |                                                             |                               |                                                             |                               |
| <b>C<sub>10</sub>mim</b>                                    | 55.8<br>57.4                                                | 38.4                          |                                                             |                               |                                                             |                               |                                                             |                               |                                                             |                               |

<sup>a</sup> visually determined

**Table 1.** Values of the melting points, MP, and of the enthalpies of fusion,  $\Delta_{\text{fus}}\text{H}$ , for the 1-alkyl-3-methylimidazolium alkanesulfonate ionic liquids, [C<sub>n</sub>mim][C<sub>k</sub>SO<sub>3</sub>].

| <b>[C<sub>n</sub>mim][C<sub>k</sub>SO<sub>3</sub>]</b>  | <b>T<sub>d</sub> /<sup>o</sup>C</b> |
|---------------------------------------------------------|-------------------------------------|
| [C <sub>1</sub> mim] [C <sub>1</sub> SO <sub>3</sub> ]  | 380                                 |
| [C <sub>4</sub> mim] [C <sub>1</sub> SO <sub>3</sub> ]  | 352                                 |
| [C <sub>6</sub> mim] [C <sub>1</sub> SO <sub>3</sub> ]  | 337                                 |
| [C <sub>10</sub> mim] [C <sub>1</sub> SO <sub>3</sub> ] | 335                                 |
| [C <sub>2</sub> mim] [C <sub>2</sub> SO <sub>3</sub> ]  | 342                                 |
| [C <sub>2</sub> mim] [C <sub>4</sub> SO <sub>3</sub> ]  | 340                                 |
| [C <sub>3</sub> mim] [C <sub>4</sub> SO <sub>3</sub> ]  | 349                                 |
| [C <sub>2</sub> mim] [C <sub>2</sub> SO <sub>4</sub> ]  | 230                                 |

**Table 2.** Values of the decomposition temperatures,  $T_d$ , for the 1-alkyl-3-methylimidazolium alkanesulfonate ionic liquids,  $[C_n\text{mim}][C_k\text{SO}_3]$  and one alkanesulfate for comparison.

The viscosity-corrected density results are reported in Table 3, along with the corresponding molar volume,  $V$ , data for each studied ionic liquid. The temperature-dependence of the density data is fitted by a simple linear regression, and the fitting parameters are also shown in Table 3. The deviations between the fitted and experimental  $V_m$  data are smaller than 0.005 % – comparable to the repeatability of the measurements – which means that a  $\ln\rho = f(T)$  function more complex than a simple straight line is not warranted in this case (as in the case of ionic liquids in general<sup>16-18</sup>). The advantage of using a linear regression to fit  $\ln(\rho)$  values is that the thermal expansion coefficient,  $\alpha_T$ , for each ionic liquid will be a constant at a given pressure and it will be easy to obtain from the slope of the regression line: if  $\ln(\rho) = mT + b$  then  $d\ln(\rho)/dT = -\alpha_T = m$ . Figure 2 shows the values of  $\alpha_T$  for the eight ionic liquids where density data were measured at different temperatures (each ionic liquid can be identified by the slopes reported in Table 3). The plot shows that although the scatter of the  $\alpha_T$  values is much larger than that of the  $\rho$  data (the former quantity is a derived property of the latter), there is a correlation between the total number of carbon atoms in the alkyl side chain and the value of  $\alpha_T$ .

| T/K                                                                      | $\rho / \text{g cm}^{-3}$ | $V_m / \text{cm}^3 \text{mol}^{-1}$ | $\delta V_m / \text{cm}^3 \text{mol}^{-1}$ |
|--------------------------------------------------------------------------|---------------------------|-------------------------------------|--------------------------------------------|
| <b><math>[C_2\text{mim}][C_1\text{SO}_3]</math></b>                      |                           |                                     |                                            |
| $\ln(\rho / \text{g cm}^{-3}) = 0.3754 - 0.5370 \cdot 10^{-3} \cdot T/K$ |                           |                                     |                                            |
| 293.15                                                                   | 1.24347                   | 165.879                             | -0.005                                     |
| 298.15                                                                   | 1.24020                   | 166.317                             | 0.003                                      |
| 313.15                                                                   | 1.23027                   | 167.658                             | 0.006                                      |
| 333.15                                                                   | 1.21706                   | 169.478                             | -0.003                                     |
| <b><math>[C_2\text{mim}][C_2\text{SO}_3]</math></b>                      |                           |                                     |                                            |
| $\ln(\rho / \text{g cm}^{-3}) = 0.3439 - 0.5315 \cdot 10^{-3} \cdot T/K$ |                           |                                     |                                            |
| 293.15                                                                   | 1.20691                   | 182.526                             | 0.002                                      |
| 298.15                                                                   | 1.20366                   | 183.019                             | -0.006                                     |
| 313.15                                                                   | 1.19419                   | 184.470                             | 0.008                                      |
| 333.15                                                                   | 1.18149                   | 186.453                             | 0.003                                      |
| <b><math>[C_2\text{mim}][C_4\text{SO}_3]</math></b>                      |                           |                                     |                                            |
| $\ln(\rho / \text{g cm}^{-3}) = 0.2982 - 0.5524 \cdot 10^{-3} \cdot T/K$ |                           |                                     |                                            |
| 293.15                                                                   | 1.14601                   | 216.705                             | -0.002                                     |
| 298.15                                                                   | 1.14287                   | 217.301                             | 0.002                                      |
| 313.15                                                                   | 1.13343                   | 219.110                             | 0.001                                      |
| 333.15                                                                   | 1.12097                   | 221.545                             | -0.001                                     |
| <b><math>[C_3\text{mim}][C_1\text{SO}_3]</math></b>                      |                           |                                     |                                            |

|                                                        |                                                                               |         |        |
|--------------------------------------------------------|-------------------------------------------------------------------------------|---------|--------|
|                                                        | $\ln(\rho/\text{g cm}^{-3}) = 0.3462 - 0.5408 \cdot 10^{-3} \cdot T/\text{K}$ |         |        |
| 313.15                                                 | 1.19351                                                                       | 184.576 | 0      |
| 333.15                                                 | 1.18067                                                                       | 186.583 | 0      |
| <b>[C<sub>3</sub>mim][C<sub>2</sub>SO<sub>3</sub>]</b> |                                                                               |         |        |
|                                                        | $\ln(\rho/\text{g cm}^{-3}) = 0.3178 - 0.5373 \cdot 10^{-3} \cdot T/\text{K}$ |         |        |
| 293.15                                                 | 1.17383                                                                       | 199.619 | -0.001 |
| 298.15                                                 | 1.17071                                                                       | 200.152 | 0.003  |
| 313.15                                                 | 1.16128                                                                       | 201.778 | -0.003 |
| 333.15                                                 | 1.14889                                                                       | 203.954 | 0.001  |
| <b>[C<sub>3</sub>mim][C<sub>4</sub>SO<sub>3</sub>]</b> |                                                                               |         |        |
|                                                        | $\ln(\rho/\text{g cm}^{-3}) = 0.2779 - 0.5547 \cdot 10^{-3} \cdot T/\text{K}$ |         |        |
| 293.15                                                 | 1.12215                                                                       | 233.813 | -0.009 |
| 298.15                                                 | 1.11912                                                                       | 234.446 | 0.007  |
| 313.15                                                 | 1.10984                                                                       | 236.407 | 0.005  |
| 333.15                                                 | 1.09756                                                                       | 239.052 | -0.003 |
| <b>[C<sub>4</sub>mim][C<sub>2</sub>SO<sub>3</sub>]</b> |                                                                               |         |        |
|                                                        | (no fit)                                                                      |         |        |
| 333.15                                                 | 1.12170                                                                       | 221.401 | -      |
| <b>[C<sub>6</sub>mim][C<sub>1</sub>SO<sub>3</sub>]</b> |                                                                               |         |        |
|                                                        | $\ln(\rho/\text{g cm}^{-3}) = 0.2791 - 0.5613 \cdot 10^{-3} \cdot T/\text{K}$ |         |        |
| 293.15                                                 | 1.12137                                                                       | 233.976 | -0.006 |
| 298.15                                                 | 1.11828                                                                       | 234.622 | 0.006  |
| 313.15                                                 | 1.10889                                                                       | 236.610 | 0.002  |
| 333.15                                                 | 1.09649                                                                       | 239.285 | -0.002 |
| <b>[C<sub>8</sub>mim][C<sub>1</sub>SO<sub>3</sub>]</b> |                                                                               |         |        |
|                                                        | $\ln(\rho/\text{g cm}^{-3}) = 0.2489 - 0.5707 \cdot 10^{-3} \cdot T/\text{K}$ |         |        |
| 293.15                                                 | 1.08499                                                                       | 267.678 | 0.005  |
| 298.15                                                 | 1.08184                                                                       | 268.458 | -0.010 |
| 313.15                                                 | 1.07268                                                                       | 270.749 | 0.007  |
| 333.15                                                 | 1.06047                                                                       | 273.866 | -0.002 |

**Table 3.** Experimental values of the density,  $\rho$ , and molar volume,  $V_m$ , of 1-alkyl-3-methylimidazolium alkanesulfonate ionic liquids,  $[\text{C}_n\text{mim}][\text{C}_k\text{SO}_3]$ , at temperatures between (293.15 and 333.15) K. The  $\delta V_m$  values represent the difference between  $V_m$  values and molar volume data calculated using the fitting equations in parentheses.

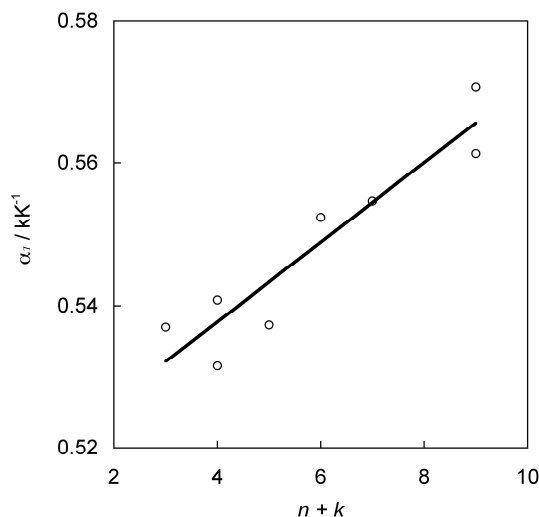


**Figure 2.** Thermal expansion coefficient,  $\alpha_T$ , as a function of the total number of carbon atoms,  $n + k$ , in the alkyl side chains of  $[\text{C}_n\text{mim}][\text{C}_k\text{SO}_3]$  ionic liquids, calculated from the density data obtained at atmospheric pressure.

The molar volume results show a striking, consistent trend along the series of 1-alkyl-3-methylimidazolium alkanesulfonate ionic liquids: as the number of methylene ( $-\text{CH}_2-$ ) groups present in the alkyl chains of the cation and/or the anion is increased, the corresponding molar volume values become equally larger per ( $-\text{CH}_2-$ ) group ( $17 \text{ cm}^3 \text{ mol}^{-1}$ ). To the best of our knowledge, it is shown herein for the first time that this change is irrespective of the ( $-\text{CH}_2-$ ) addition taking place in the cation or the anion. The added methylene groups will necessarily occupy some extra space – but the trend’s regularity is quite remarkable. An extra mole of methylene groups in the alkyl chains of a given ionic liquid of the family under study will always increase its molar volume by the same amount,  $17.06 \text{ cm}^3 \text{ mol}^{-1}$  at  $298.15 \text{ K}$ , irrespective of the ionic liquid itself. Moreover, this value compares favourably with a previous, multi-averaged determination of an increase of  $17.2 \pm 0.3 \text{ cm}^3 \text{ mol}^{-1}$  per ( $-\text{CH}_2-$ ) at  $298.15 \text{ K}$ <sup>17, 18</sup>.

Figure 3 depicts such behaviour, with the experimental molar volume points (in black) superimposed in a regular grid (white points) built taking into account only the number of methylene groups in the alkyl chains of the cation (x-axis) and the total number of methylene groups of the ionic liquid (secondary y-axis). As stated above, the nature of the family of ionic liquids studied in this work, where the size of the alkyl chains can be varied both in the anion and in the cation implies that it can be ordered not in a simple “row” but in a “matrix”. This fact is clearly denoted in Figure 3 by the above-mentioned regular grid of white points. The observation that all experimentally determined molar volumes fit that grid, with deviations always smaller than 0.2 %,

constitutes a proof of the additive character of the molar volume within this particular family of ionic liquids.

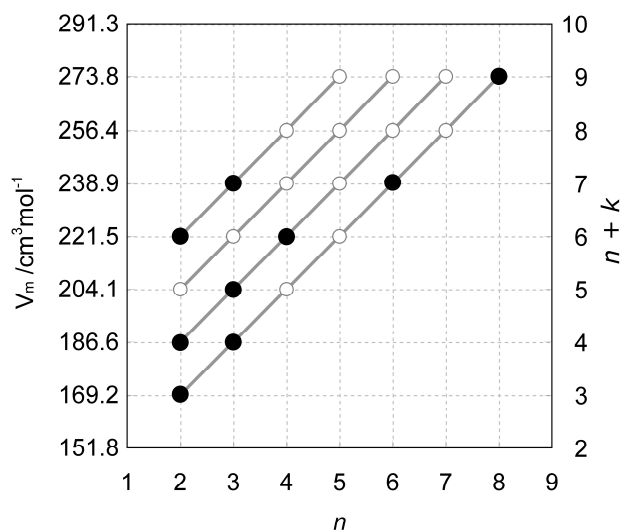


**Figure 3.** Molar volume of 1-alkyl-3-methylimidazolium alkanesulfonate,  $[C_n\text{mim}][C_k\text{SO}_3]$ , ionic liquids at 333.15 K (●) as a function of the number of carbon atoms in the alkyl chain of the cation (x-axis),  $n$ , and the total number of carbon atoms in the alkyl chains of both ions (secondary y-axis),  $(n + k)$ . The white dots represent other members of the 1-alkyl-3-methylimidazolium alkanesulfonate family whose density was not measured experimentally but can be estimated using the molar volume additive character within the family. The gray lines represent series of ionic liquids with the same number of carbon atoms in the anion, and have a slope, at 333.15 K, of  $17.45 \text{ cm}^3 \text{ mol}^{-1}$ .

The idea of estimating the density along a family of ionic liquids using the additive character of  $V_m$  via the sum of effective ion volumes was first proposed by Rebelo et al.<sup>18</sup> and further refined by other authors<sup>19-21</sup> who devised empirical group contribution methods (see Table 4). The present data confirm the general validity of those methods and extend their scope: i) alkanesulfonate-based ionic liquids were added to the list of compounds whose density can be estimated – at 298.15 K, the group,  $[C_o\text{SO}_3]^-$ , contributes with  $48.9 \text{ cm}^3 \text{ mol}^{-1}$  for those methods<sup>12,14</sup> (to be compared with  $[C_o\text{SO}_4]^- = 57.0 \text{ cm}^3 \text{ mol}^{-1}$  – taken as the difference between the molar volume of  $[C_2\text{SO}_4]^-$  and the volume of two methylene groups)<sup>20, 22</sup> where the contribution of the anion  $[\text{PF}_6]^-$  was postulated as  $73.7 \text{ cm}^3 \text{ mol}^{-1}$ ; and ii) most importantly, it was shown that these methods work not only by varying regularly the structure of one of the ions constituting the ionic liquid (along “row-like” families of ionic liquids) but also by

simultaneously changing the structure of the two ions (“matrix-like” ionic liquid families like in the 1-alkyl-3-methylimidazolium alkanesulfonate series).

|                             | Rebelo <i>et al.</i> <sup>22</sup>  | Ye and Shreeve <sup>19</sup> | Jacquemin <i>et al.</i> <sup>20</sup> | This work               |
|-----------------------------|-------------------------------------|------------------------------|---------------------------------------|-------------------------|
|                             | $V_m / \text{cm}^3 \text{mol}^{-1}$ |                              |                                       |                         |
| $[\text{C}_0\text{mim}]^+$  | 64.8 <sup>a</sup>                   | 75.9 <sup>b</sup>            | 66.0 <sup>a</sup>                     | <b>66.0<sup>a</sup></b> |
| $[\text{C}_0\text{SO}_3]^-$ | -                                   | -                            | -                                     | <b>48.9</b>             |
| $-\text{CH}_2-$             | 17.2                                | 16.9                         | 17.1                                  | <b>17.06</b>            |

<sup>a</sup> Scheme based on the hypothesis that in  $[\text{PF}_6]^-$ -based ionic liquids the contribution of  $[\text{PF}_6]^-$  to the molar volume is  $73.7 \text{ cm}^3 \text{mol}^{-1}$ .

<sup>b</sup> Scheme based on a contribution of  $[\text{PF}_6]^-$  equal to  $64.4 \text{ cm}^3 \text{mol}^{-1}$ .

**Table 4.** Effective molar volume of different constituent parts of 1-alkyl-3-methylimidazolium alkanesulfonate ionic liquids: extension of previously established contribution schemes for the estimation of the molar volume of ionic liquids. The molar volume of any ionic liquid  $[\text{C}_n\text{mim}][\text{C}_k\text{SO}_3]$  is estimated by adding the molar volumes of  $(n+k)$   $(-\text{CH}_2-)$  groups to the molar volumes of  $[\text{C}_0\text{mim}]^+$  and  $[\text{C}_0\text{SO}_3]^-$ . Values for  $T = 298.15 \text{ K}$ .

The results obtained for the viscosity of the ionic liquid samples are included in Table 5. It is observed that the ionic liquid samples based on the sulfonate anion are quite viscous with values ranging from 17 mPa·s for  $[\text{C}_2\text{mim}][\text{C}_2\text{SO}_3]$  at 356 K to 1055 mPa·s for  $[\text{C}_2\text{mim}][\text{C}_4\text{SO}_3]$  at 296 K. These values are similar to the ones found for alkylsulfate based ionic liquids or for  $[\text{C}_4\text{mim}][\text{PF}_6]$  as can be observed in Figure 4.

The experimental viscosities were correlated with temperature using both an Arrhenius-like law:

$$\eta = \eta_\infty \exp(-E_a/RT) \quad (1)$$

and a Vogel-Fulcher-Tamman (VFT) equation:

$$\eta = AT^{0.5} \exp(B/(T - T_0)) \quad (2)$$

where  $\eta_\infty$  is the viscosity at infinite temperature and  $E_a$  is the viscosity activation energy, two characteristic parameters adjusted from experimental data as a function of temperature. A, B and  $T_0$  in equation (2) are three adjustable parameters. Table 6 lists the parameters for the ionic liquids studied in the present case together with the standard relative deviations of the fits.

The viscosity of alkanesulfonate based ionic liquids decreases very rapidly with increasing temperature. For example, for  $[\text{C}_3\text{mim}][\text{C}_4\text{SO}_3]$ , one of the more viscous ionic liquids studied in this work, the viscosity decreases one order of magnitude when the temperature changes from 296 K to 330 K. This behavior is also found for

[C<sub>10</sub>mim][C<sub>1</sub>SO<sub>3</sub>], a solid at room temperature, for which the viscosity decreases four times when increasing the temperature from 326 K to 355 K.

| <i>T</i> / K                                            | $\eta$ / mPa s | Dev / % |
|---------------------------------------------------------|----------------|---------|
| <b>[C<sub>2</sub>mim] [C<sub>1</sub>SO<sub>3</sub>]</b> |                |         |
| 295.06                                                  | 184.73         | + 0.14  |
| 302.57                                                  | 113.87         | + 0.00  |
| 312.07                                                  | 68.24          | - 0.08  |
| 321.51                                                  | 45.45          | - 0.09  |
| 330.97                                                  | 31.53          | - 0.08  |
| 345.13                                                  | 20.25          | + 0.00  |
| 359.22                                                  | 14.07          | + 0.12  |
| <b>[C<sub>2</sub>mim] [C<sub>2</sub>SO<sub>3</sub>]</b> |                |         |
| 296.11                                                  | 233.61         | + 0.11  |
| 302.61                                                  | 153.51         | + 0.01  |
| 312.08                                                  | 91.71          | - 0.06  |
| 321.58                                                  | 58.53          | - 0.08  |
| 331.02                                                  | 40.36          | - 0.06  |
| 345.17                                                  | 25.14          | + 0.01  |
| 357.08                                                  | 17.65          | + 0.09  |
| <b>[C<sub>2</sub>mim] [C<sub>4</sub>SO<sub>3</sub>]</b> |                |         |
| 296.37                                                  | 531.41         | + 0.15  |
| 302.53                                                  | 328.18         | + 0.02  |
| 312.00                                                  | 175.52         | - 0.08  |
| 321.44                                                  | 103.50         | - 0.11  |
| 330.93                                                  | 66.57          | - 0.09  |
| 345.05                                                  | 37.95          | - 0.01  |
| 359.25                                                  | 23.88          | + 0.14  |
| <b>[C<sub>3</sub>mim] [C<sub>1</sub>SO<sub>3</sub>]</b> |                |         |
| 302.55                                                  | 236.95         | + 0.11  |
| 312.01                                                  | 129.09         | - 0.02  |
| 321.52                                                  | 77.49          | - 0.07  |
| 331.00                                                  | 50.17          | - 0.08  |
| 345.14                                                  | 29.31          | - 0.02  |



|                                                          |         |        |
|----------------------------------------------------------|---------|--------|
| 359.25                                                   | 18.92   | + 0.09 |
| <b>[C<sub>3</sub>mim] [C<sub>2</sub>SO<sub>3</sub>]</b>  |         |        |
| 295.29                                                   | 566.08  | + 0.13 |
| 302.51                                                   | 329.97  | + 0.01 |
| 312.02                                                   | 179.24  | - 0.06 |
| 321.45                                                   | 105.48  | - 0.10 |
| 330.89                                                   | 67.01   | - 0.08 |
| 345.06                                                   | 37.95   | + 0.00 |
| 359.22                                                   | 23.48   | + 0.13 |
| <b>[C<sub>3</sub>mim] [C<sub>4</sub>SO<sub>3</sub>]</b>  |         |        |
| 295.92                                                   | 1054.72 | + 0.20 |
| 302.52                                                   | 562.62  | - 0.02 |
| 312.00                                                   | 293.88  | - 0.08 |
| 321.44                                                   | 166.49  | - 0.10 |
| 330.95                                                   | 99.94   | - 0.09 |
| 345.14                                                   | 53.03   | - 0.01 |
| 359.25                                                   | 31.72   | + 0.15 |
| <b>[C<sub>4</sub>mim] [C<sub>2</sub>SO<sub>3</sub>]</b>  |         |        |
| 326.32                                                   | 100.89  | + 0.02 |
| 335.79                                                   | 64.49   | - 0.02 |
| 345.27                                                   | 44.50   | - 0.01 |
| 354.66                                                   | 31.58   | + 0.01 |
| <b>[C<sub>10</sub>mim] [C<sub>1</sub>SO<sub>3</sub>]</b> |         |        |
| 326.17                                                   | 248.52  | + 0.01 |
| 335.68                                                   | 149.88  | + 0.00 |
| 345.12                                                   | 91.05   | - 0.03 |
| 354.56                                                   | 62.01   | + 0.02 |

**Table 5.** Experimental values of the viscosity of [C<sub>2</sub>mim][C<sub>1</sub>SO<sub>3</sub>], [C<sub>2</sub>mim][C<sub>2</sub>SO<sub>3</sub>], [C<sub>2</sub>mim][C<sub>4</sub>SO<sub>3</sub>], [C<sub>3</sub>mim][C<sub>1</sub>SO<sub>3</sub>], [C<sub>3</sub>mim][C<sub>2</sub>SO<sub>3</sub>], [C<sub>3</sub>mim][C<sub>4</sub>SO<sub>3</sub>], [C<sub>4</sub>mim][C<sub>2</sub>SO<sub>3</sub>] and [C<sub>12</sub>mim][C<sub>1</sub>SO<sub>3</sub>] at temperatures between (295 and 360) K. The deviations are relative to the fit of the data using equation (1).

In the family of alkyimidazolium alkanesulfonate ionic liquids it is observed that the viscosity of the ionic liquids increases, as expected, when the alkyl chain increases, both/either in the cation and/or in the anion. This effect can be observed in

Figure 5 where the increase in viscosity is represented, at 323 K, as a function of the number of carbon atoms in the alkyl chains both in the cation and in the anion that compose the ionic liquid. The viscosity increases when the number of carbon atoms in the alkyl chain of the cation increases from [C<sub>2</sub>mim]<sup>+</sup> to [C<sub>4</sub>mim]<sup>+</sup>. This increase of the viscosity, although smaller than in the present case, had also been observed by Tokuda et al.<sup>4</sup> for the viscosity of 1-alkyl-3-methylimidazolium bis(trifluoromethyl)sulfonyl imide ionic liquids. Herein, an increase of the viscosity by 25 to 50 mPas is observed with the increase of one extra carbon atom in the alkyl side-chain of the 1-alkyl-3-methylimidazolium cation.

|                                                         | Arrhenius-type equation (1)     |                                |            | VFT equation (2)                        |         |           |            |
|---------------------------------------------------------|---------------------------------|--------------------------------|------------|-----------------------------------------|---------|-----------|------------|
|                                                         | $\eta_{\infty}/10^{-6}$<br>mPas | $-E_a$<br>/kJmol <sup>-1</sup> | $\sigma_r$ | $A / 10^{-3}$<br>mPa s K <sup>1/2</sup> | $B / K$ | $T_0 / K$ | $\sigma_r$ |
| [C <sub>2</sub> mim] [C <sub>1</sub> SO <sub>3</sub> ]  | 97.92                           | 35.12                          | 0.11       | 19.68                                   | 555.0   | 207.0     | 0.01       |
| [C <sub>2</sub> mim] [C <sub>2</sub> SO <sub>3</sub> ]  | 62.54                           | 37.00                          | 0.08       | 11.71                                   | 711.5   | 195.2     | 0.01       |
| [C <sub>2</sub> mim] [C <sub>4</sub> SO <sub>3</sub> ]  | 9.859                           | 43.52                          | 0.12       | 11.82                                   | 728.8   | 203.7     | 0.01       |
| [C <sub>3</sub> mim] [C <sub>1</sub> SO <sub>3</sub> ]  | 25.69                           | 40.08                          | 0.09       | 6.119                                   | 837.9   | 193.8     | 0.02       |
| [C <sub>3</sub> mim] [C <sub>2</sub> SO <sub>3</sub> ]  | 8.869                           | 43.81                          | 0.10       | 7.613                                   | 849.7   | 193.8     | 0.03       |
| [C <sub>3</sub> mim] [C <sub>4</sub> SO <sub>3</sub> ]  | 2.554                           | 48.37                          | 0.13       | 8.506                                   | 812.2   | 204.4     | 0.05       |
| [C <sub>4</sub> mim] [C <sub>2</sub> SO <sub>3</sub> ]  | 50.72                           | 39.30                          | 0.02       | 7.543                                   | 843.7   | 198.6     | 0.01       |
| [C <sub>10</sub> mim] [C <sub>1</sub> SO <sub>3</sub> ] | 6.227                           | 47.44                          | 0.02       | 9.847                                   | 844.5   | 209.6     | 0.04       |

**Table 6.** Correlation parameters of the Arrhenius-like equation (1) and of the VFT equation (2) with the deviations of the fit  $\sigma_r$  for the viscosity of studied ionic liquids as a function of temperature, determined from experimental values between 295 and 360 K.

$$\sigma_r = \left( \frac{\sum_i [(\eta_i^{\text{exp}} - \eta_i^{\text{calc}}) / \eta_i^{\text{calc}}]^2}{n - \nu} \right)^{0.5}$$

where  $n$  is the number of experimental points and  $\nu$  the number of adjustable parameters.

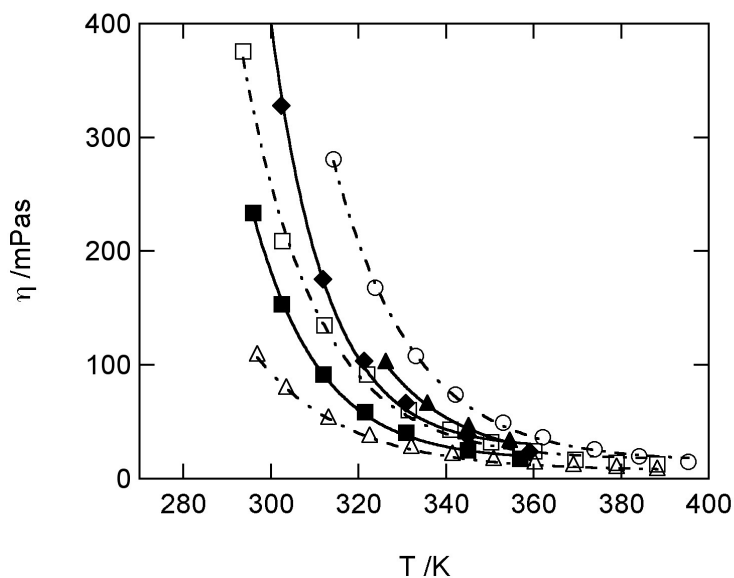


**Figure 4.** Experimental viscosities as a function of temperature. (O),  $[\text{C}_4\text{mim}][\text{C}_8\text{SO}_4]^{23}$ ; (□),  $[\text{C}_4\text{mim}][\text{PF}_6]^{13}$ ; (△),  $[\text{C}_2\text{mim}][\text{C}_2\text{SO}_4]^{13}$ ; (◆),  $[\text{C}_2\text{mim}][\text{C}_4\text{SO}_3]$ , this work; (▲),  $[\text{C}_4\text{mim}][\text{C}_2\text{SO}_3]$ , this work; (■),  $[\text{C}_2\text{mim}][\text{C}_2\text{SO}_3]$ , this work.

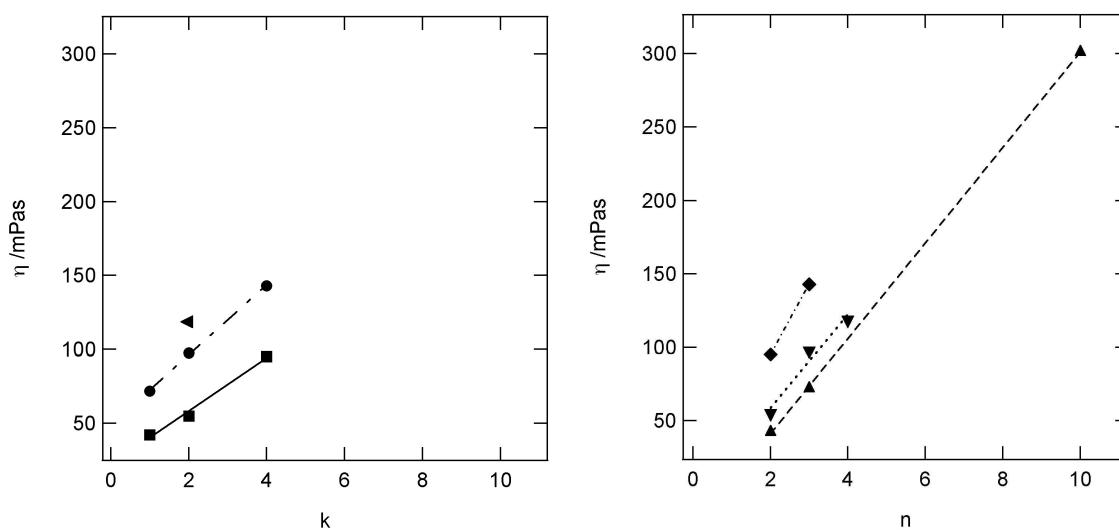


**Figure 5.** Variation of the viscosity at 323 K with the number of carbon atoms in the alkyl chains in the cation,  $n$ , and in the anion,  $k$ , forming the ionic liquid.

*Left plot:* Variation of viscosity with the number of carbon atoms in the alkyl chain of the sulfonate anion,  $k$ . ■,  $[\text{C}_2\text{mim}][\text{C}_k\text{SO}_3]$ ; ●,  $[\text{C}_3\text{mim}][\text{C}_k\text{SO}_3]$ ; ◄,  $[\text{C}_4\text{mim}][\text{C}_k\text{SO}_3]$ .  
*Right plot:* Variation of viscosity with the number of carbon atoms in the alkyl side-chain of the 1-alkyl-3-methylimidazolium cation,  $n$ . ▲,  $[\text{C}_n\text{mim}][\text{C}_1\text{SO}_3]$ ; ▼,  $[\text{C}_n\text{mim}][\text{C}_2\text{SO}_3]$ ; ◆,  $[\text{C}_n\text{mim}][\text{C}_3\text{SO}_3]$ .

The size of the alkyl side chain in the alkanesulfonate anion also influences the viscosity of the ionic liquids studied in this work. The viscosity increases by  $13 \pm 1$  mPas or by  $22 \pm 0.5$  mPas *per* extra carbon atom in the alkyl chain of the anion for [C<sub>2</sub>mim] based ionic liquids and [C<sub>3</sub>mim] based ionic liquids, respectively. This behavior confirms that, although the high-electrostatic interactions between ions determine the characteristic physico-chemical properties of ionic liquids, dispersive, van der Waals-type forces also play an important role and determine the way the viscosity changes with the size of the alkyl-side chain. Furthermore, this study confirms that the formation of non-polar molecular domains, dominated by van der Waals-type molecular interactions, determine the variation of viscosity in a family of ionic liquids and is observed when both/either the alkyl chain increases in the cation and/or in the anion. However, their impact in equilibrium (e.g. molar volume) versus transport (e.g. viscosity) properties is contrasting. While (ideal) additive behaviour is observed for the first, a much more complex response is found for the latter.

## Conclusions

A new family of ionic liquids, 1-alkyl-3-methylimidazolium alkanesulfonates, was synthesized and characterized for the first time. A possible way to place this study in perspective is to compare this family of ionic liquids with the corresponding alkanesulfates. Whereas the density and the viscosity show similar behaviour in both families, the thermal stability of alkanesulfonates shows a much better performance. However, the low-temperature limit favours the alkanesulfates that by and large have lower melting point temperatures. These differences constitute a relevant issue as far as the liquid state temperature range is concerned.

The systematic determination of selected thermodynamic properties along these exclusive families of ionic liquids – where the size of the alkyl side chain of both ions can be varied simultaneously to yield a “matrix” of pure ionic liquids – exposed different trends that can be interpreted taking into account the complex structure of ionic liquids, namely the existence of polar and non-polar nano-domains. A more complete analysis of the structural features of these families of ionic liquids is one of the future objectives of the current line of research. This includes, for example, the

study of non-isotropic phases in systems with longer alkyl side chains or the relation between structure and transport properties like viscosity or diffusion coefficients.

We anticipate that the introduction of alkanesulfonate-based ionic liquids – or other families with similar “matrix-like” structural characteristics – will promote the systematic study of the complex relation between the nano-structured molecular nature and the unique macroscopic thermodynamic properties of ionic liquids.

### Acknowledgements

This work was supported by the Fundação para a Ciência e Tecnologia (*FC&T*), Portugal (Projects POCTI/QUI/35413/2000, POCI/QUI/57716/2004). MB thanks *FC&T* for a Ph.D. grant (SFRH/BD/13763/2003) and Marie Curie Fellowships for Early Stage Research Training (EST No505613). KRS thanks the EPSRC (Portfolio Partnership Scheme, grant no. EP/D029538/1). AAHP and MFCG are thankful to the Oeiras City Hall for the attribution of Prof. António Xavier Fellowships – *Grants of Excellence*.

### References

1. N. V. Plechkova and K. R. Seddon, *Chemical Society Reviews*, 2008, **37**, 123-150.
2. J. N. Canongia Lopes and A. A. H. Padua, *J. Phys. Chem. B*, 2006, **110**, 3330-3335.
3. A. A. H. Padua, M. F. Costa Gomes and J. N. A. Canongia Lopes, *Acc. Chem. Res.*, 2007, **40**, 1087-1096.
4. H. Tokuda, K. Hayamizu, I. Kunikazu, M. A. B. H. Susan and M. Watanabe, *J. Phys. Chem. B*, 2005, **109**, 6103-6110.
5. A. Paul, P. K. Mandal and A. Samanta, *J. Phys. Chem. B*, 2005, **109**, 9148-9153.
6. J. L. Anderson and D. W. Armstrong, *Anal. Chem.*, 2003, **75**, 4851-4858.
7. S. Shigeto and H. Hamaguchi, *Chem. Phys. Lett*, 2006, **427**, 329-332.
8. Y. U. Paulechka, A. V. Blokhin, G. J. Kabo and A. A. Strechan, *J. Chem. Thermodynamics*, 2007, **39**, 866-877.
9. P. Wasserscheid, R. van Hal and A. Bösmann, *Green Chemistry*, 2002, **4**, 400-404.

10. J. D. Holbrey, W. M. Reichert, R. P. Swatloski, G. A. Broker, W. R. Pitner, K. R. Seddon and R. D. Rogers, *Green Chemistry*, 2002, **4**, 407-413.
11. E. F. Borra, O. Seddiki, R. Angel, D. Eisenstein, P. Hickson, K. R. Seddon and S. P. Worden, *Nature*, 2007, **447**, 979-981.
12. J. M. S. S. Esperança, H. J. R. Guedes, J. N. Canongia Lopes and L. P. N. Rebelo, *J. Chem. Eng. Data*, 2008, **53**, 867-870.
13. J. Jacquemin, P. Husson, A. A. H. Padua and V. Majer, *Green Chemistry*, 2006, **8**, 172-180.
14. Solvent Innovation, [www.solventinnovation.com](http://www.solventinnovation.com)
15. J. D. Holbrey and K. R. Seddon, *J. Chem. Soc., Dalton Trans.*, 1999, 2133.
16. J. W. Magee and J. A. Widegren, *J. Chem. Eng. Data*, 2007, **52**, 2331-2338.
17. J. M. S. S. Esperança, H. J. R. Guedes, M. Blesic and L. P. N. Rebelo, *J. Chem. Eng. Data*, 2006, **51**, 237-242.
18. L. P. N. Rebelo and e. al., *Phase behavior and thermodynamic properties of ionic liquids, ionic liquid mixtures and ionic liquid solutions.*, American Chemical Society, Washington, D.C., 2005.
19. C. F. Ye and J. M. Shreeve, *J. Phys. Chem. A*, 2007, **111**, 1456-1461.
20. J. Jacquemin, P. Ge, P. Nancarrow, D. Rooney, M. F. Costa Gomes, A. A. H. Padua and C. Hardacre, *J. Chem. Eng. Data*, 2008, **53**, 716-726.
21. R. L. Gardas and J. A. P. Coutinho, *Fluid Phase Equilibria*, 2008, **263**, 26-32.
22. L. P. N. Rebelo, J. N. Canongia Lopes, J. M. S. S. Esperança, J. Lachwa, H. J. R. Guedes, V. Najdanivic-Visak and Z. Visak, *Accounts of Chemical Research*, 2007, **40**, 1114-1121.
23. J. Jacquemin, P. Husson, V. Majer, A. A. H. Padua and M. F. Costa Gomes, *Green Chem.*, 2008, submitted.

## **CHAPTER 4.**

**ANION AND CATION EFFECTS ON THE  
SELF-AGGREGATION OF  
1-ALKYL-3-METHYLIMIDAZOLIUM  
ALKYLSULFONATE,  
[C<sub>n</sub>H<sub>2n+1</sub>mim][C<sub>m</sub>H<sub>2m+1</sub>SO<sub>3</sub>],  
IONIC LIQUID SURFACTANTS**

*This Chapter was submitted as a full article:*

Blesic M., Swadzba-Kwasny M., Holbrey J.D., Seddon K.R., Rebelo L.P.N.,  
“ Anion and Cation Effects on the Self-Aggregation of  
1-Alkyl-3-Methylimidazolium Alkylsulfonate,  $[C_nH_{2n+1}mim][C_mH_{2m+1}SO_3]$ ,  
Ionic Liquid Surfactants”, *Journal of Physical Chemistry B*, **2008**.

**Note:** This work is the result of the collaboration of our group with the  
QUILL, Belfast, research group. The author of the Thesis has performed a  
part of the experimental work and synthesised and characterised some ionic  
liquids used in this study.



**Anion and Cation Effects on the Self-Aggregation of  
1-Alkyl-3-Methylimidazolium Alkylsulfonate,  
[C<sub>n</sub>H<sub>2n+1</sub>mim][C<sub>m</sub>H<sub>2m+1</sub>SO<sub>3</sub>], Ionic Liquid Surfactants**

Marijana Blesic,<sup>a,b</sup> Małgorzata Swadźba-Kwaśny,<sup>b</sup> John D. Holbrey,<sup>b\*</sup>  
Kenneth R. Seddon,<sup>a,b</sup> Luís Paulo N. Rebelo<sup>a\*</sup>

<sup>a</sup>*Instituto de Tecnologia Química e Biológica, ITQB 2, Universidade Nova de Lisboa,  
Apartado 127, 2780-901 Oeiras, Portugal*

<sup>b</sup>*The QUILL Centre, The Queen's University of Belfast, Stranmillis Road, Belfast  
BT9 5AG, United Kingdom*

**Abstract**

The aggregation behaviour of seven 1-alkyl-3-methylimidazolium alkylsulfonate salts ([C<sub>n</sub>H<sub>2n+1</sub>mim][C<sub>m</sub>H<sub>2m+1</sub>SO<sub>3</sub>];  $n = 8, 10$  or  $12$ ;  $m = 1$  and  $n = 4$  or  $8$ ;  $m = 4$  or  $8$ ) has been investigated in aqueous solution under ambient conditions. Fluorescence spectroscopy and interfacial tension measurements have been used to determine the critical micelle concentrations (CMC), surface activity, and to compare the effects alkyl-substitution patterns in both the cation and anion on the surfactant properties of these salts. With relatively small methylsulfonate anions ( $n = 8, 10$  and  $12, m = 1$ ), the salts behave as conventional single chain cationic surfactants and a typical reduction in the CMC on increasing alkyl chain length ( $n$ ) in the cation is observed. Whereas, when amphiphilic character is introduced into both the cation and anion ( $n = 4$  and  $8, m = 4$  and  $8$ ), novel catanionic surfactants with lower CMC values than those of the corresponding cationic analogues, and which exhibited an unanticipated enhanced reduction of surface tension, were obtained. In addition, the thermotropic phase behaviour of [C<sub>8</sub>H<sub>18</sub>mim][C<sub>8</sub>H<sub>18</sub>SO<sub>3</sub>] ( $n = m = 8$ ) was investigated using variable temperature X-ray

scattering, polarising optical microscopy and differential scanning calorimetry and shows formation of a smectic liquid crystalline phase with a broad temperature range.

**Keywords:** ionic liquids; 1-alkyl-3-methylimidazolium; alkylsulfonate; aggregation; micelle; liquid crystalline salts.

## Introduction

The term 'ionic liquid' refers to the liquid state of matter exhibited by salts. In the ambient temperature regime, ionic liquids are typically organic salts, of which examples with 1,3-dialkylimidazolium cations probably have been the most extensively studied.<sup>1</sup> Computational<sup>2</sup> and direct experimental methods<sup>3</sup> have shown that ionic liquid systems tend to exhibit bulk isotropy yet have relatively strong local structure correlations, with cations surrounded in a first coordination sphere of anions and *vice versa*.

Structural modification of the individual ion components of an ionic liquid by, for example, increasing the length of alkyl-substituents in 1-alkyl-3-methylimidazolium cations can lead to increases in the macroscopic structural anisotropy of the liquid with microbiphasic separation of hydrocarbon and charged domains emerging. *In extremis*, with decyl- or longer substituents, liquid crystalline phases can be formed, the thermotropic mesomorphism of 1-alkyl-3-methylimidazolium<sup>4</sup> and quaternary phosphonium<sup>5</sup> salts have been widely studied. Evidence from molecular dynamics simulations<sup>6</sup> and small angle X-ray diffraction<sup>7</sup> suggests that domain separation occurs even in ionic liquids with relatively short butyl, hexyl, and octyl substituents, although the life-times of particular domain structures may be relatively small. It has also been recently reported that 1,3-dimethylimidazolium dodecylsulfonate exhibits a thermotropic liquid crystalline smectic A phase and that the phase behaviour can be tuned by modification of the substitution patterns on the imidazolium cation.<sup>8</sup>

The considerable interest in ionic liquid crystals is a consequence of the wide spectrum of potential applications: in sol-gel synthesis of macro and mesoporous silicas, hydrothermal synthesis of  $\gamma$ -alumina, preparation of gold and silver nanoparticles, or as stabilisers for suspension polymerisation.<sup>9</sup>

It has been anticipated that ionic liquid materials may have a significant potential impact on the field of surfactants.<sup>10</sup> Three possible directions for development and application, namely using ionic liquids as solvents, surfactants, or as salt additives have been discussed. Ionic liquids can be added as co-surfactants or hydrotropes to aqueous solutions of common surfactants.<sup>11,12</sup> They can be used directly as media for dissolution of many different common ionic and nonionic surfactants,<sup>13</sup> amphiphilic polymers<sup>14</sup> or ionic liquids.<sup>15</sup> Moreover due to the obvious structural similarities to conventional cationic surfactants, many ionic liquids exhibit surfactant-like behaviour and same aggregation phenomena in aqueous solution.<sup>10,11</sup> Changes in the aggregation behaviour of a range of 1-alkyl-3-methylimidazolium halide, hexafluorophosphate and bis{(trifluoromethyl)sulfonyl}imide salts in aqueous solutions as a function of alkyl chain length, concentration and the nature of the anion have been reported by our group<sup>10,11</sup> and others.<sup>16</sup> The aggregation behaviour of aqueous solutions of dodecyl-substituted pyrrolidinium, pyridinium and piperidinium bromide salts has also been examined and compared as a function of head group type.<sup>10</sup>

1-Alkyl-3-methylimidazolium alkylsulfonate salts (Figure 1) are useful examples of ionic liquid forming salts in which it is simple to systematically vary the structure of both the cations and the anions by changing the length ( $n$  and  $m$ ) of the two alkyl chains. By investigating the properties of the materials within this two dimensional array of salts, it is possible to explore whether systematic changes to the cation and anion structures of ionic liquids produce serial (cumulative) or synergistic variations in structure/property relationships. The physical properties of a range of 1-alkyl-3-methylimidazolium alkylsulfonates with alkyl groups containing six or less carbon atoms in either the cation or anion and with a total of less than eleven carbon atoms in the two alkyl chains have been investigated recently.<sup>17</sup>

Here, we report the results of investigations into the thermal and surfactant properties of seven 1-alkyl-3-methylimidazolium alkylsulfonate salts (**1-7** in Figure 1) from two regions in the  $[\text{C}_n\text{H}_{2n+1}\text{mim}][\text{C}_m\text{H}_{2m+1}\text{SO}_3]$   $n+m$  matrix, with  $n = 8, 10$  or  $12$ ;  $m = 1$  and  $n = 4$  or  $8$ ;  $m = 4$  or  $8$  in which the total number of carbon atoms in the two substituents,  $\Sigma(n+m)$ , is eight or more. In addition, the thermotropic mesomorphism of

the cationic 1-octyl-3-methylimidazolium octylsulfonate (**7**,  $n = m = 8$ ) salt in the neat anhydrous state has been investigated.

The salts investigated have amphiphilic character in either or both the cation and anion, and the results presented below demonstrate how new materials having exceptional performance characteristics comparable to those of cationic<sup>18</sup> and gemini<sup>19</sup> surfactants can be developed by applying an ionic liquid design strategy to molecular engineering.

|  | <b>Compound</b> | $n$ | $m$ | $\Sigma(m+n)$ |
|--|-----------------|-----|-----|---------------|
|  | <b>1</b>        | 8   | 1   | 9             |
|  | <b>2</b>        | 10  | 1   | 11            |
|  | <b>3</b>        | 12  | 1   | 13            |
|  | <b>4</b>        | 4   | 4   | 8             |
|  | <b>5</b>        | 4   | 8   | 12            |
|  | <b>6</b>        | 8   | 4   | 12            |
|  | <b>7</b>        | 8   | 8   | 16            |

**Figure 1.** General structure of 1-alkyl-3-methylimidazolium alkylsulfonate ionic liquids ( $[C_nH_{2n+1}mim][C_mH_{2m+1}SO_3]$ ).  $\Sigma(m+n)$  is the sum of the number of carbon atoms in the two alkyl-substituents.

## Experimental

*Materials.* 1-Methylimidazole ( $\geq 99\%$ ), dichloromethane, ethyl ethanoate, 1-butanefonyl chloride ( $\geq 98\%$ ), 1-octanesulfonyl chloride (98 %), 1-butanol ( $\geq 99.8\%$ ), 1-octanol ( $\geq 99\%$ ), 1-decanol ( $\geq 99\%$ ), 1-dodecanol ( $\geq 99\%$ ), and trimethylamine ( $\geq 99\%$ ) were purchased from Aldrich. Methyl methanesulfonate (99%) was purchased from Acros Organics. 1-Methylimidazole was distilled prior to use, all other reagents and solvents were used as received. Double-distilled deionised water was obtained from a Millipore Milli-Q water purification system (Millipore, USA). Pyrene (Fluka, Germany, 99%) was recrystallised from benzene.

$^1H$  and  $^{13}C$  NMR spectra were recorded at room temperature on a Bruker Avance spectrometer DPX 300, using  $CDCl_3$  as solvent.

*Synthesis.* The seven ionic liquids used in this study (Figure 1) were synthesised following the general procedure described below.

Alkyl alkylsulfonates ( $C_nH_{2n+1}OSO_2C_mH_{2m+1}$ ). A solution of triethylamine (1.1 mol) and the desired alcohol ( $C_nH_{2n+1}OH$ ;  $n = 4, 8, 10, 12$ ) (1.1 mol.) in dichloromethane ( $430\text{ cm}^3$ ) was cooled in an ice-bath. The respective alkylsulfonyl chloride ( $C_mH_{2m+1}SO_2Cl$ ,  $m = 1, 4, 8$ ; 1 mol eq.) dissolved in dichloromethane ( $100\text{ cm}^3$ ) was added dropwise to the cooled, rapidly stirred reaction mixture while maintaining the temperature at  $0\text{ }^\circ\text{C}$ . The reaction mixture was then stirred for several hours at room temperature, filtered, and the solvent removed under reduced pressure. The filtrate was purified by fractional vacuum distillation to yield alkyl alkylsulfonate esters as transparent, colourless or slightly yellow liquids, exception for dodecylmethanesulfonate which was obtained as a colourless solid. All products were characterised by  $^1\text{H}$  NMR spectroscopy.

1-Alkyl-3-methylimidazolium alkylsulfonates ( $[C_nH_{2n+1}mim][C_mH_{2m+1}SO_3]$ ) A solution of freshly distilled alkyl alkylsulfonate esters ( $C_nH_{2n+1}SO_3C_mH_{2m+1}$ ) (1.1 mol eq.) and 1-methylimidazole (1 mol eq.) in ethyl ethanoate ( $150\text{ cm}^3$ ) was heated under reflux with stirring overnight. The crude product formed as a dense layer and was removed, washed six times with ethyl ethanoate and any remaining solvent was removed under reduced pressure to give the corresponding ionic liquids  $[C_nH_{2n+1}mim][C_mH_{2m+1}SO_3]$  (Figure 1 and Table 1).

All the salts **1-7** (see Figure 1) were characterised by mass spectrometry and by  $^1\text{H}$  and  $^{13}\text{C}$  NMR spectroscopy (see Appendix 3) and showed no impurities other than the presence of residual water (detected independently by Karl-Fischer analysis). All samples were then thoroughly degassed and dried under vacuum (*ca.*  $0.1\text{ Pa}$ ) at moderate temperatures ( $60\text{--}80\text{ }^\circ\text{C}$ ) for typically 24 h before use.

*Differential Scanning Calorimetry (DSC).* Phase transition temperatures were measured using a TA Instruments DSC 2920 in modulated DSC mode. Cooling was accomplished by using a refrigerated cooling system capable of controlling the temperature down to  $220\text{ K}$ . Dry dinitrogen gas, with a flow rate of approximately  $20\text{ cm}^3\text{ min}^{-1}$ , was purged through the DSC cell. Transition temperatures were determined from the onset points by initially heating the sample from room temperature at a rate of  $10\text{ }^\circ\text{C min}^{-1}$  to beyond the clearing point, followed by cooling at a rate of  $5\text{ }^\circ\text{C min}^{-1}$  to

below the crystallisation temperature. The cooling-heating cycle was repeated three times. The transition temperatures and enthalpies of the transitions obtained from the second and subsequent cycles were reproducible.

*Polarising Optical Microscopy (POM).* Microscope observations were made using an Olympus BX50 microscope equipped with a Linkam TH600 hot stage and TP92 temperature controller. Neat samples were examined in the form of fine crystals placed between thin round glass plates. Contact experiments between the salts and water were performed using the Lawrence penetration experiment<sup>20</sup> by placing a few crystals of the salt between two glass slides and introducing a small drop of water into contact with the surfactant through capillary action.

*X-ray Diffraction (XRD).* X-ray diffraction data were collected using a Siemens D5000 powder diffractometer equipped with a sealed Paar heating stage with Cu-K $\alpha$  X-rays ( $\lambda = 1.542 \text{ \AA}$ ). Data were recorded from between 2 and 30° in steps of 0.05° over the temperature range 25 to 120 °C.

*Interfacial Tension (IFT).* For both IFT and fluorescence measurements, aqueous stock solutions of **1-7** were prepared using water containing  $1.74 \times 10^{-6}$  M pyrene, and all studied solutions were prepared from the stock solutions, by diluting with the same pyrene aqueous solution. Interfacial tension was measured using a Drop Shape Analysis Tensiometer (Contact Angle System OCA, Carl Stuart Ltd) working in the pendant drop mode at a constant temperature of  $23 \pm 2$  °C. IFT is derived from the fit of the pendant drop profile, and care was taken to ensure that the apparatus was calibrated with several solvents of known IFT in the range of interest. The drops were left to equilibrate close to the rupture point and at least three consistent measurements per solution were recorded.

*Fluorescence Spectroscopy.* Pyrene was used as a fluorescent probe to ascertain the onset of the aggregation of the ionic liquids in water. Steady-state fluorescence spectra of the pyrene-containing solutions in 1 cm quartz cuvettes were recorded at room temperature with a Cary Varian Eclipse Fluorescence Spectrometer collected at a 90° angle. Excitation was set to a wavelength of 337 nm. Intensities of first (I1) and third (I3) vibronic bands in the pyrene emission spectra located around 373 and 384 nm, respectively, were measured and used to determine the ratio I3/I1.

## Results and Discussion

The thermal and solution behaviour of seven  $[C_nH_{2n+1}mim][C_mH_{2m+2}SO_3]$  salts (**1-7**) have been investigated. The salts comprised two sets; a series of three salts (**1-3**) with methylsulfonate ( $m = 1$ ) anions and different length alkyl chains on the cation ( $n = 8, 10,$  and  $12$  respectively), and a matrix of four salts with intermediate length alkyl-substituents on both cation and anion, **4** ( $n = m = 4$ ), the cross terms **5** ( $n = 4, m = 8$ ) and **6** ( $n = 8, m = 4$ ), and **7** ( $n = m = 8$ ). Thermophysical data for two of the salts, **1** and **2**, have been previously reported,<sup>17</sup> whereas the remainder (**3-7**) are new and were synthesised and characterised here for the first time.

All the salts are readily soluble in water at room temperature, and produced surface active solutions. The CMC of the salts in water were determined at room temperature using interfacial surface tension and fluorescence spectroscopy.

*Thermal Behaviour.* The thermal behaviour of the salts was investigated using modulated DSC, first order endothermic transition temperatures, enthalpies, and assignments from the onset temperatures of the heating cycle from the second and subsequent cycles are given in Table 1. On the cooling cycles, all the salts showed thermal hysteresis and supercooling for the liquid to crystal transition, and (for **7**) the liquid crystalline phase to crystal transition, with the temperature depressed by  $15\text{ }^\circ\text{C}$  on average. The same phenomena were observed in the case of the crystal-crystal transformations.

The salts, **1-6**, melted directly to form ionic liquids at  $<100\text{ }^\circ\text{C}$  (conforming to the description of an ionic liquid<sup>1</sup>). **4** ( $n = m = 4$ ) also showed a reversible crystal-crystal phase transition at  $24\text{ }^\circ\text{C}$  before melting at  $60\text{ }^\circ\text{C}$ . **7** ( $n = m = 8$ ) exhibits a crystal-crystal transition at  $70\text{ }^\circ\text{C}$  and then melts to a smectic liquid crystal phase at  $79\text{ }^\circ\text{C}$ , clearing to the isotropic liquid at  $115\text{ }^\circ\text{C}$ . Confirmation that the DSC transitions were respectively crystal-crystal, melting to liquids, and melting to a liquid crystal phase was made by comparison of the transitions measured by DSC with observations from polarising hot-stage optical microscopy, and for **7**, also by small angle X-ray diffraction to elucidate the nature of the mesophase formed.

| Compound | $n$ | $m$ | CMC /mM |       | $pC_{20}^a$ | $\Pi_{CMC}^b$<br>/mN·m <sup>-1</sup> | Transition <sup>c</sup>     | $T / ^\circ\text{C}$ | $\Delta H / \text{kJ mol}^{-1}$ |
|----------|-----|-----|---------|-------|-------------|--------------------------------------|-----------------------------|----------------------|---------------------------------|
|          |     |     | IFT     | Fluor |             |                                      |                             |                      |                                 |
| <b>1</b> | 8   | 1   | 220     | -     | 1.0         | 29.0                                 | C→ <i>iso</i>               | 40.3                 | 39.3                            |
| <b>2</b> | 10  | 1   | 60      | 65    | 1.5         | 28.5                                 | C→ <i>iso</i>               | 53.6                 | 40.5                            |
| <b>3</b> | 12  | 1   | 14      | 19    | 2.1         | 28.5                                 | C→ <i>iso</i>               | 64.9                 | 47.5                            |
| <b>4</b> | 4   | 4   | -       | -     | 0.4         |                                      | C1→C2                       | 24.0                 | 10.5                            |
|          |     |     |         |       |             |                                      | C2→ <i>iso</i>              | 60.1                 | 18.3                            |
| <b>5</b> | 4   | 8   | 135     | 130   | 1.6         | 40.0                                 | C→ <i>iso</i>               | 56.3                 | 29.1                            |
| <b>6</b> | 8   | 4   | 140     | 155   | 1.6         | 28.5                                 | C→ <i>iso</i>               | 54.1                 | 32.3                            |
| <b>7</b> | 8   | 8   | 12      | 17    | 2.9         | 43.7                                 | C1→C2                       | 68.4                 | 22.5                            |
|          |     |     |         |       |             |                                      | C2→S <sub>A</sub>           | 78.9                 | 28.2                            |
|          |     |     |         |       |             |                                      | S <sub>A</sub> → <i>iso</i> | 114.9                | 2.7                             |

<sup>a</sup>  $pC_{20}$  defined as the negative logarithm to the base 10 of the concentration of amphiphilic molecules required to reduce the surface tension of the pure solvent by 20 mN m<sup>-1</sup>.

<sup>b</sup> Effectiveness of the surface tension reduction,  $\Pi_{CMC}$ , (defined as  $\Pi_{CMC} = \gamma_o - \gamma_{CMC}$ , where  $\gamma_o$  is surface tension of the pure solvent (water), and  $\gamma_{CMC}$  the surface tension of the solution at the CMC).

<sup>c</sup> C is crystal form, C1 and C2 designate lower and upper crystal phases when a crystal-crystal transition is observed, S<sub>A</sub> is smectic liquid crystalline phase and *iso* designates the isotropic liquid state.

**Table 1.** Physical data collected for the [C<sub>n</sub>H<sub>2n+1</sub>mim][C<sub>m</sub>H<sub>2m+1</sub>SO<sub>3</sub>] salts **1-7**; Critical Micelle Concentration (CMC, mM) measured by interfacial tension, *IFT*, and fluorescence emission of pyrene, *Fluor*; Absorption efficiency,  $pC_{20}$ , Effectiveness of surface tension reduction,  $\Pi_{CMC}$  (mN m<sup>-1</sup>), transition temperatures (°C) measured from the onset to the peak by DSC and transition enthalpy (kJ mol<sup>-1</sup>).

On heating a crystalline sample of **7** from ambient temperature on the hot-stage of the polarising optical microscope, a crystal-crystal transition was observed consistent with the DSC data, followed by melting of the solid into the enantiotropic liquid crystalline phase, which cleared to the isotropic liquid at 115 °C. Cooling from the isotropic liquid yielded the phase sequence, *iso*→S<sub>A</sub>→C2→C1. The mesophase forms a dark homeotropic texture under crossed polarisers (see Appendix 3), both on heating and cooling from the isotropic liquid, characteristic of the smectic A bilayer structure commonly found for neat amphiphilic salts, especially for the imidazolium-type ionic liquid crystals.<sup>4</sup>



X-ray diffraction data was collected for **7**, initially in the crystalline state at ambient temperature, then after heating to the liquid state at 120 °C, and then in 10 °C steps, while cooling to 40 °C and equilibrating for 20 min. at each temperature. The phase transitions  $iso \rightarrow S_A$  and  $S_A \rightarrow C2$  were observed, with a significant degree of supercooling for each transition such that the  $iso \rightarrow S_A$  transition occurred between 110-100 °C, and the  $S_A \rightarrow C2$  transition between 60-50 °C compared to the corresponding transition temperatures in the heating cycle of 115 °C and 79 °C respectively. Typical X-ray diffraction patterns for each phase region are shown in Figure 2.

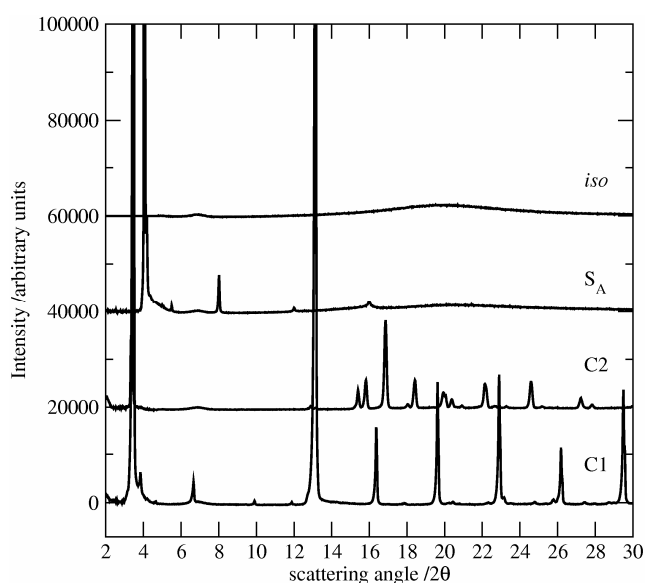


**Figure 2.** Development of the smectic ( $S_A$ ) and two consecutive solid crystalline (C2 and C1) phases for **7** ( $n = m = 8$ ) on cooling from the molten isotropic ( $iso$ ) state, followed by XRD.

The initial crystal form (C1) has a highly ordered layer structure, with a strong small angle diffraction peak  $\langle 100 \rangle$  at  $2\theta = 3.42^\circ$ , corresponding to a layer spacing of  $25.81 \text{ \AA}$ . A second set of intense peaks in the wide angle region at *ca.*  $13.12$ ,  $16.36$ , and  $19.64^\circ$  show a high degree of structure in the other two dimensions.

In the isotropic region, **7** shows a small residual peak in the small angle region at  $6.5^\circ$  and a characteristic broad diffraction band centred around  $22^\circ$  ( $\sim 4 \text{ \AA}$ ) consistent with fully mobile liquid alkyl chains. The  $S_A$  mesophase region is characterised by the presence of a sharp peak in the low angle region ( $2\theta = 2-5^\circ$ ) and a broad band centred at

22°, consistent with fully mobile alkyl chains. The change in the layer spacing ( $d$ ), determined from the position of the most intense peak in the low angle region, as a function of temperature through the different phase regions is shown in Figure 3. In the  $S_A$  phase,  $d$  decreases from 21.75 Å at 100 °C to 23.11 Å at 60 °C, corresponding to an interlayer contraction of 0.034 Å K<sup>-1</sup> consistent with decreasing mobility of the alkyl chains as the temperature is reduced. Unusually, the layer spacing in the mesophase is larger than the sum of the lengths of the two amphiphiles, and suggests formation of double-bilayer structure. This may be a result of the high density packing of the surfactant head-groups (calculated from the surface tension data, below).

Further cooling leads to crystallisation from the  $S_A$  to the crystalline C2 phase, this transition being characterised by a discontinuous increase in  $d$  (from *ca.* 23.11 Å at 60 °C in the  $S_A$  phase to 25.96 Å at 50 °C in the C2 crystalline phase, see Figure 3) and the appearance of well defined diffraction peaks in the wide angle region that support the formation of a crystalline phase. In contrast to the mesophase region, the  $d$ -spacing in the crystalline phases shows a typical contraction on cooling (0.015 Å K<sup>-1</sup>).

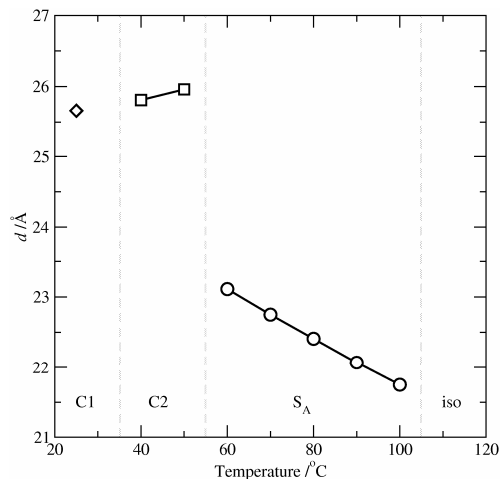


**Figure 3.** Change in the layer spacing ( $d$ ) of **7** in the liquid crystalline ( $S_A$ ,  $\circ$ ) and two crystalline phase (C1,  $\diamond$ ; C2,  $\square$ ) regions as a function of temperature, determined from the position of the peak at lowest value of  $2\theta$  in the XRD data.

The C2→C1 transition was not observed directly when samples were cooled *in situ* on the diffractometer hot stage. This is, in part, due to an absence of active cooling in the diffractometer which limits the effective minimum temperature that could be achieved in

a cooling cycle to *ca.* 40 °C. In order to demonstrate that the C2→C1 transformation is enantiotropic, a sample of **7** was heated externally until molten, then allowed to cool to room temperature and was then left to stand at room temperature overnight. The powder diffraction pattern subsequently measured was consistent with that collected on the initial crystalline sample prepared.

*Self-aggregation of [C<sub>n</sub>H<sub>2n+1</sub>mim][C<sub>m</sub>H<sub>2m+1</sub>SO<sub>3</sub>] salts in aqueous solution.* Contact experiments,<sup>20</sup> introducing a droplet of water into contact with the [C<sub>8</sub>mim][C<sub>8</sub>SO<sub>3</sub>] salt over the temperature range 25-80 °C, revealed a slight swelling of both crystalline solid and super-cooled mesophase domains on addition of water, rapidly followed by dissolution to form a fluid homogeneous solution as the contacting aqueous phase penetrated the salt. Thus, **7** showed no tendency to form lyotropic mesophases, despite the formation of a neat, anhydrous smectic (lamellar) thermotropic mesophase.

Self-aggregation of the salts in water over the lower concentration regimes was studied by surface tension and fluorescence spectroscopy with pyrene as a probe molecule.

The air-water interfacial tension of aqueous solutions of the salts **1-7** was measured as a function of concentration. Surfactant aggregation in solution leads to a decrease in the surface tension with increasing concentration, followed by a change to almost constant surface tension as the CMC is reached. Data for the salts, **1-3**, **6** and **7**, are shown in Figures 4(a) and (b). The surface tension data were used to determine the CMC, from the intersection of a linear extrapolation of the two differing regions. The two adsorption parameters: efficiency of adsorption,  $pC_{20}$ , (defined as the negative logarithm to the base 10 of the concentration of amphiphilic molecules required to reduce the surface tension of the pure solvent by 20 mN m<sup>-1</sup>) and effectiveness of the surface tension reduction,  $\Pi_{CMC}$ , (defined as  $\Pi_{CMC} = \gamma_0 - \gamma_{CMC}$ , where  $\gamma_0$  is surface tension of the pure solvent (water), and  $\gamma_{CMC}$  the surface tension of the solution at the CMC) were calculated from the data.<sup>21</sup>

Fluorescence spectroscopy, using pyrene as a molecular probe, was used to investigate the polarity of the probe domains in the solutions as a function of surfactant concentrations. By comparing the intensities of the first, I<sub>1</sub>, and third, I<sub>3</sub>, vibronic bands

of the pyrene emission spectrum, changes to the local environment of the probe molecule, and hence the bulk solution, can be monitored. The intensity ratio  $I_3/I_1$  varies as a function of the polarity of the pyrene environment and increases with decreasing solvent polarity. Figures 4(c) and (d) show the pyrene response ( $I_3/I_1$ ) for the aqueous solutions of the salts, **1-3**, **6** and **7**, as a function of concentration. The CMC is determined from the intersection points between that plateau and the descending part of the fluorescence profile.

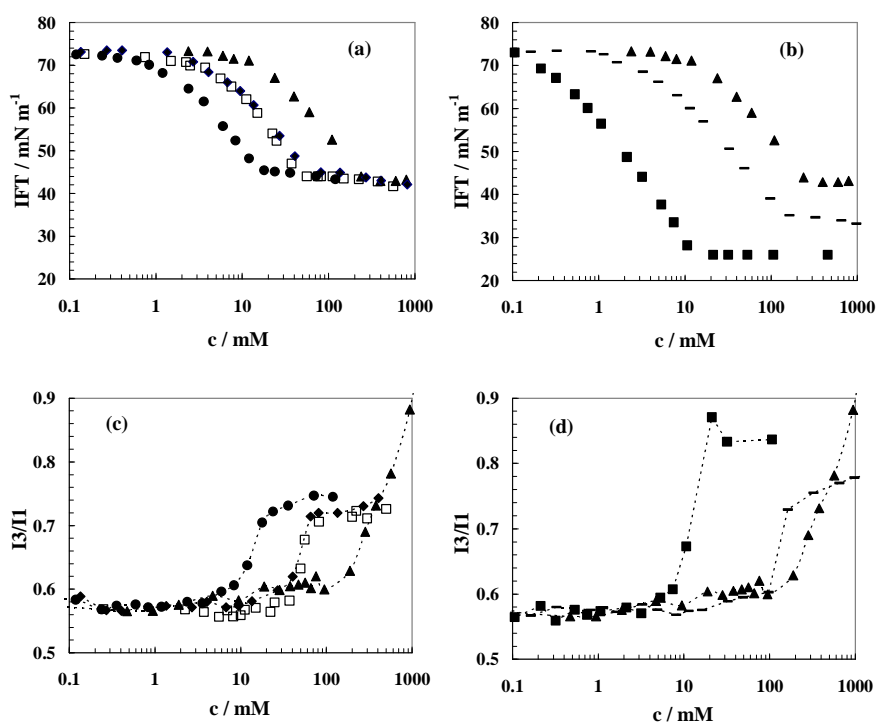


**Figure 4.** Determination of CMC by surface tension (a) and (b), and fluorescence (c) and (d) for the alkylsulfonate salts: **1** ( $n = 8$ ,  $m = 1$ ;  $\blacktriangle$ ), **2** ( $n = 10$ ,  $m = 1$ ;  $\blacklozenge$ ), **3** ( $n = 12$ ,  $m = 1$ ;  $\bullet$ ), **6** ( $n = 8$ ,  $m = 4$ ;  $-$ ), and **7** ( $n = m = 8$ ;  $\blacksquare$ ), and for comparison  $[\text{C}_{10}\text{H}_{21}\text{mim}]\text{Cl}$  ( $\square$ ).<sup>11</sup>

Experimental CMC values are presented in Table 1 calculated from both interfacial tension and fluorescence experiments. The data from the two approaches are in good agreement.

The decrease in the CMC of aqueous solutions of **1-3** containing a methylsulfonate anion is a consequence of the increased alkyl chain in the cation and follows the empirical rule that the CMC decreases by a factor of two for each  $\text{CH}_2$  group added to the alkyl chain of a single chain ionic surfactant, Figure 4(a). The dependencies,

and CMC values, found here for **1-3** are almost identical to those reported for the corresponding 1-alkyl-3-methylimidazolium chloride systems in water.<sup>11</sup> This fact indicates that chloride and methylsulfonate anions are equally efficient in decreasing the electrostatic repulsion between head groups and consequently have very similar values of adsorption efficiency and effectiveness of the surface tension reduction.

Solutions of the short alkyl chain ionic liquid **4** ( $n = m = 4$ ) showed reduced surface tensions with increasing concentration of ionic liquid in solution. However, at concentrations up to 2 M in solution no aggregation behaviour was observed (data are not shown).

The influence of increasing alkyl chain length in the anion in aqueous solution on the CMC is shown comparing the 1-octyl-3-methylimidazolium salts, **1**, **5** and **7**, in Figure 4(b). A non-linear dependence is found. For comparison purposes, the surface tension of the aqueous solution of **6** ( $n = 4, m = 8$ ) as a function of concentration is measured as well and showed almost identical aggregation behaviour to the corresponding cross-term **5** ( $n = 8, m = 4$ ).

Figure 4(a) and (b) clearly illustrates that (i) increasing the alkyl chain length in the cation is the most efficient way to decrease CMC values, and (ii) increasing the alkyl chain length in the anion (along with long alkyl chain in the cation) leads to lower CMCs and more significantly to higher effectiveness in surface tension reduction.

In common with the previously reported fluorescence studies on 1-octyl-3-methylimidazolium chloride in water,<sup>11</sup> the I3/I1 ratios for solutions of **1** show the typical increase with increasing surfactant concentration in solution indicating the formation of hydrophobic domains, however, a plateau is not reached. This may be due to the progressive dense packing of monomers in elongated aggregates without the formation a well defined micellar structure. For **7** ( $n = m = 8$ ), the plateau region of the I3/I1 ratio is significantly higher than that of the single chain surfactants (**1-3**) and implies the formation of micellar aggregates with a different structure, probably cylindrical or lamellar rather than spherical.

Surface Adsorption of Surfactants. The lowering of the surface tension,  $\gamma$ , is a consequence of the increased concentration of surfactant at the air-water surface. At concentrations greater than that of the CMC, the interfacial composition and

consequently the chemical potential changes only slightly.<sup>22</sup> Values for the efficiency of adsorption at the surface ( $pC_{20}$ ) and effectiveness of surface tension reduction ( $\Pi_{CMC}$ ) calculated in each case from the change in, and absolute values of, surface tension as a function of surfactant concentrations are listed in Table 1. The salts **1-3** (with methylsulfonate anions) show an increase in  $pC_{20}$  with increasing alkyl chain length, with only a small variation in the final value of  $\Pi_{CMC}$  between the salts. This tendency was previously described for classical cationic surfactants.<sup>21</sup>

In contrast, it was observed that both  $pC_{20}$  and  $\Pi_{CMC}$  increase with the sum of the cation and anions alkyl-substituent carbon atoms, for **5**, **6** and **7**. So that, on increasing the alkyl-chain in the cation and the anion in unison, substantial surface tension reductions are observed, see for example, Figure 4(b).

It should be noted that each molecule of catanionic surfactant yields two surface active monomers on dissolution. This is the reason why for the same concentration of surfactant much lower value of surface tension and higher absorption efficiency  $pC_{20}$  were obtained for **7** in comparison to **1**.

$\Pi_{CMC}$ , the effectiveness parameter,<sup>21</sup> is important for surface activity and reflects the detergency, foaming, emulsification, and wetting properties of surfactants. In the case of single chain ionic surfactants, repulsion between polar head groups provides a limit to dense packing of amphiphiles at the interface. In contrast, the surface tension reduction was dramatically increased for those surfactants containing both amphiphilic cations and anions. Since both the cations and anions incorporate hydrophobic alkyl chains, they both take part in the surface monolayer formation. The net electrostatic attraction between the positively and negatively charged amphiphile head groups, helped by van der Waals attractions between hydrophobic alkyl chains, enhances dense packing of monomers in the monolayer and consequently leads to lowering surface tension in the plateau region. The magnitude of the reduction reflects the efficiency of packing at the interface. From the surface tension data, by assuming that for these low concentration regimes the interfacial structure at the surface is a monolayer, the minimum area per ionic liquid molecule,  $a_o$ , can be calculated using the well known Gibbs equation.<sup>21</sup> A very low value of 0.7 nm<sup>2</sup> per ionic pair was calculated for solutions of **7**, demonstrating that, at the interface, the amphiphiles are extremely close-packed.

Closer packing increases the coherency of the interfacial film and this results, usually, in superior emulsifying and foaming properties. Additionally, for these catanionic surfactants, since they contain both cationic and anionic amphiphiles, they will be adsorbed at both negatively and positively surfaces, similar to zwitterionic surfactants. Much lower values of the surface tension were obtained in the plateau region for **7** compared with that for 1,3-didodecylimidazolium bromide,<sup>23</sup> which illustrates dominance of the electrostatic effect over the combination of hydrophobic and van der Waals effects.

Gemini surfactants,<sup>19</sup> containing two, or more, hydrophilic head groups covalently connected, have been shown to have superior properties to traditional cationic or anionic surfactants with significantly reduced surface tensions at low concentrations. Gemini surfactants have many applications, for example as solubilisers of water-insoluble materials and as agents for removal of pollutants from water.<sup>21</sup> **7** displays a high effectiveness parameter for reduction of surface tension, and has a CMC which is lower than those reported for comparable gemini surfactants with same length of alkyl chains.<sup>24</sup> Consequently there is a potential to prepare new surfactants with lower CMCs and even greater efficiencies.

Low CMC values are also associated with low irritation of biological systems since less material is required to achieve an equivalent performance. In addition, the aquatic toxicity of surfactants (and ionic liquids) has been shown to decrease with decreasing alkyl-chain length, so new surfactants such as **7** with octyl substituents may prove to have significantly lower environmental impact than single-chain cationic surfactants with equivalent activity containing dodecyl or tetradecyl substituents.

## Conclusions

The surfactant properties of 1-alkyl-3-methylimidazolium alkylsulfate ionic liquid surfactants have been investigated. In general, the low melting points and high solubility in water combine to give materials with excellent surfactant characteristics. The ionic liquids with methylsulfonate anion (**1-3**,  $n = 8, 10, \text{ and } 12$ ) behave as conventional cationic surfactants, showing CMC values comparable with those of the corresponding

imidazolium halide salts and having equivalent surface activity, reducing water-air interfacial tension from 72.5 to a minimum of *ca.* 44 mN m<sup>-1</sup>.

In contrast, when amphiphilic character is imparted into both the cation and anion, a synergistic packing effect appears to lead to the formation of novel catanionic surfactants with both lower CMC values than anticipated and enhanced surface activity. The large effect on the surface tension is interpreted in terms of a cooperative effect with both cations and anions forming the interfacial layer.

These two features: low melting points and high water solubility from the ionic liquid design methodology, and a synergistic surfactant effect where combining these two relatively poor surface active amphiphiles (octylmethylimidazolium and octylsulfonate), provides great opportunities develop new, molecularly simple yet functionally complex, modern high performance ionic surfactants that could out perform gemini and zwitterionic surfactants. In comparison to conventional single-alkyl chain ionic surfactants, corresponding gemini type surfactants or double chain ionic liquids, the presence of amphiphilic structure in both ions shows significantly higher effectiveness of the surface tension reduction. An additional interesting feature in systems such as these is that the alkyl-chains on the individual ions are relatively small which may improve biodegradability and lower the overall environmental and toxicological impact.

### **Acknowledgements**

This work was supported by the Fundação para a Ciência e Tecnologia (*FC&T*), Portugal (Projects POCTI/QUI/35413/2000, POCI/QUI/57716/2004). MB thanks *FC&T* for a Ph.D. grant (SFRH/BD/13763/2003) and Marie Curie Fellowships for Early Stage Research Training (EST No505613). KRS thanks the EPSRC (Portfolio Partnership Scheme, grant no. EP/D029538/1).

### **References**

1 Wasserscheid, P.; Welton, T. *Ionic Liquids in Synthesis*, 2nd ed. Wiley VCH: Weinheim, 2007.



- 2 Morrow, T. I.; Maginn, E. J. *J. Phys. Chem. B* **2003**, *107*, 9160-9160; Del Popolo, M. G.; Voth, G. A. *J. Phys. Chem. B* **2004**, *108*, 1744-1752; Bhargava, B. L.; Balasubramanian, S. *J. Chem. Phys.* **2005**, *123*, 144505; Shah, J. K.; Maginn, E. J. *J. Phys. Chem. B*, **2005**, *109*, 10395- 10405; Wang, Y. T.; Voth, G. A. *J. Am. Chem. Soc.*, **2005**, *127*, 12192- 12193; Canongia Lopes, J. N.; Padua, A. A. H. *J. Phys. Chem. B*, **2006**, *110*, 3330-3335.
- 3 Hardacre, C.; Holbrey, J. D.; McMath, S. E. J.; Bowron, D. T.; Soper, A. K. *J. Chem. Phys.*, **2003**, *118*, 273; Hardacre, C.; McMath, S. E. J.; Nieuwenhuyzen, M.; Bowron, D. T.; Soper, A. K. *J. Phys. C*, **2003**, *15*, S159; Deetlefs, M.; Hardacre, C.; Nieuwenhuyzen, M.; Padua, A. A. H.; Sheppard, O.; Soper, A. K. *J. Phys. Chem. B*, **2006**, *110*, 12055-12061.
- 4 Gordon, C. M.; Holbrey, J. D.; Kennedy, A. R.; Seddon, K. R. *J. Mater. Chem.* **1998**, *8*, 2627-2636; Holbrey, J. D.; Seddon, K. R. *J. Chem. Soc. Dalton Trans.* **1999**, 2133-2139; Bradley, A. E.; Hardacre, C.; Holbrey, J. D.; Johnston, S.; McMath, S. E. J.; Nieuwenhuyzen, M. *Chem. Mater.* **2002**, *14*, 629-635; Downard, A.; Earle, M. J.; Hardacre, C.; McMath, S. E. J.; Nieuwenhuyzen, M.; Teat, S. J. *Chem. Mater.* **2004**, *16*, 43-48.
- 5 Chen, H.; Kwait, D. C.; Gonen, Z. S.; Weslowski, B. T.; Abdallah D. J.; Weiss, R. G. *Chem, Mater.* **2002**, *14*, 4063-4072; Ma, K. F.; Somashekhar, B. S.; Gowda, G. A. N.; Khetrupal, C. L.; Weiss, R. G. *Langmuir* **2008**, *24*, 2746-2758.
- 6 Canongia Lopes, J. N.; Gomes, M. F. C.; Padua, A. A. H. *J. Phys. Chem. B* **2006**, *34*, 16816-16818.
- 7 Triolo, A.; Russina, O.; Bleif, H.-J.; Di Cola, E. *J. Phys. Chem. B*, **2007**, *111*, 4641-4644.
- 8 Mukai, T.; Yoshio, M.; Kato T.; Ohno, H. *Chem. Lett.* **2004**, *33*, 1630-1631.
- 9 Binnemans, K. *Chem. Rev.* **2005**, *105*, 4148-4204.
- 10 Blesic, M.; Lopes, A.; Melo, E.; Petrovski, Z.; Plechkova, N. V.; Canongia Lopes, J. N.; Seddon, K. R.; Rebelo, L. P. N. *J. Phys. Chem. B* **2008**, *112*, 8645-8650.
- 11 Blesic, M.; Marques, M. H.; Plechkova, N. V.; Seddon, K. R.; Rebelo, L. P. N.; Lopes, A. *Green Chem.* **2007**, *9*, 481-490.

- 12 Behera, K.; Dahiya P.; Pandey, S. *J. Colloid Interface Sci.* **2007**, *307*, 235-245; Behera, K.; Pandey, S. *J. Colloid Interface Sci.* **2007**, *316*, 803-814; Behera, K.; Pandey, S. *J. Phys. Chem. B* **2007**, *111*, 13307-13315; Sifaoui, H.; Lugowska, K.; Domanska, U.; Modaresi, A.; Rogalski, M. *J. Colloid and Interface Sci.* **2007**, *314*, 643-650.
- 13 Anderson, J. L.; Pino, V.; Hagberg, E. C.; Sheares V. V.; Armstrong, D. W. *Chem. Commun.* **2003**, 2444-2445; Fletcher, K. A.; Pandey, S. *Langmuir* **2004**, *20*, 33-36.
- 14 He, Y. Y.; Li, Z. B.; Simone, P.; Lodge, T. P. *J. Amer. Chem. Soc.* **2006**, *128*, 2745-2750.
- 15 Velasco, S. B.; Turmine, M.; Di Caprio D.; Letellier, P. *Colloids and Surfaces A* **2006**, *275*, 50-54.
- 16 Firestone, M. A.; Dzielawa, J. A.; Zapol, P.; Curtiss, L. A.; Seifert, S.; Dietz, M. L. *Langmuir* **2002**, *18*, 7258-7260.
- 17 Blesic, M.; Swadzba-Kwasny, M.; Belhocine, T.; Gunaratne, N.; Seddon, K. R.; Padua, A. A. H.; Costa Gomes, M. F.; Canongia Lopes, J. N.; Rebelo, L. P. N. *to be submitted*.
- 18 Kaler, E. W.; Herrington, K. L.; Methy, A. K.; Zasadzinski, J. A. N. *J. Phys. Chem.* **1992**, *96*, 6698-6707.
- 19 Menger, F. M.; Littau, C. A. *J. Am. Chem. Soc.* **1993**, *115*, 10083-10090.
- 20 Lawrence, A. C. S. in *Liquid Crystals 2*, ed. Brown, G. H. Gordon and Breach: London, 1969, part 1, p 1.
- 21 Rosen, M. J. *Surfactant and Interfacial Phenomena*, Wiley-Interscience, John Wiley & Sons, New Jersey, 2004, 208-242.
- 22 Evans, D. F.; Wennerström, H. *The Colloidal Domain: Where Physics, Chemistry, Biology and Technology Meet*, Wiley-VCH, 1999.
- 23 Baltazar, Q. Q.; Chandawalla, J.; Sawyer K.; Anderson, J. L. *Colloids and Surfaces A* **2007**, *302*, 150-156.
- 24 Frindi, M.; Michels, B.; Levy H.; Zana, R. *Langmuir* **1994**, *10*, 1140-1145.

## **CHAPTER 5.**

# **PHASE EQUILIBRIA IN IONIC LIQUID PLUS AROMATIC COMPOUND BINARY SYSTEMS**

*This Chapter will be submitted as a full article:*

Blesic M., Lopes J.N.C., Rebelo L.P.N., “Phase Equilibria in Ionic Liquid Plus Aromatic Compound Binary Systems”.

**Note:** All experimental part was done by the author of this Thesis.

## Phase Equilibria in Ionic Liquid - Aromatic Compound Mixtures

Marijana Blesic,<sup>a</sup> José N. Canongia Lopes,<sup>a,b</sup> Luís Paulo N. Rebelo<sup>a</sup>

*<sup>a</sup>Instituto de Tecnologia Química e Biológica, ITQB 2, Universidade Nova de Lisboa,  
Apartado 127, 2780-901 Oeiras, Portugal*

*<sup>b</sup>Centro de Química Estrutural, Instituto Superior Técnico, 1049-001 Lisboa,  
Portugal*

### Abstract

Binary mixtures of ionic liquids with benzene or its derivatives exhibit unusual phase diagrams characterized by a region of liquid-liquid immiscibility totally skewed towards benzene-rich compositions. This means that in some cases it is possible to dissolve up to 80% mole fraction of benzene in a given ionic liquid but effectively no ionic liquid in pure benzene. In this work we have extended previous studies on the subject by determining the solid-liquid and liquid-liquid phase diagrams of mixtures containing an ionic liquid plus a fluorinated benzene (1-ethyl-3-methylimidazolium bis(trifluoromethanesulfonyl)imide plus hexafluorobenzene or 1,3,5-trifluorobenzene), and mixtures containing triflate- or pyrrolidinium-based ionic liquids plus benzene (1-ethyl-3-methylimidazolium triflate or N-ethyl-N-methylpyrrolidinium bis(trifluoromethanesulfonyl)-imide plus benzene).

### Introduction

Binary mixtures of ionic liquids with benzene (or similar aromatic compounds) exhibit unusual properties, namely liquid-liquid immiscibility windows totally skewed towards aromatic-rich compositions, i.e., aromatic compounds are remarkably soluble in ionic liquids (in some cases up to 80% mole fraction of benzene can be dissolved in a given ionic liquid) but effectively no ionic liquid can be dissolved in a pure aromatic compound.<sup>1,2</sup> This fact has found different types of application, from improved separation techniques (aromatic-aliphatic partition using ionic liquids<sup>3</sup>, solute extraction in biphasic aromatic-ionic liquid systems<sup>4</sup>) to new

reaction or catalytic schemes involving ionic liquid solvents (polymerization<sup>5</sup>, hydrogenation<sup>6</sup>, Friedel–Crafts alkylation<sup>7</sup>).

From a more fundamental, molecular-oriented perspective, these systems were analyzed by Holbrey et al., Lynden-Bell et al., and Deetlefs et al.<sup>8-10</sup> who discussed the possibility of liquid clathrate formation in ionic liquid-aromatic systems. They were able to isolate and characterize by X-ray diffraction a 2:1 (ionic liquid)·(benzene) inclusion crystal, and elucidated by neutron diffraction and molecular dynamics studies the structure of the liquid mixtures. More recently, Lachwa et al.<sup>11, 12</sup> also made contributions to this field by showing how the fluid-phase behavior (liquid-liquid immiscibility window) could be fine-tuned by the nature of the ionic liquid or the molecular component

In this work we have extended the scope of some of the studies mentioned in the previous paragraph by determining the solid-liquid and liquid-liquid phase diagrams of benzene plus ionic liquid mixtures, where the nature of the ionic liquid and of the molecular solvent were changed in a deliberate and systematic way in order to elucidate from a molecular point of view the peculiar behaviour of this type of systems. Taking as the starting point the 1-ethyl-3-methylimidazolium bis(trifluoromethanesulfonyl)imide ionic liquid plus benzene system ( $[\text{C}_2\text{mim}][\text{NTf}_2] + \text{C}_6\text{H}_6$ ),<sup>11</sup> we have decided to study two mixtures of that ionic liquid with hexafluorobenzene or 1,3,5-trifluorobenzene ( $[\text{C}_2\text{mim}][\text{NTf}_2] + \text{C}_6\text{F}_6$  and  $[\text{C}_2\text{mim}][\text{NTf}_2] + \text{C}_6\text{H}_3\text{F}_3$ ). In this case the objective was to check the effect of changing the aromatic character and charge distribution of the benzene-derivative in the phase behaviour of the mixtures. This particular set of results was complemented by the determination of the phase diagram of the system  $[\text{C}_2\text{mim}][\text{NTf}_2]$  plus cyclohexane, ( $[\text{C}_2\text{mim}][\text{NTf}_2] + \text{c-C}_6\text{H}_{12}$ ), where the aromatic nature of the molecular component of the system is completely absent. This was followed by a system where the 1-ethyl-3-methylimidazolium cation of the ionic liquid was substituted by the N-ethyl-N-methylpyrrolidinium cation ( $[\text{C}_1\text{C}_2 \text{pyrr}][\text{NTf}_2] + \text{C}_6\text{H}_6$ ). Here the objective was to check the influence of replacing a cation containing an aromatic ring (imidazolium) by a non-aromatic cation (pyrrolidinium). Finally, the bis(trifluoromethanesulfonyl)imide anion was exchanged by the smaller trifluoromethanesulfonate anion, leading to the ( $[\text{C}_2\text{mim}][\text{OTf}] + \text{C}_6\text{H}_6$ ) system. In this case shifts in the phase diagram of the system would reflect the influence of the

benzene-anion interactions (including the loss of flexibility of the anion when changing from  $[\text{NTf}_2]^-$  to  $[\text{OTf}]^-$ ).

## Experimental

*Materials.* 1-Ethyl-3-methylimidazolium bis(trifluoromethanesulfonyl)imide,  $[\text{C}_2\text{mim}][\text{NTf}_2]$  was purchased from Solvent Innovation with 99% purity. 1-Ethyl-3-methylimidazolium trifluoromethanesulfonate,  $[\text{C}_2\text{mim}][\text{OTf}]$ , and 1-ethyl-3-methylpyrrolidinium bis(trifluoromethanesulfonyl)imide,  $[\text{C}_2\text{C}_1\text{pyrr}][\text{NTf}_2]$ , were purchased from Iolitec, both with 99% purity. Vacuum (0.1 Pa) and moderate temperature (70 °C) conditions were always applied to all ionic liquid samples for several days prior to their use, in order to reduce their water and other volatile substances content. The fluorinated molecular solvents, hexafluorobenzene and 1,3,5-trifluorobenzene, were purchased from Apollo with 99% purity and were used without further purification. Benzene and cyclohexane (Aldrich, 99.5%) were dried with 3Å molecular sieves prior to the measurements.

*Liquid - Liquid equilibrium (LLE) measurements.* All cloud-point determinations on the temperature-composition phase diagrams corresponding to liquid-liquid equilibria at a nominal pressure of 0.1 MPa were performed using a dynamic method with visual detection of the solution turbidity. For this purpose, Pyrex glass view cells with magnetic stirring were used. Samples were gravimetrically prepared directly inside the cells using an analytical high precision balance ( $\pm 0.01$  mg). The cells were then immersed in a thermostatic bath. Providing continuous stirring, we cooled off or heated the solutions usually in two or three consecutive runs with the two last runs being carried out very slowly (the rate of temperature change near the cloud point was no more than  $5 \text{ K}\cdot\text{h}^{-1}$ ). Starting from the homogeneous region, the temperature at which the first sign of turbidity appeared upon cooling was taken as the temperature of the liquid-liquid phase transition.

*Solid - Liquid equilibrium (SLE) measurements.* The solid-liquid equilibrium temperatures at 0.1 MPa nominal pressure were determined using the following method: the mixtures of the ionic liquid plus the molecular component were placed in a Pyrex glass cell. The cell was then inserted in a thermostatic water or ethanol bath and cooled by adding ice or liquid nitrogen, respectively. After solidification, the samples were heated very slowly (less than  $2 \text{ K}\cdot\text{h}^{-1}$  near the equilibrium temperature)

with continuous stirring inside the cell during melting process. The temperature at which the last crystal disappeared was taken as the temperature of the solid-liquid equilibrium.

Both the crystal-disappearance temperatures and the cloud-point temperatures were measured using a four-wire platinum resistance thermometer coupled to a *Yokogawa 7561* multimeter. The thermometer was calibrated against high accuracy mercury thermometers (0.01 K precision). The overall uncertainty of the transition temperature measurements, resulting from the visual observation of the turbidity (LLE) or the disappearance of the last crystals (SLE) is obviously greater than the instrumental error and is estimated to be  $\pm 1$  K.

## Results and Discussion

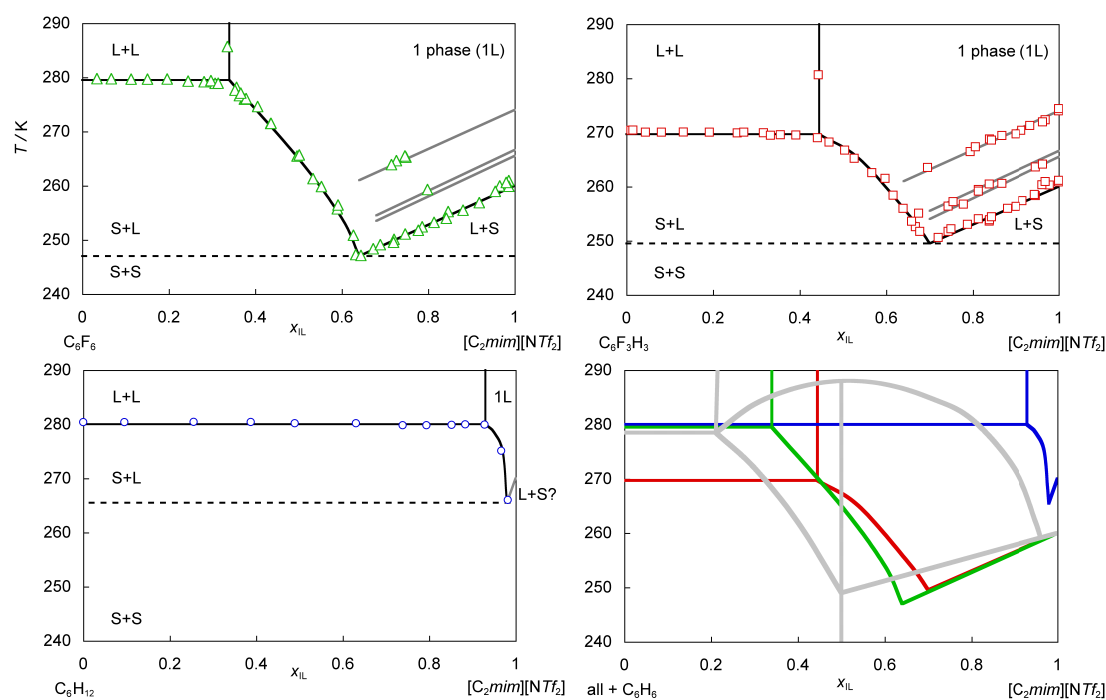


**Figure 1.** ( $T$ - $x$ ) phase diagrams of systems containing [C<sub>2</sub>mim][NTf<sub>2</sub>] mixed with (a) C<sub>6</sub>F<sub>6</sub>, (b) 1F,3F,5F-C<sub>6</sub>H<sub>3</sub>F<sub>3</sub>, or (c) c-C<sub>6</sub>H<sub>12</sub>. Figure (d) overlaps the different diagrams (keeping the same color convention used in Figures (a) to (c)) along with the schematic representation, in grey, of the phase diagram of [C<sub>2</sub>mim][NTf<sub>2</sub>] + C<sub>6</sub>H<sub>6</sub><sup>11</sup>. In Figures 1a and 1b the grey lines represent the precipitation of different polymorphs of [C<sub>2</sub>mim][NTf<sub>2</sub>] during the cooling of the mixtures.



| [C <sub>2</sub> mim][Ntf <sub>2</sub> ]      |       | [C <sub>2</sub> mim][Otf]                    |       | [C <sub>2</sub> mpyrr][Ntf <sub>2</sub> ] |       |                               |       |                               |       |
|----------------------------------------------|-------|----------------------------------------------|-------|-------------------------------------------|-------|-------------------------------|-------|-------------------------------|-------|
| x <sub>IL</sub>                              | T/K   | x <sub>IL</sub>                              | T/K   | x <sub>IL</sub>                           | T/K   |                               |       |                               |       |
| C <sub>6</sub> H <sub>3</sub> F <sub>3</sub> |       | C <sub>6</sub> H <sub>3</sub> F <sub>3</sub> |       | C <sub>6</sub> F <sub>6</sub>             |       | C <sub>6</sub> H <sub>6</sub> |       | C <sub>6</sub> H <sub>6</sub> |       |
| 0.838                                        | 0.963 | 0.963                                        | 264.2 | 0.627                                     | 250.8 | 0.916                         | 262.2 | 0.646                         | 322.5 |
| 0.838                                        | 0.944 | 0.963                                        | 272.0 | 0.590                                     | 255.7 | 0.835                         | 260.6 | 0.530                         | 306.1 |
| 0.787                                        | 0.900 | 0.944                                        | 258.5 | 0.553                                     | 259.8 | 0.796                         | 259.2 | 0.472                         | 294.6 |
| 0.011                                        | 0.900 | 0.900                                        | 256.3 | 0.502                                     | 265.7 | 0.724                         | 260.5 | 0.424                         | 286.3 |
| 0.015                                        | 0.806 | 0.900                                        | 269.7 | 0.437                                     | 271.5 | 0.000                         | 280.2 | 0.245                         | 280.0 |
| 0.044                                        | 0.778 | 0.806                                        | 267.4 | 0.406                                     | 274.6 | 0.026                         | 280.2 | 0.193                         | 281.3 |
| 0.081                                        | 0.754 | 0.778                                        | 256.7 | 0.367                                     | 277.1 | 0.095                         | 280.0 | 0.140                         | 281.4 |
| 0.132                                        | 0.443 | 0.754                                        | 257.2 | 0.314                                     | 278.9 | 0.155                         | 280.1 | 0.862                         | 352.5 |
| 0.192                                        | 0.749 | 0.443                                        | 280.6 | 0.842                                     | 254.0 | 0.271                         | 279.8 | 0.775                         | 342.3 |
| 0.256                                        | 0.695 | 0.749                                        | 252.2 | 0.798                                     | 259.3 | 0.377                         | 279.5 | 0.742                         | 337.5 |
| 0.934                                        | 0.674 | 0.695                                        | 263.5 | 0.749                                     | 265.3 | 0.919                         | 261.9 | 0.675                         | 327.7 |
| 0.880                                        | 0.658 | 0.674                                        | 255.1 | 0.715                                     | 263.9 | 0.860                         | 260.5 | 0.588                         | 315.6 |
| 0.838                                        | 0.720 | 0.658                                        | 253.6 | 0.689                                     | 249.1 | 0.767                         | 258.9 | 0.492                         | 299.4 |
| 0.838                                        | 0.677 | 0.720                                        | 250.6 | 0.721                                     | 250.1 | 0.977                         | 264.2 | 0.401                         | 283.0 |
| 0.794                                        | 0.639 | 0.677                                        | 251.7 | 0.747                                     | 251.1 | 0.818                         | 259.5 | 0.335                         | 274.0 |
| 0.743                                        | 0.616 | 0.639                                        | 256.0 | 0.645                                     | 247.1 | 0.755                         | 259.6 | 0.298                         | 274.0 |
| 0.743                                        | 0.567 | 0.616                                        | 258.4 | 0.591                                     | 256.4 | 0.684                         | 262.1 | 0.381                         | 278.5 |
| 0.667                                        | 0.526 | 0.567                                        | 262.6 | 0.534                                     | 261.3 | 0.653                         | 262.6 | 0.351                         | 274.7 |
| 0.597                                        | 0.504 | 0.526                                        | 265.2 | 0.986                                     | 260.9 | 0.624                         | 261.7 | 0.330                         | 273.4 |
| 0.978                                        | 260.3 | 0.504                                        | 266.7 | 0.965                                     | 260.0 | 0.595                         | 262.8 | 0.304                         | 272.8 |
| 0.962                                        | 260.3 | 0.333                                        | 269.5 | 0.986                                     | 259.9 | 0.547                         | 266.1 | 0.284                         | 275.1 |
| 0.969                                        | 260.9 | C <sub>6</sub> F <sub>6</sub>                |       | 0.981                                     | 260.6 | 0.936                         | 262.7 | 262.7                         | 276.9 |
| 0.969                                        | 272.4 | 0.034                                        | 279.8 | 0.955                                     | 258.9 | 0.776                         | 258.3 | 0.248                         | 279.1 |
| 0.947                                        | 258.3 | 0.067                                        | 279.7 | 0.918                                     | 256.9 | 0.651                         | 262.7 | 0.233                         | 279.6 |
| 0.947                                        | 263.6 | 0.113                                        | 279.7 | 0.881                                     | 255.5 | 0.629                         | 261.4 | 0.225                         | 330.8 |
| 0.915                                        | 257.4 | 0.151                                        | 279.7 | 0.813                                     | 253.2 | 0.709                         | 261.2 | 0.222                         | 280.1 |
| 0.867                                        | 260.6 | 0.197                                        | 279.7 | 0.777                                     | 251.8 | 0.620                         | 261.6 | 0.166                         | 281.4 |
| 0.867                                        | 269.4 | 0.245                                        | 279.3 | 0.746                                     | 265.5 | 0.637                         | 262.0 | 0.016                         | 281.2 |
| 0.843                                        | 254.4 | 0.282                                        | 279.2 | 0.720                                     | 249.5 | 0.644                         | 262.3 | 0.071                         | 281.4 |
| 0.843                                        | 268.6 | 0.307                                        | 278.9 | c-C <sub>6</sub> H <sub>12</sub>          |       | 0.612                         | 0.612 | 262.0                         | 280.9 |
| 0.812                                        | 254.0 | 0.357                                        | 278.2 | 0.883                                     | 280.0 | 0.543                         | 266.8 |                               |       |
| 0.812                                        | 259.5 | 0.375                                        | 276.0 | 0.852                                     | 279.9 | 0.512                         | 269.6 |                               |       |
| 0.812                                        | 259.2 | 0.364                                        | 276.6 | 0.794                                     | 279.8 | 0.486                         | 272.2 |                               |       |
| 0.913                                        | 270.4 | 0.353                                        | 277.6 | 0.739                                     | 279.8 | 0.432                         | 277.3 |                               |       |
| 0.271                                        | 270.0 | 0.336                                        | 285.7 | 0.630                                     | 280.2 | 0.888                         | 260.9 |                               |       |
| 0.317                                        | 269.9 | 0.632                                        | 247.3 | 0.982                                     | 266.0 | 0.786                         | 258.4 |                               |       |
| 0.355                                        | 269.6 | 0.497                                        | 265.5 | 0.967                                     | 275.1 | 0.671                         | 262.3 |                               |       |
| 0.391                                        | 269.5 | 0.436                                        | 271.5 | 0.928                                     | 279.9 | 0.653                         | 262.2 |                               |       |
| 0.441                                        | 269.0 | 0.379                                        | 276.1 | 0.489                                     | 280.2 | 0.624                         | 261.7 |                               |       |
| 0.468                                        | 268.2 | 0.297                                        | 279.4 | 0.000                                     | 280.4 | 0.591                         | 263.0 |                               |       |
| 1.000                                        | 274.0 | 0.846                                        | 255.2 | 0.095                                     | 280.4 | 0.569                         | 265.0 |                               |       |
| 1.000                                        | 260.8 | 0.786                                        | 252.4 | 0.255                                     | 280.4 | 0.466                         | 274.4 |                               |       |
| 1.000                                        | 261.2 | 0.727                                        | 264.6 | 0.387                                     | 280.4 | 0.395                         | 279.2 |                               |       |
| 1.000                                        | 274.4 | 0.673                                        | 248.4 |                                           |       | 0.346                         | 279.5 |                               |       |

**Table 1.** Experimental LLE and SLE data. The concentrations are given as mole fraction of ionic liquid in different (ionic liquid + solvent) systems.

The T-x phase diagrams of the systems ([C<sub>2</sub>mim][NTf<sub>2</sub>] + C<sub>6</sub>F<sub>6</sub>), ([C<sub>2</sub>mim][NTf<sub>2</sub>] + 1F,3F,5F-C<sub>6</sub>H<sub>3</sub>F<sub>3</sub>), and ([C<sub>2</sub>mim][NTf<sub>2</sub>] + c-C<sub>6</sub>H<sub>12</sub>) are presented in Figure 1. The data points presented in Figures 1a to 1c are also given in Table 1. For comparison

and discussion purposes Figure 1d overlaps the most important phase transition boundaries for each system along with those of the previously studied<sup>11</sup> [C<sub>2</sub>mim][NTf<sub>2</sub>] + C<sub>6</sub>H<sub>6</sub> system.

Some obvious conclusions can be taken directly from the analysis of Figure 1d: a) the solubility of the ionic liquid in any of the molecular components is always almost null (in all cases the L+L regions start just at the side of the pure molecular solvent line (upper left side of the phase diagram); b) on the other end of the L+L immiscibility window (vertical lines along the upper edge of Figure 1d) things differ a lot, with the solubility of the aliphatic compound being much smaller (less than 10% mole fraction of cyclohexane) than that of the aromatic compounds. The latter exhibit solubility mole fractions of 55, 66 and 78 % for 1F,3F,5F-C<sub>6</sub>H<sub>3</sub>F<sub>3</sub>, C<sub>6</sub>F<sub>6</sub>, and C<sub>6</sub>H<sub>6</sub>, respectively; c) benzene is the most soluble of the aromatic compounds in terms of the molar fraction of the saturated mixture; d) the most important difference between the phase diagram of the systems containing the fluorinated benzene molecules and the one corresponding to normal benzene is the absence of any congruent melting inclusion compound in the former systems, which is somehow “compensated” by the observation of multiple polymorphic forms of [C<sub>2</sub>mim][NTf<sub>2</sub>] (not shown in Figure 1d but presented in Figures 1a and 1b). In other words all the aromatic molecules are able to permeate the polar network of the ionic liquid (and dissolve much more than their aliphatic counterparts),<sup>13</sup> but the fluorinated benzenes are not able to interact so efficiently like benzene – at least in a well-defined stereochemical way<sup>11</sup> – in order to form an inclusion crystal. This is probably due to the lack or deficiency of hydrogen atoms in the equatorial positions of the aromatic ring, that are responsible for the strong connections with the oxygen atoms of the anion present in the 1:1 inclusion crystal of [C<sub>2</sub>mim][NTf<sub>2</sub>]-C<sub>6</sub>H<sub>6</sub>.

In Figure 2 we show the phase diagram of the system ([C<sub>2</sub>C<sub>1</sub>pyrr][NTf<sub>2</sub>] + C<sub>6</sub>H<sub>6</sub>). The data are also presented in Table 1. In this case we replaced the aromatic cation head group of the ionic liquid (the imidazolium ring) by the saturated pyrrolidinium ring. The liquid-liquid immiscibility region (the rectangles in the upper left corner of Figures 2a and 2b) is almost identical to that observed in the case of the ([C<sub>2</sub>mim][NTf<sub>2</sub>] + C<sub>6</sub>H<sub>6</sub>) system. A lot of emphasis has been laid in previous studies concerning ionic liquid plus aromatic systems on the existence and nature of the  $\pi$ - $\pi$  interactions between the aromatic rings of the cations (that include in most cases imidazolium or pyridinium rings) and the rings of the aromatic molecules. In some

cases the existence of those interactions was suggest to be directly linked to the performance of ionic liquid solvents as catalytic agents for reactions involving the aromatic molecule.<sup>2, 14</sup> This is certainly true but this increased catalytic activity does not necessarily translate into greater solubility of aromatic molecules in ionic liquids that have aromatic rings in their structure as compared to ionic liquids that do not have those rings (the pyrrolidinium cation used in the system under discussion is an obvious example). In other words, whenever chemical reactions that involve the aromatic molecules occur, the existence of aromatic rings in the ionic liquid can play an important part in the process, however that factor does not play a significant role in the determination of liquid-liquid immiscibility of aromatic compounds in ionic liquids.

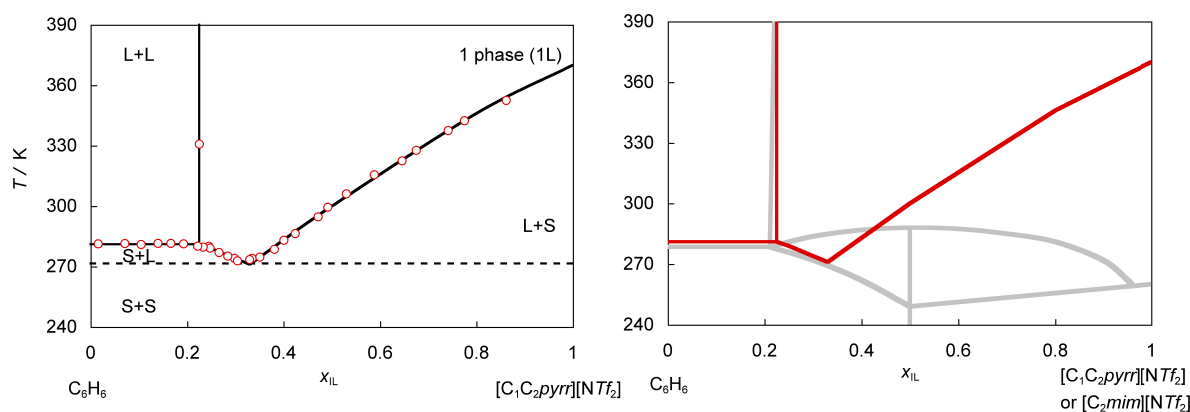


**Figure 2.** ( $T$ - $x$ ) phase diagrams of systems containing  $[C_2C_1pyrr][NTf_2]$  mixed with  $C_6H_6$ . Figure (b) overlaps the diagram of Figure (a) with the schematic representation in grey of the phase diagram of  $[C_2mim][NTf_2] + C_6H_6$ <sup>11</sup>.

One can also argue that even if the L-L immiscibility is unaffected by the absence of aromatic rings in the cations, the same is not true as regards the formation of inclusion compounds (as we have seen in the previous  $[C_2mim][NTf_2]$  plus fluorinated benzene systems, a change in the aromatic character of the molecular component precludes the formation of the inclusion compounds similar to  $[C_2mim][NTf_2] \cdot C_6H_6$ ). As a matter of fact no inclusion compound was found in the case of  $([C_2C_1pyrr][NTf_2] + C_6H_6)$  but it is dangerous to make the inference that this is caused by the absence of the aromatic ring in the cation. The reason is simple: the melting point of  $[C_2C_1pyrr][NTf_2]$  is much higher than that of  $[C_2mim][NTf_2]$ , which means that the crystalline forms of the former ionic liquid are much more stable than those of the latter and that the driving forces towards the formation of inclusion crystals are not present in the case of  $([C_2C_1pyrr][NTf_2] + C_6H_6)$  either due to the lack of the aromatic ring in the cations

(and absence of stabilizing  $\pi$ - $\pi$  interactions between benzene and the cations) or due to the much more stable (pure)  $[\text{C}_2\text{C}_1\text{pyrr}][\text{NTf}_2]$  crystals.

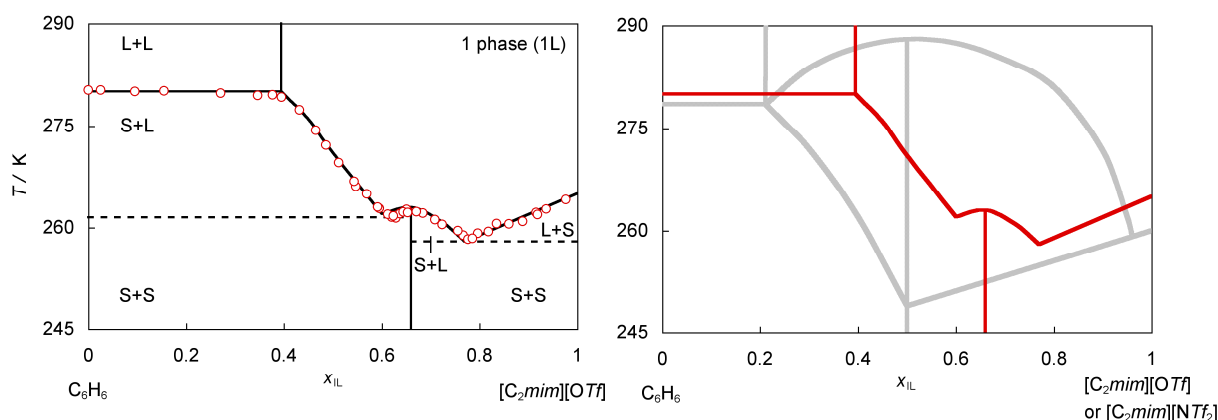


**Figure 3.** ( $T$ - $x$ ) phase diagrams of systems containing  $[\text{C}_2\text{mim}][\text{OTf}]$  mixed with  $\text{C}_6\text{H}_6$ . Figure (b) overlaps the diagram of Figure (a) with the schematic representation in grey of the phase diagram of  $[\text{C}_2\text{mim}][\text{NTf}_2] + \text{C}_6\text{H}_6$ <sup>11</sup>.

Figure 3 shows the phase diagram of the system ( $[\text{C}_2\text{mim}][\text{OTf}] + \text{C}_6\text{H}_6$ ). The experimental  $T$ - $x$  data points used to build the phase diagram are compiled in Table 1. In this case the “aromatic components” of the system were left intact relative to the ( $[\text{C}_2\text{mim}][\text{NTf}_2] + \text{C}_6\text{H}_6$ ) system and only the more flexible, larger  $[\text{NTf}_2]^-$  ion was replaced by the triflate anion, whose oxygen atoms are also capable of strong interactions with the aromatic hydrogen atoms of benzene. This means that the changes in the interaction patterns between the ionic and molecular components of the mixture are quite subtle relative to the “reference” ( $[\text{C}_2\text{mim}][\text{NTf}_2] + \text{C}_6\text{H}_6$ ) system and that is somehow reflected in the phase diagram depicted in Figure 3a that exhibits a 2:1  $[\text{C}_2\text{mim}][\text{OTf}]\cdot\text{C}_6\text{H}_6$  inclusion crystal. When one compares the two inclusion crystals in Figure 3b two conclusions are obvious: they do not occur with the same stoichiometry and their stability is quite different. The issue related to stoichiometry and stability of the inclusion crystals is under further investigation.

## Conclusion

In this work we have determined the solid - liquid and liquid-liquid phase diagrams of several ionic liquids with benzene, or totally or partially fluorinated benzene molecules. The phase diagrams exhibit different kinds of solid-liquid behaviour, ranging from the (usual) occurrence of eutectic points, the existence of

(not-so-usual) congruent melting points and the corresponding formation of inclusion crystals, or the observation of different ionic liquid crystalline phases (polymorphism). The polymorphic outcome of the crystallization is obviously determined by the solvent-influenced initial aggregation or prenucleation self-assembly of [C<sub>2</sub>mim][NTf<sub>2</sub>] molecules in solution.

These different types of behaviour are controlled by the annealing temperature during crystallization or by the nature of the aromatic compound, and could be interpreted at a molecular level taking into account the structure of the crystals.

## References

1. L. D. Simoni, Y. Lin, J. F. Brennecke and M. A. Stadtherr, *Ind. Eng. Chem. Res.*, 2008, **47**, 256-272.
2. J. K. D. Surette, L. Green and R. D. Singer, *Chemical Communications*, 1996, 2753-2754.
3. M. Krummen, D. Gruber and J. Gmehling, *Ind. Eng. Chem. Res.*, 2000, **39**, 2114-2123.
4. J. G. Huddleston, A. E. Visser, W. M. Reichert, H. D. Willauer, G. A. Broker and R. D. Rogers, *Green Chemistry*, 2001, **3**, 156-164.
5. S. Csihony, C. Fischmeister, C. Bruneau, I. T. Horvath and P. H. Dixneuf, *New Journal of Chemistry*, 2002, **26**, 1667-1670.
6. P. J. Dyson, D. J. Ellis, D. G. Parker and T. Welton, *Chemical Communications*, 1999, 25-26.
7. C. J. Adams, M. J. Earle, G. Roberts and K. R. Seddon, *Chemical Communications*, 1998, 2097-2098.
8. M. Deetlefs, C. Hardacre, M. Nieuwenhuyzen, O. Sheppard and A. K. Soper, *Journal of Physical Chemistry B*, 2005, **109**, 1593-1598.
9. J. D. Holbrey, W. M. Reichert, M. Nieuwenhuyzen, O. Sheppard, C. Hardacre and R. D. Rogers, *Chemical Communications*, 2003, 476-477.
10. R. M. Lynden-Bell, M. G. Del Popolo, T. G. A. Youngs, J. Kohanoff, C. G. Hanke, J. B. Harper and C. C. Pinilla, *Accounts of Chemical Research*, 2007, **40**, 1138-1145.
11. J. Lachwa, I. Bento, M. T. Duarte, J. N. C. Lopes and L. P. N. Rebelo, *Chemical Communications*, 2006, 2445-2447.

12. J. Lachwa, J. Szydłowski, A. Makowska, K. R. Seddon, J. Esperanca, H. J. R. Guedes and L. P. N. Rebelo, *Green Chemistry*, 2006, **8**, 262-267.
13. L. P. N. Rebelo, J. N. C. Lopes, J. Esperanca, H. Lachwa, V. Najdanovic-Visak and Z. P. Visak, *Accounts of Chemical Research*, 2007, **40**, 1114-1121.
14. T. Welton, *Coordination Chemistry Reviews*, 2004, **248**, 2459-2477.

## **CHAPTER 6.**

# **SOLUBILITY OF FLUORINATED COMPOUNDS IN A RANGE OF IONIC LIQUIDS. CLOUD-POINT TEMPERATURE DEPENDENCE ON COMPOSITION AND PRESSURE**

*This Chapter was published as a full article:*

Ferreira R., Blesic M., Trindade J., Marrucho I., Canongia Lopes J.N., Rebelo L.P.N., "Solubility of fluorinated compounds in a range of ionic liquids. Cloud-point temperature dependence on composition and pressure", *Green Chemistry*, **2008**, 10, 918.

**Note:** The author of the thesis performed the main part of the experimental work and synthesized some ionic liquids used in this study.



# Solubility of fluorinated compounds in a range of ionic liquids. Cloud-point temperature dependence on composition and pressure

Rui Ferreira,<sup>a</sup> Marijana Blesic,<sup>a</sup> Joana Trindade,<sup>a</sup> Isabel Marrucho,<sup>b</sup> José N. Canongia Lopes<sup>\*a,c</sup> and Luís Paulo N. Rebelo<sup>\*a</sup>

Received 8th April 2008, Accepted 17th June 2008

First published as an Advance Article on the web 11th August 2008

DOI: 10.1039/b805902k

In this work, we explore the mutual solubility of a number of mixtures of commonly used ionic liquids (imidazolium, pyridinium, phosphonium and ammonium ionic liquids) with partially fluorinated *n*-alcohols (C<sub>7</sub> to C<sub>10</sub>) or perfluoroheptane. The corresponding *T*-*x* diagrams at atmospheric pressure were measured through cloud-point temperature determinations. For some selected systems under near-critical isopleth conditions, pressure effects were also studied. The results are discussed in terms of (i) shifts in the immiscibility envelopes as the cation alkyl-chain length is changed, (ii) the nature of the cation or the anion, (iii) the increasing length of the fluorinated/alkylic moiety of the partially fluorinated alcohol, or (iv) comparisons with similar systems involving normal alcohols.

## 1. Introduction

One of the key-issues concerning the current importance of ionic liquids is the fact that they can simultaneously act as sophisticated solvation or reaction media while avoiding dramatic impacts in the environment due to their general low volatility and flammability combined with high thermal stability. Ionic liquids are able to dissolve (at least partially) a wide range of polar or nonpolar, organic or inorganic compounds,<sup>1</sup> providing new ways to carry out chemical reactions or industrial separations.<sup>2</sup>

It was recently reported in different molecular simulation studies<sup>3</sup> that neat ionic liquids exhibit medium-range ordering, in other words, there are persistent microscopic domains in the liquid phase. Other simulation studies<sup>4</sup> on the microscopic dynamics of ionic liquids have also pointed out their slow dynamics and the persistence of local environments, typical of the glassy state.

The segregation in polar and nonpolar domains at a nanoscale level in ionic liquids with alkyl side chains of intermediate length (for instance in 3-alkyl-1-methylimidazolium-based ionic liquids with alkyl groups larger than hexyl), has changed the way in which solvation in these liquids is understood. Some solutes dissolve preferentially in low electrical charge-density domains, while others prefer the Coulomb environment of high electrical-charge density regions, whereas some can even “be dissolved” at the interface between these polar and non-polar territories.<sup>5</sup> These facts account for the extraordinary versatility of ionic liquids as solvents.

Fluorinated organic compounds also display many exceptional physico-chemical properties that have been used in many commercial applications. Similar to ionic liquids, they are also perceived as alternative substances towards the development of

more environmentally friendly processes. Industrial production of these compounds has increased significantly since the early 1980s and fluorinated organics are commonly used as refrigerants, surfactants, polymers, as components of pharmaceuticals, fire retardants, lubricants, and insecticides.<sup>6</sup> In recent years the possibility of their use as gas-carriers (including the possibility of their use as synthetic blood substitutes),<sup>7</sup> and as solubility-promoters in supercritical extraction media<sup>8</sup> has also been explored. From a molecular point of view, the properties of fluorinated organic compounds can be rationalized in terms of the unique interactions they perform with different molecules: fluorocarbons generally exhibit low-intensity interactions with normal organic compounds<sup>9</sup> or water, a fact related not only to their “reversed” quadrupole moment (note that the carbon backbone of a perfluorocarbon molecule carries a partially positive charge, due to the high electronegativity of the fluorine atom, unlike the situation in hydrocarbons or water) but also due to their relatively rigid structure (that inhibits the existence of different conformers and introduces entropic-driven factors in mixtures with other substances).

Functionalized fluorocarbons were also studied in recent years due to their amphiphilic behaviour and their possible use as separation media or surfactant agents. Examples of such compounds are the hydrofluorocarbon molecules,<sup>10</sup> the hydrocarbon-fluorocarbon diblock molecules<sup>11</sup> and the fluorinated alcohols.<sup>12</sup> The rationale behind the synthesis and use of such molecules is the introduction of an interacting group in the otherwise inert perfluorinated chain, that will promote the “docking” of the fluorinated compound in the midst of other molecules (with the possible self-organization of the former in micelles or similar structures) or the formation of emulsions between fluorinated and organic or aqueous domains.

Systems where both types of compound, ionic liquids and fluorinated organic molecules, are inherently appealing as they are perceived as relatively benign media, combining two “clean” substances. This blend also poses very interesting challenges both from the theoretical and the applied chemistry points of

<sup>a</sup>Instituto de Tecnologia Química e Biológica, UNL, 2780 901, Oeiras, Portugal. E-mail: luis.rebelo@itqb.unl.pt

<sup>b</sup>CICECO, Universidade de Aveiro, 3810 193, Aveiro, Portugal

<sup>c</sup>Centro de Química Estrutural, IST, 1049 001, Lisboa, Portugal. E-mail: jnlopes@ist.utl.pt

view. As an example of the former aspect, one can hope to gain some insight about the interactions between the fluorinated molecules and the parts of the ionic liquid that are themselves fluorinated (generally present in anions such as bistriflamide, triflate or hexafluorophosphate). An example of the latter issue can be, for instance, the possibility of using partially fluorinated alcohols or diblock molecules to promote the miscibility (through the formation of micro-emulsions) between bistriflamide-based ionic liquids and aqueous solutions.

In this work, we explore the fluid phase diagrams of mixtures of commonly used ionic liquids with partially fluorinated alcohols. The systems are analyzed in terms of the two-phase envelopes (immiscibility regions) of the corresponding  $T-x$  diagrams at atmospheric pressure, which in turn have been determined by the measurement of cloud-point temperatures as a function of the mixture compositions. Pressure effects were also studied for some selected systems under near-critical isopleth conditions. The results are discussed in terms of shifts in those envelopes as the alkyl side chains of the cations get longer, the nature of the cation or the anion is changed, the length of the fluorinated moiety of the partially fluorinated alcohol is increased, or by comparison with systems involving normal alcohols (ethanol and propanol). We have also noticed the essentially total immiscible behaviour of a range of ionic liquids studied in this work with a linear perfluorinated alkane.

## 2. Experimental

### Materials

Table 1 shows the compounds involved in the detailed determination of the fluid phase behaviour of mixtures of ionic liquids with fluorinated alcohols. In addition to the compounds listed in Table 1, other ionic liquids and other fluorinated alcohols were used in preliminary solubility tests (see Table 2). The complete list, including name and/or commercial name (abbreviated name; CAS number, source and grade if available), is as follows: 1-ethyl-3-methylimidazolium ethylsulfate, ECOENG<sup>TM</sup> 212 ( $C_2mimEtSO_4$ ; 342573-75-5; Solvent Innovation; >99%); trioctylmethylammonium chloride, ALIQUAT<sup>TM</sup> 336 ( $N_{888}Cl$ ; 63393-96-4; Aldrich; n/a); trihexyl-(tetradecyl)phosphonium chloride ( $P_{66614}Cl$ ; 258864-54-9; Cytec; >96%); trihexyl(tetradecyl)phosphonium bis[(trifluoromethyl)sulfonyl]imide ( $P_{66614}NTf_2$ ; 460092-03-9; QUILL†; n/a); trihexyl(tetradecyl)-phosphonium trifluoromethanesulfonate ( $P_{66614}OTf$ ; CAS number; QUILL†; n/a); trihexyl(tetradecyl)-phosphonium acetate ( $P_{66614}Ac$ ; 460092-04-0; QUILL†; n/a); 1-ethyl-3-methylimidazolium bis-[(trifluoromethyl)sulfonyl]imide ( $C_2mimNTf_2$ ; 174899-82-2; QUILL†; n/a); 1-propyl-3-methylimidazolium bis[(trifluoromethyl)sulfonyl]imide ( $C_3mimNTf_2$ ; 216299-72-8; QUILL†; n/a); 1-pentyl-3-methylimidazolium bis[(trifluoromethyl)sulfonyl]imide ( $C_5mimNTf_2$ ; 280779-53-5; QUILL†; n/a); 1-octyl-3-methylimidazolium bis[(trifluoromethyl)sulfonyl]imide ( $C_8mimNTf_2$ ; 178631-04-4; QUILL†; n/a); 1-decyl-3-methylimidazolium bis[(trifluoromethyl)sulfonyl]imide ( $C_{10}mimNTf_2$ ; 433337-23-6; QUILL†; n/a); 1-dodecyl-3-methylimidazolium bis-

[(trifluoromethyl)sulfonyl]imide ( $C_{12}mimNTf_2$ ; unknown CAS; QUILL†; n/a); acetyl-cholinium bis[(trifluoromethyl)sulfonyl]imide ( $AcChNTf_2$ ; unknown CAS; QUILL†; n/a); 1-hexyl-3-methylimidazolium chloride ( $C_6mimCl$ ; 171058-17-6; QUILL†; n/a); 1-dodecyl-3-methylimidazolium chloride ( $C_{12}mimCl$ ; 114569-84-5; QUILL†; n/a); 1-butyl-3-methylimidazolium hexafluoroborate ( $C_4mimBF_4$ ; 174501-65-6; Solvent Innovation GmbH; >99%); 1-butyl-3-methylimidazolium hexafluorophosphate ( $C_4mimPF_6$ ; 174501-64-5; QUILL†; n/a); 1-octyl-3-methylimidazolium hexafluorophosphate ( $C_8mimPF_6$ ; 304680-36-2; QUILL†; n/a); 1-decyl-3-methylpyridinium bis-[(trifluoromethyl)sulfonyl]imide ( $C_{10}MePyNTf_2$ ; unknown CAS; QUILL†; n/a); 1-dodecyl-3-methylpyridinium bis[(trifluoromethyl)sulfonyl]imide ( $C_{12}MePyNTf_2$ ; unknown CAS; QUILL†; n/a); 1-tetradecyl-3-methylpyridinium bis[(trifluoromethyl)sulfonyl]imide ( $C_{14}MePyNTf_2$ ; unknown CAS; QUILL†; n/a); 1-tetradecyl-3-methylpyridinium bromide ( $C_{14}MePyBr$ ; unknown CAS; QUILL†; n/a); 1-butyl-3-methylimidazolium thiocyanate ( $C_4mimSCN$ ; 344790-87-0; Fluka; >95%) e 1-butyl-3-methylimidazolium methylsulfate ( $C_4mimMeSO_4$ ; 401788-98-5; Fluka; >97%).

All ionic liquids used in solubility tests were used without any further purification. Ionic liquids used in cloud-point data measurements were previously dried and degassed under vacuum conditions (1 to 10 Pa) at moderate temperatures (80–100 °C) for periods longer than 24 hours.

The list of alcohols used is as follows: ethanol (64-17-5; Pronalab; 99.8%); 1-propanol (71-23-8; Aldrich; 99.7%) 1*H*,1*H*,7*H*-perfluoroheptanol (117-C<sub>7</sub>FOH; 335-99-9; Apollo Scientific; 98%); 1*H*,1*H*,2*H*,2*H*-perfluorooctanol (1122-C<sub>8</sub>FOH; 647-42-7; ABCR; 98%); 1*H*,1*H*-perfluorooctanol (11-C<sub>8</sub>FOH; 307-30-2; Apollo Scientific; 98%); 1*H*,1*H*-perfluorononanol (11-C<sub>9</sub>FOH; 423-56-3; Apollo Scientific; 98%); 1*H*,1*H*-perfluorodecanol (11-C<sub>10</sub>FOH; 307-37-9; Apollo Scientific; 98%); 1*H*,1*H*,2*H*,2*H*,3*H*,3*H*-perfluorononanol (112233-C<sub>9</sub>FOH; 80806-68-4; Fluorochem; 98%) and perfluoroheptane (C<sub>7</sub>F<sub>16</sub>; 335-57-9; Apollo Scientific, 98%). All fluorinated alcohols were used without further purification.

### Preliminary solubility tests

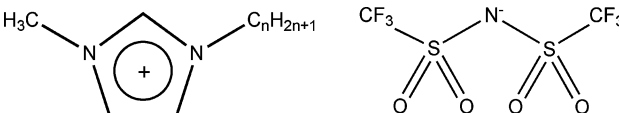
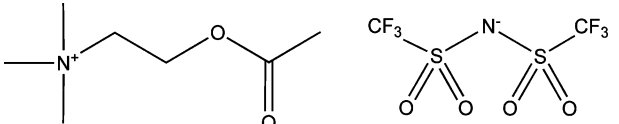
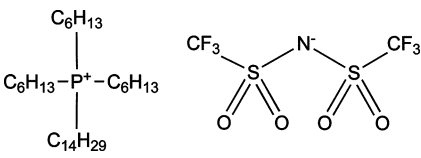
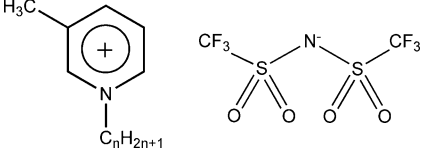
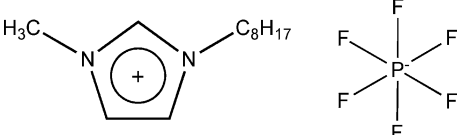
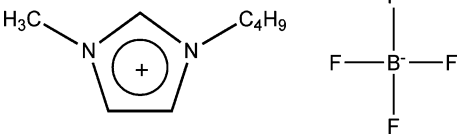
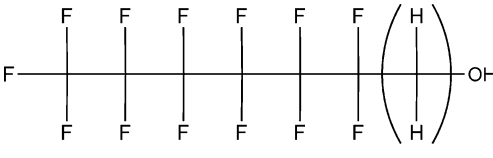
Solubility tests were performed by adding small amounts (*ca.* 100 μL) of IL and fluorinated compound into a glass (Pyrex) conical vessel containing a magnetic stirrer. Any phase separation (if present) was visually detected. Different composition ranges were tested at temperatures from *ca.* –10 °C up to 70 °C.

### Cloud-point measurements

All cloud-point determinations on the temperature-composition phase diagrams of the ionic liquid plus fluorinated alcohol systems at a nominal pressure of 0.1 MPa were performed using a dynamic method with visual detection of the solution turbidity. For this purpose, Pyrex glass view cells with magnetic stirring were used. Samples were gravimetrically prepared directly inside the cells using an analytical high precision balance (±0.01 mg). The cells were then immersed in a thermostatic bath. Providing continuous stirring, we cooled off or heated the solutions usually in two or three runs with the two last runs being carried out very slowly (the

† Queen's University Ionic Liquids Laboratories.

**Table 1** Description of the ionic liquids and fluorinated alcohols used in the cloud-point determinations

| Formal Name                                                                                                                                                                          | Structure                                                                            | Abbreviation                                                |
|--------------------------------------------------------------------------------------------------------------------------------------------------------------------------------------|--------------------------------------------------------------------------------------|-------------------------------------------------------------|
| 1-Alkyl-3-methylimidazolium bis(trifluoromethylsulfonyl)imide (alkyl = octyl, decyl and dodecyl)                                                                                     |    | $C_8mimNTf_2$<br>$C_{10}mimNTf_2$<br>$C_{12}mimNTf_2$       |
| Acetylcholinium bis(trifluoromethylsulfonyl)imide                                                                                                                                    |    | $AcChNTf_2$                                                 |
| Trihexyltetradecylphosphonium bis(trifluoromethylsulfonyl)imide                                                                                                                      |    | $P_{66614}NTf_2$                                            |
| 1-Alkyl-3-methylpyridinium bis(trifluoromethylsulfonyl)imide (alkyl = decyl, dodecyl and tetradecyl)                                                                                 |   | $C_{10}MePyNTf_2$<br>$C_{12}MePyNTf_2$<br>$C_{14}MePyNTf_2$ |
| 1-Octyl-3-methylimidazolium hexafluorophosphate                                                                                                                                      |  | $C_8mimPF_6$                                                |
| 1-Butyl-3-methylimidazolium tetrafluoroborate                                                                                                                                        |  | $C_4mimBF_4$                                                |
| 1 <i>H</i> ,1 <i>H</i> ,2 <i>H</i> ,2 <i>H</i> -Perfluorooctanol ( $n = 2$ )<br>1 <i>H</i> ,1 <i>H</i> ,2 <i>H</i> ,2 <i>H</i> ,3 <i>H</i> ,3 <i>H</i> -Perfluorononanol ( $n = 3$ ) |  | 1122- $C_8$ FOH<br>112233- $C_9$ FOH                        |

rate of temperature change near the cloud point was no more than  $5 \text{ K h}^{-1}$ ). Beginning in the homogeneous region, upon cooling, the temperature at which the first sign of turbidity appeared was taken as the temperature of the liquid–liquid phase transition. Temperature was monitored using a four-wire platinum resistance thermometer coupled to a Yokogawa 7561 multimeter. The thermometer was calibrated against high accuracy mercury thermometers (0.01 K precision). The overall accuracy in the determination of the cloud-point temperatures is estimated to be  $\pm 0.3 \text{ K}$ .

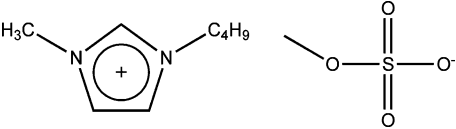
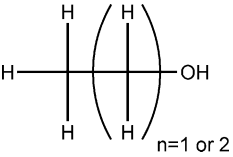
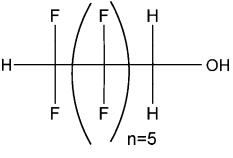
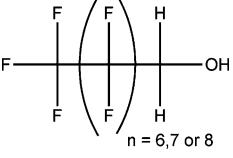
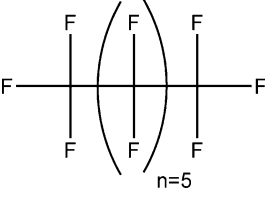
Pressure effects on the cloud-point temperature were obtained by a He–Ne laser light scattering technique. The apparatus and

the methodology used for the determination of phase transitions have already been described in detail.<sup>13</sup> Here, only a brief description is provided. The cell (with an internal volume of *ca.*  $1.0 \text{ cm}^3$  and an optical length of *ca.*  $2.6 \text{ mm}$ ) is a thick-walled Pyrex glass tube that is connected to a pressurization line and separated from it by a mercury plug. The intensity of the scattered light is captured at a very low angle ( $2^\circ < 2\theta < 4^\circ$ ) in the outer portion of a bifurcated optical cable, whereas transmitted light is captured in the inner portion of this cable. The intensity of scattered light ( $I_{sc}$ ) and transmitted light ( $I_{tr}$ ) are corrected for density fluctuations, reflections, and multiple scattering effects. The cloud-point is the point on the

**Table 2** Description of other compounds, not listed in Table 1, which were used in preliminary solubility tests

| Formal Name                                                                                            | Structure | Abbreviation                                                                                                                                             |
|--------------------------------------------------------------------------------------------------------|-----------|----------------------------------------------------------------------------------------------------------------------------------------------------------|
| 1-Ethyl-3-methylimidazolium ethylsulfate<br>(ECOENG™ 212)                                              |           | <i>C</i> <sub>2</sub> <i>mimEtSO</i> <sub>4</sub>                                                                                                        |
| Trioctylmethylammonium chloride<br>(ALIQUAT™ 336)                                                      |           | <i>N</i> <sub>8881</sub> Cl                                                                                                                              |
| Trihexyl(tetradecyl)phosphonium chloride                                                               |           | <i>P</i> <sub>66614</sub> Cl                                                                                                                             |
| Trihexyl(tetradecyl)phosphonium trifluoromethanesulfonate                                              |           | <i>P</i> <sub>66614</sub> <i>OTf</i>                                                                                                                     |
| Trihexyl(tetradecyl)phosphonium acetate                                                                |           | <i>P</i> <sub>66614</sub> <i>Ac</i>                                                                                                                      |
| 1-Alkyl-3-methylimidazolium bis-[(trifluoromethyl)sulfonyl]imide<br>(alkyl = ethyl, propyl and pentyl) |           | <i>C</i> <sub>2</sub> <i>mimNTf</i> <sub>2</sub><br><i>C</i> <sub>3</sub> <i>mimNTf</i> <sub>2</sub><br><i>C</i> <sub>5</sub> <i>mimNTf</i> <sub>2</sub> |
| 1-Alkyl-3-methylimidazolium chloride<br>(alkyl = hexyl, dodecyl)                                       |           | <i>C</i> <sub>6</sub> <i>mimCl</i><br><i>C</i> <sub>12</sub> <i>mimCl</i>                                                                                |
| 1-Butyl-3-methylimidazolium hexafluorophosphate                                                        |           | <i>C</i> <sub>4</sub> <i>mimPF</i> <sub>6</sub>                                                                                                          |
| 1-Tetradecyl-3-methylpyridinium bromide                                                                |           | <i>C</i> <sub>14</sub> <i>MePyBr</i>                                                                                                                     |
| 1-Butyl-3-methylimidazolium thiocyanate                                                                |           | <i>C</i> <sub>4</sub> <i>mimSCN</i>                                                                                                                      |

**Table 2** (Contd.)

| Formal Name                                                                                                                   | Structure                                                                           | Abbreviation                                    |
|-------------------------------------------------------------------------------------------------------------------------------|-------------------------------------------------------------------------------------|-------------------------------------------------|
| 1-Butyl-3-methylimidazolium methylsulfate                                                                                     |   | $C_4mimMeSO_4$                                  |
| Ethanol ( $n = 1$ )<br>Propanol ( $n = 2$ )                                                                                   |    | $C_2H_5OH$<br>$C_3H_7OH$                        |
| 1H,1H,7H-dodecafluoroheptanol                                                                                                 |    | 117- $C_7FOH$                                   |
| 1-(Perfluoroheptyl)methanol ( $n = 6$ )<br>1-(Perfluorooctyl)methanol ( $n = 7$ )<br>1-(Perfluorononanol)methanol ( $n = 8$ ) |   | 11- $C_8FOH$<br>11- $C_9FOH$<br>11- $C_{10}FOH$ |
| Perfluoroheptane                                                                                                              |  | $C_7F_{16}$                                     |

least-squares fits of  $(I_{sc,corr})^{-1}$  against pressure ( $p$ ) or temperature ( $T$ ) where the slope changes abruptly. Temperature accuracy is typically  $\pm 0.01$  K in the range  $240 \text{ K} < T < 380 \text{ K}$ . As for pressure, accuracy is  $\pm 0.01$  MPa in the range  $0.1 \text{ MPa} < p < 5 \text{ MPa}$ . The cell can be operated in the isobaric or isothermal mode. Whenever possible, isothermal runs are preferred over isobaric ones. Pressure transmission (isothermal mode) is many orders of magnitude faster than thermal equilibration (isobaric mode). Also, the rate at which one is able to change pressure is much greater than that for temperature. Nonetheless, many runs had to be performed in the isobaric mode due to the common low  $T$ - $p$  slope presented by the binary mixtures being studied here.

### 3. Results and discussion

The preliminary solubility tests are given in Table 3. These results were used to select the systems that would be more promising in terms of a richer fluid phase behaviour, *i.e.*, systems exhibiting liquid-liquid partial immiscibility (LLE) ending at an upper critical solution temperature, UCST, as

the temperature is increased. For systems presenting this type of phase diagrams one can easily switch between one-phase and two-phase situations either by composition or temperature change. It is important to note that not all systems exhibiting LLE behaviour were selected for the subsequent cloud-point measurements (those that were selected are highlighted in grey in Table 3). There were different types of reasons for the rejection of some of the systems: some systems contained ionic liquids with rather high melting points (an LLE line interrupted by a solid-liquid equilibrium (SLE) line), which can cause problems in terms of turbidity detection; others exhibited degradation problems at temperatures near the UCST; *etc.* The solubility tests were also used to select the “best” fluorinated alcohol—that presenting LLE behaviour in mixtures with different ionic liquids at experimentally convenient conditions. In this case, it was found that a higher number of hydrogenated carbon atoms near the hydroxyl function decreased the miscibility between the ionic liquids and the fluorinated alcohols, promoting the appearance of larger immiscibility domains. The selected fluorinated alcohol was thus 1122- $C_8FOH$  (or 112233- $C_9FOH$  in just one case, for comparison purposes only). Tests with two normal (hydrogenated) alcohols, ethanol and propanol, were

**Table 3** Solubility tests in (ionic liquid + fluorinated alcohol) and (ionic liquid + perfluoroalkane) mixtures. M: miscible (one fluid phase system); PM: partially miscible; LPM: low partial miscibility; I: immiscible; LLE: liquid–liquid equilibria; SLE: solid–liquid equilibria. Note that all these fluorinated alcohols are water immiscible. The cells highlighted in bold correspond to systems where the determination of the corresponding fluid phase diagrams was possible

|                                       | 117-C <sub>7</sub> FOH | 1122-C <sub>8</sub> FOH | 11-C <sub>8</sub> FOH | 112233-C <sub>9</sub> FOH | 11-C <sub>9</sub> FOH | 11-C <sub>10</sub> FOH | C <sub>7</sub> F <sub>16</sub> |
|---------------------------------------|------------------------|-------------------------|-----------------------|---------------------------|-----------------------|------------------------|--------------------------------|
| P <sub>66614</sub> NTf <sub>2</sub>   | M                      | <b>PM (LLE)</b>         | M                     | —                         | —                     | M                      | I to LPM                       |
| P <sub>66614</sub> Cl                 | M                      | M                       | —                     | —                         | —                     | —                      | I                              |
| P <sub>66614</sub> OTf                | M                      | —                       | M                     | —                         | M                     | M (SLE)                | I                              |
| P <sub>66614</sub> Ac                 | —                      | —                       | M (SLE)               | —                         | M                     | foam (LLE)             | —                              |
| C <sub>2</sub> mimNTf <sub>2</sub>    | M                      | —                       | M                     | —                         | M                     | M                      | —                              |
| C <sub>3</sub> mimNTf <sub>2</sub>    | —                      | PM (LLE)                | —                     | —                         | —                     | —                      | I to LPM                       |
| C <sub>5</sub> mimNTf <sub>2</sub>    | M                      | —                       | —                     | —                         | —                     | —                      | I to LPM                       |
| C <sub>8</sub> mimNTf <sub>2</sub>    | —                      | <b>PM (LLE)</b>         | —                     | —                         | —                     | —                      | —                              |
| C <sub>10</sub> mimNTf <sub>2</sub>   | M                      | <b>PM (LLE)</b>         | M                     | <b>PM (LLE)</b>           | —                     | M                      | I to LPM                       |
| C <sub>12</sub> mimNTf <sub>2</sub>   | M                      | <b>PM (LLE)</b>         | —                     | —                         | —                     | —                      | I                              |
| AcChNTf <sub>2</sub>                  | —                      | <b>PM (LLE)</b>         | —                     | —                         | —                     | —                      | —                              |
| C <sub>6</sub> mimCl                  | —                      | M                       | —                     | —                         | M                     | M                      | —                              |
| C <sub>12</sub> mimCl                 | M                      | —                       | —                     | —                         | —                     | —                      | I                              |
| C <sub>4</sub> mimBF <sub>4</sub>     | M                      | <b>PM (LLE)</b>         | M (SLE)               | —                         | —                     | M (SLE)                | —                              |
| C <sub>4</sub> mimPF <sub>6</sub>     | M                      | PM (LLE)                | —                     | —                         | —                     | —                      | I to LPM                       |
| C <sub>8</sub> mimPF <sub>6</sub>     | —                      | <b>PM (LLE)</b>         | —                     | —                         | —                     | —                      | —                              |
| C <sub>10</sub> MePy NTf <sub>2</sub> | —                      | <b>PM (LLE)</b>         | —                     | —                         | —                     | —                      | —                              |
| C <sub>12</sub> MePy NTf <sub>2</sub> | —                      | <b>PM (LLE)</b>         | —                     | —                         | —                     | —                      | —                              |
| C <sub>14</sub> MePy NTf <sub>2</sub> | —                      | <b>PM (LLE)</b>         | M                     | —                         | —                     | M                      | —                              |
| C <sub>14</sub> MePy Br               | —                      | PM (LLE)                | —                     | —                         | —                     | —                      | —                              |
| ECOENG 212                            | M                      | M                       | M                     | —                         | M                     | gel-like (LLE)         | —                              |
| AMMOENG 102                           | —                      | M                       | —                     | —                         | —                     | —                      | I                              |
| ALIQUAT 336                           | —                      | M                       | M                     | —                         | M                     | M                      | —                              |
| C <sub>4</sub> mim SCN                | —                      | M                       | —                     | —                         | —                     | —                      | —                              |
| C <sub>4</sub> mim SO <sub>4</sub>    | —                      | M                       | —                     | —                         | —                     | —                      | —                              |

also performed in order to compare the fluid phase behaviour of their mixtures with ionic liquids.

It should be noted that M. Shiflett and A. Yokozeki<sup>10,14–16</sup> determined a series of phase diagrams of several small-molecule hydrofluorocarbons with C<sub>2</sub>mimNTf<sub>2</sub>, C<sub>4</sub>mimPF<sub>6</sub>, C<sub>n</sub>mimBF<sub>4</sub> ( $n = 2$  or  $4$ ).

The results of the cloud-point determinations are given in Table 4 for the thirteen selected (ionic-liquid + alcohol) systems: ten systems with 1122-C<sub>8</sub>FOH (highlighted in Table 3), one system with 1-decyl-3-methylimidazolium bistriflamide plus 112233-C<sub>9</sub>FOH, and two with acetylcholinium bistriflamide plus ethanol or propanol.

Fig. 1 (a to d) depicts the fluid phase behaviour of mixtures of dialkylimidazolium bistriflamide ionic liquids with 1122-C<sub>8</sub>FOH or 112233-C<sub>9</sub>FOH. The figure shows that the fluid phase behaviour is affected by the length of the alkyl side-chains connected to the imidazolium ring of the ionic liquid and by the length of the hydrogenated segment between the perfluorinated chain and the hydroxyl group of the alcohol. It must be stressed that the scale ( $x$ - and  $y$ -axes ranges) in Fig. 1 was adjusted to the scale of all subsequent figures that depict the fluid phase behaviour in ionic liquid plus alcohol mixtures (Fig. 3 to 5), in order to facilitate comparisons between them—hence the apparently unused space in panels (a to d) in Fig. 1.

The general trend depicted in Fig. 1 can thus be summarized as follows: (i) ionic liquids with longer alkyl-side chains (in the imidazolium cation) show a larger immiscibility domain with fluorinated alcohols than their shorter-chain counterparts—a behaviour opposite of that shown when  $n$ -alcohols are mixed with these same ionic liquids,<sup>17,18</sup> or  $N$ -alkyl-3-methylpyridinium-

based ionic liquids;<sup>17</sup> (ii) a longer hydrogenated carbon chain—a kind of “spacer”—between the fluorinated chain and the hydroxyl group of the alcohol also decreases the miscibility between the two components of the mixture; and (iii) larger immiscibility regions (an increase in the  $T_{UCST}$ ) are accompanied by a shift in the critical composition to mixtures richer in the fluorinated alcohol.

Trend (i) can be interpreted taking into account the recently discovered nano-structure of ionic liquids, exhibiting high-charge (polar) and low-charge (non-polar) density regions,<sup>3</sup> and also their dual nature as they interact with a given solute either *via* the non-polar or polar regions, or (in the latter case) *via* the charged parts of the anion or of the cation.<sup>1</sup> Previous simulation studies,<sup>5</sup> supported by experimental evidence have shown that the hydroxyl group of alcohols interact strongly with the anions of ionic liquids and also with the hydrogen atoms directly connected to the imidazolium ring (especially the one at C2) and that the alkyl side chain of the alcohol orients itself away from the polar region and towards the non-polar domains of the ionic liquid. To confirm these facts for bistriflamide-based ionic liquids, new Molecular Dynamics simulations were performed within the scope of the present work: methanol and tetrafluoromethane molecules acting as test-solutes and C<sub>4</sub>mimNTf<sub>2</sub> acting as the solvent were modelled by explicit-atom force fields.<sup>19–22</sup> Details of the simulations were similar to those adopted for pure ionic liquids.<sup>23</sup> Due to the slow dynamics of this type of system, special care was taken to ensure that equilibrium conditions were reached, including the proper diffusion of the solutes in the ionic liquid. Equilibration and production runs were implemented for 1 ns and multiple re-equilibrations through the use of temperature annealing

**Table 4** Cloud-point temperatures as a function of the ionic liquid mole fraction in different (ionic liquid + alcohol) systems. All systems include the alcohol 1122-C<sub>8</sub>FOH, except where stated

| <i>x</i> <sub>IL</sub>                           | <i>T</i> /K | <i>x</i> <sub>IL</sub>                           | <i>T</i> /K | <i>x</i> <sub>IL</sub>               | <i>T</i> /K | <i>x</i> <sub>IL</sub>               | <i>T</i> /K | <i>x</i> <sub>IL</sub>            | <i>T</i> /K | <i>x</i> <sub>IL</sub>            | <i>T</i> /K | <i>x</i> <sub>IL</sub>               | <i>T</i> /K |
|--------------------------------------------------|-------------|--------------------------------------------------|-------------|--------------------------------------|-------------|--------------------------------------|-------------|-----------------------------------|-------------|-----------------------------------|-------------|--------------------------------------|-------------|
| C <sub>8</sub> mimNTf <sub>2</sub>               |             | C <sub>12</sub> mimNTf <sub>2</sub>              |             | C <sub>10</sub> MePyNTf <sub>2</sub> |             | C <sub>14</sub> MePyNTf <sub>2</sub> |             | AcChNTf <sub>2</sub> <sup>b</sup> |             | AcChNTf <sub>2</sub> <sup>c</sup> |             | C <sub>8</sub> mimPF <sub>6</sub>    |             |
| 0.155                                            | 263.9       | 0.533                                            | 282.0       | 0.575                                | 269.4       | 0.460                                | 292.1       | 0.008                             | 308.6       | 0.268                             | 285.4       | 0.065                                | 320.0       |
| 0.220                                            | 266.5       | 0.060                                            | 273.7       | 0.616                                | 269.0       | 0.426                                | 292.7       | 0.017                             | 319.8       | 0.231                             | 288.1       | 0.092                                | 323.5       |
| 0.302                                            | 268.3       | 0.136                                            | 283.2       | 0.655                                | 266.8       | 0.378                                | 293.2       | 0.023                             | 324.7       | 0.202                             | 290.0       | 0.115                                | 325.1       |
| 0.384                                            | 268.3       | 0.199                                            | 284.8       | 0.694                                | 263.9       | 0.340                                | 293.5       | 0.031                             | 328.2       | 0.179                             | 291.1       | 0.145                                | 326.0       |
| 0.670                                            | 264.5       | 0.739                                            | 267.3       | 0.736                                | 263.0       | 0.314                                | 293.5       | 0.041                             | 331.0       | 0.160                             | 291.8       | 0.183                                | 327.0       |
| 0.569                                            | 268.5       | 0.623                                            | 277.2       | 0.066                                | 259.4       | 0.270                                | 293.5       | 0.051                             | 332.5       | 0.122                             | 292.6       | 0.232                                | 327.6       |
| 0.466                                            | 269.2       | C <sub>10</sub> mimNTf <sub>2</sub> <sup>a</sup> |             | 0.097                                | 265.7       | 0.239                                | 293.4       | 0.063                             | 333.5       | 0.088                             | 292.7       | 0.284                                | 328.1       |
| 0.346                                            | 268.9       | 0.093                                            | 280.8       | 0.118                                | 267.8       | AcChNTf <sub>2</sub>                 |             | 0.076                             | 334.1       | C <sub>4</sub> mimBF <sub>4</sub> |             | P <sub>6,6,14</sub> NTf <sub>2</sub> |             |
| C <sub>10</sub> mimNTf <sub>2</sub> <sup>b</sup> |             | 0.118                                            | 283.3       | C <sub>12</sub> MePyNTf <sub>2</sub> |             | 0.006                                | 282.6       | 0.093                             | 334.3       | 0.313                             | 284.3       | 0.015                                | 283.8       |
| 0.038                                            | 252.3       | 0.141                                            | 285.5       | 0.050                                | 267.7       | 0.017                                | 304.6       | 0.108                             | 334.4       | 0.371                             | 287.7       | 0.021                                | 290.3       |
| 0.052                                            | 261.2       | 0.174                                            | 287.1       | 0.083                                | 275.4       | 0.028                                | 313.6       | 0.125                             | 334.3       | 0.404                             | 290.1       | 0.035                                | 295.9       |
| 0.083                                            | 267.5       | 0.222                                            | 287.9       | 0.120                                | 278.5       | 0.045                                | 319.6       | 0.153                             | 333.9       | 0.439                             | 291.9       | 0.048                                | 300.0       |
| 0.102                                            | 270.4       | 0.273                                            | 288.3       | 0.163                                | 281.0       | 0.064                                | 323.6       | 0.173                             | 333.4       | 0.480                             | 294.8       | 0.063                                | 302.4       |
| 0.760                                            | 259.9       | 0.350                                            | 287.8       | 0.200                                | 281.9       | 0.087                                | 326.1       | 0.190                             | 332.9       | 0.508                             | 297.0       | 0.084                                | 303.6       |
| 0.690                                            | 266.2       | 0.406                                            | 286.1       | 0.227                                | 282.7       | 0.106                                | 327.9       | 0.181                             | 333.2       | 0.538                             | 299.1       | 0.134                                | 305.5       |
| 0.625                                            | 270.7       | 0.048                                            | 270.3       | 0.269                                | 283.0       | 0.129                                | 329.6       | 0.212                             | 331.8       | 0.572                             | 301.2       | 0.180                                | 306.1       |
| 0.045                                            | 256.9       | 0.072                                            | 276.6       | 0.331                                | 283.1       | 0.169                                | 330.7       | 0.248                             | 329.5       | 0.601                             | 302.8       | 0.234                                | 306.1       |
| 0.067                                            | 262.9       | 0.062                                            | 274.3       | 0.418                                | 282.5       | 0.202                                | 331.4       | 0.289                             | 326.4       | 0.621                             | 303.7       | 0.381                                | 303.2       |
| 0.080                                            | 266.0       | 0.078                                            | 278.1       | 0.638                                | 273.6       | 0.227                                | 331.8       | 0.629                             | 275.7       | 0.609                             | 303.5       | 0.445                                | 300.7       |
| 0.094                                            | 268.6       | 0.291                                            | 288.2       | 0.560                                | 278.0       | 0.255                                | 332.0       | 0.553                             | 292.3       | 0.645                             | 304.8       | 0.518                                | 295.8       |
| 0.121                                            | 270.8       | 0.329                                            | 288.0       | 0.508                                | 281.0       | 0.286                                | 332.3       | 0.422                             | 311.5       | 0.696                             | 306.5       | 0.634                                | 284.3       |
| 0.139                                            | 272.2       | 0.388                                            | 286.6       | C <sub>14</sub> MePyNTf <sub>2</sub> |             | 0.318                                | 332.2       | 0.340                             | 321.4       | 0.744                             | 307.8       | 0.686                                | 278.2       |
| 0.168                                            | 274.1       | 0.451                                            | 284.9       | 0.020                                | 267.2       | 0.348                                | 332.4       | 0.242                             | 329.8       | 0.805                             | 308.7       | 0.013                                | 280.9       |
| 0.185                                            | 274.4       | 0.501                                            | 283.0       | 0.034                                | 277.5       | 0.374                                | 332.0       | AcChNTf <sub>2</sub> <sup>c</sup> |             | 0.846                             | 309.4       | 0.028                                | 293.6       |
| 0.219                                            | 275.0       | 0.573                                            | 279.3       | 0.045                                | 281.2       | 0.412                                | 332.0       | 0.009                             | 255.3       | 0.986                             | 301.3       | 0.058                                | 301.7       |
| 0.261                                            | 275.6       | 0.648                                            | 273.0       | 0.066                                | 286.7       | 0.311                                | 332.8       | 0.011                             | 258.4       | 0.942                             | 307.5       | 0.085                                | 303.9       |
| 0.313                                            | 276.0       | 0.703                                            | 269.3       | 0.082                                | 288.5       | 0.394                                | 332.4       | 0.014                             | 273.4       | 0.794                             | 307.1       | 0.114                                | 305.3       |
| 0.260                                            | 275.9       | C <sub>10</sub> MePyNTf <sub>2</sub>             |             | 0.106                                | 290.7       | 0.456                                | 332.2       | 0.018                             | 275.5       | 0.818                             | 307.1       | 0.163                                | 306.0       |
| 0.329                                            | 276.1       | 0.111                                            | 266.8       | 0.126                                | 291.7       | 0.519                                | 331.2       | 0.019                             | 276.5       | 0.851                             | 307.3       | 0.215                                | 306.0       |
| 0.382                                            | 275.8       | 0.146                                            | 271.0       | 0.153                                | 292.6       | 0.559                                | 330.5       | 0.024                             | 283.8       | 0.890                             | 306.4       | 0.268                                | 305.8       |
| 0.436                                            | 275.6       | 0.183                                            | 273.0       | 0.191                                | 293.1       | 0.594                                | 329.9       | 0.027                             | 285.5       | 0.982                             | 296.1       | 0.315                                | 304.8       |
| 0.480                                            | 274.1       | 0.220                                            | 273.7       | 0.222                                | 293.2       | 0.630                                | 328.8       | 0.030                             | 286.8       | 0.959                             | 303.0       | 0.770                                | 263.3       |
| 0.527                                            | 273.1       | 0.278                                            | 274.5       | 0.820                                | 263.5       | 0.671                                | 326.8       | 0.034                             | 288.3       | 0.924                             | 304.9       | 0.568                                | 292.0       |
| 0.565                                            | 272.2       | 0.313                                            | 274.6       | 0.768                                | 271.1       | 0.712                                | 323.4       | 0.041                             | 289.7       | 0.691                             | 304.2       |                                      |             |
| 0.605                                            | 270.6       | 0.349                                            | 274.0       | 0.705                                | 278.1       | 0.749                                | 320.4       | 0.072                             | 292.2       | 0.479                             | 294.2       |                                      |             |
| 0.653                                            | 268.3       | 0.386                                            | 273.9       | 0.647                                | 283.6       | 0.910                                | 280.4       | 0.104                             | 292.8       | 0.591                             | 300.5       |                                      |             |
| 0.730                                            | 263.0       | 0.424                                            | 273.0       | 0.610                                | 286.2       | 0.853                                | 302.5       | 0.143                             | 292.2       | 0.405                             | 293.2       |                                      |             |
| C <sub>12</sub> mimNTf <sub>2</sub> <sup>c</sup> |             | 0.438                                            | 273.6       | 0.569                                | 288.4       | 0.801                                | 314.5       | 0.520                             | 251.6       | 0.645                             | 306.6       |                                      |             |
| 0.273                                            | 285.8       | 0.483                                            | 273.0       | 0.528                                | 290.0       | 0.831                                | 308.8       | 0.400                             | 269.8       | C <sub>8</sub> mimPF <sub>6</sub> |             |                                      |             |
| 0.393                                            | 285.2       | 0.529                                            | 272.2       | 0.493                                | 291.2       | 0.722                                | 322.8       | 0.325                             | 279.4       | 0.041                             | 314.3       |                                      |             |

<sup>a</sup> 112233-C<sub>9</sub>FOH. <sup>b</sup> Propanol. <sup>c</sup> Ethanol.

and/or switching off and on of the Coulomb interactions were performed. The temperature, pressure and low concentration of the solutions ensured that they were performed in the one-phase region of each system. Solvent–solute radial distribution functions (RDFs) for selected atoms from each species (solute, cation and anion) were calculated from the structural simulation data and are shown in Fig. 2. Fig. 2a describes the position of the hydroxyl hydrogen atom of methanol (HO) relative to different atoms of the ionic liquid. The strong interaction of HO with the oxygen atom of bistriflamide (OBT) is obvious and confirms the statements produced at the beginning of this paragraph. On the other hand, the RDFs of Fig. 2b show how the methanol molecule orients itself in relation to the strong interaction centre OBT: the succession of the three peaks clearly shows that the hydrogen points towards the oxygen atom (possibly forming an hydrogen bond), while the methyl group points in the opposite direction (towards the less polar regions of the ionic liquid, *cf.* below). Finally, Fig. 2c shows the RDFs describing the position of the carbon atom of CF<sub>4</sub> (CFC) relative to different atoms of

the anion or cation of the ionic liquid. The changes are dramatic in relation to Fig. 2a: the solute is now positioned in the non-polar domains of the ionic liquid, as denoted by the RDF of CFC with the end-carbon of the butyl group of the cation, CT. However the different RDFs also show that there is a certain degree of affinity between CFC and the fluorine atoms of the CF<sub>3</sub> groups of bistriflamide (*cf.* the CFC-FBT radial distribution function), which means that probably the perfluorinated solutes will prefer to stay away from the polar regions of the ionic liquid but as close as possible to the CF<sub>3</sub> groups of bistriflamide. We must keep in mind that the interactions of perfluorocarbons with hydrocarbons are quite unfavourable and in this particular case the position of the perfluorinated solute is dictated simply by the less unfavourable position, a situation that can be partially mitigated by some (favourable) interactions with other (not so dissimilar) CF<sub>3</sub> groups.

Returning to the discussion of the systems studied experimentally, in the case of the fluorinated alcohols with an ethyl or propyl “spacer” group, 1122-C<sub>8</sub>FOH or 112233-C<sub>9</sub>FOH,

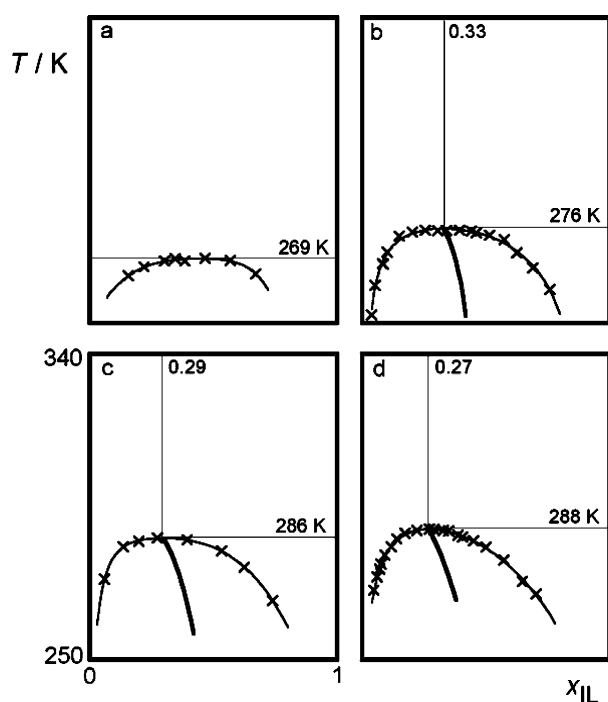


**Fig. 1** Cloud-point temperature,  $T$ , as a function of composition (mole fraction of ionic liquid,  $x_{\text{IL}}$ ) in (a)  $\text{C}_8\text{mimNTf}_2 + 1122\text{-C}_8\text{FOH}$ ; (b)  $\text{C}_{10}\text{mimNTf}_2 + 1122\text{-C}_8\text{FOH}$ ; (c)  $\text{C}_{12}\text{mimNTf}_2 + 1122\text{-C}_8\text{FOH}$ ; and (d)  $\text{C}_{10}\text{mimNTf}_2 + 112233\text{-C}_9\text{FOH}$ . (x): experimental cloud-point data; black lines represent fittings to each side of the liquid–liquid equilibrium envelope; grey lines represent the average composition as determined by the rectilinear diameter law. Also shown are the estimated values for the upper critical solution temperature,  $T_{\text{UCST}}$ , and critical composition.

respectively, the perfluorinated segment will be thrown by the hydrogenated segment deep into the non-polar region of the ionic liquid, where the interactions are unfavourable and the driving force towards phase separation is larger. When the alkyl side-chains of the cation are longer, the nano-segregation is more noticeable and the non-polar domains are larger, which means that the immiscibility regions will also increase, as can be observed in the series of mixtures depicted in Fig. 1a to 1c.

Trend (ii) is noticeable not only by the comparison between Fig. 1b and 1d—a  $T_{\text{UCST}}$  upwards shift of  $\sim 12$  K—but also by the fact that fluorinated alcohols with just one hydrogenated atom of carbon exhibit complete miscibility with the ionic liquid (*cf.* Table 3). Conversely, perfluorinated alkanes—with no spacer and no hydroxyl group—exhibit large immiscibility walls (complete immiscibility or very limited partial miscibility, *cf.* last column of Table 3) with different ionic liquids.<sup>24</sup> This trend can also be interpreted by the “dual-nature” arguments presented in the previous paragraphs. In fact, the increased miscibility of perfluorinated alcohols or fluorinated alcohols with short spacers (such as methyl) can be better understood if one also recognizes the presence of “fluorinated-friendly” residues included in (or adjacent to) the polar domains of the ionic liquid: the perfluoromethyl groups present at the ends of the bistriflamide anion. In the case of fluorinated alcohols with no or short spacers, the hydroxyl group will anchor the alcohol “head” near the polar regions and the short spacer will allow the perfluorinated chain to remain close to the polar domain

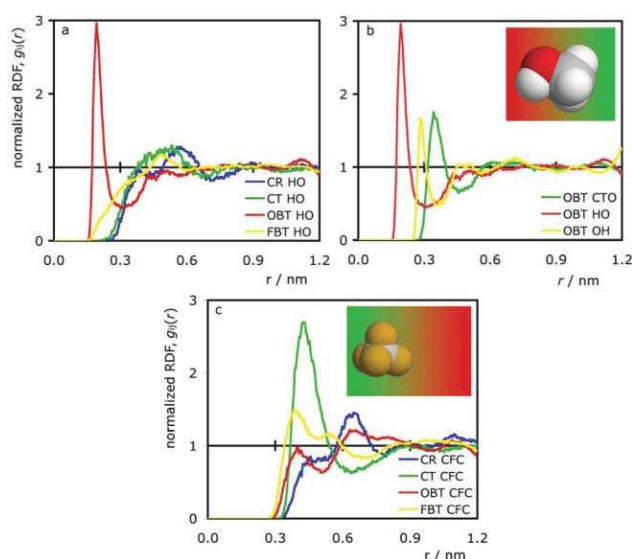


**Fig. 2** Solute–solvent radial distribution functions showing the position and orientation of methanol (a and b) and tetrafluoromethane (c) dissolved in  $[\text{C}_4\text{mim}][\text{NTF}_2]$ . The insets indicate schematically the preference of each solute for the high-charge (red) or low-charge (green) regions of the ionic liquid. HO, OH and CTO represent the hydrogen (hydroxyl), oxygen and carbon atoms of methanol, respectively; CR the carbon atom between the two nitrogens of the imidazolium ring; CT the terminal carbon in the butyl chain of the cation; and OBT and FBT the oxygen and fluorine atoms of the anion, respectively. CFC holds for the carbon atom of tetrafluoromethane.

where it can orient itself towards the end groups of bistriflamide, thus increasing the mutual miscibility of the alcohol and the ionic liquid. When the hydroxyl group is absent (as in the case of perfluoroalkanes) no anchoring process is possible and the perfluorinated compound (that has no driving force to stay close to the polar regions) will exhibit large immiscibility windows in mixtures with ionic liquids.

Trend (iii) will be discussed below, when other ionic liquids and alcohols with different volume ratios are presented.

In Fig. 3 mixtures with a different family of ionic liquids—*N*-alkyl-3-methylpyridinium bistriflamide—are shown. The only difference between the previous systems and the present ones is the “head” of the cation that was “switched” from a methyl-imidazolium ring to a methyl-pyridinium one (*cf.* Table 1).

The differences between Fig. 1 and 3, especially when ionic liquids with the same alkyl side-chain length are compared (Fig. 1b and 3a; Fig. 1c and 3b), are very small both in terms of the upper critical solution temperatures and concentrations. This lends support to the view that no specific interactions between the fluorinated alcohol and the charged part of these two particular ionic liquid cations are present in the mixture. The structural similarity between the two head groups of the cations (both alkyl-substituted hetero-aromatic rings) also explains the similarity of the fluid phase behaviour.

The acetylcholinium cation was tested in the systems represented in Fig. 4. The most obvious difference in relation to the systems presented in Fig. 1 and 3 is that by changing the structural nature of the cation (the long alkyl side chain was changed into a shorter, functionalized one; the hetero-aromatic head group was replaced by a tetra-alkyl ammonium cation)



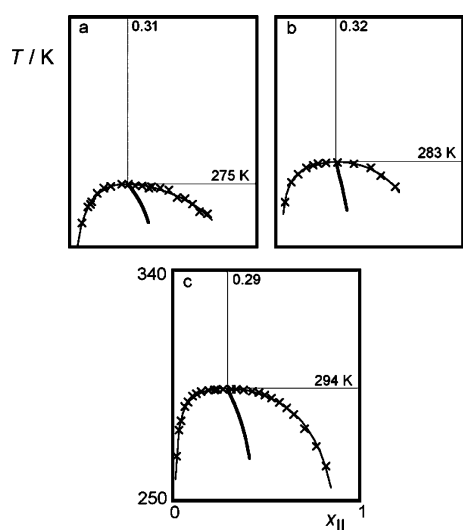


**Fig. 3** Cloud-point temperature as a function of composition (mole fraction of ionic liquid) in (a)  $C_{10}MePyNTf_2 + 1122-C_8FOH$ ; (b)  $C_{12}MePyNTf_2 + 1122-C_8FOH$ ; and (c)  $C_{14}MePyNTf_2 + 1122-C_8FOH$ . Symbols and lines as in Fig. 1.

the immiscibility window with the fluorinated alcohol increases dramatically.

It is hard to interpret these results in terms of the polar/non-polar structure of the ionic liquid and of the specific interactions of the fluorinated alcohol with the anion. In acetylcholinium-based ionic liquids one can argue that the functionalization of the alkyl side-chain with an ester group increases the charge density of the non-polar regions, eventually reducing the segregated character of the ionic liquid and decreasing the size of its non-polar domains. This can be discussed in terms of the results presented in Fig. 4b, where the solubility of ethanol and propanol in  $AcChNTf_2$  is shown. At room temperature (298 K) ethanol is completely miscible with  $AcChNTf_2$ , exhibiting an upper critical solution temperature at around 293 K. The corresponding value for the propanol mixtures is 338 K, signalling a much larger immiscibility domain. This can be easily understood in terms of the inability of the ionic liquid to accommodate the longer alkyl moieties of the propanol among its functionalized, high charge-density, alkyl side-chains. However, the increased immiscibility of the fluorinated alcohol in  $AcChNTf_2$  cannot be understood considering only the partial destruction of the non-polar regions of the latter substance. In fact, we saw in previous systems that a smaller non-bonded region increased

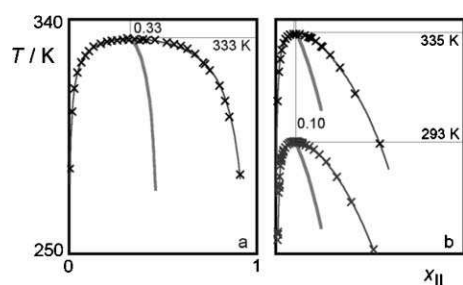


**Fig. 4** Cloud-point temperature as a function of composition (mole fraction of ionic liquid) in (a)  $AcChNTf_2 + 1122-C_8FOH$ ; (b)  $AcChNTf_2 + C_3H_8OH$  (top);  $AcChNTf_2 + C_2H_5OH$  (bottom). Symbols and lines as in Fig. 1.

the miscibility. The detail that is missing is that now the hydroxy group of the fluorinated alcohol can interact not only with the oxygen atoms of bistriflamide (and orient its fluorinated moiety towards the  $CF_3$  end-groups of that anion) but also interact with the oxygen atoms of the ester group (which implies the presence of the fluorinated residue in the midst of the alkyl side chain of the cation). This competition will promote the immiscibility of the fluorinated alcohol in the acetylcholinium-based ionic liquid.

Fig. 5 presents the results for mixtures of different types of ionic liquid with the fluorinated alcohol 1122- $C_8FOH$ . In this case both the cation and the anion were changed.

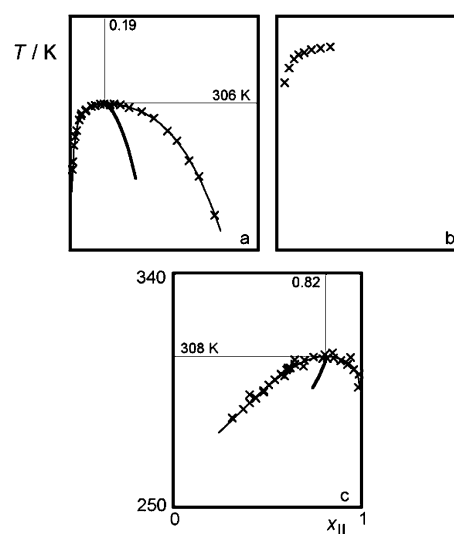


**Fig. 5** Cloud-point temperature as a function of composition (mole fraction of ionic liquid) in (a)  $P_{66614}NTf_2 + 1122-C_8FOH$ ; (b)  $C_8mimPF_6 + 1122-C_8FOH$ ; (c)  $C_4mimBF_4 + 1122-C_8FOH$ . Symbols and lines as in Fig. 1.

In Fig. 5a we show the fluid phase diagram of mixtures of the fluorinated alcohol with a tetra-alkylphosphonium-based ionic liquid with bistriflamide as counter-ion. The immiscibility envelope lies somewhere in between those of imidazolium- and pyridinium-based ionic liquids (Fig. 1 and 3) and that of the acetylcholinium-based ionic liquid (Fig. 4a). Immiscibility is larger than in the former cases because the non-polar regions are bigger (four alkyl side-chains) and surround the charged part of the ionic liquid (the phosphorus atom in the cation and the bistriflamide anion), making it more difficult for the alcohol to anchor and orient itself favourably in the vicinity of the anion. On the other hand, miscibility is larger than in the acetylcholinium case due to the absence of the ester groups in the alkyl-side chains (*cf.* discussion above).

In Fig. 5b, the bistriflamide anion of the ionic liquid was substituted by the hexafluorophosphate anion. The fluid phase diagram is incomplete due to decomposition problems at the temperatures that needed to be attained to measure the corresponding cloud-points (one of the reasons behind the increasing popularity of bistriflamide as the “standard” anion in many recent studies involving ionic liquids is its enhanced thermal stability relative to other anions such as  $PF_6$  or  $BF_4$ ). Nevertheless, it is possible to conclude that the immiscibility is quite high, probably due to the size and rigidity of the anion

that while interacting with the hydroxyl group of the fluorinated alcohol does not allow at the same time the interaction of the fluorinated residue of the latter with the fluorinated atoms of the former.

In Fig. 5c, we tested a tetrafluoroborate anion-based ionic liquid. In order to decrease the working temperatures and avoid decomposition problems we decided to use an imidazolium cation with a shorter alkyl side-chain (as we saw in previous cases, smaller non-polar domains in the ionic liquid increase the solubility of the fluorinated alcohol). The fluid phase diagram of the mixture still exhibits a relatively high upper critical solution temperature (higher than the corresponding bistriflamide imidazolium-based ionic liquid of Fig. 1) for the same reasons pointed out in the previous paragraph.

However, the most interesting feature of the diagram in Fig. 5c is the shift to higher ionic liquid mole fraction of the upper critical solution concentration. Part of the shift can be attributed to the difference in size between the components of the mixture: components with similar size generally exhibit symmetrical  $T-x$  immiscibility windows centred at the equimolar concentration, whereas mixtures with components very dissimilar in size will have the LLE envelope leaning towards the smaller component. This can explain trend (iii) observed in Fig. 1 (see above): as the alkyl side-chain of the ionic liquid is increased (its volume is larger) the diagrams shift to the side of the alcohol (lower ionic liquid mole fraction) and the corresponding critical concentration is decreased. The same applies to Fig. 4: when the fluorinated alcohol is substituted by (the much smaller) ethanol or propanol molecules, the corresponding diagrams and critical concentrations also shift (markedly) to more alcohol-rich compositions. In this case, we have the smallest of all studied ionic liquids, which means that we would anticipate a shift of the critical concentration to the ionic-liquid-rich side of the diagram. That is indeed the case, but the surprise is the magnitude of the shift: the molar volumes of the fluorinated alcohol and of  $C_4mimBF_4$  are quite similar (216.7 and 187.6  $\text{cm}^3 \text{mol}^{-1}$ , respectively, cf. Table 5), which would indicate a critical concentration close to the equimolar, not  $x_{iL} = 0.82$ .

Lattice models like the modified Flory–Huggins, FH, theory proved to be valuable tools to interpret liquid–liquid equilibrium behaviour, namely the prediction of the locus of the critical solution concentration in binary mixtures containing ionic liquids.<sup>31</sup> According to those models, the critical solution concentration, expressed in mole fraction of component 1, can be expressed as  $x_{1,c} = 1/(1 + r^{3/2})$ , where  $r$  is the ratio between the molar volume of the components,  $r = V_{m,1}/V_{m,2}$ . The aforementioned relation was applied to the systems studied in this work and it was found (cf. Table 5) that the relation yields good results for all of them except for the  $C_4mimBF_4 + 1122-C_8FOH$  mixtures. This fact suggests that there is some degree of association between the fluorinated molecules in the one-phase region above the USCT—the mixture is not completely random. For instance, if we consider that, on average, the fluorinated alcohol molecules form dimers (with a volume twice that of the isolated molecules) than the corresponding value of  $x_{1,c}$  would rise from the 0.544 value presented in Table 5 to a value of 0.778, in better agreement with the experimental value. Such self-aggregation (possibly through the fluorinated “tails” of the alcohol) would compensate for the possible loss of F–F interactions when the anion of the ionic liquid is changed from bistriflamide to tetrafluoroborate and would explain the sudden change in the shape of the liquid–liquid immiscibility envelope in Fig. 5c.

The effect of pressure on the liquid–liquid immiscibility window of selected ionic liquid plus partially fluorinated alcohol was also investigated. The shift of the cloud point temperature as a function of pressure for four mixtures containing 1122- $C_8FOH$  and  $C_8mimNTf_2$ ,  $C_{10}mimNTf_2$ ,  $C_{12}mimNTf_2$ , or  $C_{12}MePyNTf_2$ , each at their corresponding critical composition (cf. Fig. 1a–1c and 3b), is presented in Fig. 6. The graph shows that in these systems the cloud-point temperatures are almost not affected by pressure—less than 0.2 K per MPa increase in all cases (see caption to figure).

The fact that these slopes,  $dT/dp$ , are positive imply that the mixing process at temperatures near and above the UCST in these systems (fluorinated alcohols + bistriflamide- and imidazolium-based or pyridinium-based ionic liquids) is accompanied by a volume expansion (positive excess volume,

**Table 5** Critical solution concentration (estimated, FH, and experimental, exp) in different (ionic liquid(1) + alcohol(2)) systems. All systems include the alcohol 1122- $C_8FOH$ , except where stated. The molar volume of each component at 298 K is also given. Numbers as superscripts hold for references

|                                      | $C_8mimNTf_2$       | $C_{10}mimNTf_2$    | $C_{12}mimNTf_2$         | $C_{10}MePyNTf_2$   | $C_{12}MePyNTf_2$   | $C_{14}MePyNTf_2$   |
|--------------------------------------|---------------------|---------------------|--------------------------|---------------------|---------------------|---------------------|
| $V_{m1}/\text{cm}^3 \text{mol}^{-1}$ | 362.1 <sup>25</sup> | 404.1 <sup>25</sup> | 429.8 <sup>1,26, e</sup> | 407.6 <sup>27</sup> | 440.1 <sup>27</sup> | 473.2 <sup>27</sup> |
| $V_{m2}/\text{cm}^3 \text{mol}^{-1}$ | 216.4 <sup>d</sup>  | 216.4 <sup>d</sup>  | 216.4 <sup>d</sup>       | 216.4 <sup>d</sup>  | 216.4 <sup>d</sup>  | 216.4 <sup>d</sup>  |
| $x_{1,c}$ (FH)                       | 0.317               | 0.283               | 0.264                    | 0.279               | 0.257               | 0.237               |
| $x_{1,c}$ (exp)                      | 0.47                | 0.330               | 0.294                    | 0.309               | 0.323               | 0.291               |
|                                      | $C_{10}mimNTf_2^a$  | $AcChNTf_2$         | $AcChNTf_2^b$            | $AcChNTf_2^c$       | $P_{6,6,14}NTf_2$   | $C_4mimBF_4$        |
| $V_{m1}/\text{cm}^3 \text{mol}^{-1}$ | 404.1 <sup>25</sup> | 287.4 <sup>28</sup> | 287.4 <sup>28</sup>      | 287.4 <sup>28</sup> | 716.3 <sup>26</sup> | 187.6 <sup>29</sup> |
| $V_{m2}/\text{cm}^3 \text{mol}^{-1}$ | 234.2 <sup>d</sup>  | 216.4 <sup>d</sup>  | 75.2 <sup>30</sup>       | 58.7 <sup>30</sup>  | 216.4 <sup>d</sup>  | 216.4 <sup>d</sup>  |
| $x_{1,c}$ (FH)                       | 0.304               | 0.396               | 0.118                    | 0.084               | 0.143               | 0.554               |
| $x_{1,c}$ (exp)                      | 0.269               | 0.334               | 0.109                    | 0.101               | 0.186               | 0.815               |

All systems include the alcohol 1122- $C_8FOH$ , except<sup>a</sup> 112233- $C_9FOH$ . <sup>b</sup> Propanol. <sup>c</sup> Ethanol. <sup>d</sup> Density measured in the present work using an Anton-Paar DMA 5000 vibrating-tube densimeter. <sup>e</sup> Molar volume estimated as the sum of the effective volumes occupied by the cation and anion (see ref. 1,26).

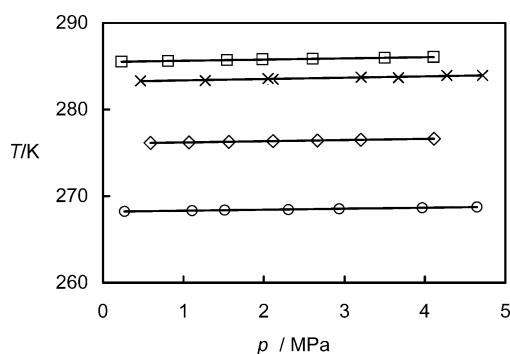


**Fig. 6** Pressure dependence of cloud-point temperature in partially fluorinated alcohol plus ionic liquid systems near their critical composition. Values for the slope in mK/MPa are given between parentheses for each system. (□) 1122-C<sub>8</sub>FOH + C<sub>8</sub>mimNTf<sub>2</sub> (118); (◇) 1122-C<sub>8</sub>FOH + C<sub>10</sub>mimNTf<sub>2</sub> (140); (○) 1122-C<sub>8</sub>FOH + C<sub>12</sub>mimNTf<sub>2</sub> (138); (×) 1122-C<sub>8</sub>FOH + C<sub>12</sub>MePyNTf<sub>2</sub> (158).

$\Delta V^E > 0$ ). The rationale for this fact is found at the recently revisited<sup>32,33</sup> Prigogine–Defay relation, which states that under some restrictive assumptions (in practice, the two excess properties,  $\Delta V^E$  and  $\Delta H^E$ , have to have a similar form in respect to composition and present no inflection points), one obtains a Clapeyron-type of relation, which can be expressed as:

$$\left(\frac{dT}{dp}\right)_c \cong T_c(p) \frac{\Delta V^E(T_c(p), x)}{\Delta H^E(T_c(p), x)} \quad (1)$$

Then, one should recognize that demixing upon cooling (UCST-type of phase diagram) is an exothermic process, thus, conversely, mixing is endothermic ( $\Delta H^E > 0$ ).

#### 4. Conclusions

In this work, liquid–liquid equilibria (cloud-point temperature determinations) of binary mixtures of fluorinated alcohols plus different ionic liquids were studied and measured by turbidimetry. These systems comprise two classes of fluids that, due to their unique characteristics, are very interesting both from the pure and applied chemistry points of view and have, in recent years, received increasing attention from the scientific community.

The corresponding  $T$ – $x$  phase diagrams exhibit a rich fluid-phase behaviour that can be rationalized semi-quantitatively at the molecular level in terms of the different and complex interactions between the fluorinated alcohol—composed of a polar head group, an alkylated “spacer”, and a fluorinated moiety—and the ionic liquid—a micro-segregated fluid exhibiting non-polar domains permeated by a polar network.

The possibility of using fluorinated alcohols (or other diblock molecules with fluorinated residues) together with bistriflamide-based ionic liquids in order to promote the miscibility of the latter with water (and water-soluble molecules) is one of the potential future developments of the present work.

#### Acknowledgements

This work was supported by the *Fundação para a Ciência e Tecnologia (FC & T)*, Portugal (POCI/QUI/57716/2004 and PTDC/CTM/73850/2006). M. B. thanks *FC & T* for a Ph.D.

grant SFRH/BD/13763/2003. We would like to thank the QUILL team, Belfast, for the synthesis and characterization of several ionic liquids used in this work.

#### References

- 1 L. P. N. Rebelo, J. N. Canongia Lopes, J. M. S. S. Esperança, J. Lachwa, V. Najdanovic-Visak and Z. P. Visak, *Acc. Chem. Res.*, 2007, **40**, 1114–1121.
- 2 N. V. Plechkova and K. R. Seddon, *Chem. Soc. Rev.*, 2008, **37**, 123–150.
- 3 J. N. Canongia Lopes and A. A. H. Pádua, *J. Phys. Chem. B*, 2006, **110**, 3330–3335.
- 4 M. S. Kelkar and E. J. Maginn, *J. Chem. Phys.*, 2005, **123**.
- 5 J. N. Canongia Lopes, M. F. Costa Gomes and A. A. H. Pádua, *J. Phys. Chem. B*, 2006, **110**, 16816–16818.
- 6 R. E. Banks, B. E. Smart, J. C. Tatlow, *Organofluorine Chemistry – Principles and Commercial Applications*, Plenum Press, New York, 1994.
- 7 J. G. Riess, *Chem. Rev.*, 2001, **101**, 2797–2919.
- 8 C. A. Eckert, B. L. Knutson and P. G. Debenedetti, *Nature*, 1996, **383**, 313–318.
- 9 M. J. P. de Melo, A. M. A. Dias, M. Blesic, L. P. N. Rebelo, L. F. Vega, J. A. P. Coutinho and I. M. Marrucho, *Fluid Phase Equilib.*, 2006, **242**, 210–219.
- 10 M. B. Shiflett and A. Yokozeki, *Ind. Eng. Chem. Res.*, 2008, **47**, 926–934.
- 11 P. Morgado, H. G. Zhao, F. J. Blas, C. McCabe, L. P. N. Rebelo and E. J. M. Filipe, *J. Phys. Chem. B*, 2007, **111**, 2856–2863.
- 12 J. R. Trindade, A. M. A. Dias, M. Blesic, N. Pedrosa, L. P. N. Rebelo, L. F. Vega, J. A. P. Coutinho and I. M. Marrucho, *Fluid Phase Equilib.*, 2007, **251**, 33–40.
- 13 H. C. de Sousa and L. P. N. Rebelo, *J. Chem. Thermodyn.*, 2000, **32**, 355–387.
- 14 M. B. Shiflett and A. Yokozeki, *J. Chem. Eng. Data*, 2008, **53**, 492–497.
- 15 M. B. Shiflett and A. Yokozeki, *Fluid Phase Equilib.*, 2007, **259**, 210–217.
- 16 M. B. Shiflett and A. Yokozeki, *J. Chem. Eng. Data*, 2007, **52**, 2413–2418.
- 17 J. M. Crosthwaite, M. J. Muldoon, S. Aki, E. J. Maginn and J. F. Brennecke, *J. Phys. Chem. B*, 2006, **110**, 9354–9361.
- 18 J. M. Crosthwaite, S. Aki, E. J. Maginn and J. F. Brennecke, *J. Phys. Chem. B*, 2004, **108**, 5113–5119.
- 19 W. L. Jorgensen, D. S. Maxwell and J. TiradoRives, *J. Am. Chem. Soc.*, 1996, **118**, 11225–11236.
- 20 E. K. Watkins and W. L. Jorgensen, *J. Phys. Chem. A*, 2001, **105**, 4118–4125.
- 21 J. N. C. Lopes, J. Deschamps and A. A. H. Padua, *J. Phys. Chem. B*, 2004, **108**, 11250.
- 22 J. N. C. Lopes, J. Deschamps and A. A. H. Padua, *J. Phys. Chem. B*, 2004, **108**, 2038–2047.
- 23 J. Lopes and A. A. H. Padua, *J. Phys. Chem. B*, 2006, **110**, 3330–3335.
- 24 T. L. Merrigan, E. D. Bates, S. C. Dorman and J. H. Davis, *Chem. Commun.*, 2000, 2051–2052.
- 25 J. N. C. Lopes, T. C. Cordeiro, J. Esperanca, H. J. R. Guedes, S. Huq, L. P. N. Rebelo and K. R. Seddon, *J. Phys. Chem. B*, 2005, **109**, 3519–3525.
- 26 J. Esperanca, H. J. R. Guedes, M. Blesic and L. P. N. Rebelo, *J. Chem. Eng. Data*, 2006, **51**, 237–242.
- 27 P. Natalia, *PhD Thesis*, Queens University of Belfast, 2007.
- 28 G. W. Driver, *PhD Thesis*, Queens University of Belfast, 2007.
- 29 R. G. de Azevedo, J. Esperanca, V. Najdanovic-Visak, Z. P. Visak, H. J. R. Guedes, M. N. da Ponte and L. P. N. Rebelo, *J. Chem. Eng. Data*, 2005, **50**, 997–1008.
- 30 G. C. Benson and H. D. Pflug, *J. Chem. Eng. Data*, 1970, **15**, 382.
- 31 V. Najdanovic-Visak, J. Esperanca, L. P. N. Rebelo, M. N. da Ponte, H. J. R. Guedes, K. R. Seddon, H. C. de Sousa and J. Szydowski, *J. Phys. Chem. B*, 2003, **107**, 12797–12807.
- 32 L. P. N. Rebelo, *Phys. Chem. Chem. Phys.*, 1999, **1**, 4277–4286.
- 33 H. C. De Sousa and L. P. N. Rebelo, *J. Polym. Sci., Part B: Polym. Phys.*, 2000, **38**, 632–651.

## **CHAPTER 7.**

# **LIQUID-LIQUID EQUILIBRIUM OF ALKANE PLUS PERFLUOROALKANE, AND PERFLUOROALKANE PLUS PERFLUOROALCOHOLS BINARY MIXTURES**

*This Chapter was published as the articles:*

Trindade J.R., Dias A.M.A., Blesic M., Pedrosa N., Rebelo L.P.N., Vega L.F., Coutinho J.A.P., Marrucho I.M., "Liquid-liquid equilibrium of (1H,1H,7H-perfluoroheptan-1-ol plus perfluoroalkane) binary mixtures", *Fluid Phase Equilibria*, **2007**, 25, 33.

de Melo M.J.P., Dias A.M.A., Blesic M., Rebelo L.P.N., Vega L.F., Coutinho J.A.P., Marrucho I.M., "Liquid-liquid equilibrium of (perfluoroalkane plus alkane) binary mixtures", *Fluid Phase Equilibria*, **2006**, 242, 210

**Note:** The author of the thesis took part in the experimental determination of phase diagrams.



## Liquid–liquid equilibrium of (perfluoroalkane + alkane) binary mixtures

Maria J. Pratas de Melo<sup>a</sup>, Ana M.A. Dias<sup>a</sup>, Marijana Blesic<sup>b</sup>, Luís P.N. Rebelo<sup>b</sup>,  
Lourdes F. Vega<sup>c</sup>, João A.P. Coutinho<sup>a</sup>, Isabel M. Marrucho<sup>a,\*</sup>

<sup>a</sup> CICECO, Universidade de Aveiro, 3810-193 Aveiro, Portugal

<sup>b</sup> Instituto de Tecnologia Química e Biológica, ITQB2, Universidade Nova de Lisboa, Av. República,  
Apartado 127, 2780-901 Oeiras, Portugal

<sup>c</sup> Institut de Ciència de Materials de Barcelona, Consejo Superior de Investigaciones Científicas (ICMAB-CSIC),  
Campus de la U.A.B., 08193 Bellaterra, Barcelona, Spain

Received 1 February 2006; accepted 2 February 2006

### Abstract

Despite the structural similarity between perfluoroalkanes (PFCs) and alkanes (HCs), mixtures containing these two classes of compounds present large deviations from Raoult's law and extended immiscibility regions. The study of these mixtures is of great interest for both practical applications and testing or improving theories of mixtures as well as for the general understanding of solute–solvent interactions. In this work, new liquid–liquid equilibrium (LLE) data for mixtures of perfluoro-*n*-octane and linear alkanes from C<sub>6</sub> to C<sub>9</sub> are presented. Data were measured at atmospheric pressure by turbidimetry and at pressures up to 150 MPa using a laser light scattering technique. The binary liquid–liquid equilibrium data were correlated using relations derived from renormalization group (RG) theory and the Modified UNIFAC with temperature dependent interaction parameters. The soft-SAFT equation of state (EoS) was also used, with parameters taken from vapour–liquid equilibrium (VLE) data to study their transferability to liquid–liquid equilibrium data. It is shown that using those parameters soft-SAFT can provide a good description of the data measured far from the critical point at atmospheric pressure and a correct dependence of the critical temperature up to 150 MPa if the size interaction parameter is also considered.

© 2006 Elsevier B.V. All rights reserved.

**Keywords:** Perfluoro-*n*-octane; Linear alkanes; Liquid–liquid equilibrium; Soft-SAFT EoS; Renormalization group theory; Modified UNIFAC

### 1. Introduction

The mutual incompatibility between perfluoroalkanes (PFCs) and alkanes (HCs) generates a set of interesting phenomena in all states of matter expressed as large regions of liquid–liquid immiscibility, large positive deviations from Raoult's law, and large positive excess properties [1,2]; microphase separation, segregation, and self-assembly [3], negative aneutropy or minima in the surface tension versus composition diagrams [4], among others are also found. All these phenomena reflect the bulk thermodynamics of these mixtures, which are characterized by weak, unlike interactions.

Since the late 1940s, the potential application of these systems as refrigerant mixtures or as immiscible solvents has motivated their study. The hydrophobicity of fluorinated compounds (that makes them immiscible at room temperature with water and with many common organic solvents) as well as their ability to form a homogenous solution at elevated temperatures with several of these solvents together with their inertness, their solubility in supercritical CO<sub>2</sub>, and their ability to dissolve gases, assemble them and their mixtures interesting materials to be used in new applications. These include their use as two-phase reaction media in a novel technique known as “*Fluorous Phase Organic Synthesis*” (FPOS) [5–7].

A bibliographic review on available experimental data of (PFC + HC) systems is compiled in Table 1. It summarizes the methods and experimental conditions used to perform liquid–liquid solubility measurements for mixtures of linear,

\* Corresponding author. Tel.: +351 234 370200; fax: +351 234 380074.  
E-mail address: [imarrucho@dq.ua.pt](mailto:imarrucho@dq.ua.pt) (I.M. Marrucho).

Table 1  
Compilation of references reporting experimental liquid–liquid solubility data for perfluoroalkane + alkane systems

| System                                                          | Method    | <i>T</i> range (K) | <i>P</i> range (MPa) | Reference                  |
|-----------------------------------------------------------------|-----------|--------------------|----------------------|----------------------------|
| C <sub>7</sub> F <sub>14</sub> + C <sub>6</sub> H <sub>6</sub>  | Synthetic | 308–359            | 0.1                  | Hildebrand and Cochran [8] |
| C <sub>7</sub> F <sub>14</sub> + C <sub>7</sub> H <sub>8</sub>  |           | 316–362            |                      |                            |
| C <sub>7</sub> F <sub>16</sub> + C <sub>6</sub> H <sub>6</sub>  | Synthetic | 330–387            | 0.1                  | Hildebrand et al. [9]      |
| C <sub>7</sub> F <sub>16</sub> + C <sub>7</sub> H <sub>16</sub> |           | 300–323            |                      |                            |
| C <sub>5</sub> F <sub>12</sub> + C <sub>5</sub> H <sub>12</sub> | Synthetic | 300–341            | 0.1                  | Simons and Dunlap [10]     |
| C <sub>4</sub> F <sub>10</sub> + C <sub>4</sub> H <sub>10</sub> | Synthetic |                    | 0.1                  | Simons and Mausteller [11] |
| C <sub>7</sub> F <sub>16</sub> + C <sub>8</sub> H <sub>18</sub> | Synthetic |                    | 0.1                  | Campbell and Hickman [12]  |
| C <sub>7</sub> F <sub>16</sub> + C <sub>6</sub> H <sub>14</sub> | Synthetic |                    | 283–302              | Hickman [13]               |
| C <sub>6</sub> F <sub>14</sub> + C <sub>6</sub> H <sub>14</sub> | Synthetic |                    | 250–294              | 0.1                        |
| C <sub>6</sub> F <sub>14</sub> + C <sub>6</sub> H <sub>14</sub> | Synthetic | 290–295            | 0.1                  | Lepori et al. [1]          |
| C <sub>6</sub> F <sub>14</sub> + C <sub>7</sub> H <sub>16</sub> |           | 300–315            |                      |                            |
| C <sub>6</sub> F <sub>14</sub> + C <sub>8</sub> H <sub>18</sub> |           | 286–325            |                      |                            |
| C <sub>8</sub> F <sub>18</sub> + C <sub>6</sub> H <sub>14</sub> | Synthetic | 260–314            | 0.1                  | Lo Nostro et al. [3]       |
| C <sub>8</sub> F <sub>18</sub> + C <sub>7</sub> H <sub>16</sub> |           | 293–331            |                      |                            |
| C <sub>8</sub> F <sub>18</sub> + C <sub>8</sub> H <sub>18</sub> |           | 295–349            |                      |                            |

cyclic and aromatic alkanes with perfluoroalkanes that are liquid at ambient temperature. Although significant experimental data have been reported, the fact is that, to date, there are aspects related to these mixtures that are not yet completely understood. As a consequence, there is no single method/model able to correctly predict or describe this type of mixtures.

In the early 1950s, it was believed that (PFC + HC) mixtures would be completely miscible in all proportions and that the regular solution theory [15] would describe these mixtures, at least qualitatively. When the first results for LLE data begun to be published – revealing their high non-ideality – new explanations had to be considered to account for their anomalous behaviour. Several approaches or proposals to solve this issue were presented. For instance, the failure of the geometric combining rule due to the interpenetration between neighboring C–H groups which leads to an abnormally strong hydrocarbon–hydrocarbon interaction energy, were corrected by an empirical shift in the solubility parameter,  $\delta$ , of the hydrocarbons. Additionally, corrections to the regular solution theory to include the effect of volume changes that occur on mixing and modifications of regular solution theory to take into account size and ionization potential differences between the two components were considered. However, as reported by Scott [16] none of the suggestions fully accounted for the anomalous behaviour of all systems investigated. In the 1970s, Siebert and Knobler [17] measured the second virial coefficients of *n*-alkanes, perfluoro-*n*-alkanes, and their mixtures and concluded that the anomalous behaviour of alkane + perfluoroalkane systems was due to the failure of the geometric-mean rule to describe the unusually weak hydrocarbon–fluorocarbon attractive interaction. They discussed possible reasons for such a weak, unlike interaction between the two components: non-central forces, large ionization potential differences, and large size differences, concluding that the observed deviation from the geometric-mean prediction was most likely due to the latter. This explanation had previously been suggested by Dyke et al. [18] and Rowlinson [19] from studies of the gas–liquid critical line and a review of the

data available, respectively. The results indicated that the interactions between perfluoroalkanes and alkanes were about 10% weaker than the geometric mean of the like-molecule interactions.

Similar conclusions were drawn by Mousa et al. [20] when they tried to apply the theory of conformal solutions to calculate the critical properties of several perfluoroalkane + alkane mixtures. The authors observed that accurate results were obtained only when an unlike parameter equal to 0.92 was used to calculate the mixed interaction constant. Archer et al. [21] reported the first attempt to account for the liquid–liquid thermodynamics of alkane + perfluoroalkanes mixtures using the bonded hard-sphere (BHS) theory, that has its roots in the theory of Wertheim [22], as the soft-SAFT equation of state (EoS) used in this work, and that incorporates in its development the same structural idea. The authors used the BHS theory to account for repulsive interactions and the van der Waals one-fluid theory to describe attractive interactions. They found this approach accurate enough to describe properly the critical properties of alkanes, perfluoroalkanes and their mixtures. They observed that to correctly describe the UCST of the alkane + perfluoroalkanes mixtures, the correction parameter  $\xi$  in the geometric-mean rule for the van der Waals cross-term must be equal to 0.909 for all the mixtures studied. By applying this correction, they usually found that the difference between calculated and experimental values would not exceed 7%.

Recently, renewed interest on the subject came out with the work of McCabe et al. [23] and Colina et al. [24], both modelling the solution thermodynamics of alkane + perfluoroalkanes mixtures using the statistical associating fluid SAFT-VR approach. Interestingly, these authors found that to reproduce the observed mixing behaviour within the SAFT-VR model, the interaction energies between perfluoroalkane and alkane interaction sites had to be reduced by ca. 8% relative to the geometric-mean prediction, a result which is similar to that found by Knobler and co-workers. McCabe et al. [23] studied the high-pressure phase behaviour of a number of perfluoro-*n*-alkane (C<sub>1</sub>–C<sub>4</sub>) + *n*-alkane

(C<sub>1</sub>–C<sub>7</sub>) binary mixtures, and suggested a value  $\xi = 0.9234$ . Later, Colina et al. [24] slightly modified this value to  $\xi = 0.929$  in order to provide a better fit to the upper critical solution temperature (UCST) of the C<sub>6</sub>F<sub>14</sub> + C<sub>6</sub>H<sub>14</sub> system. The unlike parameter was then used in a transferable way to predict liquid–liquid envelopes and the vapour–liquid phase behaviour of some of the mixtures measured by Lepori et al. [1]. As presented, the model could describe quite well the UCST of the mixtures but predicted narrower phase envelopes than the experimental ones. Also, the  $P$ – $x$ – $y$  diagrams were broader than those inferred from experimental data as a result of the overestimation of the pure component vapour pressures. In turn, the latter was due to a rescaling of the parameters to match the critical point, which made the predictions for subcritical properties less accurate.

Trying to overcome the higher deviations that McCabe et al. [23] observed when the chain length of the  $n$ -alkane component increased, Morgado et al. [2], also using the SAFT-VR EoS, concentrated on the behaviour of alkane + perfluoroalkane binary mixtures with chain lengths between five and eight carbon atoms for both components. They determined a set of binary interaction parameters that can be used to accurately predict the phase behaviour of alkane + perfluoroalkane systems of longer chain molecules and focused on the liquid–liquid immiscibility found close to ambient temperatures, rather than the high-pressure phase behaviour.

Song et al. [25] examined the use of typical all atom Lennard–Jones 12-6 plus Coulomb potential functions for simulating the interactions between perfluorinated molecules and alkanes together with the Lorentz–Berthelot combining rules usually employed with such potentials. This model had already been applied to accurately account for many of the liquid-phase properties of pure perfluoroalkanes [26] and alkanes [27], and the authors believed that departures from the geometric-mean rule mentioned above possibly resulted from inadequate treatment of molecular geometries or from charge distributions in the models employed in these earlier studies. However, they noticed that the special character of perfluoroalkane + alkane interactions was definitely not captured if standard combining rules were used. The authors compared their calculations with experimental data for second virial coefficients, gas–liquid solubilities and enthalpies of liquid mixing and observed that a reduction of ca. 10% in the interactions between unlike pairs of molecules was required, which is the same reduction required when simple single-site representations of molecules are used. Alternatively, the authors tried the use of two-parameter combining rules as well as more sophisticated approaches to calculate the cross-interaction parameters but the results were not conclusive. Ultimately, the underlying physical origins of the unusual mixing behaviour remained unclear.

In a recent work, Zhang and Siepmann [28] presented phase diagrams for selected  $n$ -alkanes,  $n$ -perfluoroalkanes and carbon dioxide ternary mixtures, as a function of pressure, from Monte Carlo simulations. They used two binary interaction parameters for the alkane–perfluoroalkane mixtures, fitted to a particular mixture, and used them in a transferable manner for the rest of the mixtures involving the two compounds. The agreement

with the available data for the binary phase diagrams is fair, and hence a qualitative agreement with the ternary mixtures is expected.

In a previous study [29], our group used the soft-SAFT equation of state to model the experimental vapour–liquid equilibrium (VLE) and liquid–liquid equilibrium (LLE) data for PFCs + HCs measured by Lepori et al. [1]. The unlike energy parameter was treated as adjustable, and it was set at the optimum value  $\xi = 0.9146$  for the correct prediction of the experimental azeotrope of the perfluoro- $n$ -hexane +  $n$ -hexane mixture at 298.15 K. The unlike size parameter was not adjusted ( $\eta = 1$ ), because the simple Lorentz combination rule provided satisfactory results. It is interesting to notice that the value of the unlike energy parameter agrees well with the values found by other authors using different models to describe these systems.

In this work, we present new data at both atmospheric pressure and high pressures for the LLE of perfluoro- $n$ -octane with alkanes ranging from  $n$ -hexane to  $n$ -nonane. The experimental data measured is correlated using relations derived from renormalization group (RG) theory and Modified UNIFAC model with temperature dependent interaction parameters. Data are also modelled using the soft-SAFT equation of state in a predictive way by using the energetic interaction parameter obtained in our previous work [29] in a transferable manner. It is also shown that, to correctly describe the pressure dependence of the LLE data with the soft-SAFT EoS, both size and energy binary interaction parameters have to be considered.

## 2. Experimental

Liquid–liquid equilibria of binary mixtures of perfluoro- $n$ -octane + alkanes,  $n$ -C<sub>*n*</sub>H<sub>2*n*+2</sub> ( $n = 6$ – $9$ ), were measured using synthetic methods: by turbidimetry at atmospheric pressure, and using laser light scattering techniques for measurements at pressures up to 150 MPa. All chemicals, from Aldrich, with claimed purities of 98% (perfluoro- $n$ -octane) and 99% (alkanes) underwent further drying using 3 Å molecular sieves except the perfluoro- $n$ -octane, which was used as received. Binary mixtures were gravimetrically prepared with an estimated weight fraction uncertainty of  $\pm 2 \times 10^{-5}$ .

In the case of measurements at a nominal pressure of 0.1 MPa, different samples of perfluoro- $n$ -octane +  $n$ -alkane were prepared in ampoules containing a magnetic stirrer. Due to the density difference between the components, the heavier bottom phase is richer in PFC, and the upper phase contains mostly the hydrogenated component. The ampoules were sealed while frozen using liquid nitrogen to avoid changes in the composition of the samples. The ampoules containing mixtures at different compositions were then immersed in a thermostatic bath equipped with a calibrated Pt100 temperature sensor with an uncertainty of 0.05 K. Cloud points were determined by visual observation while heating the samples until a homogeneous phase is obtained followed by slow cooling of the mixtures until phase separation is detected.

Pressure effects on the liquid–liquid equilibrium temperature were obtained by He–Ne laser light scattering techniques using two apparatus. One of them, which operates up to pressures



of 5 MPa, has a thick-walled Pyrex glass tube cell (internal volume  $\sim 1.0 \text{ cm}^3$ , optical length  $\sim 2.6 \text{ mm}$ ) connected to a pressurization line and separated from it by a mercury plug. The apparatus is easy, fast and safe to operate since both temperature and pressure are computer controlled and it is fully automated (including data acquisition and treatment). The apparatus, as well as the methodology used for the determination of phase transitions, have been recently described in detail [30]. Here, only a brief description is provided. Scattered light intensity is captured at a very low angle ( $2^\circ < 2\theta < 4^\circ$ ) in the outer part of a bifurcated optical cable, while transmitted light is captured in the inner portion of this cable. The cloud point is the point on the  $(I_{\text{sc,corr}})^{-1}$  against pressure ( $p$ ) or temperature ( $T$ ) least-squares fits where the slope changes abruptly. Temperature accuracy is typically  $\pm 0.01 \text{ K}$  in the range  $240 \text{ K} < T < 400 \text{ K}$ . As for pressure, accuracy is  $\pm 0.01 \text{ MPa}$  up to 5 MPa. The other apparatus uses a stainless-steel cylindrical cell [31] closed on both sides with thick sapphire windows. It was used for experiments in which pressure was raised up to 150 MPa. In this case, the hydraulic fluid is the pure alkane in contact with a sufficiently long (1/16) in. stainless-steel tube filled with the solution (buffer volume), in order to avoid contamination during compression/expansion cycles. The total volume (buffer + optical) of injected solution is typically  $1.6 \text{ cm}^3$ , although the optical volume roughly corresponds to a mere  $0.5 \text{ cm}^3$ . In the case of isothermal runs, temperature accuracy is maintained ( $\pm 0.01 \text{ K}$ ) but it worsens a bit for isobaric runs. As for pressure, the uncertainty is  $\pm 0.1 \text{ MPa}$  in this higher-pressure range. Either cell can be operated in the isobaric or isothermal mode. Abrupt changes in either the transmitted or scattered light upon phase transition sharpen as the thermodynamic path approaches a perpendicular angle to the one-phase/two-phase surface. Pressure can be changed much more quickly than temperature, but, nonetheless, some experimental runs had to be performed in the isobaric mode due to the relatively low critical  $T$ - $p$  slope presented by the current binary mixtures.

### 3. Modelling

#### 3.1. Critical point estimation and data correlation

Systems with liquid–liquid equilibria present long-range concentration fluctuations in the vicinity of their consolute critical temperature. Asymptotically close to the critical point the thermodynamic properties vary as a simple power of the temperature difference or concentration difference (referred to their critical point values) with universal critical exponents, apart from a regular classical part. The non-classical behaviour of these systems as they approach their critical point is correctly taken into account from the renormalization group theory [32]. Since our liquid–liquid equilibria measurements are very close to the critical consolute temperature, we have correlated our experimental data using relations derived from the RG theory. According to Sengers et al. [33] the following relation is verified in the close vicinity of the critical point,

$$\Delta M = B(\tau)^\beta \quad (1)$$

where  $\Delta M$  is the difference in the order parameter between the coexisting phases,  $\beta$  the exponent,  $B$  the amplitude, and  $\tau = (T - T_c)/T_c$  holds for the reduced temperature that expresses the distance from the critical point. The order parameter is a quantity (mole fraction, volume fraction, density, etc.) chosen to measure the difference between the two coexisting phases. In the non-asymptotic region Eq. (1) is modified by the presence of corrections to scaling [34],

$$\Delta M = B_0 \tau^\beta [1 + B_1 \tau^{\Delta_1} + B_2 \tau^{2\Delta_1} + \dots] \quad (2)$$

where  $\Delta_1$  is the correction exponent. The so-called diameter of the coexisting curve is given by the relationship [35]

$$\frac{M_1^I + M_1^{II}}{2} = M_c [1 + A_1 \tau + A_2 \tau^{1-\alpha} + \dots] \quad (3)$$

where  $\alpha$  is a critical exponent and  $M_1^I + M_1^{II}$ , and  $M_c$  represent the property chosen for order parameter of component 1 in phases I, II, and at the critical point, respectively. When Eqs. (2) and (3) are combined (and perturbation terms are neglected) the result is the equation used in this work to correlate the experimental data:

$$\phi - \phi_c = fA \left( \frac{T - T_c}{T_c} \right)^\beta \quad (4)$$

where  $f = 1$  for  $x > x_c$  and  $f = -1$  for  $x < x_c$ .

#### 3.2. Modified UNIFAC model

Low pressure liquid–liquid equilibrium data are frequently modelled using an excess Gibbs energy model. The Modified UNIFAC model [36] was also used in this work to correlate the experimental data. The parameters required for the use of UNIFAC are group volumes ( $R_k$ ), group surface areas ( $Q_k$ ) and group-interaction parameters ( $a_{mn}$  and  $a_{nm}$ ). The volume and area parameters for the groups involved in the mixtures studied ( $\text{CF}_2$ ,  $\text{CF}_3$ ,  $\text{CH}_2$  and  $\text{CH}_3$ ) are already available in the UNIFAC parameter table [37]. The group interaction parameters between the two main groups  $\text{CF}_2$  and  $\text{CH}_2$  have also been published for VLE predictions [37]. However, as discussed by Magnussen et al. [38], it is not possible to quantitatively predict LLE compositions using model parameters based on VLE data. In order to obtain a reliable prediction of multicomponent LLE using excess Gibbs energy models, it is necessary to establish the model parameters based on binary and ternary LLE data. In their work, the authors presented a set of interaction parameters adjusted to LLE data but that did not include the  $\text{CF}_2/\text{CH}_2$  interaction. These interaction parameters were adjusted in this work using the experimental data measured.

The temperature dependence of the interaction parameters is described by the equation:

$$a_{mn} = a_{mn,1} + a_{mn,2}(T - T_0) \quad (5)$$

with  $a_{mn} \neq a_{nm}$  and where  $T_0$  is an arbitrary reference temperature, chosen to be 298.15 K in this work. The adjusted parameters  $a_{mn,1}$  and  $a_{mn,2}$  are equal to 146 and  $-0.3914$  for the  $\text{CF}_2/\text{CH}_2$  interaction and  $-7.66$  and  $0.2237$  for the  $\text{CH}_2/\text{CF}_2$  interaction.

The parameters were adjusted discarding the experimental data near the critical region giving a higher priority to the description of the diagrams far from that region.

### 3.3. The soft-SAFT EoS

We have also used a molecular-based EoS to describe the experimental data. The model was already used to study the vapour–liquid and liquid–liquid equilibrium data for PFCs + HCs mixtures [29]. More details about the model for these particular systems can be found in that work and in references therein. In this work, only the main equation is presented for completeness.

As usually done in SAFT-type equations, the soft-SAFT EoS is formulated in terms of the residual molar Helmholtz energy,  $A^{\text{res}}$ , defined as the molar Helmholtz energy of the fluid relative to that of an ideal gas at the same temperature and density.  $A^{\text{res}}$  is written as the sum of three contributions:

$$A^{\text{res}} = A^{\text{total}} - A^{\text{ideal}} = A^{\text{ref}} + A^{\text{chain}} + A^{\text{assoc}} \quad (6)$$

where  $A^{\text{ref}}$  accounts for the pairwise intermolecular interactions of the reference system,  $A^{\text{chain}}$  evaluates the free energy due to the formation of a chain from units of the reference system, and  $A^{\text{assoc}}$  takes into account the contribution due to site–site association. For molecules that do not associate, as those that are being studied in this work, the association term is null.

The SAFT model describes a pure non-associating fluid as homonuclear chains composed of equal spherical segments bonded tangentially. Different fluids will have different number of segments,  $m$ , segment diameter,  $\sigma$ , and segment interaction energy,  $\varepsilon$ . These parameters are usually obtained by adjusting the equation to density and vapour pressure data of the pure compounds. The molecular parameters for the compounds studied in this work had already been obtained and previously reported for perfluoro-*n*-octane [29] and for the linear alkanes from  $C_6$  to  $C_9$  [39]. When dealing with mixtures that are highly non-ideal, the Lorentz–Berthelot cross-interaction size and energy parameters need also to be adjusted to experimental data:

$$\sigma_{ij} = \eta_{ij} \frac{\sigma_{ii} + \sigma_{ij}}{2}, \quad (7)$$

$$\varepsilon_{ij} = \xi_{ij} \sqrt{\varepsilon_{ii} \varepsilon_{jj}} \quad (8)$$

The soft-SAFT equation has been accurately applied by our group to model VLE data for pure perfluoroalkanes [40], solubility data of gases as oxygen [29,41] and carbon dioxide [42] in these compounds and also VLE data for alkane and perfluoroalkanes systems [29]. In this last case, we have obtained that a single, temperature independent, energy binary parameter ( $\xi_{ij} = 0.9146$ ), fitted to VLE equilibria for the system perfluoro-*n*-hexane + *n*-hexane mixture at 298.15 K is able to accurately describe the behaviour of this and other PFC–HC mixtures in a transferable manner [29]. We have further investigated the reliability of these parameters for describing the behaviour of other mixtures of PFC + HCs. Fig. 1 depicts experimental data for the  $C_6H_{14} + C_7F_{16}$  mixture at 317.65 K and for the  $C_6H_{14} + C_8F_{18}$  mixture at 313.15 K, both taken from ref. [43], as compared with

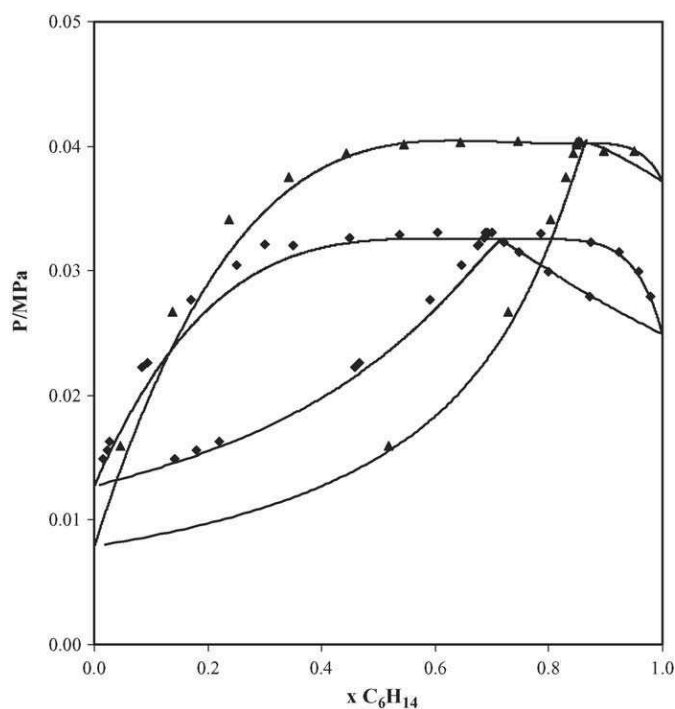


Fig. 1.  $P$ - $x$ - $y$  diagrams for  $C_6H_{14} + C_7F_{16}$  at 317.65 K (diamonds) and  $C_6H_{14} + C_8F_{18}$  at 313.15 K (triangles). Symbols represent experimental data by Duce et al. [43] and lines correspond to the predictions from the soft-SAFT EoS.

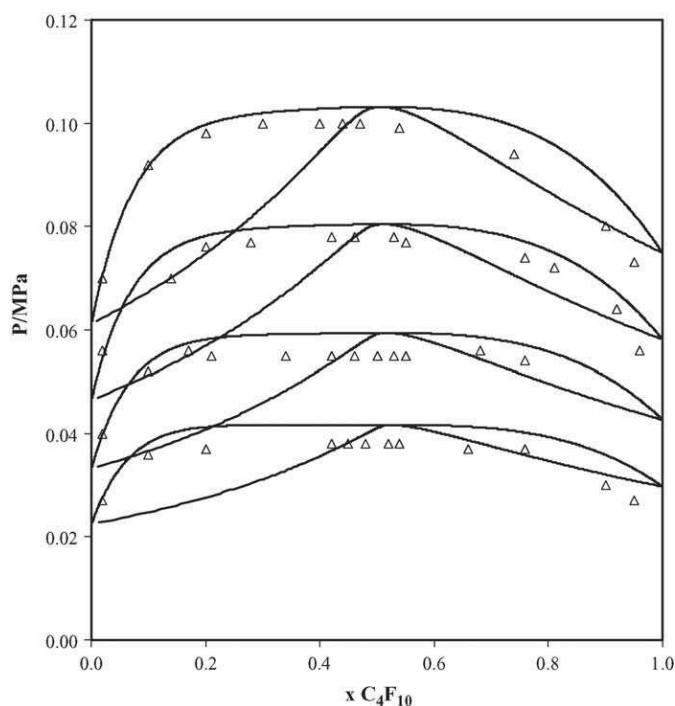


Fig. 2.  $P$ - $x$ - $y$  diagrams at 259.95, 253.62, 246.35 and 238.45 K for  $C_4F_{10} + C_4H_{10}$  mixture compared with soft-SAFT predictions. The triangles describe the experimental data [44] and the solid curves the theoretical predictions as obtained by soft-SAFT.

soft-SAFT predictions using parameters from reference [29]. The predictive capability of these parameters is further shown in Fig. 2, where we show  $P$ - $x$  diagrams at 259.95, 253.62, 246.35

and 238.45 K for C<sub>4</sub>F<sub>10</sub> + C<sub>4</sub>H<sub>10</sub> mixture [44] compared with soft-SAFT predictions. The excellent agreement found between the experimental data and the soft-SAFT predictions in all these cases has encouraged the use of an identical set of parameters for the LLE data measured in this work, in order to further check their transferability for other regions of the phase diagram.

#### 4. Results and discussion

Experimental data measured for the studied systems at atmospheric pressure and high pressure are reported in Tables 2 and 3, respectively. Experimental data at a nominal pressure of 0.1 MPa are presented in Fig. 3a and b where compositions are expressed in terms of mole and volume fraction, respectively. Compositions in terms of volume fractions ( $\phi$ ) are calculated using the relation:

$$\phi_i = \frac{x_i}{x_i + K(1 - x_i)} \quad (9)$$

where  $K = \rho_i M_j / \rho_j M_i$ , being  $\rho$  and  $M$  the mass density and the molecular weight, respectively, of components  $i$  and  $j$ . As for most systems, it occurs that the temperature versus composition diagrams of PFCs + HCs mixtures are more symmetric when represented in terms of volume fraction as compared to mole fraction.

Fig. 3a also compares the data measured in this work with the experimental data recently published by Lo Nostro et al. [3]. It can be observed that the results agree well for the perfluoro- $n$ -octane +  $n$ -octane mixture but significant deviations are observed for perfluoro- $n$ -octane with  $n$ -hexane and especially with  $n$ -heptane. The higher deviations found in mixtures involving volatile compounds, as is the case of  $n$ -hexane and  $n$ -heptane, may be justified by changes in the composition of the mixtures during the measurement procedure.

As mentioned in the previous section our experimental data were correlated using relations derived from renormalization group theory, in which the volume fraction was chosen to be the order parameter. Eq. (4) was used to correlate our mutual solubility experimental data in the entire temperature interval,

Table 2

Experimental liquid–liquid solubility data for perfluoro- $n$ -octane (1) + alkane (2) (C<sub>6</sub>–C<sub>9</sub>) mixtures at atmospheric pressure

| C <sub>8</sub> F <sub>18</sub> + C <sub>6</sub> H <sub>14</sub> |                | C <sub>8</sub> F <sub>18</sub> + C <sub>7</sub> H <sub>16</sub> |                | C <sub>8</sub> F <sub>18</sub> + C <sub>8</sub> H <sub>18</sub> |                | C <sub>8</sub> F <sub>18</sub> + C <sub>9</sub> H <sub>20</sub> |                |
|-----------------------------------------------------------------|----------------|-----------------------------------------------------------------|----------------|-----------------------------------------------------------------|----------------|-----------------------------------------------------------------|----------------|
| T (K)                                                           | x <sub>1</sub> | T (K)                                                           | x <sub>1</sub> | T (K)                                                           | x <sub>1</sub> | T (K)                                                           | x <sub>1</sub> |
| 293.98                                                          | 0.0806         | 319.13                                                          | 0.1024         | 334.24                                                          | 0.0991         | 352.09                                                          | 0.1116         |
| 306.36                                                          | 0.1222         | 328.21                                                          | 0.1772         | 345.48                                                          | 0.1669         | 362.24                                                          | 0.1650         |
| 308.95                                                          | 0.1683         | 330.76                                                          | 0.2611         | 349.16                                                          | 0.2374         | 367.65                                                          | 0.2526         |
| 310.83                                                          | 0.2518         | 330.76                                                          | 0.3185         | 350.52                                                          | 0.3013         | 368.85                                                          | 0.3505         |
| 310.81                                                          | 0.2997         | 330.96                                                          | 0.3818         | 350.44                                                          | 0.4026         | 368.49                                                          | 0.4342         |
| 310.71                                                          | 0.3470         | 330.58                                                          | 0.4967         | 349.70                                                          | 0.4984         | 367.46                                                          | 0.5395         |
| 310.65                                                          | 0.3959         | 329.80                                                          | 0.5437         | 346.09                                                          | 0.5964         | 362.59                                                          | 0.6391         |
| 309.61                                                          | 0.4425         | 316.24                                                          | 0.7048         | 336.01                                                          | 0.7245         | 349.16                                                          | 0.7639         |
| 308.49                                                          | 0.4891         |                                                                 |                | 327.71                                                          | 0.7640         | 322.99                                                          | 0.8805         |
| 305.74                                                          | 0.5440         |                                                                 |                | 299.71                                                          | 0.8919         |                                                                 |                |
| 303.05                                                          | 0.6000         |                                                                 |                |                                                                 |                |                                                                 |                |
| 296.93                                                          | 0.6657         |                                                                 |                |                                                                 |                |                                                                 |                |
| 293.89                                                          | 0.6924         |                                                                 |                |                                                                 |                |                                                                 |                |

Table 3

Experimental liquid–liquid solubility data for perfluoro- $n$ -octane (1) + alkane (2) (C<sub>6</sub>–C<sub>9</sub>) mixtures at pressures higher than atmospheric

| C <sub>8</sub> F <sub>18</sub> + C <sub>6</sub> H <sub>14</sub> |       |                         |       |                         |        |
|-----------------------------------------------------------------|-------|-------------------------|-------|-------------------------|--------|
| x <sub>1</sub> = 0.2552                                         |       | x <sub>1</sub> = 0.2678 |       | x <sub>1</sub> = 0.2644 |        |
| T/K                                                             | P/MPa | T/K                     | P/MPa | T/K                     | P/MPa  |
| 311.58                                                          | 1.48  | 311.13                  | 0.85  | 311.72                  | 1.43   |
| 312.08                                                          | 2.18  | 311.80                  | 1.74  | 312.52                  | 2.45   |
| 312.59                                                          | 2.88  | 311.41                  | 1.23  | 313.29                  | 3.40   |
| 313.31                                                          | 3.78  | 310.89                  | 0.53  | 314.02                  | 4.42   |
| 314.12                                                          | 4.95  | 313.24                  | 3.60  | 314.81                  | 5.45   |
| 310.98                                                          | 0.71  | 312.42                  | 2.57  | 322.99                  | 16.70  |
| 310.53                                                          | 0.13  |                         |       | 332.97                  | 31.00  |
|                                                                 |       |                         |       | 342.95                  | 46.50  |
|                                                                 |       |                         |       | 353.00                  | 62.80  |
|                                                                 |       |                         |       | 363.07                  | 80.20  |
|                                                                 |       |                         |       | 373.16                  | 98.00  |
|                                                                 |       |                         |       | 383.43                  | 118.50 |
|                                                                 |       |                         |       | 394.15                  | 143.00 |

C<sub>8</sub>F<sub>18</sub> + C<sub>7</sub>H<sub>16</sub>

| x <sub>1</sub> = 0.2567 |       | x <sub>1</sub> = 0.3446 |       |
|-------------------------|-------|-------------------------|-------|
| T/K                     | P/MPa | T/K                     | P/MPa |
| 331.90                  | 1.52  | 330.88                  | 0.14  |
| 333.29                  | 3.20  | 331.33                  | 0.60  |
| 333.78                  | 3.83  | 331.92                  | 1.37  |
| 332.48                  | 2.24  | 332.82                  | 2.41  |
|                         |       | 333.50                  | 3.28  |
|                         |       | 334.49                  | 4.46  |

C<sub>8</sub>F<sub>18</sub> + C<sub>8</sub>H<sub>18</sub>

| x <sub>1</sub> = 0.3608 |       | x <sub>1</sub> = 0.7510 |       |
|-------------------------|-------|-------------------------|-------|
| T/K                     | P/MPa | T/K                     | P/MPa |
| 349.80                  | 0.15  | 332.302                 | 4.02  |
| 350.18                  | 0.60  | 331.999                 | 3.55  |
| 350.93                  | 1.48  | 331.619                 | 3.04  |
| 351.80                  | 2.49  | 331.124                 | 2.54  |
| 352.64                  | 3.46  | 330.628                 | 1.87  |
| 353.44                  | 4.42  | 332.604                 | 4.26  |
|                         |       | 329.668                 | 0.70  |
|                         |       | 329.308                 | 0.29  |
|                         |       | 330.127                 | 1.27  |

C<sub>8</sub>F<sub>18</sub> + C<sub>9</sub>H<sub>20</sub>

| x <sub>1</sub> = 0.0828 |       |
|-------------------------|-------|
| T/K                     | P/MPa |
| 344.34                  | 0.16  |
| 344.68                  | 0.84  |
| 345.34                  | 1.85  |
| 345.78                  | 2.50  |
| 346.46                  | 3.48  |
| 347.12                  | 4.41  |

including the critical region. Values for  $A$  and  $\beta$  to be used in Eq. (4) together with the calculated values for the critical temperature, mole fraction, and volume fraction for each mixture are reported in Table 4. The solid lines in Fig. 3a and b represent the correlations.

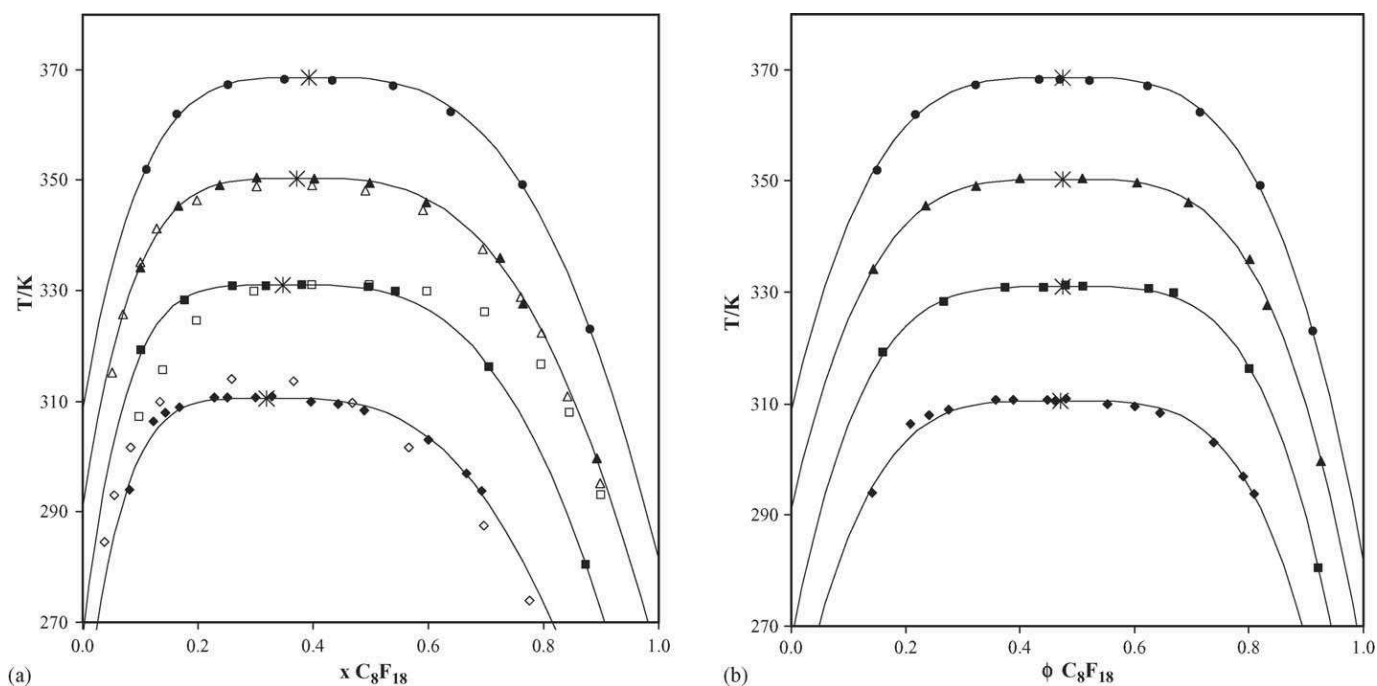


Fig. 3. Experimental and correlated coexisting curve of perfluoro- $n$ -octane + alkanes ( $C_6$ – $C_9$ ) in terms of mole fraction (a) and volume fraction (b). Symbols represent solubility in  $n$ -hexane ( $\blacklozenge$ ),  $n$ -heptane ( $\blacksquare$ ),  $n$ -octane ( $\blacktriangle$ ) and  $n$ -nonane ( $\bullet$ ). (\*) Represents the critical point for each mixture. The non-filled symbols in Fig. 1a represent data measured by Lo Nostro et al. [3]. The lines represent the correlated data calculated from renormalization group theory.

Fig. 4 shows a comparison between the experimental LLE data for  $C_8F_{18} + C_nH_{2n+2}$  at 1MPa and two models: the modified UNIFAC model (dashed lines) and the soft-SAFT EoS (solid lines). Note that the UNIFAC model has been fitted to the binary data using four adjustable parameters, while results from soft-SAFT are pure predictions since the parameters used were obtained from fitting VLE data. Even though the agreement of soft-SAFT with the experimental data is not as accurate at that shown in Figs. 1 and 2, the EoS provides an acceptable description of the experimental data in the region far from the critical point and even the trend of the critical point shift with the alkane chain length change in the mixture is well captured. Since most classical models are not accurate in describing LLE and, in addition, no fitting to these data has been performed, those should be considered as good predictions. Also, notice that no long-range fluctuations are included in the version of soft-SAFT used here, and hence, a correct description of the critical region should not be expected. An alternative approach would be to use the crossover-soft-SAFT EoS [45,46], which correctly describes both the regions far from and close to the VLE critical point of pure fluids and binary mixtures. However, two reasons have prevented us from using the crossover equation

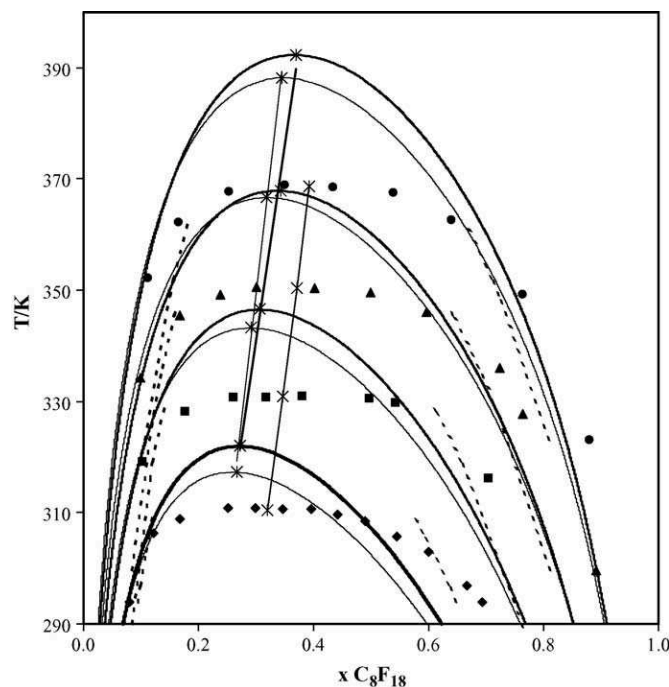


Table 4  
Parameters to be used in Eq. (4) together with critical constants for the studied mixtures

| System                  | $A$     | $\beta$ | $\phi_c$ | $x_c$ | $T_c$  |
|-------------------------|---------|---------|----------|-------|--------|
| $C_8F_{18} + C_6H_{14}$ | 0.71426 | 0.25801 | 0.471    | 0.320 | 310.54 |
| $C_8F_{18} + C_7H_{16}$ | 0.71572 | 0.25017 | 0.474    | 0.348 | 330.99 |
| $C_8F_{18} + C_8H_{18}$ | 0.77238 | 0.27603 | 0.473    | 0.371 | 350.33 |
| $C_8F_{18} + C_9H_{20}$ | 0.79521 | 0.28589 | 0.473    | 0.393 | 368.65 |

Fig. 4. Comparison between experimental LLE data for  $C_8F_{18} + C_nH_{2n+2}$  mixtures at 0.1 MPa and the predictions obtained from the soft-SAFT EoS. Symbols represent the experimental data as in Fig. 1. The full lines represent the predictions given by the soft-SAFT EoS when  $\eta = 1$  and  $\xi = 0.9146$  (—) and  $\eta = 1.011$  and  $\xi = 0.9146$  (—) and the dashed lines the correlation results obtained with the Modified UNIFAC model. Stars represent the upper critical solution temperature for each mixture.



in this work: first of all, our purpose here was to check the transferability of the parameters obtained from other regions of the phase diagram of these mixtures and of related ones (which were fitted with the classical soft-SAFT EoS), and secondly, as discussed in ref. [46], the crossover-soft-SAFT equation is not ready, yet, for LLE, since the isomorphism assumption used to develop it does not apply to this type of phase equilibria.

The soft-SAFT model has also been used to predict the pressure dependence of the phase diagrams. In this case, the size binary interaction parameter had to be slightly adjusted to a value equal to 1.011 in order to correctly describe the pressure dependence of the experimental data. This change is related with the excess volume description of the mixtures by the soft-SAFT model and has little influence on the description of the LLE data at atmospheric pressure as shown in Fig. 4. It is interesting to observe that the size and energy binary interaction parameters used in this work are very similar to the adjusted unlike  $\text{CH}_x/\text{CF}_y$  cross-interaction parameters used by Zhang and Siepmann [28] when using molecular simulation to model alkane + perfluoroalkane mixtures.

The results given by the model to describe the high-pressure data are compared with the experimental results in Fig. 5 for the  $\text{C}_8\text{F}_{18} + \text{C}_6\text{H}_{14}$  mixture at  $x = 0.2644$ . Table 5 compares the experimental and calculated  $(\partial T/\partial P)_x$  for distinct fixed compositions of all the mixtures studied. Although the model overpredicts the experimental temperature, as expected because there was not a perfect match at atmospheric pressure, the pressure dependence is correctly predicted. A comparison between the predictive results obtained with the soft-SAFT and the correlated data obtained with the Modified UNIFAC model, using

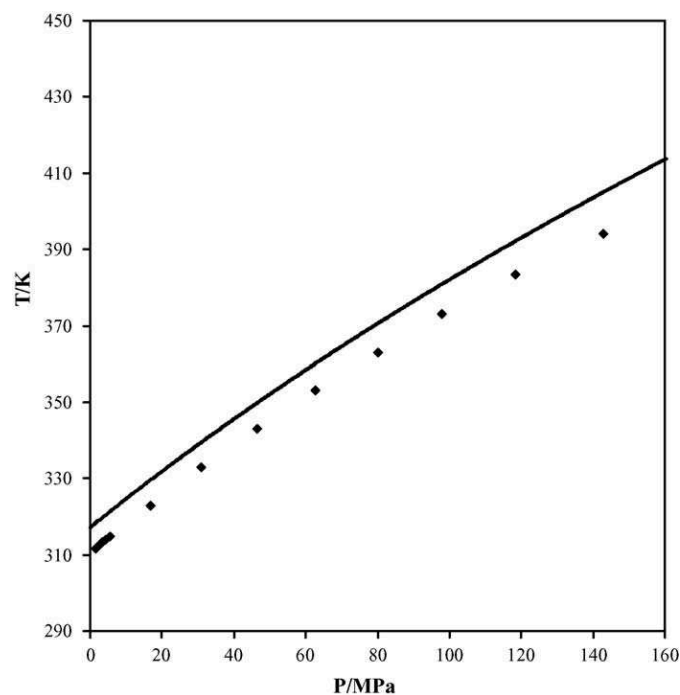


Fig. 5. Effect of the pressure on the LLE of  $\text{C}_8\text{F}_{18} + \text{C}_6\text{H}_{14}$  mixtures at  $x_{\text{C}_8\text{F}_{18}} = 0.2644$ . The line represents the predictions given by the soft-SAFT EoS when  $\eta = 1.011$  and  $\xi = 0.9146$ .

Table 5

Experimental and calculated  $(\partial T/\partial P)_x$  for distinct fixed compositions of all the mixtures studied

| System                                              | $x_{\text{C}_8\text{F}_{18}}$ | $(\partial T/\partial P)_x$ (K bar <sup>-1</sup> ) |                              |
|-----------------------------------------------------|-------------------------------|----------------------------------------------------|------------------------------|
|                                                     |                               | Experimental ( $\times 10^2$ )                     | Calculated ( $\times 10^2$ ) |
| $\text{C}_8\text{F}_{18} + \text{C}_6\text{H}_{14}$ | 0.2552                        | 7.47                                               | 7.51                         |
|                                                     | 0.2678                        | 7.63                                               | 7.56                         |
| $\text{C}_8\text{F}_{18} + \text{C}_7\text{H}_{16}$ | 0.2567                        | 8.18                                               | 7.70                         |
|                                                     | 0.3446                        | 8.29                                               | 8.20                         |
| $\text{C}_8\text{F}_{18} + \text{C}_8\text{H}_{18}$ | 0.3608                        | 8.54                                               | 8.37                         |
|                                                     | 0.7510                        | 8.17                                               | 7.73                         |
| $\text{C}_8\text{F}_{18} + \text{C}_9\text{H}_{20}$ | 0.0828                        | 6.61                                               | 5.04                         |

interaction parameters explicitly adjusted to describe LLE data, let us conclude that the predictive capacity of the soft-SAFT model is superior.

In the case of one of the systems studied,  $\text{C}_8\text{F}_{18} + \text{C}_6\text{H}_{14}$ , it is possible to estimate the magnitude of the molar excess enthalpy, a quantity that has seldom been investigated in these systems. Under some restrictive assumptions [47], the Prigogine–Defay equation establishes a Clapeyron-type of relationship in which the pressure dependence of the critical temperature is directly related to the excess properties themselves:

$$\left(\frac{dT}{dP}\right)_c \cong T_c \frac{v^E(T_c(p), x)}{h^E(T_c(p), x)} \quad (10)$$

Recently, Rebelo et al. [48] demonstrated that Eq. (10) can also be successfully applied at temperatures and finite concentrations not too far from critical. At 298.15 K, the  $\text{C}_8\text{F}_{18} + \text{C}_6\text{H}_{14}$  system is heterogeneous for the equimolar composition. Nonetheless, by Redlich–Kister interpolation it is possible to determine the hypothetical, equimolar reference value for any excess property provided there are sufficient data in the homogeneous region. This was done by Lepori et al. [1] who reported a value of  $5.1 \text{ cm}^3 \text{ mol}^{-1}$  for the equimolar excess volume at 298.15 K. The use of the Prigogine and Defay relation (Eq. (10)) thus establishes  $2.03 \text{ kJ mol}^{-1}$  for the endothermic equimolar excess enthalpy at 298.15 K to be compared with the experimental values  $2.16$  and  $2.37 \text{ kJ mol}^{-1}$  [49,50] for the similar  $\text{C}_6\text{F}_{14} + \text{C}_6\text{H}_{14}$  system.

## 5. Conclusions

In this work, we have presented liquid–liquid equilibrium of binary mixtures of perfluoro-*n*-octane + alkanes,  $n\text{-C}_n\text{H}_{2n+2}$  ( $n = 6\text{--}9$ ), as measured by turbidimetry at atmospheric pressure, and using a laser light scattering technique for measurements at pressures up to 150 MPa. A group renormalization theory was used to calculate the critical temperature and mole fraction for each mixture, which are difficult to observe experimentally due to the extended flatness region that these systems exhibit. The Modified UNIFAC model was used to correlate the experimental data using interaction parameters that are temperature dependent. Results obtained from the correlation were compared with the predictive results obtained with the soft-SAFT model using

interactions parameters adjusted to VLE data. The comparison showed that the results obtained with the soft-SAFT model are of better quality than those correlated by UNIFAC, corroborating the higher predictive capacity of the soft-SAFT model.

#### List of symbols

|            |                                                                 |
|------------|-----------------------------------------------------------------|
| $a_{mn}$   | UNIFAC group-interaction parameters                             |
| $A$        | Helmholtz free energy                                           |
| $h^E$      | excess enthalpy                                                 |
| $m$        | chain length (for Lennard–Jones segments)                       |
| $M$        | molecular weight                                                |
| $\Delta M$ | difference in the order parameter between the coexisting phases |
| $P$        | pressure                                                        |
| $Q_k$      | UNIFAC group surface areas                                      |
| $R_k$      | UNIFAC group volumes                                            |
| $T$        | temperature                                                     |
| $T_0$      | reference temperature equal to 298.15 K                         |
| $v^E$      | excess volume                                                   |
| $x$        | mole fraction                                                   |

#### Greek letters

|               |                                                                                      |
|---------------|--------------------------------------------------------------------------------------|
| $\alpha$      | critical exponent                                                                    |
| $\beta$       | critical exponent                                                                    |
| $\Delta_1$    | correction exponent                                                                  |
| $\varepsilon$ | segment interaction energy (between Lennard–Jones segments)                          |
| $\eta$        | size parameter of the generalized Lorentz–Berthelot combination rules                |
| $\xi$         | energy parameter of the generalized Lorentz–Berthelot combination rules              |
| $\rho$        | mass density ( $\text{kg}/\text{m}^3$ )                                              |
| $\sigma$      | size parameter of the intermolecular potential/diameter (for Lennard–Jones segments) |
| $\tau$        | reduced temperature that expresses the distance from the critical point              |
| $\phi$        | volume fraction                                                                      |

#### Indices

|       |                                    |
|-------|------------------------------------|
| assoc | association term for soft-SAFT EoS |
| c     | critical                           |
| Chain | chain term for soft-SAFT EoS       |
| $i$   | component                          |
| ref   | reference term for soft-SAFT EoS   |
| I     | phase one                          |
| II    | phase two                          |

#### Acknowledgements

Several helpful discussions with Fèlix Llovel (Institut de Ciència de Materials de Barcelona, Barcelona, Spain) are gratefully acknowledged. This project was financed by Fundação para a Ciência e Tecnologia, POCTI/35435/EQU/2000. A.M.A. Dias is grateful to Fundação para a Ciência e Tecnologia for the Ph.D. grant SFRH/BD/5390/2001. Partial support has been provided by the Spanish government, under projects HP2002-0089, CTQ2004-05985-C02-01 and CTQ2005-00296/PPQ.

#### References

- [1] L. Lepori, E. Matteoli, A. Spanedda, C. Ducè, M.R. Tine, *Fluid Phase Equilib.* 201 (2002) 119–134.
- [2] P. Morgado, C. McCabe, E.J.M. Filipe, *Fluid Phase Equilib.* 228–229 (2005) 389–393.
- [3] P. Lo Nostro, L. Scalise, P. Baglioni, *J. Chem. Eng. Data* 50 (2005) 1148–1152.
- [4] I.A. McLure, R. Whitfield, J. Bowers, *J. Colloid Interface Sci.* 203 (1998) 31–40.
- [5] I.T. Horvath, J. Rabai, *Science* 266 (1994) 72–75.
- [6] A. Studer, S. Hadida, R. Ferritto, S.Y. Kim, P. Jeger, P. Wipf, D.P. Curran, *Science* 275 (1997) 823–826.
- [7] B. Betzemeier, P. Knochel, *Top. Curr. Chem.* 206 (1999) 61–78.
- [8] J.H. Hildebrand, D.R.F. Cochran, *J. Am. Chem. Soc.* 71 (1949) 22–25.
- [9] J.H. Hildebrand, B.B. Fisher, H.A. Benesi, *J. Am. Chem. Soc.* 72 (1950) 4348–4351.
- [10] J.H. Simons, R.D. Dunlap, *J. Chem. Phys.* 18 (1950) 335–346.
- [11] J.H. Simons, J.W. Mausteller, *J. Chem. Phys.* 20 (1952) 1516–1519.
- [12] D.N. Campbell, J.B. Hickman, *J. Am. Chem. Soc.* 75 (1953) 2879–2881.
- [13] J.B. Hickman, *J. Am. Chem. Soc.* 77 (1955) 6154–6156.
- [14] R.G. Bedford, R.D. Dunlap, *J. Am. Chem. Soc.* 80 (1958) 282–285.
- [15] J.H. Hildebrand, R.L. Scott, *Solubility of Nonelectrolytes*, third ed., Reinhold Publishing Corp., New York, 1950.
- [16] R.L. Scott, *J. Phys. Chem.* 62 (1958) 136–145.
- [17] E.M.D. Siebert, C.M. Knobler, *J. Phys. Chem.* 75 (1971) 3863–3870.
- [18] D.E.L. Dyke, J.S. Rowlinson, R. Thacker, *Trans. Faraday Soc.* 55 (1959) 903–910.
- [19] J.S. Rowlinson, *Liquids and Liquid Mixtures*, second ed., Butterworth Scientific, London, 1969.
- [20] A.E.H.N. Mousa, A. Kreglews, W.B. Kay, *J. Chem. Thermodyn.* 4 (1972) 301–305.
- [21] A.L. Archer, M.D. Amos, G. Jackson, I.A. McLure, *Int. J. Thermophys.* 17 (1966) 201–206.
- [22] M.S. Wertheim, *J. Stat. Phys.* 35 (1984) 35–47.
- [23] C. McCabe, A. Galindo, A. Gil-Villegas, G. Jackson, *J. Phys. Chem. B* 102 (1998) 8060–8069.
- [24] C.M. Colina, A. Galindo, F.J. Blas, K.E. Gubbins, *Fluid Phase Equilib.* 222 (2004) 77–85.
- [25] W. Song, P.J. Rossky, M. Maroncelli, *J. Chem. Phys.* 119 (2003) 9145–9162.
- [26] E.K. Watkins, W.L. Jorgensen, *J. Phys. Chem. A* 105 (2001) 4118–4125.
- [27] W.L. Jorgensen, D.S. Maxwell, J. Tirado-Rives, *J. Am. Chem. Soc.* 118 (1996) 11225–11236.
- [28] L. Zhang, J.I. Siepmann, *J. Phys. Chem. B* 109 (2005) 2911–2919.
- [29] A.M.A. Dias, J.C. Pàmies, J.A.P. Coutinho, I.M. Marrucho, L.F. Vega, *J. Phys. Chem. B* 108 (2004) 1450–1457.
- [30] H.C. Sousa, L.P.N. Rebelo, *J. Chem. Thermodyn.* 32 (2000) 355–387.
- [31] L.P.N. Rebelo, Z.P. Visak, H.C. Sousa, J. Szydłowski, R. Gomes de Azevedo, A.M. Ramos, V. Najdanovic-Visak, M. Nunes da Ponte, J. Klein, *Macromolecules* 35 (2002) 1887–1895.
- [32] T. Narayanan, A. Kumar, E.S.R. Gopal, S.C. Greer, *J. Phys. Chem.* 84 (1980) 2883–2887.
- [33] J.M.H.L. Sengers, W.L. Greer, J.V. Sengers, *J. Phys. Chem. Ref. Data* 5 (1976) 1–52.
- [34] F.J. Wegner, *Phys. Rev. B* 5 (1972) 4529–4536.
- [35] L. Koo, M.S. Green, *Phys. Rev. A* 16 (1977) 2483–2487.
- [36] B.L. Larsen, P. Rasmussen, A. Fredenslund, *Ind. Eng. Chem. Res.* 26 (1987) 2274–2286.
- [37] H.K. Hansen, P. Rasmussen, A. Fredenslund, M. Schiller, J. Gmehling, *Ind. Eng. Chem. Res.* 30 (1991) 2352–2355.
- [38] T. Magnussen, P. Rasmussen, A. Fredenslund, *Ind. Eng. Chem. Process Des. Dev.* 20 (1981) 331–339.
- [39] J.C. Pàmies, L.F. Vega, *Ind. Eng. Chem. Res.* 40 (2001) 2532–2543.
- [40] A.M.A. Dias, C.M. Gonçalves, A.I. Caço, L.M.N.B.F. Santos, M.M. Piñeiro, L.F. Vega, J.A.P. Coutinho, I.M. Marrucho, *J. Chem. Eng. Data* 50 (2005) 1328–1333.

- [41] A.M.A. Dias, J.C. Pamiés, L.F. Vega, J.A.P. Coutinho, I.M. Marrucho, *J. Polish Chem.* 80 (2006) 143–152.
- [42] A.M.A. Dias, J.C. Pamiés, H. Carrier, J.L. Daridon, L.F. Vega, J.A.P. Coutinho, I.M. Marrucho, *IECR* (2006) in press.
- [43] C. Duce, M. Tine, L. Lepori, E. Matteoli, *Fluid Phase Equilib.* 199 (2002) 197–212.
- [44] J.A. Brown, W.H. Mears, *J. Phys. Chem.* 62 (1958) 960–962.
- [45] F. Llovel, J.C. Pamiés, L.F. Vega, *J. Chem. Phys.* 121 (2004) 10715–10724.
- [46] F. Llovel, L.F. Vega, *J. Phys. Chem.* 110 (2006) 1350–1362.
- [47] L.P.N. Rebelo, *Phys. Chem. Chem. Phys.* 1 (1999) 4277–4286.
- [48] L.P.N. Rebelo, V. Najdanovic-Visak, Z.P. Visak, M. Nunes da Ponte, J. Troncoso, C.A. Cerdeiriña, L. Romani, *Phys. Chem. Chem. Phys.* 4 (2002) 2251–2259.
- [49] A.G. Williamson, R.L. Scott, *J. Phys. Chem.* 65 (1961) 275–279.
- [50] R.D. Dunlap, R.G. Bedford, J.C. Woodbrey, S.D. Furrow, *J. Am. Chem. Soc.* 81 (1959) 2927–2930.



# Liquid–liquid equilibrium of (1H,1H,7H-perfluoroheptan-1-ol + perfluoroalkane) binary mixtures

J.R. Trindade<sup>a,b</sup>, A.M.A. Dias<sup>a,1</sup>, M. Blesic<sup>b</sup>, N. Pedrosa<sup>a</sup>, L.P.N. Rebelo<sup>b</sup>,  
L.F. Vega<sup>c</sup>, J.A.P. Coutinho<sup>a</sup>, I.M. Marrucho<sup>a,\*</sup>

<sup>a</sup> CICECO, Universidade de Aveiro, 3810-193 Aveiro, Portugal

<sup>b</sup> Instituto de Tecnologia Química e Biológica, ITQB2, Universidade Nova de Lisboa, Av. República, Apartado 127, 2780-901 Oeiras, Portugal

<sup>c</sup> Institut de Ciència de Materials de Barcelona, Consejo Superior de Investigaciones Científicas (ICMAB-CSIC),  
Campus de la U.A.B., 08193 Bellaterra, Barcelona, Spain

Received 6 September 2006; received in revised form 26 October 2006; accepted 30 October 2006

Available online 7 November 2006

## Abstract

This work presents new liquid–liquid equilibrium data for mixtures of 1H,1H,7H-perfluoroheptan-1-ol and linear perfluoroalkanes from C<sub>6</sub> to C<sub>9</sub>. Data were measured at atmospheric pressure by turbidimetry and at pressures up to 5 MPa using a laser light scattering technique. The coexistence curves have been fitted to renormalization group extended-scaling expressions with the critical temperature and molar fraction obtained from the fit.

The soft-SAFT equation of state (EoS) was also used to describe the experimental data at both low and high pressures. A good description of the immiscibility gap was obtained with this approach although results seem to deteriorate at high pressures showing that the model cannot simultaneously describe the equilibrium and excess thermodynamic properties.

© 2006 Elsevier B.V. All rights reserved.

**Keywords:** 1H,1H,7H-perfluoroheptan-1-ol; Linear perfluoroalkanes; Liquid–liquid equilibrium; soft-SAFT EoS; Renormalization group theory

## 1. Introduction

Phase equilibrium studies of mixtures involving perfluoroalkanes are an actual and promising subject due to the important applications that these mixtures can find in a broad range of areas.

Extended attention has been given to perfluoroalkane (PFC) + alkane (HC) mixtures due to their use for industrial and environmental applications and also because of the unexpected non-ideal behaviour that these mixtures present. On the basis of the Scott and Hildebrand regular solution theory, these mixtures should be close to ideal, due to the small difference (ca. 1–2 cal<sup>1/2</sup> cm<sup>-3/2</sup>) of their solubility parameters that is insufficient to account for the characteristic incidence of liquid/liquid immiscibility in PFCs + HCs mixtures [1].

In previous publications [2,3] attention has been devoted to the measurement and modelling of vapour–liquid equilibrium (VLE) and liquid–liquid equilibrium (LLE) data for PFCs + HCs mixtures. These works and references therein, mention the unexpected immiscibility of these mixtures and the different attempts to justify this behaviour. The most accepted idea is that it is related with the weakness of the unlike forces governing the liquid mixture.

McLure et al. [1] studied the liquid–liquid co-existence curves of linear methylsiloxane-perfluoroalkane mixtures in order to study the influence of chain flexibility, where other effects as size and energy differences are also important. In this case, the difference in the solubility parameters is lower than in PFCs + HCs mixtures (ca. 1 cal<sup>1/2</sup> cm<sup>-3/2</sup>) although, as the authors noticed, dimethylsiloxane-perfluoroalkane mixtures actually exhibit positive deviations from ideality as large as those of the alkane-perfluoroalkane mixtures whose solubility parameter difference is larger. Following these studies, the LLE of mixtures of a perfluoroalcohol and linear perfluoroalkanes was measured and modelled and the results are presented in this work.

\* Corresponding author. Tel.: +351 234 370200; fax: +351 234 380074.

E-mail address: [imarrucho@dq.ua.pt](mailto:imarrucho@dq.ua.pt) (I.M. Marrucho).

<sup>1</sup> Present address: Departamento de Engenharia Biológica, Universidade do Minho, Campus de Gualtar, 4710-057 Braga, Portugal.



The importance of this study stems from both a practical and a fundamental point of view. The practical importance is justified by the considerable number of applications of perfluoroalcohols in a wide range of areas. Owing to their unique properties as high hydrogen bonding donor ability, low nucleophilicity, high ionising power and ability to solvate water, fluorinated alcohols have been used to allow reactions, which usually require the use of added reagents or metal catalysts to be carried out under neutral and mild conditions [4]. Another example is the “pseudo-hydroxide extraction”, proposed as a method for separating alkali metal hydroxide from alkaline salt solutions using weakly acidic hydroxy compounds such as fluorinated alcohols. In both cases, the use of the fluoroalcohol facilitates the isolation of the products originating high yields, and the fluoroalcohols could be directly recovered from the reaction medium and reused. These processes bring an improvement from an environmental point of view, by suppression of effluents, in particular heavy metals, and they are particularly simple, since most of the reactions do not require any work-up [5].

Other recent applications of fluoroalcohols take advantage of their ability to originate and stabilize the formation of microemulsions for diverse medical and industrial applications [6,7] as well as their effect on protein conformations, notably the induction of  $\alpha$ -helix formation. It was observed that the effectiveness of helix induction was found to increase exponentially with increasing number of fluorine atoms per alcohol molecule [8].

The hydrophobicity of such highly fluorinated molecules has also been used to polymerise an epoxy monomer in their presence with the aim of inducing a surface modification toward more hydrophobicity using cationic UV-curing as technique which is solvent free, giving high production rates and low energy requirements when compared to traditional polymerisation techniques [9].

However, it has also been recently reported that fluorinated telomer alcohols (FTOHs) may act as precursors to the perfluorinated acids (PFCAs) that have been detected widely in the environment as being ambient persistent and prejudicial for human beings [10]. Efficient techniques to recover these compounds before they react are also important from an environmental point of view.

From a theoretically point of view, this study can give new insights regarding the interactions between the constituents of the mixture helping to understand and develop accurate theoretical models to describe and predict the thermodynamic behaviour of this class of mixtures. Having in mind that the difference between the solubility parameters for the compounds studied in these mixtures is ca  $2.6 \text{ cal}^{1/2} \text{ cm}^{-3/2}$ , higher than those mentioned before, it is interesting to test the soft-SAFT EoS in the description of these systems.

The experimental LLE data were measured by turbidimetry at atmospheric pressure and using a light scattering technique for higher pressures up to 4.5 MPa. Whenever possible comparisons with previously results for the alkane + perfluoroalkane mixtures [3] will be done, to conclude about the similarity of the thermodynamics of these two classes of mixtures.

The soft-SAFT EoS [11] was used to model the experimental data measured. The soft-SAFT EoS [11] was used to model the experimental data measured. This work appears as a continuation of previous publications [2,3,12] intending to characterize perfluoroalkanes and their mixtures with other classes of compounds using a versatile and robust EoS, in this case the *soft* version of the original SAFT EoS. The molecular parameters that characterize the pure perfluoroalcohol, according to the soft-SAFT model, were adjusted to densities and vapour pressures and are here presented. The molecular parameters of the PFC are taken from our previous work [2].

## 2. Experimental

Liquid–liquid equilibria of binary mixtures of 1H,1H,7H-perfluoroheptan-1-ol (CAS no. 335-99-9) + linear perfluoroalkanes,  $n\text{-C}_n\text{F}_{2n+2}$  ( $n=6\text{--}9$ ), were measured using synthetic methods: by turbidimetry at atmospheric pressure, and using a laser light scattering technique for measurements at pressures up to 5 MPa. 1H,1H,7H-perfluoroheptan-1-ol was obtained from Apollo Scientific with a purity of 98%. Perfluoro-*n*-hexane was bought from Sigma–Aldrich (99%), perfluoro-*n*-heptane from Apollo Scientific (98%) and both perfluoro-*n*-octane and perfluoro-*n*-nonane are from Fluorochem (99%). All the compounds were used without further purification. This decision was supported by the work of McLure et al. [1] who concluded that impurities in the mentioned range do not induce appreciable changes on the LLE data.

The experimental procedure applied was the same as previously used [3]. At a nominal pressure of 0.1 MPa, different samples of 1H,1H,7H-perfluoroheptan-1-ol + perfluoro-*n*-alkane were prepared in ampoules containing a magnetic stirrer. Samples with different compositions were prepared by weighting using an analytical high precision balance ( $\pm 0.01$  mg) model *Precisa 40 SM-200A*. The ampoules containing the mixtures at different compositions were then immersed in a thermostatic bath equipped with a calibrated Pt 100 temperature sensor with an uncertainty of 0.05 K connected to a multimeter, *Yokogawa 7561*. The water or alcohol thermostatic bath was sufficiently large to avoid temperature gradients. Cloud points were determined by visual observation by heating the samples until a homogeneous phase was obtained followed by slow cooling of the mixtures until phase separation was observed.

Measurements at pressure higher than the 0.1 MPa nominal pressure were obtained by a He–Ne laser light scattering technique. The fully automated apparatus [3] has a thick-walled Pyrex glass tube cell connected to a pressurization line and separated from it by a mercury plug. Scattered light intensity ( $I_{sc}$ ) is captured at a very low angle ( $2 < 2\theta$  ( $^\circ$ )  $< 4$ ) in the outer part of a bifurcated optical cable, while the transmitted light is captured in the inner portion of this cable. The cloud-point is the point on the  $(I_{sc,corr})^{-1}$  against pressure ( $P$ ) or temperature ( $T$ ) least-squares fits where the slope changes abruptly. The cell can be operated in the isobaric or isothermal mode. Abrupt changes in either the transmitted or scattered light upon phase transition sharpen as the thermodynamic path approaches a perpendicular angle to the one-phase/two-phase surface. Temperature accuracy

is typically  $\pm 0.01$  K in the range  $240 < T$  (K)  $< 400$ . As for pressure, accuracy is  $\pm 0.01$  MPa up to 5 MPa.

The density data for the 1H,1H,7H-perfluoroheptan-1-ol compound was measured with a vibrating tube Antón Paar DMA 4500 densimeter between 293.15 and 343.15 K at atmospheric pressure. The measuring principle is based on the calculation of the frequency of resonance of a mechanic oscillator with a given mass and volume, which is excited to be in resonance. The uncertainty of the measurements is  $\pm 5 \times 10^{-4}$  g cm $^{-3}$ . The vapour pressure data were taken from the literature [13]. These data were used to fit the molecular parameters for the soft-SAFT model [11] of this compound.

### 3. Modelling

#### 3.1. Renormalization group theory

Systems with liquid–liquid equilibria present long-range concentration fluctuations in the vicinity of their consolute critical temperature. Asymptotically close to the critical point the thermodynamic properties vary as a simple power of the temperature difference or concentration difference with universal critical exponents, apart from a regular classical part. The non-classical behaviour of these systems as they approach their critical point is correctly taken into account from the renormalization group theory (RG) [14]. Since our experimental conditions were very close to the consolute critical temperature, we have used the RG theory [14] to correlate the experimental data and to obtain the critical temperatures and molar fractions of the studied systems. These properties are difficult to measure directly from experiments due to the extended flat critical region observed. According to the theory [15], asymptotically close to the critical point the thermodynamic properties vary as a simple power of the temperature difference or concentration difference (referred to their critical point values) with universal critical exponents and can be extended to describe the non-asymptotic region by the introduction of correction factors [16].

$$\Delta M = B_0 \tau^\beta [1 + B_1 \tau^{\Delta_1} + B_2 \tau^{2\Delta_1} + \dots] \quad (1)$$

where  $\Delta M$  is the difference in the order parameter between the coexisting phases,  $\beta$  the critical exponent,  $B$  the amplitude,  $\Delta_1$  the correction exponent and  $\tau = (T - T_c)/T_c$  holds for the reduced temperature that expresses the distance from the critical point. The order parameter is a quantity (mole fraction, volume fraction, density, etc.) chosen to measure the difference between the two coexisting phases.

By further considering the definition of the diameter of the coexisting curve [17] the following final equation is obtained:

$$x - x_c = fA \left( \frac{T - T_c}{T_c} \right)^\beta \quad (2)$$

where  $x$  stands for the molar fraction, being  $f=1$  for  $x > x_c$  and  $f=-1$  for  $x < x_c$ .  $A$  and  $\beta$  are parameters to be adjusted to the experimental data. In this work, we have used the mole fraction as the order parameter. This choice is usually guided by the symmetry of the equilibrium curves. The property that originates

the most symmetric curves is usually chosen to be the order parameter.

#### 3.2. Soft-SAFT model

The experimental data were also correlated with the soft-SAFT EoS [11]. The model was already used to study the vapour–liquid and liquid–liquid equilibrium data of mixtures of perfluoroalkanes both as a correlation and prediction method [2,3]. As usually done in SAFT-type equations, the soft-SAFT EoS is formulated in terms of the residual molar Helmholtz energy,  $A^{\text{res}}$ , defined as the molar Helmholtz energy of the fluid relative to that of an ideal gas at the same temperature and density.  $A^{\text{res}}$  is written as the sum of three contributions:

$$A^{\text{res}} = A^{\text{total}} - A^{\text{ideal}} = A^{\text{ref}} + A^{\text{chain}} + A^{\text{assoc}} \quad (3)$$

where  $A^{\text{ref}}$  accounts for the pairwise intermolecular interactions of the reference system,  $A^{\text{chain}}$ , evaluates the free energy due to the formation of a chain from units of the reference system, and  $A^{\text{assoc}}$ , takes into account the contribution due to site–site association. More details about the model for these particular systems can be found in references [11,17] and in the references therein.

The SAFT model describes a pure non-associating fluid as homonuclear chains composed of equal spherical segments bonded tangentially. Different fluids will have different number of segments,  $m$ , segment diameter,  $\sigma$ , and segment interaction energy,  $\varepsilon$ . The molecular parameters for the linear perfluoroalkane compounds had already been obtained and previously reported [2]. In this work, new molecular parameters are presented for 1H,1H,7H-perfluoroheptan-1-ol. The molecule was modelled as an associating compound with two associating sites that mimic the hydrogen bonds characterizing the perfluoroalcohol. These associating sites require two more molecular parameters to be considered, namely the energy and the volume of the associating site. For consistency with previous works, the associating parameters were chosen to be equal to those previously adjusted for normal alkanols, in a transferable manner [19].

When dealing with mixtures that are highly non-ideal, the Lorentz–Berthelot cross-interaction size and energy parameters need also to be adjusted to experimental data:

$$\sigma_{ij} = \eta_{ij} \frac{\sigma_{ii} + \sigma_{jj}}{2} \quad (4)$$

$$\varepsilon_{ij} = \xi_{ij} \sqrt{\varepsilon_{ii} \varepsilon_{jj}} \quad (5)$$

### 4. Results and discussion

Density data for 1H,1H,7H-perfluoroheptan-1-ol measured in this work is presented in Table 1. For the temperature range studied, experimental data were found to be correctly described by a linear equation of the type:

$$\rho_{\text{calc}} = a - bT \quad (6)$$

where  $T$  is the temperature in K and  $\rho$  is the density in g/cm $^3$ . Coefficients for Eq. (6) are also reported in Table 1.

Table 1  
Density data for the pure 1H,1H,7H-perfluoroheptan-1-ol and coefficients of  $\rho_{\text{calc}} = a - bT$  with  $T$  in K and  $\rho$  in  $\text{g/cm}^3$

| $T$ (K)      | $\rho$ ( $\text{g cm}^{-3}$ ) |
|--------------|-------------------------------|
| Density      |                               |
| 293.15       | 1.7501                        |
| 293.15       | 1.7502                        |
| 303.15       | 1.7327                        |
| 313.15       | 1.7150                        |
| 323.15       | 1.6969                        |
| 333.15       | 1.6785                        |
| 343.15       | 1.6597                        |
| Coefficients |                               |
| $a$          | 2.2792                        |
| $b$          | $1.8033 \times 10^{-3}$       |
| AAD          | 0.0004                        |

Experimental LLE equilibrium data measured for the studied systems at atmospheric pressure and high pressure are reported in Tables 2 and 3, respectively. Experimental data at a nominal pressure of 0.1 MPa are presented in Fig. 1a and b in which compositions are expressed in terms of mole and volume fraction, respectively. Compositions in terms of volume fractions ( $\phi$ ) are calculated using the relation:

$$\phi_i = \frac{x_i}{x_i + K(1 - x_i)} \quad (7)$$

where  $K = \rho_i M_j / \rho_j M_i$ , being  $\rho$  and  $M$  the mass density and the molecular weight, respectively, of components  $i$  and  $j$ . It is interesting to remark that unlike most systems, the temperature versus composition diagrams of 1H,1H,7H-perfluoroheptan-1-ol +  $n$ -PFC mixtures are more symmetric when represented in terms of mole fractions than volume fractions. However, even in

Table 2  
Experimental liquid–liquid solubility data for 1H,1H,7H-perfluoroheptan-1-ol (1) +  $n$ -perfluoroalkane (2) mixtures at atmospheric pressure

| $\text{C}_6\text{F}_{14}$   |        | $\text{C}_7\text{F}_{16}$ |        | $\text{C}_8\text{F}_{18}$ |        | $\text{C}_9\text{F}_{20}$ |        |
|-----------------------------|--------|---------------------------|--------|---------------------------|--------|---------------------------|--------|
| $T$ (K)                     | $x_1$  | $T$ (K)                   | $x_1$  | $T$ (K)                   | $x_1$  | $T$ (K)                   | $x_1$  |
| 1H,1H-perfluoro-1-heptanol+ |        |                           |        |                           |        |                           |        |
| 277.48                      | 0.6649 | 275.97                    | 0.7396 | 294.77                    | 0.6991 | 299.15                    | 0.7465 |
| 280.17                      | 0.6314 | 280.44                    | 0.7005 | 296.82                    | 0.6710 | 305.75                    | 0.6467 |
| 283.04                      | 0.6012 | 285.53                    | 0.6500 | 298.19                    | 0.6483 | 307.42                    | 0.5719 |
| 284.50                      | 0.5753 | 289.23                    | 0.5818 | 299.45                    | 0.6265 | 307.92                    | 0.5020 |
| 285.31                      | 0.5591 | 287.42                    | 0.6174 | 299.93                    | 0.6058 | 307.93                    | 0.4556 |
| 286.05                      | 0.5388 | 284.38                    | 0.6637 | 301.08                    | 0.5582 | 307.78                    | 0.4125 |
| 287.14                      | 0.5050 | 281.61                    | 0.6878 | 301.23                    | 0.5427 | 307.74                    | 0.3699 |
| 287.50                      | 0.4874 | 277.35                    | 0.7290 | 301.42                    | 0.5264 | 305.71                    | 0.2640 |
| 287.98                      | 0.4579 | 289.50                    | 0.5798 | 301.55                    | 0.5087 | 304.86                    | 0.2454 |
| 288.22                      | 0.4339 | 290.88                    | 0.5386 | 301.65                    | 0.4864 | 303.49                    | 0.2229 |
| 288.38                      | 0.4026 | 291.47                    | 0.5109 | 301.89                    | 0.4113 | 302.36                    | 0.2018 |
| 288.56                      | 0.3536 | 292.07                    | 0.4682 | 301.64                    | 0.4838 | 298.05                    | 0.1562 |
| 288.56                      | 0.3094 | 292.10                    | 0.4483 | 301.78                    | 0.4596 | 295.11                    | 0.1279 |
| 287.89                      | 0.2291 | 292.15                    | 0.4078 | 301.90                    | 0.4397 | 271.97                    | 0.8831 |
| 288.42                      | 0.2857 | 292.18                    | 0.3835 | 301.93                    | 0.4256 | 279.07                    | 0.8477 |
| 288.65                      | 0.3429 | 292.15                    | 0.3623 | 301.81                    | 0.3779 | 291.22                    | 0.8008 |
| 288.41                      | 0.2959 | 292.15                    | 0.3399 | 301.72                    | 0.3380 | 297.11                    | 0.7625 |
| 288.36                      | 0.2568 | 291.95                    | 0.2863 | 301.43                    | 0.3068 | 301.97                    | 0.7131 |
| 287.63                      | 0.2167 | 291.89                    | 0.2741 | 301.16                    | 0.2933 | 304.83                    | 0.6681 |
| 287.11                      | 0.1900 | 291.20                    | 0.2494 | 301.91                    | 0.4135 | 306.86                    | 0.6045 |
| 286.70                      | 0.1716 | 292.20                    | 0.3418 | 301.80                    | 0.3643 | 307.93                    | 0.5410 |
| 285.46                      | 0.1495 | 292.20                    | 0.3040 | 301.73                    | 0.3478 | 301.03                    | 0.1864 |
| 285.20                      | 0.1419 | 291.52                    | 0.2532 | 301.52                    | 0.3205 | 306.26                    | 0.2862 |
| 283.36                      | 0.1265 | 291.18                    | 0.2321 | 301.29                    | 0.3027 | 306.80                    | 0.3152 |
| 279.83                      | 0.1066 | 290.37                    | 0.2112 | 300.98                    | 0.2840 | 307.33                    | 0.3391 |
| 279.58                      | 0.1026 | 289.35                    | 0.1874 | 300.25                    | 0.2539 | 286.03                    | 0.0827 |
| 277.66                      | 0.0919 | 288.18                    | 0.1670 | 299.92                    | 0.2449 | 292.73                    | 0.1137 |
| 276.37                      | 0.0877 | 286.94                    | 0.1528 | 299.18                    | 0.2246 |                           |        |
|                             |        | 285.59                    | 0.1391 | 298.29                    | 0.2060 |                           |        |
|                             |        | 283.71                    | 0.1257 | 296.95                    | 0.1836 |                           |        |
|                             |        | 278.03                    | 0.0946 | 295.13                    | 0.1650 |                           |        |
|                             |        |                           |        | 287.11                    | 0.7616 |                           |        |
|                             |        |                           |        | 294.46                    | 0.7033 |                           |        |
|                             |        |                           |        | 293.19                    | 0.7188 |                           |        |
|                             |        |                           |        | 290.35                    | 0.7403 |                           |        |
|                             |        |                           |        | 279.03                    | 0.8058 |                           |        |
|                             |        |                           |        | 297.17                    | 0.1889 |                           |        |
|                             |        |                           |        | 294.57                    | 0.1589 |                           |        |
|                             |        |                           |        | 292.53                    | 0.1416 |                           |        |
|                             |        |                           |        | 290.65                    | 0.1298 |                           |        |

Table 3

Experimental liquid–liquid solubility data for 1H,1H,7H-perfluoroheptan-1-ol (1) + *n*-perfluoroalkane (2) mixtures at pressures higher than atmospheric and resulting  $(\partial T/\partial P)$  for distinct fixed compositions near the critical point

| C <sub>6</sub> F <sub>14</sub> ( $x_1 = 0.3710$ )              |              | C <sub>7</sub> F <sub>16</sub> ( $x_1 = 0.3991$ ) |              | C <sub>8</sub> F <sub>18</sub> ( $x_1 = 0.4277$ ) |              | C <sub>9</sub> F <sub>20</sub> ( $x_1 = 0.4531$ ) |              |
|----------------------------------------------------------------|--------------|---------------------------------------------------|--------------|---------------------------------------------------|--------------|---------------------------------------------------|--------------|
| <i>P</i> (MPa)                                                 | <i>T</i> (K) | <i>P</i> (MPa)                                    | <i>T</i> (K) | <i>P</i> (MPa)                                    | <i>T</i> (K) | <i>P</i> (MPa)                                    | <i>T</i> (K) |
| 1H,1H,7H-perfluoro-1-heptanol+                                 |              |                                                   |              |                                                   |              |                                                   |              |
| 0.589                                                          | 288.75       | 0.542                                             | 291.99       | 0.179                                             | 301.78       | 0.226                                             | 307.97       |
| 0.630                                                          | 288.75       | 0.890                                             | 292.02       | 0.535                                             | 301.82       | 0.594                                             | 308.03       |
| 0.822                                                          | 288.73       | 1.273                                             | 292.04       | 1.071                                             | 301.89       | 1.160                                             | 308.14       |
| 1.066                                                          | 288.73       | 2.011                                             | 292.10       | 1.585                                             | 301.95       | 1.746                                             | 308.25       |
| 1.560                                                          | 288.70       | 2.523                                             | 292.14       | 2.304                                             | 302.04       | 2.171                                             | 308.33       |
| 2.185                                                          | 288.67       | 3.240                                             | 292.19       | 2.757                                             | 302.08       | 2.821                                             | 308.45       |
| 2.234                                                          | 288.67       | 3.825                                             | 292.24       | 3.077                                             | 302.12       | 3.339                                             | 308.54       |
| 2.647                                                          | 288.64       | 4.450                                             | 292.28       | 3.721                                             | 302.20       | 3.819                                             | 308.62       |
| 3.282                                                          | 288.61       |                                                   |              | 4.150                                             | 302.26       | 4.406                                             | 308.73       |
| 3.984                                                          | 288.58       |                                                   |              | 4.425                                             | 302.30       |                                                   |              |
| 4.252                                                          | 288.57       |                                                   |              |                                                   |              |                                                   |              |
| $(\partial T/\partial P)_c \times 10^2$ (K MPa <sup>-1</sup> ) |              |                                                   |              |                                                   |              |                                                   |              |
| -5.00                                                          |              | 7.53                                              |              | 12.2                                              |              | 18.2                                              |              |

terms of molar fraction the mixtures are less symmetric than the perfluoro-*n*-octane + *n*-alkanes measured previously as is also shown in Figure 1. The LLE equilibrium data for the mixture perfluoro-*n*-octane + *n*-octane measured in a previous work [3] is here used to elucidate about the difference in symmetry and immiscibility range characterizing each of these classes of mixtures.

The pressure dependence of the studied systems is given in Table 3. It was measured for a fixed composition near the critical point. Also given in Table 3 are the  $(\partial T/\partial P)_c$  ratios calculated from the experimental data measured. It is important to mention that this ratio increases along the *n*-perfluoroalkane series studied passing from negative values for the mixture of the perfluoro-alcohol with C<sub>6</sub>F<sub>14</sub> to positive values for the other mixtures. This change in the signal of the pressure dependence derivative reflects a signal change in the excess volume. In fact, according to the Prigogine-Defay equation recently discussed by Rebelo et al. [20], near the critical region and under some restrictive assumptions [21], a Clapeyron-type of relationship can be established in which the pressure dependence of the critical temperature is directly related to the excess properties themselves,

$$\left(\frac{dT}{dP}\right)_x \cong T_c \frac{v^E(T_c(p), x)}{h^E(T_c(p), x)} \quad (8)$$

As a final comment on the symmetry of the coexistence curves, the experimental data were plotted as reduced *T*, defined as  $T_{red} = T/T_c$ , as a function of the molar fraction. The diagrams obtained are shown in Fig. 2 along with those for the perfluoro-*n*-octane + *n*-alkanes mixtures studied in a previous work [3]. It can be observed that a *global LLE diagram* can be visualized helping to support the universality theory reported by Munson [22] and Gilmour [23].

As mentioned in the previous section our experimental data at 0.1 MPa were correlated using relations derived from renormalization group (RG) theory. Eq. (2) was used to correlate our mutual solubility experimental data in the entire temperature

interval, including the critical region. Values for *A* and  $\beta$  to be used in Eq. (2) together with the calculated values for the critical temperature, mole fraction and volume fraction for each mixture are reported in Table 4. The solid lines in Fig. 1a and b represent the correlations.

Fig. 3 presents the correlation obtained with the RG theory and the correlation given by the soft-SAFT EoS. As mentioned before, the molecular parameters for 1H,1H,7H-perfluoroheptan-1-ol were adjusted using the liquid density and vapour pressure data. The associative energy and volume parameters were chosen to be equal to the ones of a normal alcohols being equal to 3450 K and 2250 Å<sup>3</sup>, respectively [18]. The remaining molecular parameters namely, the number of segments, *m*, segment diameter,  $\sigma$ , and segment interaction energy,  $\varepsilon$ , are 3.744, 4.245 Å and 252.7 K, respectively. Liquid densities and vapour pressures are fitted to experimental data with an AAD less than 0.08% and 0.6%, respectively.

In the case of the mixtures, the binary interaction parameters were adjusted to the experimental LLE data measured. A fixed size interaction binary parameter equal to 1.05 was used in a transferable way for all the mixtures. In this way, the energy interaction parameter was the only adjusted parameter and it was found to increase along the linear perfluoro-*n*-alkane series. Their values were equal to 0.9607, 0.9638, 0.9647 and 0.9655 from C<sub>6</sub> to C<sub>9</sub>. In previous studies of LLE of mixtures with PFCs using the original soft-SAFT model [3] it was found that the EoS was not able to adequately describe the entire equilibrium diagram. It could provide an acceptable description of the

Table 4

Parameters to be used in Eq. (2) together with critical constants for the studied mixtures

| System                                                                                              | <i>A</i> | $\beta$ | $\phi_{1c}$ | $x_{1c}$ | <i>T<sub>c</sub></i> (K) |
|-----------------------------------------------------------------------------------------------------|----------|---------|-------------|----------|--------------------------|
| CF <sub>2</sub> H(CF <sub>2</sub> ) <sub>6</sub> H <sub>2</sub> OH + C <sub>6</sub> F <sub>14</sub> | 0.6478   | 0.2510  | 0.380       | 0.371    | 288.36                   |
| CF <sub>2</sub> H(CF <sub>2</sub> ) <sub>6</sub> H <sub>2</sub> OH + C <sub>7</sub> F <sub>16</sub> | 0.8301   | 0.3144  | 0.349       | 0.399    | 292.31                   |
| CF <sub>2</sub> H(CF <sub>2</sub> ) <sub>6</sub> H <sub>2</sub> OH + C <sub>8</sub> F <sub>18</sub> | 0.8225   | 0.2963  | 0.326       | 0.428    | 301.81                   |
| CF <sub>2</sub> H(CF <sub>2</sub> ) <sub>6</sub> H <sub>2</sub> OH + C <sub>9</sub> F <sub>20</sub> | 0.7718   | 0.2749  | 0.304       | 0.453    | 307.73                   |

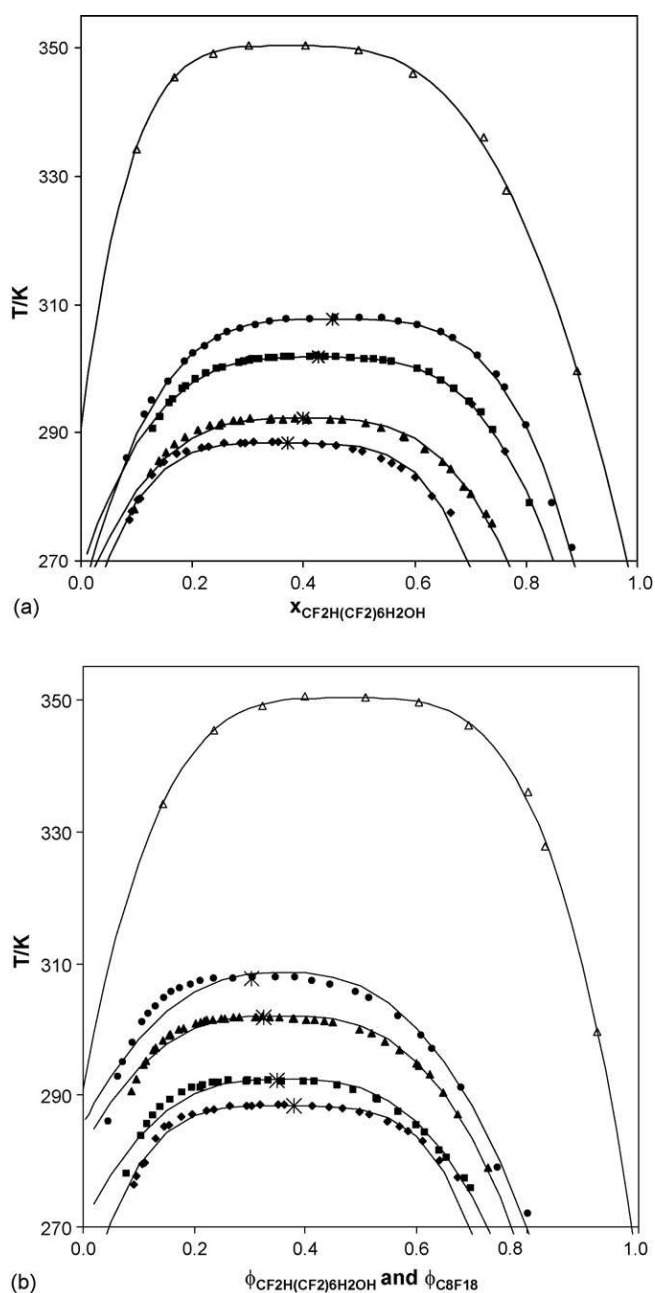


Fig. 1. Experimental and correlated coexisting curve of 1H,1H,7H-perfluoroheptan-1-ol + *n*-perfluoroalkanes ( $C_6$ – $C_9$ ) in terms of mole fraction (a) and volume fraction (b). Symbols represent solubility in *n*-hexane ( $\blacklozenge$ ), *n*-heptane ( $\blacksquare$ ), *n*-octane ( $\blacktriangle$ ) and *n*-nonane ( $\bullet$ ). Asterisk (\*) represents the critical point for each mixture. The non-filled symbols represent data for *n*-octane + perfluoro-*n*-octane ( $\triangle$ ) measured by our group in a previous work [3]. The lines represent the correlated data calculated from renormalization group theory.

experimental data in the region far from the critical point and even the trend of the critical point shift with the alkane chain length change in the mixture, but it failed to describe the critical region. This is not the case for the mixtures studied in this work, where it was possible to accurately describe the LLE diagram both far and close to the critical point as shown in Fig. 3.

The binary interaction parameters adjusted using experimental data at 0.1 MPa have also been used to predict the pressure

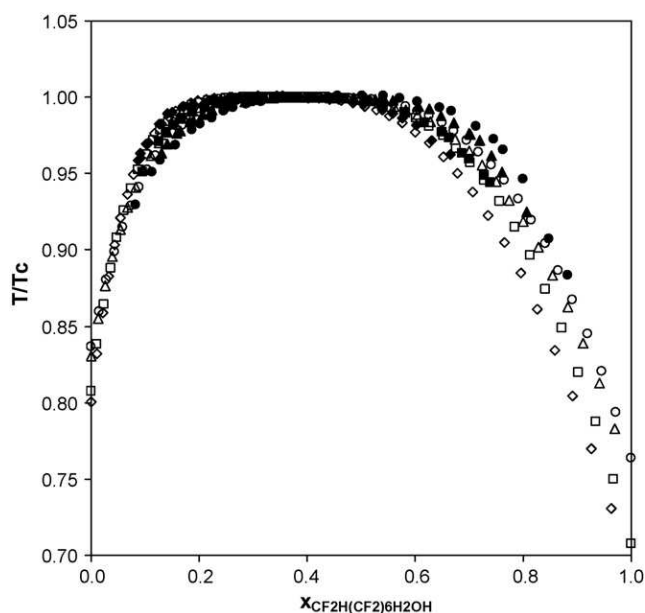


Fig. 2. Reduced temperature as a function of the molar fractions for all the mixtures studied in this work (full symbols) and also for perfluoro-*n*-octane + *n*-alkanes (non-filled symbols) using experimental data measured in a previous work [3]. Symbols as in Fig. 1.

dependence of the phase diagrams. However, these parameters were not capable of correctly describe the pressure dependence, being the theoretical predictions higher than the experimental ones as can be seen in Fig. 4. It was tried to fit binary parameters to the data measured at higher pressures to achieve an adequate representation of the pressure dependence of the phase diagrams.

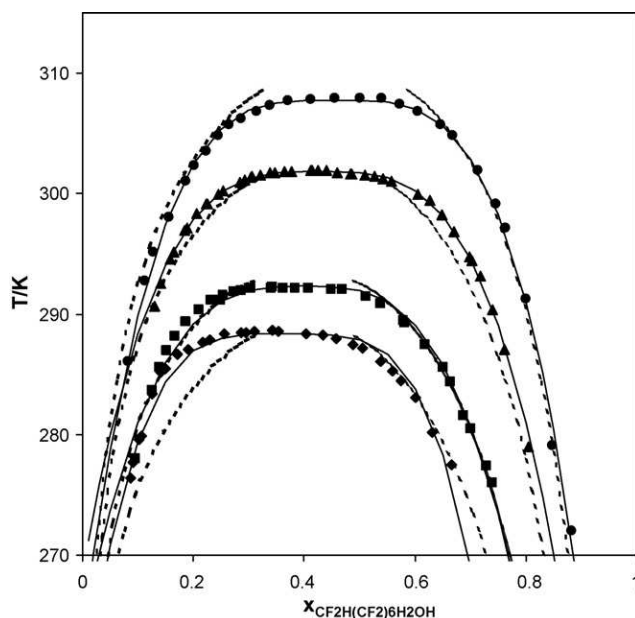


Fig. 3. Comparison between experimental LLE data for 1H,1H,7H-perfluoroheptan-1-ol +  $C_nF_{2n+2}$  mixtures at 0.1 MPa and the predictions obtained from the soft-SAFT EoS. Symbols represent the experimental data as in Fig. 1. The dashed lines represent the description obtained with soft-SAFT EoS when  $\eta = 1.05$  and  $\xi = 0.9607, 0.9638, 0.9647$  and  $0.9655$  from  $C_6$  to  $C_9$ . The full lines represent the correlated data calculated from renormalization group theory.



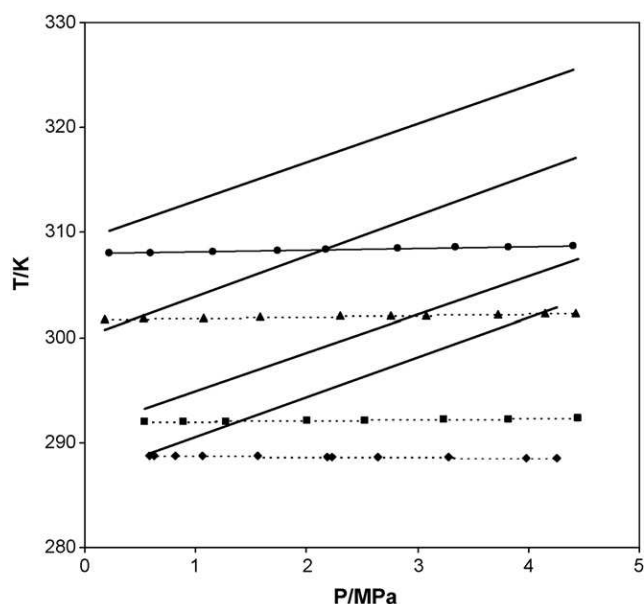


Fig. 4. Prediction of the high pressure experimental data obtained with the soft-SAFT EoS using the binary parameters adjusted for data at atmospheric pressure (full lines). Symbols as in Fig. 1 (with thinner lines being guides for the eye).

Nevertheless, using these parameters to describe the LLE data at 0.1 MPa, makes it possible to identify and locate the phase diagram on the composition scale but leads to an overprediction of the two phase region as expected from results reported in a previous work [3]. This shows that the soft-SAFT EoS is not able to simultaneously describe the  $g^E$  and the  $h^E$  and  $v^E$ . A good description of the  $g^E$  results in an accurate description of the phase diagram while a poor description of the  $h^E$  and/or  $v^E$  leads to a wrong pressure dependency of the critical point, according to Eq. (8). If one forces a good representation of the pressure dependence of the critical temperature, and hence, of the  $v^E/h^E$  ratio, a poor description of the phase diagram, and thus of  $g^E$  is obtained.

These results show that the soft-SAFT EoS, as it was presented in this work, cannot simultaneously describe the equilibrium properties (the LLE diagram) and the excess thermodynamic properties when using the same set of binary interaction parameters. Recent works presented derivations of two versions of the SAFT EoS, the soft-SAFT EoS [24] and the SAFT-VR Mie [25], and they are attempts to deal with situations as the one mentioned above. Both works, using different methodologies, intend to generalize the SAFT EoS in order to make it broad enough to be able to simultaneously describe equilibrium and excess properties, using a same set of parameters, that would also be more physically robust. In future work, it would be interesting to test the ability of these “extended versions” to predict the experimental data measured in this work.

## 5. Conclusions

In this work, liquid–liquid equilibria results of binary mixtures of 1H,1H,7H-perfluoroheptan-1-ol + perfluoro- $n$ -alkanes,  $n$ -C $_n$ F $_{2n+2}$  ( $n = 6$ – $9$ ), as measured by turbidimetry at atmospheric

pressure, and using a laser light scattering technique, for measurements at pressures up to 5 MPa, are presented. A group renormalization theory was used to calculate the critical temperature and mole fraction for each mixture, which are difficult to observe experimentally due to the extended flatness of this region that these systems exhibit.

The soft-SAFT EoS was used to correlate the experimental data measured at atmospheric pressure. Using a fixed and transferable size binary interaction parameter, it was possible to accurately describe the equilibrium data measured including the critical region. The same binary interaction parameters proved to be inefficient to predict the higher pressure data measured. As future work, it would be interesting to look for the possibility of the existence of a set of molecular and/or interaction parameters that could simultaneously describe both equilibrium and excess data.

### List of symbols

|            |                                                                 |
|------------|-----------------------------------------------------------------|
| $A$        | Helmholtz free energy                                           |
| $h^E$      | excess enthalpy                                                 |
| $m$        | chain length (for Lennard-Jones segments)                       |
| $M$        | molecular weight                                                |
| $\Delta M$ | difference in the order parameter between the coexisting phases |
| $p$        | pressure                                                        |
| $T$        | temperature                                                     |
| $v^E$      | excess volume                                                   |
| $x$        | mole fraction                                                   |

### Greek letters

|               |                                                                                      |
|---------------|--------------------------------------------------------------------------------------|
| $\beta$       | critical exponent                                                                    |
| $\Delta_1$    | correction exponent                                                                  |
| $\varepsilon$ | segment interaction energy (between Lennard-Jones segments)                          |
| $\eta$        | size parameter of the generalized Lorentz-Berthelot combination rules                |
| $\xi$         | energy parameter of the generalized Lorentz-Berthelot combination rules              |
| $\rho$        | mass density ( $\text{kg m}^{-3}$ )                                                  |
| $\sigma$      | size parameter of the intermolecular potential/diameter (for Lennard-Jones segments) |
| $\tau$        | reduced temperature that expresses the distance from the critical point              |
| $\phi$        | volume fraction                                                                      |

### Indices

|       |                                    |
|-------|------------------------------------|
| $c$   | critical                           |
| $i$   | component                          |
| assoc | association term for soft-SAFT EoS |
| calc  | calculated                         |
| chain | chain term for soft-SAFT EoS       |
| ref   | reference term for soft-SAFT EoS   |
| res   | residual term for soft-SAFT EoS    |

## Acknowledgements

This project was financed by Fundação para a Ciência e Tecnologia, POCI/QUI/57716/2004. Partial support from the

Spanish government was provided under project CTQ2005-00296/PPQ.

## References

- [1] I.A. McLure, A. Mokhtari, J. Bowers, *J. Chem. Soc., Faraday Trans.* 93 (1997) 249–256.
- [2] A.M.A. Dias, J.C. Pàmies, J.A.P. Coutinho, I.M. Marrucho, L.F. Vega, *J. Phys. Chem. B* 108 (2004) 1450–1457.
- [3] M.J.P. Melo, A.M.A. Dias, M. Blesic, L.P.N. Rebelo, L.F. Vega, J.A.P. Coutinho, I.M. Marrucho, *Fluid Phase Equilib.* 242 (2006) 210–219.
- [4] J.P. Bégué, D. Bonnet-Delpon, B. Crousse, *ChemInform* (2004) 35–40.
- [5] H. Kang, N.L. Engle, P.V. Bonnessen, L.H. Delmau, T.J. Haverlock, B.A. Moyer, *Symposia Papers presented before the Division of Environmental Chemistry American Chemical Society*, 2004.
- [6] F. Giulieri, M.P. Krafft, *Thin Solid Films* 284/285 (1996) 195–199.
- [7] A.N. Dobрева-Veleva, E.W. Kaler, K.V. Schubert, A.E. Feiring, W.B. Farnham, *Langmuir* 15 (1999) 4480–4485.
- [8] N. Hirota, K. Mizuno, Y. Goto, *J. Mol. Biol.* 275 (1998) 365–378.
- [9] M. Sangermano, R. Bongiovanni, A. Priola, D. Pospiech, *J. Polym. Sci.: A: Polym. Chem.* 43 (2005) 4144–4150.
- [10] M.J. Dinglasan-Panlilio, S. Mabury, *Environ. Sci. Technol.* 40 (2006) 1447–1452.
- [11] F.J. Blas, L.F. Vega, *Mol. Phys.* 92 (1997) 135–150.
- [12] A.M.A. Dias, H. Carrier, J.L. Daridon, J.C. Pàmies, L.F. Vega, J.A.P. Coutinho, I.M. Marrucho, *Ind. Eng. Chem. Res.* 45 (2006) 2341–2350.
- [13] L.M.N.B.F. Santos, M.J.M. Monte, M. Fulhem, J.A.P. Coutinho, *J. Chem. Eng. Data*, submitted for publication.
- [14] N. Nagarajan, A. Kumar, E.S.R. Gopal, S.C. Greer, *J. Phys. Chem.* 84 (1980) 2883–2887.
- [15] J.M.H.L. Sengers, W.L. Greer, J.V. Sengers, *J. Phys. Chem. Ref. Data* 5 (1976) 1–52.
- [16] F.J. Wegner, *Phys. Rev. B* 5 (1972) 4529–4533.
- [17] M. LeyKoo, M.S. Green, *Phys. Rev. A* 16 (1977) 2483–2487.
- [18] J.C. Pàmies, L.F. Vega, *Ind. Eng. Chem. Res.* 40 (2001) 2532–2543.
- [19] J.C. Pàmies, Ph.D. Thesis, Universitat Rovira i Virgili, 2003.
- [20] L.P.N. Rebelo, V. Najdanovic-Visak, Z.P. Visak, M. Nunes da Ponte, J. Trancoso, C.A. Cerdeiriña, L. Romani, *Phys. Chem. Chem. Phys.* 4 (2002) 2251–2259.
- [21] L.P.N. Rebelo, *Phys. Chem. Chem. Phys.* 1 (1999) 4277–4286.
- [22] M.S.B. Munson, *J. Phys. Chem.* 68 (1964) 796–800.
- [23] J.B. Gilmour, J.O. Zwicker, J. Katz, *J. Phys. Chem.* 71 (1967) 3259–3264.
- [24] F. Llovel, C.J. Peters, L.F. Vega, *Fluid Phase Equilib.* 248 (2006) 115–122.
- [25] T. Lafitte, D. Bessieres, M.M. Pineiro, J.L. Daridon, *J. Chem. Phys.* 124 (2006).

# GENERAL DISCUSSION

Each chapter of this Thesis includes a comprehensive discussion of the presented work. Therefore, this part offers only a brief review.

The Thesis is mainly focused on the phase behaviour in nano (Chapters 1, 2, and 4) and macro domains (Chapters 5-7) and thermophysical properties of neat ionic liquids (Chapter 3) or mixtures containing ionic liquids and water, fluorinated or organic solvents.

Aqueous solutions of ionic liquids of the 1-alkyl-3-methylimidazolium chloride family,  $[C_n\text{mim}]\text{Cl}$ , and 1-alkyl-3-methylpyridinium chloride family,  $[C_n\text{mpy}]\text{Cl}$ , with  $n$  ranging from 8 to 14 and  $n$  ranging from 8 to 18, respectively, when scrutinised using interfacial tension, fluorescence, and  $^1\text{H}$  NMR measurements, present evidence for the self-aggregation of the  $[C_n\text{mim}]^+$  and  $[C_n\text{mpy}]^+$  cations into micellar aggregates. Although the interfacial tension results show a decrease in IFT even for  $n < 8$ , these compounds do not show a IFT plateau at higher  $[C_n\text{mim}]\text{Cl}$  and  $[C_n\text{mpy}]\text{Cl}$  concentrations which indicates that the hydrophobicity is not enough to build up micelles in these cases. The observed critical micelle concentration, CMC, for both families of ionic liquids, shows a good free energy correlation as a function of  $n$  and the dependence for micellisation is similar to that of the alkyltrimethylammonium and alkylammonium chloride families,  $C_n\text{TAC}$  and  $C_n\text{AC}$ .

The effect of the anion of the ionic liquid on the surface tension of aqueous solutions of  $[C_{10}\text{mim}]\text{X}$  (where X is  $\text{Cl}^-$ ,  $[\text{NTf}_2]^-$  or  $[\text{PF}_6]^-$ ) was studied as well. In the cases of the  $[\text{NTf}_2]^-$  and  $[\text{PF}_6]^-$  anions no micelle formation was detected, as the low solubility of the corresponding ionic liquids induced phase separation before any bulk aggregation occurred.

It was observed that 1-alkyl-3-methylpyridinium-based ionic liquids can be used as quenchers for some fluorescence probes (fluorophores). In order to verify that the 1-alkyl-3-methylpyridinium group is able to quench the fluorescence of these probes, Stern-Volmer quenching constants,  $K_{\text{SV}}$ , for the steady-state fluorescence quenching for pyrene and anthracene were determined from the variation of fluorescence intensity in the absence ( $I_0$ ) and presence ( $I$ ) of low concentrations, of 1-alkyl-3-methylpyridinium,  $c$ , in ethanenitrile. From the slopes of the Stern-Volmer



plots values of  $K_{SV} = 0.3 \text{ mM}^{-1}$  and  $0.07 \text{ mM}^{-1}$ , respectively, for pyrene and anthracene, were obtained. The fact that the  $[\text{C}_n\text{mpy}]\text{Cl}$  family may act as fluorescence quenchers opens the possibility of determining CMCs by detecting the surfactant concentration for which the quenching deviates from the normal Stern-Volmer equation, *i.e.*, from a slope comparable to that which occurs in homogeneous media. The start-point of micellisation defined as CMC can be recognised as a pronounced break-point in the dependence of  $I_0 / I$  versus the concentration of  $[\text{C}_n\text{mpy}]\text{Cl}$  in aqueous solution. The ability of pyridinium ionic liquids to act as a quencher for some fluorophores can be used as a very sensitive method for monitoring their concentration change. This method can be used in a broad concentration range and in the presence many other species in solution, since quenching requires a specific contact pyridinium nucleus-fluorophore.

A family of ionic liquids based on alkanesulfonate anions,  $[\text{C}_k\text{SO}_3]^-$ , and 1-alkyl-3-methylimidazolium cations,  $[\text{C}_n\text{mim}]^+$ , was synthesized, where the size of the alkyl side chain simultaneously was varied in the cation or in the anion. In order to characterize this family of ionic liquids, their melting and decomposition temperatures, and the density and the viscosity as a function of temperature were determined. No clear pattern was found in the variation of the melting point temperatures. The ionic liquids studied have shown very good thermal stability, with decomposition temperatures ranging from 600 to 700 K measured by TGA. The absence of the ester bond in the sulfonate anion,  $[\text{C}_m\text{SO}_3]^-$ , contributes to a better thermal stability of these ionic liquids in comparison to those with sulfate anions,  $[\text{C}_m\text{SO}_4]^-$ , which at high temperature and in the presence of traces of impurities (water, amines) undergo hydrolysis. The molar volume results show a consistent trend along the series of 1-alkyl-3-methylimidazolium alkanesulfonate ionic liquids: the “addition” of a  $(-\text{CH}_2-)$  group in either a short or a long alkyl chain, either in the cation or in the anion, always increases the molar volume by the same universal amount,  $17.06 \text{ cm}^3\text{mol}^{-1}$  at 298.15 K, irrespective of the ionic liquid itself. It is observed that the ionic liquid samples based on the sulfonate anion are quite viscous with values ranging from 17 mPa s for  $[\text{C}_2\text{mim}][\text{C}_2\text{SO}_3]$  at 356 K to 1055 mPa s for  $[\text{C}_2\text{mim}][\text{C}_4\text{SO}_3]$  at 296 K. The viscosity of alkanesulfonate based ionic liquids decreases very rapidly with increasing temperature. For example, for  $[\text{C}_3\text{mim}][\text{C}_4\text{SO}_3]$ , one of the more viscous ionic liquids studied in this work, the viscosity decreases one order of magnitude when the temperature changes from 296 K

to 330 K. Viscosity of the ionic liquids increases, as expected, when the alkyl chain increases, both/either in the cation and/or in the anion.

The aggregation behaviour of seven members of the same family 1-alkyl-3-methylimidazolium alkylsulfonate ionic liquids ( $[C_n\text{mim}][C_m\text{SO}_3]$ ,  $n = 8, 10$  or  $12$ ;  $m = 1$  and  $n = 4$  or  $8$ ;  $m = 4$  or  $8$ ) has been investigated in aqueous solution under ambient conditions, as well. The ionic liquids with the methylsulfonate anion ( $[C_n\text{mim}][C_1\text{SO}_3]$ ,  $n = 8, 10,$  and  $12$ ) behave as conventional cationic surfactants, showing CMC values comparable with those of the aforementioned imidazolium and pyrrolidinium halide salts and having equivalent surface activity, reducing water-air interfacial tension from 72.5 to a minimum of *ca.* 44 mN m<sup>-1</sup>. In contrast, when amphiphilic character is imparted into both the cation and anion, a synergistic packing effect appears to lead to the formation of novel catanionic surfactants with both lower CMC values and enhanced surface activity. The large effect on the surface tension can be explained by a cooperative effect with both cations and anions forming the interfacial layer. In comparison to conventional single-alkyl chain ionic surfactants, corresponding gemini type surfactants or double chain ionic liquids, the presence of amphiphilic structure in both ions shows significantly higher effectiveness of the surface tension reduction. Contrary to single chain ionic surfactants where repulsion between equally charged polar heads is present, in the case of catanionic surfactants the net electrostatic attraction between the positively and negatively charged amphiphile head groups, helped by van de Waals attractions between hydrophobic alkyl chains, enhances dense packing of monomers in the monolayer and consequently leads to lowering surface tension in the plateau region.

In addition, the thermotropic phase behaviour of  $[C_8\text{mim}][C_8\text{SO}_3]$  was investigated by variable temperature X-ray scattering, polarizing optical microscopy and differential scanning calorimetry. This salt shows formation of a smectic liquid crystalline phase with a broad temperature range.

Solid-liquid and liquid-liquid phase diagrams of mixtures containing an ionic liquid plus a fluorinated benzene (hexafluorobenzene or 1,3,5-trifluorobenzene), and mixtures containing triflate- or pyrrolidinium-based ionic liquids plus benzene (1-ethyl-3-methylimidazolium triflate or N-ethyl-N-methylpyrrolidinium bis(trifluoromethanesulfonyl)-imide plus benzene) were determined. The phase diagrams exhibit different kinds of solid-liquid behaviour, ranging from the

occurrence of eutectic points, the existence of congruent melting points and the corresponding formation of inclusion crystals, or the observation of different ionic liquid crystalline phases (polymorphism). These different types of behaviour can be controlled by temperature annealing during crystallization or by the nature of the aromatic compound.

The mutual solubilities of many mixtures of commonly used ionic liquids (imidazolium, pyridinium, phosphonium and ammonium ionic liquids) with partially fluorinated alcohols (C7 to C10 carbon chain length) or perfluoroheptane were explored. It was found that ionic liquids with longer alkyl-side chains in the imidazolium cation show a larger immiscibility domain with fluorinated alcohols than their shorter-chain counterparts – a behaviour opposite of that shown when *n*-alcohols are mixed with these same ionic liquids. Also, a longer hydrogenated carbon chain – a kind of “spacer” - between the fluorinated chain and the hydroxyl group of the alcohol also decreases the miscibility between the two components of the mixture.

We have also measured cloud-points corresponding to liquid–liquid equilibrium (LLE) for mixtures of perfluoro-*n*-octane and linear alkanes from C6 to C9. The Modified UNIFAC and the soft-SAFT model were used to correlate the experimental data using interaction parameters that are temperature dependent. The comparison showed that the results obtained with the soft-SAFT model are of better quality than those correlated by UNIFAC, corroborating the higher predictive capacity of the soft-SAFT model

Liquid–liquid equilibria of binary mixtures of 1H,1H,7H-perfluoroheptan-1-ol + perfluoro-*n*-alkanes,  $n\text{-C}_n\text{F}_{2n+2}$  ( $n = 6\text{--}9$ ) were investigated. It was shown that using the soft-SAFT EoS with a fixed and transferable size binary interaction parameter to correlate the experimental data it is possible to accurately describe the equilibrium data measured at atmospheric pressure including the critical region. The same binary interaction parameters proved to be inefficient to predict the higher pressure data measured.

# **Appendix 1**

# On the Self-Aggregation and Fluorescence Quenching Aptitude of Surfactant Ionic Liquids

**Chemicals.** *Ionic liquids and ionic liquids preparation.* The 1-alkyl-3-methylpyridinium chlorides,  $[C_n\text{mpy}]\text{Cl}$  ( $n = 4, 10, 12, 14, 16, 18$ ), 1-dodecyl-1-methylpyrrolidinium bromide, 1-dodecyl-3-methylpyridinium bromide, and 1-dodecyl-1-methylpiperidinium bromide  $[C_{12}\text{Y}]\text{Br}$  ( $\text{Y} = \text{mpyrr}, \text{mpy}$  and  $\text{mpip}$  – see Scheme 1 of main text) were synthesized by reaction of 1 mol of 3-methylpyridine, 1-methylpyrrolidine or 1-methylpiperidine with an excess of the appropriate haloalkane (1.3 mol). This excess also allows for the reactants to be stirred without additional solvent at 70 °C and the progress of reactions was monitored by  $^1\text{H-NMR}$  spectroscopy in  $\text{CDCl}_3$ . Upon completion of the reaction there was no evidence for the presence of 3-methylpyridine, 1-methylpyrrolidine or 1-methylpiperidine. The ionic liquids were purified with ethyl ethanoate. The volume of ethyl ethanoate used for the recrystallization was approximately half that of the halide salt. The ethyl ethanoate was decanted, followed by the addition of fresh ethyl ethanoate, and this step was repeated five times. The remaining ethyl ethanoate was removed *in vacuo* and the ionic liquids were dried to remove any small traces of volatile compounds by applying vacuum (0.1 Pa) at moderate temperatures (60–80 °C) for typically 72 h. All chemicals were purchased from Sigma-Aldrich; the more volatile liquids were purified by distillation under vacuum before use. For the NMR experiments,  $d^1$  trichloromethane (D+0.03%) (Euriso-top) was used.

**Chemicals.** *IFT, Fluorescence, and NMR measurements.* Doubly-distilled deionised water was obtained from a Millipore Milli-Q water purification system (Millipore, USA). Both for the IFT and fluorescence measurements  $[C_n\text{mpy}]\text{Cl}$  stock solutions were prepared in either  $1.74 \times 10^{-6}$  M pyrene or  $1.06 \times 10^{-5}$  M anthracene aqueous solution, and all studied solutions were prepared from the stock solutions diluting with the same pyrene or anthracene aqueous solution. Pyrene (Fluka, Germany, 99%) was recrystallized from benzene. Anthracene (Fluka, Germany, *puriss.*, for scintillation) and ethanenitrile (Merck, Germany, gradient grade) were used without further purification. For the NMR experiments,  $\text{D}_2\text{O}$  (Cambridge Isotope Lab., USA, D, 99.9%) was used.

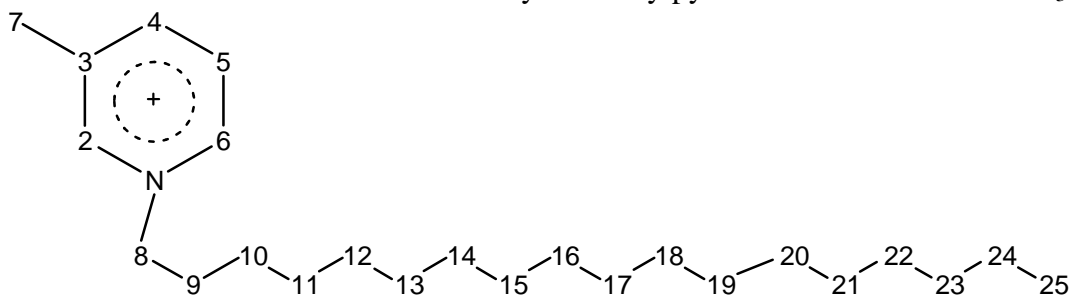
**Spectra for purity assessment.**  $^1\text{H}$ - and  $^{13}\text{C}$ -NMR analyses showed no major impurities in the ionic liquids as prepared above. All NMR spectra were recorded at room temperature on a Bruker Avance spectrometer DPX 300, using deuterated chloroform as solvent.

#### **Techniques and methodologies.**

*Interfacial tension.* Interfacial tension (IFT) was measured using a Drop Shape Analysis Tensiometer Kruss DSA1 v 1.80 working in the pendant drop mode at a constant temperature of  $(23 \pm 2)$  °C. IFT is derived from the fit of the pendant drop profile, and care was taken to ensure that the apparatus was calibrated with several solvents of known IFT in the range of interest. The drops were left to equilibrate close to the rupture point and at least three consistent measurements per solution were recorded.

*Fluorescence spectroscopy.* Fluorescent probes, anthracene and pyrene, were used in order to ascertain the onset of the aggregation of ionic liquids in water. Steady-state fluorescence spectra of the pyrene-containing and anthracene-containing solutions in 1 cm quartz cuvettes were recorded with a Cary Varian Eclipse Fluorescence Spectrometer and collected at a  $90^\circ$  angle. All measurements were done at room temperature. The excitation wavelength used for pyrene and anthracene-containing samples was 337 nm or 357 nm, respectively. Anthracene emission spectra were recorded between 350 and 450 nm and the total fluorescence intensity calculated by integration. In the case of pyrene, the fluorescence was collected at 373 nm, the wavelength of the first vibronic emission band.

*$^1\text{H}$  NMR spectroscopy.* Proton NMR spectra were recorded on a BRUKER Avance 400 ultrashield Plus spectrometer, operating at 400.13 MHz and equipped with 5 mm diameter inverse detection broadband probe head, with the following acquisition parameters: spectral width, 6 kHz; pulse width, 4  $\mu\text{s}$  ( $45^\circ$  flip angle); data points, 64K; repetition delay, 1.5 s; number of transients, 32; temperature, 303 K. The water resonance was suppressed with a pre-saturation pulse.

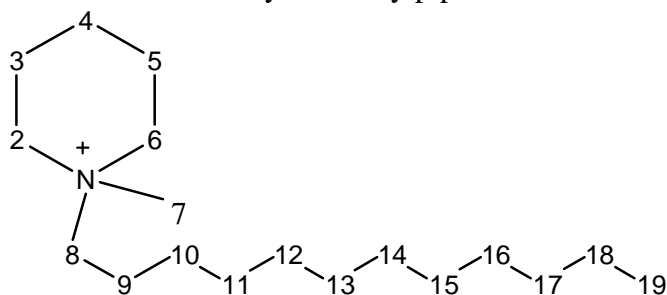
**Table 1.**  $^1\text{H}$  chemical shift data of 1-alkyl-3-methylpyridinium chlorides in  $\text{CDCl}_3$ 

| n         | CH(2) | CH <sub>3</sub> (7) | CH(4)            | CH(5)         | CH(6)         | CH <sub>2</sub> (8) | CH <sub>2</sub> (9) | CH <sub>2</sub> (10...(n+6)) | CH <sub>3</sub> (n+7) |
|-----------|-------|---------------------|------------------|---------------|---------------|---------------------|---------------------|------------------------------|-----------------------|
| <b>4</b>  |       |                     |                  |               |               |                     |                     |                              |                       |
| nr        | 1     | 3                   | 1                | 1             | 1             | 2                   | 2                   | 10                           | 3                     |
| $\delta$  | 9.8   | 2.68                | 8.29             | 8.08          | 9.48          | 5.01                | 2.07                | 1.4                          | 0.97                  |
| m         | s     | s                   | d<br>( $J=7.8$ ) | t ( $J=6$ )   | d ( $J=6$ )   | t ( $J=7.5$ )       | m                   | m                            | t ( $J=6.6$ )         |
| <b>10</b> |       |                     |                  |               |               |                     |                     |                              |                       |
| nr        | 1     | 3                   | 1                | 1             | 1             | 2                   | 2                   | 14                           | 3                     |
| $\delta$  | 9.7   | 2.67                | 8.29             | 8.1           | 9.44          | 4.98                | 2.07                | 1.27                         | 0.86                  |
| m         | s     | s                   | d<br>( $J=8.1$ ) | t ( $J=6$ )   | d ( $J=6$ )   | t ( $J=7.2$ )       | m                   | bp                           | t ( $J=6.3$ )         |
| <b>12</b> |       |                     |                  |               |               |                     |                     |                              |                       |
| nr        | 1     | 3                   | 1                | 1             | 1             | 2                   | 2                   | 18                           | 3                     |
| $\delta$  | 9.53  | 2.66                | 8.25             | 8.03          | 9.42          | 4.99                | 2.05                | 1.29                         | 0.87                  |
| m         | s     | s                   | d<br>( $J=7.8$ ) | t ( $J=6.3$ ) | d ( $J=5.7$ ) | t ( $J=7.5$ )       | m                   | bp                           | t ( $J=6.3$ )         |
| <b>14</b> |       |                     |                  |               |               |                     |                     |                              |                       |
| nr        | 1     | 3                   | 1                | 1             | 1             | 2                   | 2                   | 22                           | 3                     |
| $\delta$  | 9.49  | 2.66                | 8.25             | 8.03          | 9.39          | 4.99                | 2.04                | 1.28                         | 0.88                  |
| m         | s     | s                   | d<br>( $J=8.1$ ) | t ( $J=6.3$ ) | d ( $J=6$ )   | t ( $J=7.5$ )       | m                   | bp                           | t ( $J=6.3$ )         |
| <b>16</b> |       |                     |                  |               |               |                     |                     |                              |                       |
| nr        | 1     | 3                   | 1                | 1             | 1             | 2                   | 2                   | 26                           | 3                     |
| $\delta$  | 9.59  | 2.66                | 8.26             | 8.05          | 9.45          | 4.99                | 2.04                | 1.28                         | 0.88                  |
| m         | s     | s                   | d<br>( $J=8.1$ ) | t ( $J=6.3$ ) | d ( $J=6$ )   | t ( $J=7.5$ )       | m                   | bp                           | t ( $J=6.6$ )         |
| <b>18</b> |       |                     |                  |               |               |                     |                     |                              |                       |
| nr        | 1     | 3                   | 1                | 1             | 1             | 2                   | 2                   | 30                           | 3                     |
| $\delta$  | 9.67  | 2.67                | 8.28             | 8.08          | 9.47          | 4.99                | 2.05                | 1.28                         | 0.88                  |
| m         | s     | s                   | d<br>( $J=8.1$ ) | t ( $J=6$ )   | d ( $J=6$ )   | t ( $J=7.2$ )       | m                   | bp                           | t ( $J=6.6$ )         |

**Table 2.**  $^{13}\text{C}$  chemical shift data of 1-alkyl-3-methylpyridinium chlorides in  $\text{CDCl}_3$

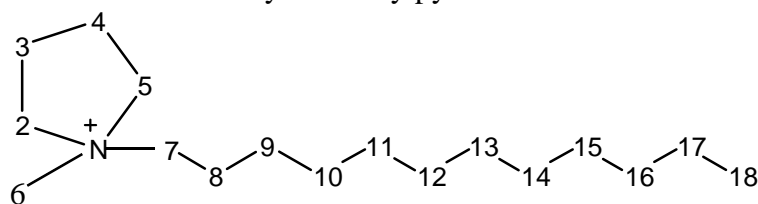
| <i>n</i>  | CH(1)  | C(2)   | CH <sub>3</sub> (3) | CH(4)  | CH(5)  | CH(6)  | CH <sub>2</sub> (7) | CH <sub>2</sub> (8) | CH <sub>2</sub> (9) | CH <sub>2</sub> (10..(n+3)) | CH <sub>2</sub> (n+4) | CH <sub>2</sub> (n+5) | CH <sub>3</sub> (n+6) |
|-----------|--------|--------|---------------------|--------|--------|--------|---------------------|---------------------|---------------------|-----------------------------|-----------------------|-----------------------|-----------------------|
| <b>10</b> | 145.22 | 139.94 | 19.02               | 145.77 | 128.22 | 142.91 | 62.04               | 32.41               | 32.13               | 29,5                        | 26.45                 | 22.95                 | 14.42                 |
| <b>12</b> | 145.20 | 140.00 | 19.17               | 145.72 | 128.10 | 142.97 | 62.29               | 32.52               | 32.30               | 29,7                        | 26.54                 | 23.08                 | 14.53                 |
| <b>14</b> | 145,16 | 140.00 | 19.15               | 145,76 | 128.16 | 142,97 | 62,27               | 32.49               | 32.32               | 29,7                        | 26.54                 | 23.09                 | 14.53                 |
| <b>16</b> | 145,26 | 139.97 | 19.10               | 145.75 | 128.20 | 142.97 | 62.14               | 32.49               | 32.29               | 29.7                        | 26.20                 | 23.06                 | 14.5                  |
| <b>18</b> | 145,10 | 139.99 | 19.16               | 145,74 | 128.15 | 142,93 | 62,32               | 32.47               | 32.33               | 29,7                        | 26.54                 | 23.09                 | 14.53                 |

$^1\text{H}$  NMR of 1-dodecyl-3-methylpiperidinium bromide



$^1\text{H-NMR}$  ( $\text{CDCl}_3$ , 300MHz):  $\delta/\text{ppm}$  = 3.669-3.552 (m,  $\text{CH}_2$  (2,6,8)); 3.268 (s,  $\text{CH}_3$ (7)); 1.864-1.668 (m, $\text{CH}_2$  (3,4,5)); 1.294-1.184 (bp,  $\text{CH}_2$  (10-18)); 0.811 (t,  $J=7$ ,  $\text{CH}_3$  (19)).

$^1\text{H}$  NMR of 1-dodecyl-3-methylpyrrolidinium bromide



$^1\text{H-NMR}$  ( $\text{CDCl}_3$ , 300MHz):  $\delta/\text{ppm}$  = 3.867-3.842 (m,  $\text{CH}_2$  (2,5)); 3.686-3.626 (t,  $J=6.3$ ,  $\text{CH}_2$  (7)); 3.299 (s,  $\text{CH}_3$ (6)); 2.314-2.311 (m, $\text{CH}_2$  (3,4)); 1.798-1.783 (m,  $\text{CH}_2$  (8)); 1.360-1.1255 (bp,  $\text{CH}_2$  (9-17)); 0.859-0.904 (t,  $J=7$ ,  $\text{CH}_3$  (18)).



**Table 3.** Melting, decomposition and freezing points of 1-alkyl-3-methylpyridinium chlorides

| Compounds studied           | Tmp / °C | T decomp/°C | Tfr / °C |
|-----------------------------|----------|-------------|----------|
| [C <sub>4</sub> (3)mpy] Cl  | 111.3    | 242         | -        |
| [C <sub>6</sub> (3)mpy] Cl  | 81.9     | 238         | -        |
| [C <sub>8</sub> (3)mpy] Cl  | 80.0     | 232         | -        |
| [C <sub>10</sub> (3)mpy] Cl | 79.3     | 227         | 52.4     |
| [C <sub>12</sub> (3)mpy] Cl | 87.6     | 227         | 51.8     |
| [C <sub>14</sub> (3)mpy] Cl | 93.6     | 227         | 60.0     |
| [C <sub>16</sub> (3)mpy] Cl | 109.8    | 228         | 78.7     |
| [C <sub>18</sub> (3)mpy] Cl | 112.2    | 228         | 72.7     |

**Table 4.** Charge distribution and geometry of isolated N,N-dimethylpyrrolidinium (pyrr) and N,N-dimethylpiperidinium (pip) cations obtained *ab initio* (cf. experimental section). The numbering of the atoms is different from the rest of the manuscript but, on the one hand, it reflects the ordering of the z matrices used to build the files from MD calculations, and on the other hand it constitutes an ambiguous self-contained set.

| Atomic definition and atomic point charges (in a.c.u.) |       |       |                  |      |      |
|--------------------------------------------------------|-------|-------|------------------|------|------|
|                                                        | pyrr  | pip   |                  | pyrr | pip  |
| N1                                                     | 0.13  | 0.20  | H13 (cycle,meta) | 0.06 | 0.06 |
| C2 (cycle,ortho)                                       | 0.07  | -0.09 | H14 (cycle,meta) | 0.06 | 0.02 |
| C3 (cycle,ortho)                                       | 0.07  | -0.09 | H15 (cycle,meta) | 0.06 | 0.02 |
| C4 (cycle,meta)                                        | -0.04 | 0.02  | H16 (cycle,meta) | 0.06 | 0.06 |
| C5 (cycle,meta)                                        | -0.04 | 0.02  | H17 (cycle,para) | -    | 0.04 |
| C6 (cycle,para)                                        | -     | -0.07 | H18 (cycle,para) | -    | 0.06 |
| C7 (methyl)                                            | -0.22 | -0.36 | H19 (methyl)     | 0.13 | 0.17 |
| C8 (methyl)                                            | -0.22 | -0.33 | H20 (methyl)     | 0.13 | 0.19 |
| H9 (cycle,ortho)                                       | 0.05  | 0.10  | H21 (methyl)     | 0.14 | 0.17 |
| H10 (cycle,ortho)                                      | 0.05  | 0.09  | H22 (methyl)     | 0.13 | 0.16 |
| H11 (cycle,ortho)                                      | 0.05  | 0.09  | H23 (methyl)     | 0.13 | 0.17 |
| H12 (cycle,ortho)                                      | 0.05  | 0.10  | H24 (methyl)     | 0.14 | 0.17 |
| Bond lengths (in pm)                                   |       |       |                  |      |      |
| R(1,2)                                                 | 152   | 151   | R(4,13)          | 108  | 108  |
| R(1,3)                                                 | 152   | 151   | R(4,14)          | 108  | 108  |
| R(1,7)                                                 | 150   | 149   | R(5,6)           | -    | 153  |
| R(1,8)                                                 | 150   | 149   | R(5,15)          | 108  | 108  |
| R(2,4)                                                 | 153   | 152   | R(5,16)          | 108  | 108  |
| R(2,9)                                                 | 108   | 108   | R(6,17)          | -    | 109  |
| R(2,10)                                                | 108   | 108   | R(6,18)          | -    | 108  |
| R(3,5)                                                 | 153   | 152   | R(7,19)          | 108  | 108  |
| R(3,11)                                                | 108   | 108   | R(7,20)          | 108  | 108  |

|                            |     |     |            |     |     |
|----------------------------|-----|-----|------------|-----|-----|
| $R(3,12)$                  | 108 | 108 | $R(7,21)$  | 108 | 108 |
| $R(4,5)$                   | 154 | -   | $R(8,22)$  | 108 | 108 |
| $R(4,6)$                   | -   | 153 | $R(8,23)$  | 108 | 108 |
|                            |     |     | $R(8,24)$  | 108 | 108 |
| Angles (in degrees of arc) |     |     |            |     |     |
| A(2,1,3)                   | 108 | 110 | A(3,5,4)   | 108 |     |
| A(2,1,7)                   | 110 | 111 | A(3,5,6)   | -   | 111 |
| A(2,1,8)                   | 110 | 109 | A(3,5,15)  | 110 | 111 |
| A(3,1,7)                   | 110 | 111 | A(3,5,16)  | 110 | 107 |
| A(3,1,8)                   | 110 | 109 | A(4,5,15)  | 111 | -   |
| A(7,1,8)                   | 109 | 108 | A(4,5,16)  | 111 | -   |
| A(1,2,4)                   | 108 | 113 | A(6,5,15)  | -   | 111 |
| A(1,2,9)                   | 108 | 106 | A(6,5,16)  |     | 111 |
| A(1,2,10)                  | 108 | 107 | A(15,5,16) | 107 | 106 |
| A(4,2,9)                   | 113 | 110 | A(4,6,5)   | -   | 111 |
| A(4,2,10)                  | 113 | 112 | A(4,6,17)  |     | 110 |
| A(9,2,10)                  | 108 | 108 | A(4,6,18)  | -   | 110 |
| A(1,3,5)                   | 108 | 113 | A(5,6,17)  | -   | 110 |
| A(1,3,11)                  | 108 | 107 | A(5,6,18)  | -   | 110 |
| A(1,3,12)                  | 108 | 106 | A(17,6,18) | -   | 107 |
| A(5,3,11)                  | 113 | 112 | A(1,7,19)  | 109 | 109 |
| A(5,3,12)                  | 113 | 110 | A(1,7,20)  | 109 | 110 |
| A(11,3,12)                 | 108 | 108 | A(1,7,21)  | 109 | 109 |
| A(2,4,5)                   | 108 | -   | A(19,7,20) | 110 | 110 |
| A(2,4,6)                   | -   | 111 | A(19,7,21) | 110 | 110 |
| A(2,4,13)                  | 110 | 107 | A(20,7,21) | 110 | 110 |
| A(2,4,14)                  | 110 | 111 | A(1,8,22)  | 109 | 109 |
| A(5,4,13)                  | 111 | -   | A(1,8,23)  | 109 | 109 |
| A(5,4,14)                  | 111 | -   | A(1,8,24)  | 109 | 109 |
| A(6,4,13)                  | -   | 111 | A(22,8,23) | 110 | 110 |
| A(6,4,14)                  | -   | 111 | A(22,8,24) | 110 | 110 |
| A(13,4,14)                 | 107 | 106 | A(23,8,24) | 110 | 110 |

## **Appendix 2**

# 1-Alkyl-3-methylimidazolium alkanesulfonate ionic liquids: synthesis and physicochemical properties

**[CH<sub>3</sub>mim][SO<sub>3</sub>CH<sub>3</sub>].** Methyl methanesulfonate (25 g, 1.05 mol eq) dissolved in ethyl ethanoate (50 ml) was placed in a 500 ml round-bottomed flask and stirred vigorously. The mixture was cooled in an ice-bath, and 1-methylimidazole (17.8 g, 1 mol eq) dissolved in ethanoate (50 ml) was added dropwise using a dropping funnel. Strongly exothermic reaction was observed upon adding. After stirring for 8 h, the crude product was washed 4 times with ethyl ethanoate in order to remove unreacted reagents. Removal of the remaining solvent *in vacuo* gave the desired product **1-methyl-3-methylimidazolium methanesulfonate** as a white solid (40.5 g, 97.4% yield).

**<sup>1</sup>H-NMR** (CDCl<sub>3</sub>, 300 MHz): δ/ppm = 2.75 (s, 3H, SCH<sub>3</sub>); 4.03 (s, 6H, NCH<sub>3</sub>); 7.61 (s, 2H, NCH); 9.70 (s, 1H, NCHN).

**<sup>13</sup>C-NMR** (CDCl<sub>3</sub>, 75 MHz): δ/ppm = 36.50 (SCH<sub>3</sub>); 40.13 (NCH<sub>3</sub>); 124.00 (NCH); 138.89 (NCHN).

**MS ES<sup>+</sup> m/z** (% rel. Intensity): 97 M<sup>+</sup> (100). Calcd. for C<sub>5</sub>H<sub>9</sub>N<sub>2</sub>: 97.0776; found: 97.0770.

**MS ES<sup>-</sup> m/z** (% rel. Intensity): 95 M<sup>-</sup> (100). Calcd. for CH<sub>3</sub>O<sub>3</sub>S: 94.9803; found: 94.9795.

**[C<sub>2</sub>H<sub>5</sub>mim][CH<sub>3</sub>SO<sub>3</sub>].** Following the general procedure 1b (50 °C, 72 h), **1-ethyl-3-methylimidazolium methanesulfonate** was obtained as a yellowish liquid in *ca.* 91 % yield.

**<sup>1</sup>H-NMR** (CDCl<sub>3</sub>, 300 MHz): δ/ppm = 1.00 (t, 3H, J = 7.5 Hz, CH<sub>2</sub>CH<sub>3</sub>); 2.15 (s, 3H, SCH<sub>3</sub>); 3.50 (s, 3H, NCH<sub>3</sub>); 3.80 (q, 2H, J = 7.5 Hz, NCH<sub>2</sub>); 7.16 (s, 1H, NCHCH); 7.19 (s, 1H, NCHCH); 9.13 (s, 1H, NCHN).

**<sup>13</sup>C-NMR** (CDCl<sub>3</sub>, 75 MHz): δ/ppm = 10.01 (CH<sub>2</sub>CH<sub>3</sub>); 36.01 (SCH<sub>3</sub>); 44.14 (NCH<sub>3</sub>); 44.39 (NCH<sub>2</sub>); 122.12 (NCH); 124.03 (NCH); 138.81 (NCHN).

**MS ES<sup>+</sup> m/z** (% rel. Intensity): 111 M<sup>+</sup> (100). Calcd. for C<sub>6</sub>H<sub>11</sub>N<sub>2</sub>: 111.0922; found: 111.0922

**MS ES<sup>-</sup> m/z** (% rel. Intensity): 95 M<sup>-</sup> (100). Calcd. for CH<sub>3</sub>O<sub>3</sub>S: 94.9803; found: 94.9800.

**[C<sub>3</sub>H<sub>7</sub>mim][SO<sub>3</sub>CH<sub>3</sub>].** Following the general procedure 1a (12 h) and 1b (70 °C, 96 h), **1-propyl-3-methylimidazolium methanesulfonate** was obtained as a very pale yellow liquid in *ca.* 94 % yield.

**<sup>1</sup>H-NMR** (CDCl<sub>3</sub>, 300 MHz): δ/ppm = 0.69 (t, 3H, J = 7.5 Hz, CH<sub>2</sub>CH<sub>3</sub>); 1.63-1.71 (m, 2H, J = 7.5 Hz, CH<sub>2</sub>CH<sub>3</sub>); 2.47 (s, 3H, SCH<sub>3</sub>); 3.70 (s, 3H, NCH<sub>3</sub>); 3.98 (t, 2H, J = 7.2 Hz, NCH<sub>2</sub>); 7.33 (d, 1H, J = 1.8 Hz, NCH); 7.41 (d, 1H, J = 1.8 Hz, NCH); 9.49 (s, 1H, NCHN).

**<sup>13</sup>C-NMR** (CDCl<sub>3</sub>, 75 MHz): δ/ppm = 10.88 (CH<sub>2</sub>CH<sub>3</sub>); 23.78 (CH<sub>2</sub>CH<sub>3</sub>); 36.45 (SCH<sub>3</sub>); 40.03 (NCH<sub>3</sub>); 51.40 (NCH<sub>2</sub>); 122.64 (NCH); 124.10 (NCH); 137.76 (NCHN).

**MS ES<sup>+</sup> m/z** (% rel. Intensity): 125 M<sup>+</sup> (100). Calcd. for C<sub>7</sub>H<sub>13</sub>N<sub>2</sub>: 125.1079; found: 125.1076

**MS ES<sup>-</sup> m/z** (% rel. Intensity): 95 M<sup>-</sup> (100). Calcd. for CH<sub>3</sub>O<sub>3</sub>S: 94.9803; found: 94.9801.

**[C<sub>4</sub>H<sub>9</sub>mim][SO<sub>3</sub>CH<sub>3</sub>].** Following the general procedure 1a (12 h) and 1b (70 °C, 50 h), **1-butyl-3-methylimidazolium methanesulfonate** was obtained as a white crystalline solid (86% yield).

**<sup>1</sup>H-NMR** (CDCl<sub>3</sub>, 300MHz): δ/ppm = 0.96 (t, 3H, J=7.5 Hz, CH<sub>2</sub>CH<sub>3</sub>); 1.31-1.41 (m, 2H, J=7.5 Hz, CH<sub>2</sub>CH<sub>3</sub>); 1.84-1.94 (m, 2H, J=7.5 Hz, NCH<sub>2</sub>CH<sub>2</sub>); 2.76 (s, 3H, SCH<sub>3</sub>); 4.06 (s, 3H, NCH<sub>3</sub>); 4.28 (t, 2H, J=7.2 Hz, NCH<sub>2</sub>); 7.55 (s, 1H, NCH); 7.66 (s, 1H, NCH); 9.81 (s, 1H, NCHN).

**<sup>13</sup>C-NMR** (CDCl<sub>3</sub>, 75 MHz): δ/ppm = 13.65 (CH<sub>2</sub>CH<sub>3</sub>); 19.63 (CH<sub>2</sub>CH<sub>3</sub>); 32.35 (CH<sub>2</sub>CH<sub>2</sub>CH<sub>3</sub>); 36.51 (SCH<sub>3</sub>); 40.05 (NCH<sub>3</sub>); 49.80 (NCH<sub>2</sub>); 122.56 (NCH); 124.17 (NCH); 137.88 (NCHN).

**MS ES<sup>+</sup> m/z** (% rel. Intensity): 139 M<sup>+</sup> (100). Calcd. for C<sub>8</sub>H<sub>15</sub>N<sub>2</sub>: 139.1235; found: 139.1228

**MS ES<sup>-</sup> m/z** (% rel. Intensity): 95 M<sup>-</sup> (100). Calcd. for CH<sub>3</sub>O<sub>3</sub>S: 94.9803; found: 94.9799.

**[C<sub>5</sub>H<sub>11</sub>mim][SO<sub>3</sub>CH<sub>3</sub>].** Following the general procedure 1a (12 h) and 1b (70 °C, 72 h), **1-pentyl-3-methylimidazolium methanesulfonate** was obtained as a white solid (86% yield).

**<sup>1</sup>H-NMR** (CDCl<sub>3</sub>, 300MHz): δ/ppm = 0.89 (t, 3H, J=6.8 Hz, CH<sub>2</sub>CH<sub>3</sub>); 1.28-1.40 (m, 4H, J=7.5 Hz, (CH<sub>2</sub>)<sub>2</sub>CH<sub>3</sub>); 1.85-1.95 (m, 2H, J=7.5 Hz, NCH<sub>2</sub>CH<sub>2</sub>); 2.76 (s, 3H, SCH<sub>3</sub>); 4.06 (s, 3H, NCH<sub>3</sub>); 4.27 (t, 2H, J=7.5 Hz, NCH<sub>2</sub>); 7.52 (d, 1H, J=1.8 Hz, NCH); 7.66 (d, 1H, J=1.8 Hz, NCH); 9.81 (s, 1H, NCHN).

**<sup>13</sup>C-NMR** (CDCl<sub>3</sub>, 75MHz): δ/ppm = 14.09 (CH<sub>2</sub>CH<sub>3</sub>); 22.29 (CH<sub>2</sub>CH<sub>3</sub>); 28.49 (CH<sub>2</sub>CH<sub>2</sub>CH<sub>3</sub>); 30.19 (NCH<sub>2</sub>CH<sub>2</sub>); 36.57 (SCH<sub>3</sub>); 40.08 (NCH<sub>3</sub>); 50.11 (NCH<sub>2</sub>); 122.49 (NCH); 124.20 (NCH); 137.98 (NCHN).

**MS ES<sup>+</sup> m/z** (% rel. Intensity): 153 M<sup>+</sup> (100). Calcd. for C<sub>9</sub>H<sub>17</sub>N<sub>2</sub>: 153.1392; found: 153.1383.

**MS ES<sup>-</sup> m/z** (% rel. Intensity): 95 M<sup>-</sup> (100). Calcd. for CH<sub>3</sub>O<sub>3</sub>S: 94.9803; found: 94.9796.

**[C<sub>6</sub>H<sub>13</sub>mim][SO<sub>3</sub>CH<sub>3</sub>].** Following the general procedure 1a (48 h) and 1b (70 °C, 72 h), **1-hexyl-3-methylimidazolium methanesulfonate** was obtained as a pale yellow liquid (67 % yield).

**<sup>1</sup>H-NMR** (CDCl<sub>3</sub>, 300MHz): δ/ppm = 0.41 (t, 3H, J=6.8 Hz, CH<sub>2</sub>CH<sub>3</sub>); 0.85 (br, 6H, (CH<sub>2</sub>)<sub>3</sub>CH<sub>3</sub>); 1.42 (br, 2H, NCH<sub>2</sub>CH<sub>2</sub>); 2.76 (s, 3H, SCH<sub>3</sub>); 3.61 (s, 3H, NCH<sub>3</sub>); 3.81 (t, 2H, J=6.3 Hz, NCH<sub>2</sub>); 7.18 (d, 1H, J=1.5 Hz, NCHCH); 7.29 (d, 1H, J=1.5 Hz, NCHCH); 9.25 (s, 1H, NCHN).

**<sup>13</sup>C-NMR** (CDCl<sub>3</sub>, 75MHz): δ/ppm = 13.92 (CH<sub>2</sub>CH<sub>3</sub>); 22.31 (CH<sub>2</sub>CH<sub>3</sub>); 25.77 (CH<sub>2</sub>CH<sub>2</sub>CH<sub>3</sub>); 30.19 (N(CH<sub>2</sub>)<sub>2</sub>CH<sub>2</sub>); 31.02 (NCH<sub>2</sub>CH<sub>2</sub>); 36.19 (SCH<sub>3</sub>); 39.84 (NCH<sub>3</sub>); 49.71 (NCH<sub>2</sub>); 122.48 (NCH); 124.01 (NCH); 137.39 (NCHN).

**MS ES<sup>+</sup> m/z** (% rel. Intensity): 167 M<sup>+</sup> (100). Calcd. for C<sub>10</sub>H<sub>19</sub>N<sub>2</sub>: 167.1548; found: 167.1499.

**MS ES<sup>-</sup> m/z** (% rel. Intensity): 95 M<sup>-</sup> (100). Calcd. for CH<sub>3</sub>O<sub>3</sub>S: 94.9803; found: 94.9796.

**[C<sub>8</sub>H<sub>17</sub>mim][SO<sub>3</sub>CH<sub>3</sub>].** Following the general procedure 1a (48 h) and 1b (70 °C, 72 h), **1-octyl-3-methylimidazolium methanesulfonate** was obtained as a pale yellow liquid (82 % yield).

**<sup>1</sup>H-NMR** (CDCl<sub>3</sub>, 300MHz): δ/ppm = 0.56 (t, 3H, J=6.8 Hz, CH<sub>2</sub>CH<sub>3</sub>); 0.98 (br, 10H, (CH<sub>2</sub>)<sub>5</sub>CH<sub>3</sub>); 1.59 (br, 2H, NCH<sub>2</sub>CH<sub>2</sub>); 2.46 (s, 3H, SCH<sub>3</sub>); 3.70 (s, 3H, NCH<sub>3</sub>); 3.98 (t, 2H, J=6.9 Hz, NCH<sub>2</sub>); 7.27 (d, 1H, J=1.2 Hz, NCHCH); 7.41 (d, 1H, J=1.2 Hz, NCHCH); 9.48 (s, 1H, NCHN).

**<sup>13</sup>C-NMR** (CDCl<sub>3</sub>, 75MHz): δ/ppm = 14.21 (CH<sub>2</sub>CH<sub>3</sub>); 22.69 (CH<sub>2</sub>CH<sub>3</sub>); 26.36 (CH<sub>2</sub>CH<sub>2</sub>CH<sub>3</sub>); 29.08 (CH<sub>2</sub>(CH<sub>2</sub>)<sub>2</sub>CH<sub>3</sub>); 29.15 (N(CH<sub>2</sub>)<sub>3</sub>CH<sub>2</sub>); 30.47 (N(CH<sub>2</sub>)<sub>2</sub>CH<sub>2</sub>); 31.79 (NCH<sub>2</sub>CH<sub>2</sub>); 36.42 (SCH<sub>3</sub>); 39.98 (NCH<sub>3</sub>); 49.99 (NCH<sub>2</sub>); 122.67 (NCH); 124.18 (NCH); 137.74 (NCHN).

*[C<sub>10</sub>H<sub>21</sub>mim][SO<sub>3</sub>CH<sub>3</sub>]*. Following the general procedure 1a (48 h) and 1b (70 °C, 96 h), **1-decyl-3-methylimidazolium methanesulfonate** was obtained as a white solid (85% yield).

<sup>1</sup>H-NMR (CDCl<sub>3</sub>, 300MHz): δ/ppm = 0.79 (t, 3H, J=6.6 Hz, CH<sub>2</sub>CH<sub>3</sub>); 1.18 (br, 14H, (CH<sub>2</sub>)<sub>7</sub>CH<sub>3</sub>); 1.81 (t, 2H, J=6.6 Hz, NCH<sub>2</sub>CH<sub>2</sub>); 2.67 (s, 3H, SCH<sub>3</sub>); 3.97 (s, 3H, NCH<sub>3</sub>); 4.18 (t, 2H, J=7.5 Hz, NCH<sub>2</sub>); 7.45 (s, 1H, NCHCH); 7.61 (s, 1H, NCHCH); 9.68 (s, 1H, NCHN).

<sup>13</sup>C-NMR (CDCl<sub>3</sub>, 75MHz): δ/ppm = 14.29 (CH<sub>2</sub>CH<sub>3</sub>); 22.81 (CH<sub>2</sub>CH<sub>3</sub>); 26.43 (CH<sub>2</sub>CH<sub>2</sub>CH<sub>3</sub>); 29.19 (CH<sub>2</sub>(CH<sub>2</sub>)<sub>2</sub>CH<sub>3</sub>); 29.40 (CH<sub>2</sub>(CH<sub>2</sub>)<sub>3</sub>CH<sub>3</sub>); 29.56 (CH<sub>2</sub>(CH<sub>2</sub>)<sub>4</sub>CH<sub>3</sub>); 29.63 (N(CH<sub>2</sub>)<sub>3</sub>CH<sub>2</sub>); 30.49 (N(CH<sub>2</sub>)<sub>2</sub>CH<sub>2</sub>); 31.99 (NCH<sub>2</sub>CH<sub>2</sub>); 36.40(SCH<sub>3</sub>); 40.00(NCH<sub>3</sub>); 50.05 (NCH<sub>2</sub>); 122.48 (NCH); 124.22 (NCH); 137.80 (NCHN).

MS ES<sup>+</sup> m/z (% rel. Intensity): 223 M<sup>+</sup> (100). Calcd. for C<sub>14</sub>H<sub>27</sub>N<sub>2</sub>: 223.2174; found: 223.2164.

MS ES<sup>-</sup> m/z (% rel. Intensity): 95 M<sup>-</sup> (100). Calcd. for CH<sub>3</sub>O<sub>3</sub>S: 94.9803; found: 94.9798.

*[C<sub>2</sub>H<sub>5</sub>mim][SO<sub>3</sub>C<sub>2</sub>H<sub>5</sub>]*. Following the general procedure 1a (12 h) and 1b (50 °C, 48 h), **1-ethyl-3-methylimidazolium ethanesulfonate** was obtained as a pale yellow liquid (87 % yield).

<sup>1</sup>H-NMR (CDCl<sub>3</sub>, 300MHz): δ/ppm = 0.99 (t, 3H, J=7.5 Hz, NCH<sub>2</sub>CH<sub>3</sub>); 1.23 (t, 3H, J=7.5 Hz, SCH<sub>2</sub>CH<sub>3</sub>); 2.50 (q, 2H, J=7.5 Hz, SCH<sub>2</sub>); 3.72 (s, 3H, NCH<sub>3</sub>); 4.02 (q, 2H, J=7.5 Hz, NCH<sub>2</sub>); 7.34 (s, 1H, NCHCH); 7.35 (s, 1H, NCHCH); 9.48 (s, 1H, NCHN);

<sup>13</sup>C-NMR (CDCl<sub>3</sub>, 75MHz): δ/ppm = 10.06 (NCH<sub>2</sub>CH<sub>3</sub>); 15.75 (SCH<sub>2</sub>CH<sub>3</sub>); 36.30 (SCH<sub>2</sub>CH<sub>3</sub>); 45.01 (NCH<sub>3</sub>); 45.99 (NCH<sub>2</sub>); 122.35 (NCH); 124.02 (NCH); 137.35 (NCHN).

MS ES<sup>+</sup> m/z (% rel. Intensity): 111 M<sup>+</sup> (100). Calcd. for C<sub>6</sub>H<sub>11</sub>N<sub>2</sub>: 111.0922; found: 111.0966.

MS ES<sup>-</sup> m/z (% rel. Intensity): 109 M<sup>-</sup> (100). Calcd. for C<sub>2</sub>H<sub>5</sub>O<sub>3</sub>S: 108.9959; found: 108.9980.

*[C<sub>3</sub>H<sub>7</sub>mim][SO<sub>3</sub>C<sub>2</sub>H<sub>5</sub>]*. Following the general procedure 1a (12 h) and 1b (60 °C, 72 h), **1-propyl-3-methylimidazolium ethanesulfonate** was obtained as a pale yellow liquid (90 % yield).

<sup>1</sup>H-NMR (CDCl<sub>3</sub>, 300MHz): δ/ppm = 0.97 (t, 3H, J=7.5 Hz, N(CH<sub>2</sub>)<sub>2</sub>CH<sub>3</sub>); 1.34 (t, 3H, J=7.5 Hz, SCH<sub>2</sub>CH<sub>3</sub>); 1.90-2.05 (m, 2H, J=7.5 Hz, NCH<sub>2</sub>CH<sub>2</sub>); 2.85 (q, 2H, J=7.5 Hz, SCH<sub>2</sub>); 4.06 (s, 3H, NCH<sub>3</sub>); 4.26 (t, 2H, J=7.2 Hz, NCH<sub>2</sub>); 7.60 (d, 1H, J=6.6 Hz, NCHCH); 7.69 (d, 1H, J=6.6 Hz, NCHCH); 9.85 (s, 1H, NCHN).

<sup>13</sup>C-NMR (CDCl<sub>3</sub>, 75MHz): δ/ppm = 10.19 ((CH<sub>2</sub>)<sub>2</sub>CH<sub>3</sub>); 10.92 (SCH<sub>2</sub>CH<sub>3</sub>); 23.85 (NCH<sub>2</sub>CH<sub>2</sub>); 36.50 (SCH<sub>2</sub>CH<sub>3</sub>); 46.15 (NCH<sub>3</sub>); 51.44 (NCH<sub>2</sub>); 122.63 (NCH); 124.16 (NCH); 137.94 (NCHN).

MS ES<sup>+</sup> m/z (% rel. Intensity): 125 M<sup>+</sup> (100). Calcd. for C<sub>7</sub>H<sub>13</sub>N<sub>2</sub>: 125.1079; found: 125.1073.

MS ES<sup>-</sup> m/z (% rel. Intensity): 109 M<sup>-</sup> (100). Calcd. for C<sub>2</sub>H<sub>5</sub>O<sub>3</sub>S: 108.9959; found: 108.9950.

*[C<sub>4</sub>H<sub>9</sub>mim][SO<sub>3</sub>C<sub>2</sub>H<sub>5</sub>]*. Following the general procedure 1a (48 h) and 1b (50 °C, 72 h), **1-butyl-3-methylimidazolium ethanesulfonate** was obtained as a white solid (84 % yield).

<sup>1</sup>H-NMR (CDCl<sub>3</sub>, 300MHz): δ/ppm = 0.96 (t, 3H, J=7.2 Hz, (CH<sub>2</sub>)<sub>3</sub>CH<sub>3</sub>); 1.36 (m, 5H, J=7.5 Hz, N(CH<sub>2</sub>)<sub>2</sub>CH<sub>2</sub>, SCH<sub>2</sub>CH<sub>3</sub>); 1.88 (m, 2H, J=7.5 Hz, CH<sub>2</sub>CH<sub>2</sub>); 2.89 (q, 2H, J=7.5 Hz, SCH<sub>2</sub>); 4.06 (s, 3H, NCH<sub>3</sub>); 4.28 (t, 2H, J=7.5 Hz, NCH<sub>2</sub>); 7.28 (t, 1H, J= 1.8 Hz, NCHCH); 7.39 (t, 1H, J=1.8 Hz, NCHCH); 10.06 (s, 1H, NCHN).

<sup>13</sup>C-NMR (CDCl<sub>3</sub>, 75MHz): δ/ppm= 10.32 ((CH<sub>2</sub>)<sub>3</sub>CH<sub>3</sub>); 13.82 (SCH<sub>2</sub>CH<sub>3</sub>); 19.87 (N(CH<sub>2</sub>)<sub>2</sub>CH<sub>2</sub>); 32.52 (NCH<sub>2</sub>CH<sub>2</sub>); 36.89 (SCH<sub>2</sub>CH<sub>3</sub>); 46.27 (NCH<sub>3</sub>); 51.19 (NCH<sub>2</sub>); 121.96 (NCH); 123.66(NCH); 139.11 (NCHN).

MS ES<sup>+</sup> m/z (% rel. Intensity): 139 M<sup>+</sup> (100). Calcd. for C<sub>8</sub>H<sub>15</sub>N<sub>2</sub>: 139.1235; found: 139.1231

MS ES<sup>-</sup> m/z (% rel. Intensity): 109 M<sup>-</sup> (100). Calcd. for C<sub>2</sub>H<sub>5</sub>O<sub>3</sub>S: 108.9959; found: 108.9953.

[C<sub>5</sub>H<sub>11</sub>mim][SO<sub>3</sub>C<sub>2</sub>H<sub>5</sub>]. Following the general procedure 1a (12 h) and 1b (50 °C, 72 h), **1-pentyl-3-methylimidazolium ethanesulfonate** was obtained as a white solid (52 % yield).

<sup>1</sup>H-NMR (CDCl<sub>3</sub>, 300MHz): δ/ppm = 0.90 (t, 3H, J=6.9 Hz, (CH<sub>2</sub>)<sub>4</sub>CH<sub>3</sub>); 1.34 (m, 7H, J=7.5 Hz, NCH<sub>2</sub>(CH<sub>2</sub>)<sub>2</sub>, SCH<sub>2</sub>CH<sub>3</sub>); 1.89 (m, 2H, J=7.5 Hz, NCH<sub>2</sub>CH<sub>2</sub>); 2.88 (q, 2H, J=7.5 Hz, SCH<sub>2</sub>); 4.06 (s, 3H, NCH<sub>3</sub>); 4.26 (t, 2H, J=7.5 Hz, NCH<sub>2</sub>); 7.32 (t, 1H, J= 1.5 Hz, NCHCH); 7.44 (t, 1H, J=1.8 Hz, NCHCH); 10.02 (s, 1H, NCHN).

<sup>13</sup>C-NMR (CDCl<sub>3</sub>, 75MHz): δ/ppm = 0.90 (t, 3H, J=6.9 Hz, (CH<sub>2</sub>)<sub>4</sub>CH<sub>3</sub>); 1.34 (m, 7H, J=7.5 Hz, NCH<sub>2</sub>(CH<sub>2</sub>)<sub>2</sub>, SCH<sub>2</sub>CH<sub>3</sub>); 1.89 (m, 2H, J=7.5 Hz, NCH<sub>2</sub>CH<sub>2</sub>); 2.88 (q, 2H, J=7.5 Hz, SCH<sub>2</sub>); 4.06 (s, 3H, NCH<sub>3</sub>); 4.26 (t, 2H, J=7.5 Hz, NCH<sub>2</sub>); 7.32 (t, 1H, J= 1.5 Hz, NCHCH); 7.44 (t, 1H, J=1.8 Hz, NCHCH); 10.02 (s, 1H, NCHN).

MS ES<sup>+</sup> m/z (% rel. Intensity): 153 M<sup>+</sup> (100). Calcd. for C<sub>9</sub>H<sub>17</sub>N<sub>2</sub>: 153.1392; found: 153.1389.

MS ES<sup>-</sup> m/z (% rel. Intensity): 109 M<sup>-</sup> (100). Calcd. for C<sub>2</sub>H<sub>5</sub>O<sub>3</sub>S: 108.9959; found: 108.9952.

[C<sub>6</sub>H<sub>13</sub>mim][SO<sub>3</sub>C<sub>2</sub>H<sub>5</sub>]. Following the general procedure 1a (12 h) and 1b (50 °C, 72 h), **1-hexyl-3-methylimidazolium ethanesulfonate** was obtained as a white solid (55 % yield).

<sup>1</sup>H-NMR (CDCl<sub>3</sub>, 300MHz): δ/ppm = 0.55 (t, 3H, J=6.9 Hz, (CH<sub>2</sub>)<sub>5</sub>CH<sub>3</sub>); 1.01 (m, 9H, (CH<sub>2</sub>)<sub>3</sub>CH<sub>3</sub>; SCH<sub>2</sub>CH<sub>3</sub>); 1.57 (k, 2H, J=6.6 Hz, NCH<sub>2</sub>CH<sub>2</sub>); 2.50 (q, 2H, J=7.5 Hz, SCH<sub>2</sub>CH<sub>3</sub>); 3.74 (s, 3H, N-CH<sub>3</sub>); 3.96 (t, 2H, J=7.5 Hz, NCH<sub>2</sub>); 7.27 (d, 1H, J=1.8 Hz, NCHCH); 7.42 (d, 1H, J=1.5 Hz, NCHCH); 9.50 (s, 1H, NCHN).

<sup>13</sup>C-NMR (CDCl<sub>3</sub>, 75MHz): δ/ppm = 10.11 (N(CH<sub>2</sub>)<sub>5</sub>CH<sub>3</sub>); 14.06 (SCH<sub>2</sub>CH<sub>3</sub>); 22.49 (N(CH<sub>2</sub>)<sub>4</sub>CH<sub>2</sub>); 25.97 (N(CH<sub>2</sub>)<sub>3</sub>CH<sub>2</sub>); 30.38 (N(CH<sub>2</sub>)<sub>2</sub>CH<sub>2</sub>); 31.21 (NCH<sub>2</sub>CH<sub>2</sub>); 36.39 (SCH<sub>2</sub>CH<sub>3</sub>); 46.06 (NCH<sub>3</sub>); 49.94 (NCH<sub>2</sub>); 122.48 (NCH); 124.18 (NCH); 137.80 (NCHN).

MS ES<sup>+</sup> m/z (% rel. Intensity): 167 M<sup>+</sup> (100). Calcd. for C<sub>10</sub>H<sub>19</sub>N<sub>2</sub>: 167.1548; found: 167.1550.

MS ES<sup>-</sup> m/z (% rel. Intensity): 109 M<sup>-</sup> (100). Calcd. for C<sub>2</sub>H<sub>5</sub>O<sub>3</sub>S: 108.9959; found: 108.9970.

[C<sub>2</sub>H<sub>5</sub>mim][SO<sub>3</sub>C<sub>3</sub>H<sub>7</sub>]. Following the general procedure 1a (12 h) and 1b (50 °C, 48 h), **1-ethyl-3-methylimidazolium propylsulfonate** was obtained as a yellow liquid (42 % yield).

<sup>1</sup>H-NMR (CDCl<sub>3</sub>, 300MHz): δ/ppm = 1.01 (t, 3H, J=7.5 Hz, NCH<sub>2</sub>CH<sub>3</sub>); 1.57 (t, 3H, J=7.5 Hz, S(CH<sub>2</sub>)<sub>2</sub>CH<sub>3</sub>); 1.85 (m, 2H, J=7.5 Hz, SCH<sub>2</sub>CH<sub>2</sub>); 2.80 (k, 2H, J=3.3 Hz, SCH<sub>2</sub>); 4.05(s, 3H, NCH<sub>3</sub>); 4.35 (q, 2H, J=7.5 Hz, NCH<sub>2</sub>); 7.63(d, 1H, J=1.8 Hz, NCHCH); 7.64(d, 1H, J=1.8 Hz, NCHCH); 9.85(s, 1H, NCHN).

<sup>13</sup>C-NMR (CDCl<sub>3</sub>, 75MHz): δ/ppm = 13.80 (NCH<sub>2</sub>CH<sub>3</sub>); 15.88 (S(CH<sub>2</sub>)<sub>2</sub>CH<sub>3</sub>); 19.19 (SCH<sub>2</sub>CH<sub>2</sub>); 36.50 (SCH<sub>2</sub>); 42.22 (NCH<sub>3</sub>); 54.36 (NCH<sub>2</sub>); 122.36 (NCH); 124.12 (NCH); 137.71 (NCHN).

MS ES<sup>+</sup> m/z (% rel. Intensity): 111 M<sup>+</sup> (100). Calcd. for C<sub>6</sub>H<sub>11</sub>N<sub>2</sub>: 111.0922; found: 111.0924.

**MS ES<sup>-</sup> m/z** (% rel. Intensity): 123 M<sup>-</sup> (100). Calcd. for C<sub>3</sub>H<sub>7</sub>O<sub>3</sub>S: 123.0116; found: 123.0106.

**[C<sub>3</sub>H<sub>7</sub>mim][SO<sub>3</sub>C<sub>3</sub>H<sub>7</sub>]**. Following the general procedure 1a (12 h) and 1b (70 °C, 72 h), **1-propyl-3-methylimidazolium propylsulfonate** was obtained as a white solid (71 % yield).

**<sup>1</sup>H-NMR** (CDCl<sub>3</sub>, 300MHz): δ/ppm = 0.504-0.603 (m, 6H, J= 7.2 Hz N(CH<sub>2</sub>)<sub>2</sub>CH<sub>3</sub>, S(CH<sub>2</sub>)<sub>2</sub>CH<sub>3</sub>); 1.36-1.54 (m, 4H, J= 7.2 Hz, NCH<sub>2</sub>CH<sub>2</sub>, SCH<sub>2</sub>CH<sub>2</sub>); 2.35 (t, 2H, J= 6 Hz, SCH<sub>2</sub>); 3.63 (s, 3H, NCH<sub>3</sub>); 3.84(t, 2H, J=7.5 Hz, NCH<sub>2</sub>); 7.31 (d, 1H, J=1.5 Hz, NCHCH); 7.25 (d, 1H, J=1.5 Hz, NCHCH); 9.32 (s, 1H, NCHN);

**<sup>13</sup>C-NMR** (CDCl<sub>3</sub>, 75MHz): δ/ppm = 10.71 (N(CH<sub>2</sub>)<sub>2</sub>CH<sub>3</sub>); 13.66 (S(CH<sub>2</sub>)<sub>2</sub>CH<sub>3</sub>); 18.96 (SCH<sub>2</sub>CH<sub>2</sub>); 23.67 (NCH<sub>2</sub>CH<sub>2</sub>); 36.27 (SCH<sub>2</sub>); 51.16 (NCH<sub>3</sub>); 54.15 (NCH<sub>2</sub>); 122.61 (NCH); 124.03 (NCH); 137.55 (NCHN).

**MS ES<sup>+</sup> m/z** (% rel. Intensity): 125 M<sup>+</sup> (100). Calcd. for C<sub>7</sub>H<sub>13</sub>N<sub>2</sub>: 125.1079; found: 125.1077.

**MS ES<sup>-</sup> m/z** (% rel. Intensity): 123 M<sup>-</sup> (100). Calcd. for C<sub>3</sub>H<sub>7</sub>O<sub>3</sub>S: 123.0116; found: 123.0112.

**[C<sub>2</sub>H<sub>5</sub>mim][SO<sub>3</sub>C<sub>4</sub>H<sub>9</sub>]**. Following the general procedure 1a (12 h) and 1b (50 °C, 72 h), **1-ethyl-3-methylimidazolium butylsulfonate** was obtained as a yellow liquid (70 % yield).

**<sup>1</sup>H-NMR** (CDCl<sub>3</sub>, 300MHz): δ/ppm = 0.91 (t, 3H, J=7.2 Hz, (CH<sub>2</sub>)<sub>3</sub>CH<sub>3</sub>); 1.37-1.49 (m, 2H, J= 7.5 Hz, CH<sub>2</sub>CH<sub>2</sub>CH<sub>3</sub>); 1.57 (t, 3H, J=7.2 Hz, NCH<sub>2</sub>CH<sub>3</sub>); 1.81(q, 2H, J= 1.5 Hz, SCH<sub>2</sub>CH<sub>2</sub>); 2.80 (q, 2H, J= 1.8 Hz, SCH<sub>2</sub>); 4.05 (s, 3H, NCH<sub>3</sub>); 4.36 (q, 2H, J=7.5 Hz, NCH<sub>2</sub>); 7.63 (q, 2H, J=1.5 Hz, NCHCH); 9.86 (s, 1H, NCHN).

**<sup>13</sup>C-NMR** (CDCl<sub>3</sub>, 75MHz): δ/ppm =13.08 (NCH<sub>2</sub>CH<sub>3</sub>); 14.87 (S(CH<sub>2</sub>)<sub>3</sub>CH<sub>3</sub>); 21.28 (S(CH<sub>2</sub>)<sub>2</sub>CH<sub>2</sub>); 26.71 (SCH<sub>2</sub>CH<sub>2</sub>); 35.46 (SCH<sub>2</sub>); 44.16 (NCH<sub>3</sub>); 51.15 (NCH<sub>2</sub>); 121.40 (NCH); 123.13 (NCH); 138.48 (NCHN).

**MS ES<sup>+</sup> m/z** (% rel. Intensity): 111 M<sup>+</sup> (100). Calcd. for C<sub>6</sub>H<sub>11</sub>N<sub>2</sub>: 111.0922; found: 111.0921.

**MS ES<sup>-</sup> m/z** (% rel. Intensity): 137 M<sup>-</sup> (100). Calcd. for C<sub>4</sub>H<sub>9</sub>O<sub>3</sub>S: 137.0272; found: 137.0264.

**[C<sub>3</sub>H<sub>7</sub>mim][SO<sub>3</sub>C<sub>4</sub>H<sub>9</sub>]**. Following the general procedure 1a (12 h) and 1b (50 °C, 72 h), **1-propyl-3-methylimidazolium butylsulfonate** was obtained as a yellow liquid (68 % yield).

**<sup>1</sup>H-NMR** (CDCl<sub>3</sub>, 300MHz): δ/ppm = 0.89-0.99 (m, 6H, J= 7.5 Hz, S(CH<sub>2</sub>)<sub>3</sub>CH<sub>3</sub>, N(CH<sub>2</sub>)<sub>2</sub>CH<sub>3</sub>); 1.36-1.49 (m, 2H, J=7.5 Hz, S(CH<sub>2</sub>)<sub>2</sub>CH<sub>2</sub>); 1.76-1.84 (m, 4H, J= 7.5 Hz, SCH<sub>2</sub>CH<sub>2</sub>, NCH<sub>2</sub>CH<sub>2</sub>); 2.83(q, 2H, J=6.5 Hz, SCH<sub>2</sub>); 4.05(s, 3H, NCH<sub>3</sub>); 4.25 (t, 2H, J=7.2 Hz, NCH<sub>2</sub>); 7.55(d, 1H, J=1.5 Hz, NCHCH); 7.65(d, 1H, J=1.5 Hz, NCHCH); 9.87 (s, 1H, NCHN).

**<sup>13</sup>C-NMR** (CDCl<sub>3</sub>, 75MHz): δ/ppm = 10.98 (N(CH<sub>2</sub>)<sub>2</sub>CH<sub>3</sub>); 14.16 (S(CH<sub>2</sub>)<sub>3</sub>CH<sub>3</sub>); 22.42 (S(CH<sub>2</sub>)<sub>2</sub>CH<sub>2</sub>); 23.91 (NCH<sub>2</sub>CH<sub>2</sub>); 27.83 (SCH<sub>2</sub>CH<sub>2</sub>); 36.59 (SCH<sub>2</sub>); 51.53 (NCH<sub>3</sub>); 52.27 (NCH<sub>2</sub>); 122.60 (NCH); 124.16 (NCH); 138.16 (NCHN).

**MS ES<sup>+</sup> m/z** (% rel. Intensity): 125 M<sup>+</sup> (100). Calcd. for C<sub>7</sub>H<sub>13</sub>N<sub>2</sub>: 125.1079; found: 125.1076.

**MS ES<sup>-</sup> m/z** (% rel. Intensity): 137 M<sup>-</sup> (100). Calcd. for C<sub>4</sub>H<sub>9</sub>O<sub>3</sub>S: 137.0272; found: 137.0263.

**[C<sub>2</sub>H<sub>5</sub>mim][SO<sub>3</sub>C<sub>6</sub>H<sub>13</sub>]**. 10g of C<sub>6</sub>H<sub>13</sub>SO<sub>3</sub>Na and 7,8g of C<sub>2</sub>H<sub>5</sub>mimCl were dissolved separately in minimum amount of methanol (molar ratio 1:1). Due to the low solubility of C<sub>6</sub>H<sub>13</sub>SO<sub>3</sub>Na in methanol,



vigorous stirring in a large amount of methanol were required. Both solutions were joined in a 500 ml round-bottomed flask and stirred for 5 days. Afterwards, methanol was removed under reduced pressure at 25°C. Subsequently, 100ml of acetone was added to the mixture in order to precipitate sodium chloride. The precipitation was separated by filtration and acetone was removed under reduced pressure to give the **1-ethyl-3-methylimidazolium hexylsulfonate** as a yellow liquid (10.32 g, 58.1 % yield).

**<sup>1</sup>H-NMR** (CDCl<sub>3</sub>, 300MHz): δ/ppm = 0.54 (t, 3H, J= 6.6 Hz, (CH<sub>2</sub>)<sub>5</sub>CH<sub>3</sub>); 0.94-0.97 (m, 4H, J=6.6 Hz, (CH<sub>2</sub>)<sub>2</sub>CH<sub>3</sub>); 1.02-1.09 (m, 2H, J=7.2 Hz, S(CH<sub>2</sub>)<sub>2</sub>CH<sub>2</sub>); 1.24(t, 3H, J= 7.5 Hz, NCH<sub>2</sub>CH<sub>3</sub>); 1.43-1.51 (m, 2H, J=7.5 Hz, SCH<sub>2</sub>CH<sub>2</sub>); 2.48 (t, 2H, J= 7.8 Hz, SCH<sub>2</sub>) 3.76 (s, 3H, NCH<sub>3</sub>); 4.03 (t, 2H, J=7.2 Hz, NCH<sub>2</sub>); 7.36(s, 2H, NCHCH); 9.55(s, 1H, NCHN).

**<sup>13</sup>C-NMR** (CDCl<sub>3</sub>, 75MHz): δ/ppm = 14.18; 15.81; 22.58; 25.58; 28.75; 31.72; 6.38; 45.08; 52.43; 122.34; 124.05;137.48.

**MS ES<sup>+</sup> m/z** (% rel. Intensity): 111 M<sup>+</sup> (100). Calcd. for C<sub>6</sub>H<sub>11</sub>N<sub>2</sub>: 111.0922; found: 111.0921.

**MS ES<sup>-</sup> m/z** (% rel. Intensity): 165 M<sup>-</sup> (100). Calcd. for C<sub>6</sub>H<sub>13</sub>O<sub>3</sub>S: 165.0585; found: 165.0580.

## **Appendix 3**

## Catanionic Surfactant Ionic Liquids: Micelles and Ionic Liquid Crystals

$^1\text{H}$ - and  $^{13}\text{C}$ -NMR analyses showed no major impurities in the ionic liquids. All NMR spectra were recorded at room temperature on a Bruker Avance spectrometer DPX 300, using deuterated chloroform as solvent.

**[C<sub>8</sub>H<sub>17</sub>mim][SO<sub>3</sub>CH<sub>3</sub>]**. Following the general procedure 1a (48 h) and 1b (70 °C, 72 h), **1-octyl-3-methylimidazolium methanesulfonate** was obtained as a pale yellow liquid (82 % yield).

$^1\text{H}$ -NMR(CDCl<sub>3</sub>, 300MHz):  $\delta$ /ppm = 0.56 (t, 3H, J=6.8 Hz, CH<sub>2</sub>CH<sub>3</sub>); 0.98 (br, 10H, (CH<sub>2</sub>)<sub>5</sub>CH<sub>3</sub>); 1.59 (br, 2H, NCH<sub>2</sub>CH<sub>2</sub>); 2.46 (s, 3H, SCH<sub>3</sub>); 3.70 (s, 3H, NCH<sub>3</sub>); 3.98 (t, 2H, J=6.9 Hz, NCH<sub>2</sub>); 7.27 (d, 1H, J=1.2 Hz, NCHCH); 7.41 (d, 1H, J=1.2 Hz, NCHCH); 9.48 (s, 1H, NCHN).

$^{13}\text{C}$ -NMR(CDCl<sub>3</sub>, 75MHz):  $\delta$ /ppm = 14.21, 22.69, 26.36, 29.08, 29.15, 30.47, 31.79, 36.42, 39.98, 49.99, 122.67, 124.18, 137.74.

MS ES<sup>+</sup> m/z (% rel. Intensity): 195 M<sup>+</sup> (100). Calcd. for C<sub>12</sub>H<sub>23</sub>N<sub>2</sub>: 195.1861; found: 195.1857.

MS ES<sup>-</sup> m/z (% rel. Intensity): 95 M<sup>-</sup> (100). Calcd. for CH<sub>3</sub>O<sub>3</sub>S: 94.9803; found: 94.9798.

**[C<sub>10</sub>H<sub>21</sub>mim][SO<sub>3</sub>CH<sub>3</sub>]**. Following the general procedure 1a (48 h) and 1b (70 °C, 96 h), **1-decyl-3-methylimidazolium methanesulfonate** was obtained as a white solid (85% yield).

$^1\text{H}$ -NMR(CDCl<sub>3</sub>, 300MHz):  $\delta$ /ppm = 0.79 (t, 3H, J=6.6 Hz, CH<sub>2</sub>CH<sub>3</sub>); 1.18 (br, 14H, (CH<sub>2</sub>)<sub>7</sub>CH<sub>3</sub>); 1.81 (t, 2H, J=6.6 Hz, NCH<sub>2</sub>CH<sub>2</sub>); 2.67 (s, 3H, SCH<sub>3</sub>); 3.97 (s, 3H, NCH<sub>3</sub>); 4.18 (t, 2H, J=7.5 Hz, NCH<sub>2</sub>); 7.45 (s, 1H, NCHCH); 7.61 (s, 1H, NCHCH); 9.68 (s, 1H, NCHN).

$^{13}\text{C}$ -NMR(CDCl<sub>3</sub>, 75MHz):  $\delta$ /ppm = 14.29, 22.81, 26.43, 29.19, 29.40, 29.56, 29.63, 30.49, 31.99, 36.40, 40.00, 50.05, 122.48, 124.22, 137.80.

MS ES<sup>+</sup> m/z (% rel. Intensity): 223 M<sup>+</sup> (100). Calcd. for C<sub>14</sub>H<sub>27</sub>N<sub>2</sub>: 223.2174; found: 223.2164.

MS ES<sup>-</sup> m/z (% rel. Intensity): 95 M<sup>-</sup> (100). Calcd. for CH<sub>3</sub>O<sub>3</sub>S: 94.9803; found: 94.9798.

**[C<sub>8</sub>H<sub>17</sub>mim][SO<sub>3</sub>C<sub>4</sub>H<sub>9</sub>]**. Following the general procedure 1a (48 h) and 1b (70 °C, 96 h), **1-octyl-3-methylimidazolium butanesulfonate** was obtained as white crystals (79 % yield).

$^1\text{H}$ -NMR(CDCl<sub>3</sub>, 300MHz):  $\delta$ /ppm = 0.90 (br, 6H, CH<sub>2</sub>CH<sub>3</sub>); 1.29 (br, 10H, (CH<sub>2</sub>)<sub>5</sub>CH<sub>3</sub>); 1.43 (m, 2H, J=7.5 Hz, S(CH<sub>2</sub>)<sub>2</sub>CH<sub>2</sub>); 1.85 (br, 4H, SCH<sub>2</sub>CH<sub>2</sub>, NCH<sub>2</sub>CH<sub>2</sub>); 2.84 (br, 2H, SCH<sub>2</sub>); 4.05 (s, 3H, NCH<sub>3</sub>); 4.25 (t, 2H, J=7.4 Hz, NCH<sub>2</sub>); 7.33 (s, 1H, NCHCH); 7.48 (s, 1H, NCHCH); 9.98 (s, 1H, NCHN).

$^{13}\text{C}$ -NMR(CDCl<sub>3</sub>, 75MHz):  $\delta$ /ppm = 13.91, 14.08, 22.21, 22.61, 26.29, 27.55, 28.99, 29.07, 30.31, 31.71, 36.47, 50.03, 51.97, 121.71, 123.53, 138.41

MS ES<sup>+</sup> m/z (% rel. Intensity): 195 M<sup>+</sup> (100). Calcd. for C<sub>12</sub>H<sub>23</sub>N<sub>2</sub>: 195.1861; found: 195.1855.

MS ES<sup>-</sup> m/z (% rel. Intensity): 137 M<sup>-</sup> (100). Calcd. for C<sub>4</sub>H<sub>9</sub>O<sub>3</sub>S: 137.0272; found: 137.0271.

**[C<sub>4</sub>H<sub>9</sub>mim][SO<sub>3</sub>C<sub>4</sub>H<sub>9</sub>]**. Following the general procedure 1a (48 h) and 1b (70 °C, 72 h), **1-butyl-3-methylimidazolium butanesulfonate** was obtained as a white powder (81 % yield).

<sup>1</sup>H-NMR(CDCl<sub>3</sub>, 300MHz): δ/ppm = 0.92 (br, 6H, CH<sub>2</sub>CH<sub>3</sub>); 1.38 (br, 4H, CH<sub>2</sub>CH<sub>3</sub>); 1.84 (br, 4H, NCH<sub>2</sub>CH<sub>2</sub>, SCH<sub>2</sub>CH<sub>2</sub>); 2.86 (br, 2H, SCH<sub>2</sub>); 4.05 (s, 3H, NCH<sub>3</sub>); 4.27 (t, 2H, J=7.3 Hz, NCH<sub>2</sub>); 7.41 (s, 1H, NCHCH); 7.54 (s, 1H, NCHCH); 9.93 (s, 1H, NCHN).

<sup>13</sup>C-NMR(CDCl<sub>3</sub>, 75MHz): δ/ppm = 14.15, 14.54, 20.87, 23.40, 28.61, 33.53, 36.85, 50.98, 52.94, 124.04, 125.35

MS ES<sup>+</sup> m/z (% rel. Intensity): 139 M<sup>+</sup> (100). Calcd. for C<sub>12</sub>H<sub>23</sub>N<sub>2</sub>: 139.1235; found: 139.1235.

MS ES<sup>-</sup> m/z (% rel. Intensity): 137 M<sup>-</sup> (100). Calcd. for CH<sub>3</sub>O<sub>3</sub>S: 137.0272; found: 137.0270.

**[C<sub>4</sub>H<sub>9</sub>mim][SO<sub>3</sub>C<sub>8</sub>H<sub>17</sub>]**. Following the general procedure 1a (48 h) and 1b (70 °C, 72 h), **1-butyl-3-methylimidazolium octanesulfonate** was obtained as white crystals (78 % yield).

<sup>1</sup>H-NMR(CDCl<sub>3</sub>, 300MHz): δ/ppm = 0.92 (t, 3H, J=6.7 Hz, S(CH<sub>2</sub>)<sub>7</sub>CH<sub>3</sub>); 1.01 (t, 3H, J=7.4 Hz, N(CH<sub>2</sub>)<sub>3</sub>CH<sub>3</sub>); 1.32 (br, 10H, S(CH<sub>2</sub>)<sub>2</sub>(CH<sub>2</sub>)<sub>5</sub>CH<sub>3</sub>); 1.40 (br, 2H, N(CH<sub>2</sub>)<sub>2</sub>CH<sub>2</sub>CH<sub>3</sub>); 1.80 (br, 2H, SCH<sub>2</sub>CH<sub>2</sub>); 1.89 (br, 2H, NCH<sub>2</sub>CH<sub>2</sub>); 2.79 (br, 2H, SCH<sub>2</sub>); 3.95 (s, 3H, NCH<sub>3</sub>); 4.24 (t, 2H, J=7.3 Hz, NCH<sub>2</sub>); 7.60 (s, 1H, NCHCH); 7.66 (s, 1H, NCHCH); 8.97 (s, 1H, NCHN).

<sup>13</sup>C-NMR(CDCl<sub>3</sub>, 75MHz): δ/ppm = 14.17, 14.85, 20.88, 24.14, 26.50, 30.32, 30.68, 30.85, 36.90, 51.02, 53.24, 124.11, 125.42, 138.37.

MS ES<sup>+</sup> m/z (% rel. Intensity): 139 M<sup>+</sup> (100). Calcd. for C<sub>12</sub>H<sub>23</sub>N<sub>2</sub>: 139.1235; found: 139.1233.

MS ES<sup>-</sup> m/z (% rel. Intensity): 193 M<sup>-</sup> (100). Calcd. for CH<sub>3</sub>O<sub>3</sub>S: 193.0898; found: 193.0899.

**[C<sub>12</sub>H<sub>23</sub>mim][SO<sub>3</sub>CH<sub>3</sub>]**. Following the general procedure 1a (48 h) and 1b (70 °C, 96 h), **1-dodecyl-3-methylimidazolium methanesulfonate** was obtained as a pale yellow crystalline powder (61 % yield).

<sup>1</sup>H-NMR(CDCl<sub>3</sub>, 300MHz): δ/ppm = 0.88 (t, 3H, J=6.6 Hz, CH<sub>2</sub>CH<sub>3</sub>); 1.25 (br, 18H, (CH<sub>2</sub>)<sub>9</sub>CH<sub>3</sub>); 1.87 (br, 2H, NCH<sub>2</sub>CH<sub>2</sub>); 2.76 (s, 3H, SCH<sub>3</sub>); 4.04 (s, 3H, NCH<sub>3</sub>); 4.25 (t, 2H, J=7.4 Hz, NCH<sub>2</sub>); 7.34 (s, 1H, NCHCH); 7.49 (s, 1H, NCHCH); 9.73 (s, 1H, NCHN).

<sup>13</sup>C-NMR(CDCl<sub>3</sub>, 75MHz): δ/ppm = 14.53, 22.09, 26.67, 29.38, 29.73, 29.77, 29.90, 29.99, 30.62, 32.31, 36.96, 40.01, 50.54, 121.82, 123.52, 138.97

MS ES<sup>+</sup> m/z (% rel. Intensity): 251 M<sup>+</sup> (100). Calcd. for C<sub>12</sub>H<sub>23</sub>N<sub>2</sub>: 251.2487; found: 251.2481.

MS ES<sup>-</sup> m/z (% rel. Intensity): 95 M<sup>-</sup> (100). Calcd. for CH<sub>3</sub>O<sub>3</sub>S: 94.980; found: 94.9803.

**[C<sub>8</sub>H<sub>17</sub>mim][SO<sub>3</sub>C<sub>8</sub>H<sub>17</sub>]**. Following the general procedure 1a (48 h) and 1b (70 °C, 96 h), **1-octyl-3-methylimidazolium octanesulfonate** was obtained as white crystals (69 %).

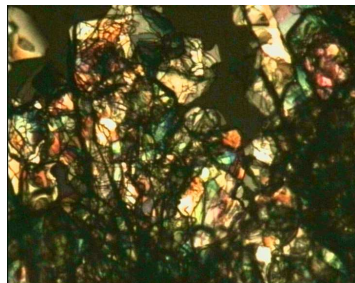
<sup>1</sup>H-NMR(CDCl<sub>3</sub>, 300MHz): δ/ppm = 0.87 (br, 6H, N(CH<sub>2</sub>)<sub>7</sub>CH<sub>3</sub>, S(CH<sub>2</sub>)<sub>7</sub>CH<sub>3</sub>); 1.26 (br, 20H, N(CH<sub>2</sub>)<sub>2</sub>(CH<sub>2</sub>)<sub>5</sub>CH<sub>3</sub>, S(CH<sub>2</sub>)<sub>2</sub>(CH<sub>2</sub>)<sub>5</sub>CH<sub>3</sub>); 1.86 (br, 4H, NCH<sub>2</sub>CH<sub>2</sub>, SCH<sub>2</sub>CH<sub>2</sub>); 2.86 (br, 2H, SCH<sub>2</sub>); 4.05 (s, 3H, NCH<sub>3</sub>); 4.25 (t, 2H, J=7.4 Hz, NCH<sub>2</sub>); 7.26 (s, 1H, NCHCH); 7.38 (s, 1H, NCHCH); 10.05 (s, 1H, NCHN).

<sup>13</sup>C-NMR(CDCl<sub>3</sub>, 75MHz): δ/ppm = 14.45, 14.51, 22.99, 23.07, 25.87, 26.68, 29.36, 29.44, 29.48, 29.60, 29.84, 30.64, 32.09, 32.27, 36.96, 50.53, 52.65, 121.75, 123.44, 139.32

MS ES<sup>+</sup> m/z (% rel. Intensity): 195 M<sup>+</sup> (100). Calcd. for C<sub>12</sub>H<sub>23</sub>N<sub>2</sub>: 195.1861; found: 195.1856.

MS ES<sup>-</sup> m/z (% rel. Intensity): 193 M<sup>-</sup> (100). Calcd. for CH<sub>3</sub>O<sub>3</sub>S: 193.0865; found: 193.0898.

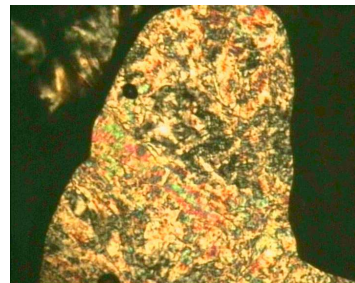
Photomicrographs of  $[\text{C}_8\text{H}_{17}\text{mim}][\text{SO}_3\text{C}_8\text{H}_{17}]$  in the three phase regions; C1 (20 °C), C2 (72 °) and  $\text{S}_\text{A}$  (82 °C).



20 °C, C1



72 °C, C2



82 °C,  $\text{S}_\text{A}$